Target separation of arsenic from contaminated raw water

A thesis

submitted in fulfilment

of the requirements for the degree

of

Doctor of Philosophy in Engineering

at

The University of Waikato

by

JAMES OYEDIJI AREMU

THE UNIVERSITY OF
WAIKATO
Te Whare Wānanga o Waikato

2020

Abstract

Arsenic is known to be one of the most toxic and carcinogenic elements known to have affected millions of people worldwide. Arsenic in surface and groundwater originates from both natural and anthropogenic sources. Prolonged exposure to arsenic can lead to skin disease, cancer, diabetes and cardiovascular disease. This thesis investigates target separation of arsenic from contaminated water using the adsorption and coagulation/flocculation/dissolved air flotation (C/F/DAF) processes.

DMI-65, a silica based catalytic media was used as an adsorbent to investigate As (III) and As (V) removal from a contaminated drinking water. Batch adsorption studies were conducted at different pH (5, 6, 7 and 8.5) to determine adsorption kinetics. Equilibrium was achieved after 6 hours of contact time and experimental data were best fitted to the pseudo second-order kinetic model for As (III) and As (V). The adsorption data were best fitted to Langmuir isotherm models and the maximum adsorption capacity of DMI-65 for As (III) and As (V) were estimated to be 0.318 mg/g and 0.237 mg/g respectively. Thermodynamics studies revealed that adsorption capacity and arsenic removal percentage using DMI-65 increased with increase in temperature. The adsorption process can be attributed to physisorption as a result of Van der Waals interaction at the surface of the adsorbent. Regeneration and reusability of a media is an important economic factor. DMI-65 was able to demonstrate its ability to regenerate after several cycles using sodium hydroxide (NaOH) and performed well over a wide pH range. The maximum removal efficiency for As (III) was 96.55 % at pH 5 and 90.40 % for As (V) at pH 8.5.

A continuous adsorption study was conducted in a fixed-bed column to remove arsenic from the Waikato River using DMI-65. The dynamic adsorption capacity and breakthrough time was well predicted by Thomas and Yoon-Nelson models. The maximum adsorption capacity was found to be 11.96 mg/g using DMI-65 as adsorbent for initial concentration, flowrate and pH of ~ 13.00 – 20.00 µg/L, 20 mL/min and 5, respectively. Results obtained showed that DMI-65 is effective in removing arsenic from contaminated drinking water. It is also effective in reducing turbidity but fouling of the adsorption column is a major drawback and leads to increased pressure drop in the fixed-bed column.

Competing ions in the form of organic anions such as nitrate (NO_3^-), silicate (SiO_4^{4-}), sulfate (SO_4^{2-}), bicarbonate (CO_3^{2-}) and phosphate ($H_2PO_4^-$) are known to interfere with arsenic removal in natural waters. This interference is also influenced by the pH of the solution and anionic concentration. The study was conducted at pH levels (5 – 9) and anionic concentration strength (1, 5 and 10 mM). The most significant interference with the removal of As (V) by polyaluminium chloride (PAC) occurred in the presence of phosphate at pH 6 with a removal rate of 5.52 % at 10 mM phosphate concentration. Overall, the major impact of the competing anions on As (V) removal followed the following order of $H_2PO_4^- > CO_3^{2-} > NO_3^- > SO_4^{2-}$.

Target separation of arsenic from other contaminants was investigated in a two-stage C/F/DAF process. The results of this study indicated that increase in flotation time (10 – 30 minutes) and saturation pressure (2 – 4 bar) did not result in any significant increase in arsenic removal efficiency. Turbidity removal efficiency was poor at pH 5 and 6 despite recording higher arsenic removal efficiency. The first stage DAF process showed that 88.10 % of arsenic and 3.44 % turbidity removal efficiency was achieved using 9.4 mg/L of PAC at pH 6. Increasing the pH of the remaining solution to 8 in the second-stage DAF process resulted in 83.55 % arsenic removal and 64.08 % turbidity removal after adding 0.47 mg/L PAC. These findings showed that the amount of arsenic leaving the water treatment plant (WTP) to the wastewater treatment plant (WWTP) can be reduced from the current 0.942 kg/day to 0.16 kg/day. This represents an overall reduction of 83.01 % in the amount of arsenic that would have end up in the biosolids thereby making it unfit for agricultural purposes. This result showed that arsenic can successfully be separated from other contaminants in a two-stage C/F/DAF process by change in pH from 6 to 8 and under optimised operating conditions.

Acknowledgements

I am forever grateful to Almighty God for his grace and blessings upon my life. To him be all the glory, honour and praise.

I would like to sincerely thank my supervisors Dr. Mark Lay and Dr. Graeme Glasgow who supported me throughout my PhD research with their endless patience, motivation, guidance and encouragement. Both of you have been incredibly generous with your time and energy. Your extensive feedback has had an enormous impact not only in this thesis, but also on my thinking, research and writing. I would like to thank you for giving me an opportunity to have valuable experience working with students as a sessional assistant and providing me the platform to work for and alongside external partners on projects. These experiences I believe would stay with me forever and shape my career in the water and wastewater sector. I would like to thank Mr Gaurav Ahuja for his technical advice, suggestions, and continuous encouragement. You are indeed a friend. I would like to appreciate the contribution of Karl Palos at the start of this thesis for your suggestions and technical input. Thank you.

I want to express my gratitude to all the technical staff who supported me in this project. Particularly Dr. Lisa Li, Ms Helen Turner, Dr. Amanda French, Mrs Annette Rodgers, Mrs Jenny Stockdill and Mr Renat Radosinsky. I thank you all. Special thanks to the administrators of the School of Engineering, Ms Mary Dalbeth and Ms Natalie Shaw for being helping during these years. I also appreciate Dr. Debbie Dada, the librarian of the School of Engineering for her support in making sure the thesis is in good shape for submission. I would like to thank Mr Sukhjit Singh (from Vertex Engineers Ltd, Hamilton New Zealand) for his contribution to technical discussions and suggestions. Thank you to Aaron Low and Norton Holtz of Ligar polymers Ltd, Hamilton, New Zealand for their support and technical advice. I would like to thank everyone in the research group, especially Asaf, Muhammad, Levi, Steve, Tim, Jia, Sohaib, Nicole, Aaron and other undergraduate students I have worked with, it has been great to share the journey with you.

I would like to express my gratitude for the financial support I received during this project from WSP OPUS Consultants (external study award) and Faculty of Science,

and Engineering Student Trust research Grant, 2017 (University of Waikato, Hamilton, New Zealand).

Thank you to all my friends for making life interesting and joyful. Many thanks to Dr. Jerome Odebunmi, Akeem Iyanda, Dr. Omoniyi Alimi, Dimeji Fayomi, Dr. Amir Tarighaleslami and Abdul Kaggwa, I would like to thank the family of Mr and Mrs Kola Fatokun for being there for me, and for your enormous support and kindness.

I would like to acknowledge the unconditional love and financial support I received from my family throughout these years. Special thanks go to my Dad, Engr. Daniel.A. Aremu and my Mum, Dr. Dorcas.A. Aremu. Without you, this would not have been possible. Thank you for all the advice, support, sacrifices and words of encouragement you gave me even when things were not going as planned. To my siblings, Mr Sunday Aremu, Mrs Felicia Akano and Mrs Sabina Adegoke. I love you all.

Finally, special thanks to my beloved son, Jason Ayodele Aremu for putting smile on my face everyday. I feel blessed with you in my life. Daddy loves you.

Contributing Publications

1. **James .O. Aremu**, Mark Lay, Graeme Glasgow., Kinetic and isotherm studies on adsorption of arsenic using silica based catalytic media. Journal of Water Process Engineering (32) 2019. https://doi.org/10.1016/j.jwpe.2019.100939.

2. **James Oyediji Aremu**, Hanan Nabilah Rozi, Dr. Mark Lay, Dr. Graeme Glasgow. Arsenic removal from drinking water using silica based catalytic media. Water New Zealand Conference and Expo, 20 – 22 September, 2017, Hamilton, New Zealand.

3. N. Holtz, A. Low, A. McElroy, N. Evans, T. Madden (Ligar LP); **J. O. Aremu**, M. Lay, G. Glasgow (The University of Waikato). Arsenic removal from contaminated water using non-imprinted polymers. Water New Zealand Conference and Expo, 20 – 22 September, 2017, Hamilton, New Zealand.

4. **James Oyediji Aremu**, Dr. Mark Lay, Dr. Graeme Glasgow, Karl Palos. Challenges of heavy metals in drinking water of North Island, New Zealand, Chemeca Conference, 25 – 28, September, 2016, Adelaide, Australia.

Table of Contents

List of Tables

List of Figures

Nomenclature

Symbols

1/n	adsorption intensity
μg/L	microgram per liter
μm	micrometer
^{o}C	degree centigrade (celcius)
ΔG^{o}	Gibbs free energy (kJ/mol)
ΔH^{o}	enthalpy (kJ/mol)
ΔS^{o}	entropy (J/mol K)
a_s	air solubility (mL/L)
A_T	Temkin isotherm equilibrium binding constant (L/g)
C	concentration of the gas dissolved in the solution
CD	drag coefficient
C_e	equilibrium concentration in solution (mg/L)
cm^{-1}	per centimeter
cm^3/g	centimeter cube per gram
C_o	concentration of adsorbent at initial time zero (mg/L)
C_t	concentration of adsorbent at time t (mg/L)
d_{cb}	critical bubble diameter
D	effective diameter of the agglomerate, (m)
Eh	redox potential
EM	electrophoretic mobility (μm/s/volt/cm)
f	fraction of air dissolved at a given pressure

F	fractional attainment of equilibrium
Fig.	Figure
g	grams
g	gravitational constant, 9.81 (m/s^2)
g/L	gram per liter
g/mg	gram per milligram
g/mg.min	gram per milligram per minute
J/mol/K	joule per mole kelvin
k	Henry`s Law constant
K	kelvin
k_1	pseudo-first-order rate constant (min^{-1})
k_2	pseudo-second-order rate constant (g/mg.min)
K_{DR}	Dubinin – Radushkevich isotherm constant (mol^2/KJ^2)
kg/day	kilogram per day
kJ/mol	kilojoule per mole
K_{id}	Intra-particle diffusion rate constant ($mg/g\ min^{1/2}$)
K_{fd}	film diffusion rate constant
K_F	Freundlich constant (mg/g)
K_L	Lanmuir constant (L/mg)
km	kilometer
km^2	kilometer square
kV	kilovolt
L/g	liter per gram
L/mg	liter per milligram

M	Molarity
M Ω cm^{-1}	Megohm per centimeter
mg/g min	milligram per gram per minute
m^2/g	meters square per gram
m^3/day	meter cube per day
mA	milliamp
mg/kg	milligram per kilogram
mg/L	milligram per liter
min	minute
min^{-1}	per minute
mL	mililiter
mL/min	millimeter per minute
mol^2/KJ^2	mole square per kilojoule square
MW	Megawatt
Mw	molecular weight
nm	nanometer
nm^2	square nanometer
pKa	dissociation constant
Pa	absolute pressures in atmospheres
P/Po	pressure of adsorbate relative to its saturation pressure
ppm	parts per million
Q	volumetric flowrate (mL/min)
q_e	amount of adsorbent adsorbed at equilibrium (mg/g)
q_m	maximum adsorption capacity (mg/g)

q_s	isotherm saturation capacity (mg/g)
q_t	amount of adsorbent adsorbed at time t (mg/g)
R	gas constant (J/mol K)
R	recycle stream flowrate
Re	Reynolds number
R^2	correlation factor
R %	percentage removal
rpm	revolutions per minute
SS	suspended solids concentration (mg/L)
t	time (min)
V	volume (L)
V_{eff}	effluent volume (L)
Vt	terminal rise velocity of the agglomerate, (m/s)
W	mass (g)

Greek

α	initial adsorption rate constant (mg/g min)
β	Elovich adsorption constant (g/mg)
ε	Polanyi potential
ζ	zeta potential (mv)
λ	gamma
ρ_a	density of the agglomerate (kg/m^3)
ρ_o	density of the aqueous phase (kg/m^3)
μ	viscosity of the aqueous phase (kg/m.s)
σ	surface tension of water

∑	summation of parameters

Abbreviations

ARMCANZ	Agriculture and Resource Management Council for Australia and New Zealand
ATSDR	Agency for Toxic Substances and Disease Registry
BET	Brunauer-Emmett-Teller
C/F/DAF	Coagulation/Flocculation/Dissolved air flotation
CVD	Cardiovascular disease
DAF	Dissolved air flotation
DAFF	Dissolved air flotation/filtration
DMA	Dimethylarsinous acid
DWSNZ	Drinking Water Standards for New Zealand
EBCT	Empty bed contact time
FTIR	Fourier transform infrared spectroscopy
GSH	Glutathione
HM	Heavy metal
IARC	International Agency for Research on Cancer
ICP-MS	Inductively Coupled Plasma Mass Spectrometry
IHD	Ischemic heart disease
JCPDS	Joint Committee on Powder Diffraction Standards
MCL	Maximum contamination level
MAC	Maximum acceptable concentration
MAV	Maximum acceptable value
MIP	Molecular imprinted polymer
MMA	Monomethylarsonic acid

NA	Not Available
NIP	Non-Imprinted Polymer
NOM	Natural organic matter
NRDC	National Resources Defence Council
PC	Phytochelatin
PMAV	Permissible maximum acceptable value
RBCs	Red Blood Cells
SEM	Scan electron microscope
SEM-EDX	Scan electron microscope microscopy coupled with energy dispersive X-ray
SPL	Substance Priority List
STP	Standard Temperature and Pressure
T2DM	Type 2 Diabetes Mellitus
UNICEF	United Nations International Children`s Emergency Fund
US EPA	United States Environmental Protection Agency
WHO	World Health Organization
WTP	Water treatment plant
WWTP	Wastewater treatment plant
XRD	X-ray diffraction
XRF	X-ray fluorescence

List of chemicals used

Name	Formula	Hazard Classes
Arsenic (III) Oxide	As_2O_3	6.1D 8.2B 8.3A 6.7A 9.1A
Arsenic (V) Oxide	As_2O_5	6.1B 6.1C 6.7A 9.1A
Chitosan		-
Ethanol	C_2H_5OH	3.1B 6.4A
Ferric Chloride	$FeCl_3$	6.1D 8.2B 8.3A
Hydrochloric Acid	HCl	-
Nitric Acid	HNO_3	5.1.1C 8.1A 8.2A
Nitrogen gas	N_2	Non-flammable compressed gas
Polyaluminium Chloride (PAC)	$Al_2Cl(OH)_5$	6.1E 8.2A 8.3A 9.1A
PolyDADMAC	$(C_8H_{16}NCl)_n$	-
Potassium Bromide	KBr	6.1E 6.3A 6.4A 9.1D
Sodium Carbonate Decahydrate	$Na_2CO_3.10H_2O$	6.4A
Sodium dihydrogen Phosphate dihydrate	$NaH_2PO_4.2H_2O$	-
Sodium Hypochlorite	NaOCl	8.2B 8.3A 9.1A
Sodium Hydroxide	NaOH	8.2A 8.3A 9.1D
Sodium Nitrate	$NaNO_3$	5.1.1C 6.1D 6.3A 6.4A
Sodium Sulfate Decahydrate	$Na_2SO_4.10H_2O$	-

CHAPTER ONE

INTRODUCTION

1.1 Background

Water is not only an essential component for life but also a basic building block to maintain quality of life. Water scarcity has already resulted in adverse effects for all populations in every continent (Jadhav et al., 2015). United Nations International Children's Emergency Fund (UNICEF) and the World Health Organization (WHO) reports confirmed that 748 million people do not have adequate and safe water resources and over 2.5 billion people do not have access to a potable water supply. The WHO further estimates that 1.8 billion people use faecally contaminated sources of drinking water (UNICEF/WHO, 2014). Contamination of heavy metals in the aquatic environment has attracted global attention due to their abundance, persistence and environmental toxicity (Ali et al., 2016).

Heavy metals in general have a density greater than 5 g per cubic centimetre and atomic weights between 63.5 and 200.6 (Fu and Wang, 2011; Srivastava and Majumder, 2008). With the rapid development of industries such as metal plating facilities, mining operations, fertilizer industries, batteries, paper industries and pesticides etc., heavy metals in water/wastewater are directly or indirectly discharged into the environment (Ihsanullah et al., 2016). Unlike organic contaminants, heavy metals are not biodegradable and tend to accumulate in living organisms. Many heavy metal ions are known to be toxic or carcinogenic. Toxic heavy metals of particular concern in water treatment include arsenic, manganese, lead, cadmium, chromium, iron, nickel, copper, and zinc (Fu and Wang, 2011). Table 1-1 summarizes the allowable concentration limits of selected heavy metals as reported by the WHO, United States Environmental Protection Agency (U.S.EPA) and the Drinking Water Standards for New Zealand (DWSNZ).

Heavy metals such as zinc (Zn), cobalt (Co) and copper (Cu) are required for normal body growth, for the physiological functions of living tissue and many biological processes. However, having too much zinc can cause health problems such as skin irritation, nausea, anaemia, vomiting and stomach cramps (Ihsanullah et al., 2016; Nathan Oyaro, 2007). Likewise excess intake of copper causes serious toxicological concerns such as convulsions, cramps, vomiting and even death (Paulino et al., 2006). Cobalt (Co) is also required for normal body functions as a metal component of vitamin B_{12} (Strachan, 2010) but excess intake of it can result in polycythaemia,

an abnormal thyroid artery and over production of red blood cells (RBCs) (Robert and Mari, 2003). According to Dieter et al. (2005) high concentrations of Mn and Cu in drinking water can cause mental diseases such as Manganism and Alzheimer`s. In addition, high Mn contamination of drinking water also affects how children function intellectually (Wasserman et al., 2006). Lead (Pb) causes chronic health risks, including irritability, headache, abdominal pain, kidney damage, blood pressure, stomach cancer, lung cancer due to its high toxicity and being a carcinogenic metal (Järup, 2003; Mortada et al., 2001; Steenland and Boffetta, 2000). Cadmium (Cd) exposure can cause both acute and chronic health effects in living organisms such as kidney damage and skeletal damage (Barbee and Prince, 1999; Jarup et al., 2000). Lastly, arsenic (As) is well known to cause kidney, liver, lung, skin and bladder cancer. Accumulation of arsenic in the body can cause gastrointestinal problems and arsenicosis (Sharma and Sohn, 2009; Villaescusa and Bollinger, 2008).

Table 1-1: WHO, US EPA and DWSNZ limitations of selected heavy metals in drinking water (DWSNZ, 2008; US EPA, 2016; WHO, 2011)

Contaminant	EPA maximum contamination level (MCL) (mg/L)	WHO provisional guideline value (mg/L)	DWSNZ maximum acceptable value (MAV) (mg/L)
Arsenic	0.01	0.01	0.01
Chromium	0.1	0.05	0.05
Cadmium	0.005	0.003	0.004
Copper	1.3	2.0	2.0
Nickel	-	0.07	0.08
mercury	0.002	0.006	0.007
Zinc	5.0	3.0	-
Lead	0.015	0.01	0.01
Antimony	0.006	0.02	0.02

Water and wastewater treatment plants generate millions of tons of residual sludge worldwide every year. The management of this sludge is a major part of waste treatment (Babel and del Mundo Dacera, 2006). The basic disposal methods for such large quantities of sludge are land application, landfilling, incineration, ocean

dumping and lagooning. Until a few years ago, sewage sludge could be re-used directly in agriculture as fertilizer. Recently, however, there has been increased concern because of increased legislation around heavy metal concentration limits in sewage sludge (Lue-Hing et al., 1998). Concern for heavy metals is due to its non-biodegradability, toxicity and consequent persistence (Dutta, 2002). The Water Technology Committee of the Agriculture and Resource Management Council of Australia and New Zealand (ARMCANZ) provides guidelines for sewage sludge for use and disposal. Three grades of biosolids are established based on chemical contaminants. Grade C biosolids are only suitable for disposal at landfills, Grade B is suitable for disposal as landscape enhancement material and for addition to soil used for food production, forestry, and rehabilitation; Grade A biosolids have unrestricted application. Table 1-2 lists the maximum heavy metal concentrations for different grades of biosolids.

Table 1-2: Biosolids classification according to chemical contaminant levels (Ogilvie, 1998).

Contaminants mg/kg	**Grade A**	**Grade B**	**Grade C**
Arsenic	20	75	Any one or more contaminants with concentration levels exceeding Grade B; or untested product
Cadmium	3	85	
Chromium	400	3000	
Copper	200	4300	
Lead	200	840	
Mercury	1	57	
Molybdenum	4	7	
Nickel	60	420	
Selenium	3	100	
Zinc	250	7500	

The Hamilton wastewater treatment (WWTP) plant located at Pukete has a C grade solid sludge due to high arsenic concentrations. The arsenic is removed from raw water from the Waikato River at the Hamilton drinking water plant. The water treatment plant sludge is sent to the wastewater treatment plant.

At 425 km long, the Waikato River (Fig. 1-1) is New Zealand`s longest and most significant river. The Waikato River drains a total catchment area of 14,260 km^2 or 12 % of the total area of the North Island of New Zealand with more than 300,000 people living within its catchment (Waikato Regional Council, 2008; Wilson and Webster-Brown, 2009). The river originates from the central North Island volcanic zone, flows into Lake Taupo and cuts through the volcanic plateau flowing north, passing through eight major hydroelectric dams capable of generating 1,450 MW of electricity before emptying into the Tasman Sea (Waikato Regional Council, 2008). In addition to geothermal activities that lie at the banks of the Waikato River, at least 12 sewage treatment plants discharge into the river alongside discharges from intensive dairying and from major industries. The Waikato River is a source of drinking water to more than 30 communities, including Hamilton, a major city of more than 150,000 people (McLaren and Kim, 1995).

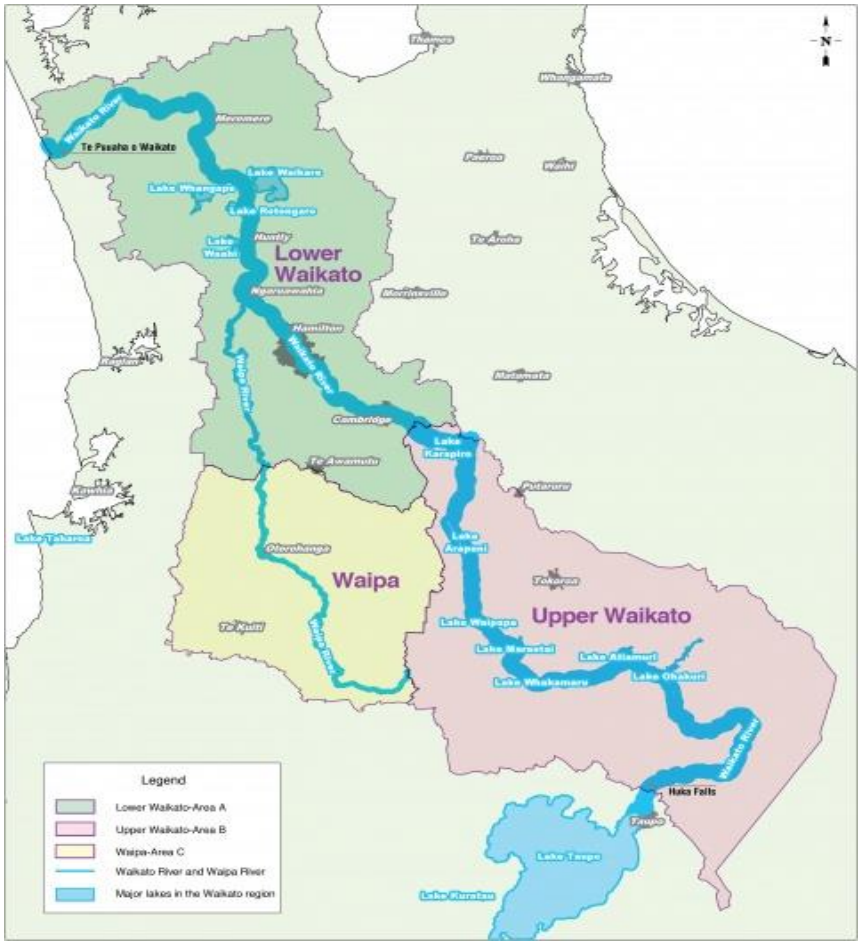

Figure 1-1: The Waikato River (Waikato River Authority, 2016).

The Hamilton water treatment plant (WTP) processes around 106,000 m^3/day of water from the Waikato River. Table 1-3 shows the summary data of Hamilton WTP alum sludge composition.

Table 1-3: Summary data of Hamilton water treatment plant alum sludge composition (Hamilton City Council).

Parameter Name	Results (Average)
Treated water production (m^3/day)	106,000
Sludge to wastewater treatment plant (m^3/day)	371
Total suspended solids in sludge (kg/day)	924
Arsenic in sludge (kg/day)	0.94
Aluminium in sludge (kg/day)	118.80
Mercury in sludge (kg/day)	0.0008
Lead in sludge (kg/day)	0.0032
Zinc in sludge (kg/day)	0.0224
Nickel in sludge (kg/day)	0.0041
Copper in sludge (kg/day)	0.0235
Cadmium in sludge (kg/day)	0.0004
Chromium in sludge (kg/day)	0.0056

Hamilton WWTP processes an average of 40,000 m^3/day of wastewater (including sludge from the WTP) and produces 14.3 tonnes (wet)/ day of biosolids. The wet biosolids produced contain 22.2 % solids thereby producing 3.17 tonnes (dry)/day of biosolids. Currently, the sludge from Hamilton WWTP is sent to Tokoroa for vermicasting with waste wood chips/pulp from the Kinleith pulp and paper mill (now called OJI Fibre Solutions – formerly Carter Holt Harvey).

From Table 1-4, the WTP produces about 0.94 kg/day arsenic which contributes most of the arsenic found in the biosolids at the WWTP (112.6 mg/kg) dry biosolids – the upper limit for B grade sludge is 30 mg/kg dry), causing it to be a grade C biosolid (unsuitable for reuse).

Table 1-4: Metals composition of Pukete wastewater treatment plant sludge (Hamilton City Council).

Metal	Concentration (mg recoverable/kg dry)	A grade (mg recoverable/kg dry)	B grade (mg recoverable/kg dry)	From WWTP (kg/day)	From WTP (kg/day)
Aluminium	41465.5	No limit	No limit	131.636	118.800
Arsenic	112.6	20	30	0.357	0.942
Cadmium	0.9	1	10	0.003	0.000
Chromium	152.6	600	1500	0.484	0.006
Copper	261.3	100	1250	0.830	0.024
Lead	28.8	300	300	0.091	0.003
Lithium	3.5	No limit	No limit	0.011	NA
Mercury	1.4	1	7.5	0.004	0.001
Nickel	42.8	60	135	0.136	0.004
Zinc	517.8	300	1500	1.644	0.022

NA = Not available

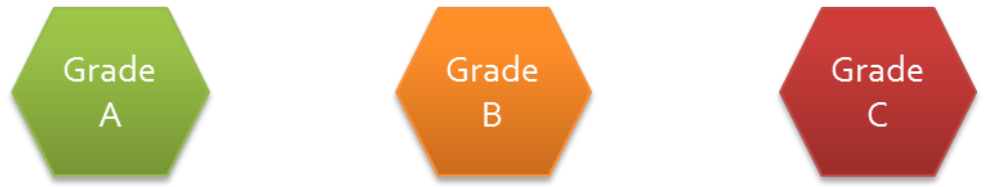

Unrestricted application

Suitable for disposal as landscape enhancement material and for addition to soil used for forestry and rehabilitation

Suitable for disposal at landfills

1.2 Research Objectives

Faced with more and more stringent regulations nowadays, removal of heavy metals from water/wastewater to protect people and the environment is a priority. Several techniques, both conventional and advanced are being used to remove these contaminants from drinking water. Therefore the aim of this research is to investigate selectively removing arsenic from raw water to reduce heavy metal content in the water treatment sludge so that arsenic content in the subsequent biosolids at the waste water treatment plant can at least achieve B grade and thus find reuse application in agriculture. One promising approach is catalytic media for metals adsorption. DMI-65 is a manganese coated silica media that is used in water

treatment for manganese and iron removal ("Quantum Filtration Medium," 2019). It is activated using chlorine as an oxidant, and it catalyses the oxidation of manganese from +4 to +7 oxidation states and iron from +2 to +3 oxidation states after which these ions precipitate out and are removed by filtration or clarification. DMI-65 should also be effective for arsenic removal as a result of bonding with iron complex formed during oxidation and precipitation process. DMI-65 has been used by OPUS (WSP) for removing iron and manganese from Waikeria Prison, New Zeland which has high Mn and Fe. It was therefore recommended by OPUS (WSP) to evaluate its use for arsenic removal.

DMI-65 has the following advantages listed below:

- Stable and satisfactory performance over wide pH range.
- Long life span (5 – 10) years.
- Regeneration is not required after initial activation.
- Reaction is rapid.

The main disadvatages of DMI-65 includes:

- Cost – currently $10/kg.
- Disposal cost after end of life.

A review of the literature has found that there is no literature on the use of DMI-65 or other catalytic media for arsenic removal. Likewise, no study has been conducted to to successfully separate arsenic from other contaminants in a contaminated drinking water. In addition, there is no evidence from literature which looked at effect of competing anions on arsenic removal in a coagulation/flocculation/dissolved air flotation process.

The aim of this research is to evaluate DMI-65 for arsenic removal and its potential for use in the treatment of Waikato river water. The specific research objectives of this thesis are:

1. Evaluate the kinetic, adsorption isotherms and thermodynamic properties of DMI-65 for removing arsenic under varying experimental condition (batch and fixed bed column study)

2. Establish the effect of competing anions on arsenic removal in a batch coagulation/flocculation/dissolved air flotation (C/F/DAF) process at different ionic strengths.
3. Examine the fate of arsenic by comparing the removal percentage in a coagulation/flocculation/dissolved air flotation (C/F/DAF) and conventional sedimentation process using Polydiallyldimethylammonium chloride (polyDADMAC) and Chitosan from crab shell.
4. Investigate separation of arsenic from contaminated raw water in a C/F/DAF process using polyaluminium chloride (PAC).

1.3 Thesis framework

Chapter 1:

Outlines the objectives, experimental approach and organization of this thesis.

Chapter 2:

This chapter provides background information on heavy metal contamination in drinking water, sources of contamination and health effects resulting from these contaminants. Arsenic contamination of Waikato River and ground water is addressed. Arsenic chemistry and health effects of arsenic exposure on various organ on the human body are discussed. An overview of the treatment technologies (conventional and advanced) used for arsenic removal, as well as the advantages, disadvantages and removal efficiencies of each are covered in detail.

Chapter 3:

This chapter presents results of experiments that evaluate the chemical and physical properties of DMI-65 using X-ray fluorescence (XRF), X-ray diffraction (XRD), Fourier transform infrared (FTIR), Scanning electron microscope (SEM), Brunauer-Emmett-Teller (BET) and particle size distribution before and after activation. The effects of pH on As (III) and As (V) were investigated. Different kinetic models were applied to determine the kinetic data for As (III) and As (V) adsorption and to select the most suitable model. The models applied are the pseudo-first order, pseudo-second and Elovich kinetic models.

An adsorption isotherm study was conducted to evaluate the interaction between As (III) and As (V) on DMI-65 at different pH values (5, 6, 7, and 8.5). The models used for determining DMI-65 adsorption capacity are Langmuir, Freundlich, Langmuir-Freundlich (L-F) and Dubinin-Radushkevich (D-R). Thermodynamics studies were conducted to determine adsorption capacity, Gibbs free energy, enthalpy, and entropy at different temperatures (283 K, 288 K, 293 K and 298 K) for both As (III) and As (V). Lastly, regeneration studies were carried out to determine the reusability of DMI-65 in removing As (III) and As (V).

Chapter 4:

This chapter presents results that investigate the performance of a fixed bed column in removing arsenic from contaminated raw water in terms of the breakthrough curve. In this study, the effect of flowrate (10 mL/min, 12.5 mL/min and 20 mL/min) and pH (5, 7 and 9) on the performance of DMI-65 was carried out. The following adsorption models were used in predicting the breakthrough curve of the effluent namely: Thomas model, Yoon-Nelson model, Adams-Bohart model and Clark model. Lastly, a nonlinear regression analysis was used in performing error analysis.

Chapter 5:

This chapter presents results of experiments that compare arsenic, UV_{254nm} and turbidity removal from contaminated drinking water between dissolved air flotation (DAF) and sedimentation processes. Impact of pH and coagulant dose were equally investigated. Bench jar tests were conducted using polyDADMAC (2.0, 2.2, 2.4, 2.6 and 3 mg/L) and Chitosan from crab shell (0.2, 0.4, 0.6, 0.8 and 1.0 mg/L) and at various pH levels (4, 5, 6, 7, 8 and 9). Other operating conditions are rapid mixing (100 rpm, G value = 60 s^{-1}), slow mixing (30 rpm, G value = 10 s^{-1}), setting time and flotation time (10 min) and a saturated pressure of 4 bar.

Chapter 6:

This chapter presents the results of an investigation of the effect of competing anions on arsenic removal from a contaminated drinking water using a batch DAF process. PAC was used as a coagulant (concentration = 23.5 mg/L) at different pH levels (5, 6, 7, 8 and 9). The anions investigated are sulfate (SO_4^{2-}), nitrate (NO_3^-), carbonate (CO_3^{2-}) and phosphate ($H_2PO_4^-$). The effect of three concentration levels

(1, 5 and 10 mM) for each competing anion was studied with flotation time (10 min), saturated pressure (4 bar), rapid mixing (100 rpm) and slow mixing (30 rpm).

Chapter 7:

This chapter investigates the effect of coagulant (PAC) dose (2.35, 4.70, 9.40, 14.10 and 18.80 mg/L), pH (5, 6, 7, 8 and 9), flotation time (10, 20 and 30 min), phosphate concentration (0.5 mM, 2.5 mM and 10 mM) and saturated pressure (2, 3 and 4 bar) on separating arsenic from contaminated raw water. The efficiency of the treatment/separation process was evaluated by measuring arsenic, UV_{254nm} and turbidity before and after treatment. Modification to the current Hamilton water treatment plant is also suggested including the cost analysis.

Chapter 8:

This chapter summarizes the results in this thesis and then concludes with overall recommendations for future work in separating arsenic from other contaminants in drinking water.

References

Ali, M.M., Ali, M.L., Islam, M.S., Rahman, M.Z., 2016. Preliminary assessment of heavy metals in water and sediment of Karnaphuli River, Bangladesh. Environ. Nanotechnol. Monit. Manag. 5, 27–35. https://doi.org/10.1016/j.enmm.2016.01.002

Babel, S., del Mundo Dacera, D., 2006. Heavy metal removal from contaminated sludge for land application: A review. Waste Manag. 26, 988–1004. https://doi.org/10.1016/j.wasman.2005.09.017

Barbee, J.Y., Prince, T.S., 1999. Acute respiratory distress syndrome in a welder exposed to metal fumes. South. Med. J. 92, 510–512.

Dieter, H.H., Bayer, T.A., Multhaup, G., 2005. Environmental Copper and Manganese in the Pathophysiology of Neurologic Diseases (Alzheimer's Disease and Manganism). Acta Hydrochim. Hydrobiol. 33, 72–78. https://doi.org/10.1002/aheh.200400556

Dutta, S., 2002. Environmental Treatment Technologies for Hazardous and Medical Waste (Remedial Scope and Efficacy). Tata McGraw-Hill, New Delhi, India.

DWSNZ, 2008. Drinking-water Standards for New Zealand.

Fu, F., Wang, Q., 2011. Removal of heavy metal ions from wastewaters: A review. J. Environ. Manage. 92, 407–418. https://doi.org/10.1016/j.jenvman.2010.11.011

Ihsanullah, Abbas, A., Al-Amer, A.M., Laoui, T., Al-Marri, M.J., Nasser, M.S., Khraisheh, M., Atieh, M.A., 2016. Heavy metal removal from aqueous solution by advanced carbon nanotubes: Critical review of adsorption applications. Sep. Purif. Technol. 157, 141–161. https://doi.org/10.1016/j.seppur.2015.11.039

Jadhav, S.V., Bringas, E., Yadav, G.D., Rathod, V.K., Ortiz, I., Marathe, K.V., 2015. Arsenic and fluoride contaminated groundwaters: A review of current technologies for contaminants removal. J. Environ. Manage. 162, 306–325. https://doi.org/10.1016/j.jenvman.2015.07.020

Järup, L., 2003. Hazards of heavy metal contamination. Br. Med. Bull. 68, 167–182.

Jarup, L., Hellstrom, L., Alfven, T., Carlsson, M., Grubb, A., Persson, B., Pettersson, C., Spang, G., Schutz, A., Elinder, C., 2000. Low level exposure to cadmium and early kidney damage: the OSCAR study. Occup. Environ. Med. 57, 668–672. https://doi.org/10.1136/oem.57.10.668

Lue-Hing, C., Zenz, D.R., Kuchenrither, R., Manila, J., sawyer, B., 1998. Municipal sewage sludge management: a reference text on processing, 2nd edition. ed, Utilization and Disposal. Technomic Publishing CO, USA.

McLaren, S.J., Kim, N.D., 1995. Evidence for a seasonal fluctuation of arsenic in New Zealand's longest river and the effect of treatment on concentrations in drinking water. Environ. Pollut. 90, 67–73. https://doi.org/10.1016/0269-7491(94)00092-R

Mortada, W.I., Sobh, M.A., El-Defrawy, M.M., Farahat, S.E., 2001. Study of lead exposure from automobile exhaust as a risk for nephrotoxicity among traffic policemen. Am. J. Nephrol. 21, 274–279. https://doi.org/46261

Nathan Oyaro, O.J., 2007. The contents of Pb, Cu, Zn and Cd in meat in Nairobi, Kenya. J. Food Agric. Environ. 5.

Ogilvie, D., 1998. National Study of the Composition of Sewage Sludge.

Paulino, A.T., Minasse, F.A.S., Guilherme, M.R., Reis, A.V., Muniz, E.C., Nozaki, J., 2006. Novel adsorbent based on silkworm chrysalides for removal of heavy metals from wastewaters. J. Colloid Interface Sci. 301, 479–487. https://doi.org/10.1016/j.jcis.2006.05.032

Quantum Filtration Medium, 2019.

Robert, G., Mari, G., 2003. Human Health effects of Metals, US Environmental Protection Agency Risk Assessment Forum. Wash. DC.

Sharma, V.K., Sohn, M., 2009. Aquatic arsenic: Toxicity, speciation, transformations, and remediation. Environ. Int. 35, 743–759. https://doi.org/10.1016/j.envint.2009.01.005

Srivastava, N.K., Majumder, C.B., 2008. Novel biofiltration methods for the treatment of heavy metals from industrial wastewater. J. Hazard. Mater. 151, 1–8. https://doi.org/10.1016/j.jhazmat.2007.09.101

Steenland, K., Boffetta, P., 2000. Lead and Cancer in humans: where are we now ? Am J Ind Med 38, 295–299.

Strachan, S., 2010. Heavy metal. Curr Anaesth Crit Care 21, 44–48.

U.S.EPA, 2016. U.S. Environmental Agency, Drinking Water Contaminants.

Villaescusa, I., Bollinger, J.-C., 2008. Arsenic in drinking water: sources, occurence and health effects (a review). Rev Env. Sci Biotechnol 7, 307–323.

Waikato Regional Council, 2008. The health of the Waikato River and Catchment.

Waikato River Authority, 2016. . Waikato, New Zealand.

Wasserman, G.A., Liu, X., Parvez, F., Ahsan, H., Levy, D., Factor-Litvak, P., Kline, J., van Geen, A., Slavkovich, V., LoIacono, N.J., Cheng, Z., Zheng, Y., Graziano, J.H., 2006. Water manganese exposure and children's intellectual function in Araihazar, Bangladesh. Environ. Health Perspect. 114, 124–129.

WHO, 2011. Guidelines for drinking water quality, fourth edition.

Wilson, N., Webster-Brown, J., 2009. The fate of antimony in a major lowland river system, the Waikato River, New Zealand. Appl. Geochem., Geochemistry and Mineralogy of Metalliferous Minewastes: An Issue in Honor of John Jambor 24, 2283–2292. https://doi.org/10.1016/j.apgeochem.2009.09.016

CHAPTER TWO

Literature Review

2.1 Introduction

Water scarcity and water pollution are major global issues. Rapid population growth and the consequent increase in anthropogenic activities have resulted in high demand for scarce water resources, generation of large volumes of water requiring treatment, and various types of physico-chemical contaminants and pathogens in surface and groundwater sources (Bektaş and Kara, 2004; Can et al., 2010; Fu and Wang, 2011; Pichel et al., 2019). According to the World Health Organization (WHO), two billion people globally use a drinking water source contaminated with faeces.

Heavy metals (HMs) contamination is a subject of continuous interest within the scientific community, due to the toxic effect on the entire biosphere (atmosphere, hydrosphere, lithosphere and pedosphere) (Morselli et al., 2003; Varol, 2011). Some heavy metals such as Copper (Cu), Colbalt (Co), and Zinc (Zn) are required for normal body growth and functions of living organisms, while the high concentrations of other metals like Cadmium (Cd), Chromium (Cr), Manganese (Mn), and Lead (Pb) are considered highly toxic for human and aquatic life (Ouyang et al., 2002). A specific amount of Cr is needed for normal body functions; while its high concentrations may cause toxicity, including liver and kidney problems and genotoxic carcinogen (Knight et al., 1997; Loubières et al., 1999). Like Cr, Co is also one of the required metals and needed for normal body functions as a metal component of vitamin B_{12}. However high intake of Co via consumption of contaminated food and water can cause abnormal thyroid artery, polycythemia, over-production of red blood cells (RBCs) and right coronary artery problems (Muhammad et al., 2011). Generally, high concentrations of Mn and Cu in drinking water can cause mental diseases such as Alzheimer's and Manganism (Dieter et al., 2005). According to (Wasserman et al., 2006) high Mn contamination in drinking water also affects the intellectual functions of 10 year old children. Pb is also a highly toxic and carcinogenic metal and may cause chronic health risks, including headache, irritability, abdominal pain, nerve damage, kidney damage, blood pressure, lung cancer, stomach cancer and gliomas (Järup, 2003; Mortada et al., 2001). As children are most susceptible to Pb toxicity, their exposure to high levels of Pb cause severe health complexities such as behavioural disturbances, memory deterioration and reduced ability to understand, while long term Pb exposure may

lead to anaemia (Järup, 2003). Like other HM, sufficient amount of Zn is also important for normal body functions. Its deficiency can lead to poor wound healing, reduced work capacity of respiratory muscles, immune dysfunction, anorexia, diarrhoea, hair loss, dermatitis and depression. Cd exposure can cause both chronic and acute health effects in living organisms (Barbee and Prince, 1999).

2.2 Heavy metals in drinking water

2.2.1 Arsenic

Arsenic (atomic number 33) is ubiquitous and ranks 20th in natural abundance, comprising about 0.00005 % of the earth's crust, 14th in the seawater, and 12th in the human body (Mandal and Suzuki, 2002). Contamination of the environment with arsenic from both natural and anthropogenic sources is widespread, occurs in many parts of the world and may be regarded as a global issue (Zaw and Emett, 2002).

More than 100 million people are reported to be at risk. The US Environmental Protection Agency (EPA) also had to reduce the permissible values of arsenic in drinking water from 50 to 10 µg L^{-1} in the light of its carcinogenic nature and its connection with liver, lung and kidney diseases and other dermal effect (Krishna et al., 2001).

Arsenic exists in the -3, 0, +3, and +5 oxidation states. Environmental forms include arsenious acids (H_3AsO_3, H_3AsO_3, $H_3AsO_3^{2-}$), arsenic acids (H_3AsO_4, $H_3AsO_4^{-}$, $H_3AsO_4^{2-}$), arsenites, arsenates, methylarsenic acid, dimethylarsinic acid, arsine, etc. Arsenic (III) is a hard acid and preferentially complexes with oxides and nitrogen. Conversely, arsenic (V) behaves like a soft acid, forming complexes with sulphides (Mohan and Pittman Jr., 2007). Inorganic forms of arsenic most often exist in water supplies. Arsenic is uniquely sensitive to mobilization (pH 6.5 – 8.5) and under both oxidizing and reducing conditions among heavy metalloids. Two forms are common in natural waters: arsenite (AsO_3^{3-}) and arsenate (AsO_4^{3-}), referred to as arsenic (III) and arsenic (V). Pentavalent (+5) or arsenate species are AsO_4^{3-}, $HAsO_4^{2-}$ and H_2AsO^{4-} while trivalent (+3) or arsenites include $As(OH)_3$, $As(OH)_4^{-}$, AsO_2OH^{2-} and AsO_3^{3-}. Pentavalent species predominate and are stable in oxygen rich aerobic environment. Trivalent arsenites predominate in moderately reducing anaerobic environments such as groundwater (Mohan and Pittman Jr., 2007).

2.2.2 Chromium

Chromium is a metal found in natural deposits as ores containing other elements such as ferric chromite ($FeCr_2O_4$), crocoite ($PbCrO_4$), and chrome ochre (Cr_2O_3). Chromium is considered one of the earth crust`s most abundant elements and it is estimated to be the sixth most abundant transition metal (Mohan and Pittman Jr., 2006). It is a known highly toxic metal in drinking water. Chromium is naturally found in different oxidation states ranging from +2, +3 and +6 with the trivalent Cr (III) and hexavalent Cr (VI) being the most stable forms in nature. The redox potential Eh-pH diagram (Fig. 2-1) presents equilibrium data and indicates the different oxidation states and chemical forms which exist within specified Eh and pH ranges. Cr (III) is much less toxic than Cr (VI) and it is an essential element in human bodies (Ihsanullah et al., 2016). Cr (VI) is extremely toxic and found in various industrial waters and can cause severe diarrhoea, vomiting, pulmonary congestions, liver and kidney damage (Hu et al., 2009; Mohan et al., 2006). Chromium is used in textile industries, electroplating, leather tanning, metal finishing, and chromate preparation (Ihsanullah et al., 2016). Therefore, the main source of chromium contamination of drinking water is industrial discharge to the environment. Cr (VI) is present mainly in the form of dichromate ($Cr_2O_7^{2-}$) and chromate (CrO_4^{2-}) ions. Depending on solution pH (Fig. 2-2), Cr (VI) can exist in water as dichromate ($Cr_2O_7^{2-}$) ions, chromate ion (CrO_4^{2-}), hydrogen chromate ion ($HCrO^{4-}$) and chromic acid (H_2CrO_4) (Liu et al., 2011).

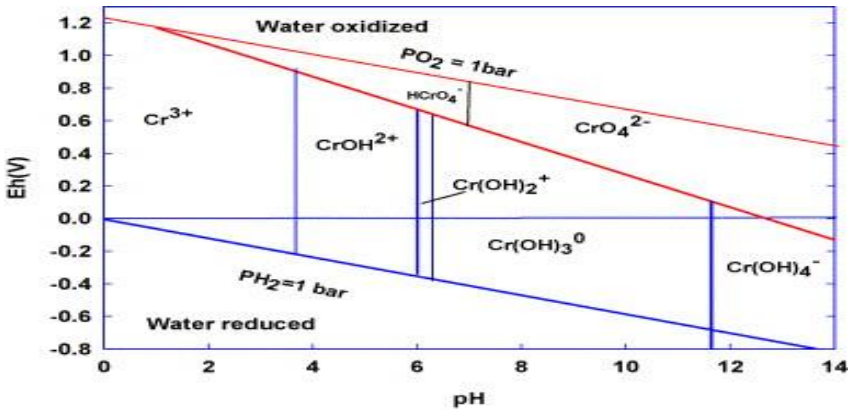

Figure 2-1: Eh-pH diagram for chromium (Radovic et al., 2000).

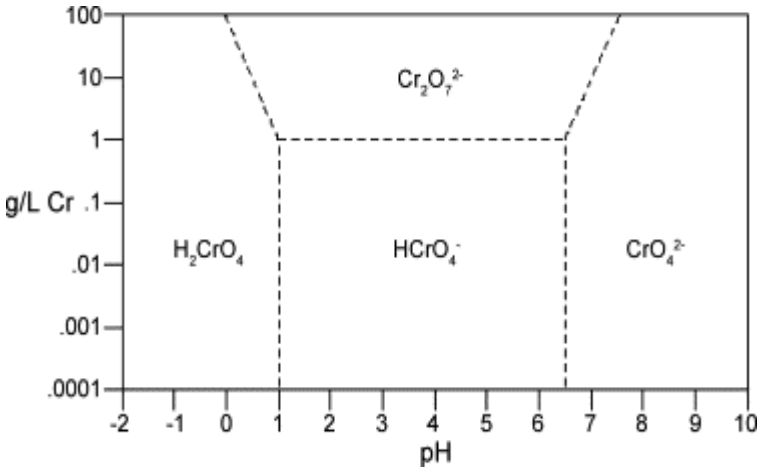

Figure 2-2: Speciation diagram of Cr (VI) (Dionex, 1996).

2.2.3 Cadmium

Cadmium is a heavy metal found in natural deposits containing other elements. It is highly toxic and considered as one of major priority to eliminate in drinking water. Cadmium is found to accumulate primarily in the kidney and has a relatively long biological half-life in human bodies of 10 - 35 years (Ihsanullah et al., 2015). As a drinking water pollutant, the kidney is the main target organ for cadmium toxicity.

Cadmium is used mainly in steel and plastic industries. Therefore, the potential sources of cadmium contamination in drinking water are the industrial wastewater discharges to the environment. Other industrial sources of cadmium contamination include cooling tower blow down, electroplating, metal plating and coating operations, etc. Cadmium is also used in nickel-cadmium batteries, in Cd-Te thin film solar cells and in pigments. One major source of non-industrial contamination in drinking water is impurities in the zinc of galvanized pipes and some metal fittings (Li et al., 2004).

2.2.4 Mercury

Mercury biodegradability and toxicity is known to cause serious damage to the environment and human health. Being an element, mercury cannot be degraded and broken down into harmless substances. Methyl mercury is an inorganic form of mercury and it is the most toxic and readily available (Ihsanullah et al., 2016). Volcanoes are responsible for most mercury contamination of the environment and from industrial activities such as in coal fired plants, non-ferrous metal production,

cement production and from municipal and hazardous waste. The toxic effect of mercury includes damage to the brain, respiratory systems, kidney and cardiovascular system (Bonzongo et al., 1996; Ihsanullah et al., 2016).

2.2.5 Nickel

Industrial applications of nickel include the production of alloys, battery manufacturing, printing, zinc base casting, and electroplating. Nickel exceeding the maximum allowable limit can cause lung cancer, chest pain, kidney problems, dry cough, shortness of breath and nausea. The main source of nickel pollution of drinking water include processes involved in battery manufacturing, production of alloys and electroplating (Ihsanullah et al., 2016; Yang et al., 2009).

2.2.6 Zinc

Zinc is a trace element and very important in regulating many biochemical processes and physiological functions of living tissue. However, excess of zinc in the body can result in serious health problems such as skin irritation, vomiting, stomach nausea, and cramps (Fu and Wang, 2011). Zinc has a number of applications in brass plating, steel works with galvanising lines, zinc-manganese batteries, household electrical appliances, zinc and brass works and these can be released into the environment from agricultural activities, industrial wastewaters, sediment remobilization or entrainment or a combination of these sources (Deliyanni et al., 2007; Ihsanullah et al., 2016).

2.2.7 Lead

Lead is a poisonous heavy metal that affects humans and animals if ingested or inhaled. The major source of lead accumulation in the body is through drinking water. It can enter the body via the lungs and digestive systems and the blood spreads it to other parts of the body. Lead in drinking water can cause damage to the kidney and liver, can cause anaemia and headache, and also damage the central nervous system (Fu and Wang, 2011; Ihsanullah et al., 2016; Srivastava and Majumder, 2008). Major applications include production of batteries, pigments, paint manufacturing and textile dyeing.

2.2.8 Copper

Copper plays an important role in animal metabolism but excessive ingestion can result in vomiting, cramps, convulsions, kidney and liver damage (Paulino et al., 2006). Copper has a number of applications in semiconductors, electronic chips, catalysts, and thus can be released into the environment through various sources such as mining of copper and from factories that use metallic copper or copper compounds (Bertinato and L'Abbé, 2004; Fu and Wang, 2011).

2.3 Chemistry of Arsenic

Arsenic (atomic number 33; atomic mass 74.921) is a group 15 element on the periodic table along with nitrogen, phosphorus, antimony and bismuth. It is the 20th most abundant element in the world, thereby accounting for about 0.00005 % of the earth crust, 14th in the seawater and 12th in the human body (Mandal and Suzuki, 2002). It is a silver-grey brittle crystalline solid with atomic weight 74.9, specific gravity 5.73, melting point 817 ^{o}C (at 28 atm), boiling point 613 ^{o}C and vapour pressure 1 mm Hg at 372 ^{o}C (Mohan and Pittman Jr., 2007). Arsenic – 75 (^{75}As) is the only nonradioactive and naturally occurring isotope of arsenic while ^{73}As has the longest half-life, which is 80.3 days. The elemental form of arsenic, A^0 has electron configuration of $1s^2 2s^2 2p63s^2 3p^6 3d^{10} 4s^2 4p^3$ (Henke, 2009).

Arsenic species are present in water due to various physical, chemical and biogeochemical processes such as precipitation/solubilisation, adsorption/desorption, oxido-reduction and microbiological processes (Issa et al., 2011a; Jovanovic et al., 2011; Lièvremont et al., 2009). Arsenic exists in -3, 0, +3 and +5 oxidation states but is mostly common in natural waters as +3 and +5 (Mohan and Pittman Jr., 2007). As^{3+} and As^{5+} usually form bonds with oxygen to form inorganic arsenite (As (III)) and arsenate (As (V)) respectively. As (III) is predominantly common in low-oxygen environments such as groundwaters and hydrothermal waters. Depending on pH (Fig. 2-3), As (III) may mainly exist as $H_3AsO_3^0$, $H_2AsO_3^-$, $HAsO_3^{2-}$ and AsO_3^{3-} and in sulfide-rich and anoxic waters, sulfur substitutes for one or more oxygen atoms to form thioarsenic species namely: $HAs_3S_6^{2-}$, $H_3As_3S_6^0$, $H_3AsO_3S^-$, and $H_2AsS_2O_2^-$ (Henke, 2009; Mohan and Pittman Jr., 2007). Depending on pH, As (V) is more dominant in oxidizing environments such as surface waters and typically occurs as $H_3AsO_{4,}^0$ $H_2AsO_4^-$, $HAsO_4^{2-}$, and AsO_4^{3-} (Ansari and Sadegh, 2007; Asmel et al., 2017; Vojoudi et al., 2017).

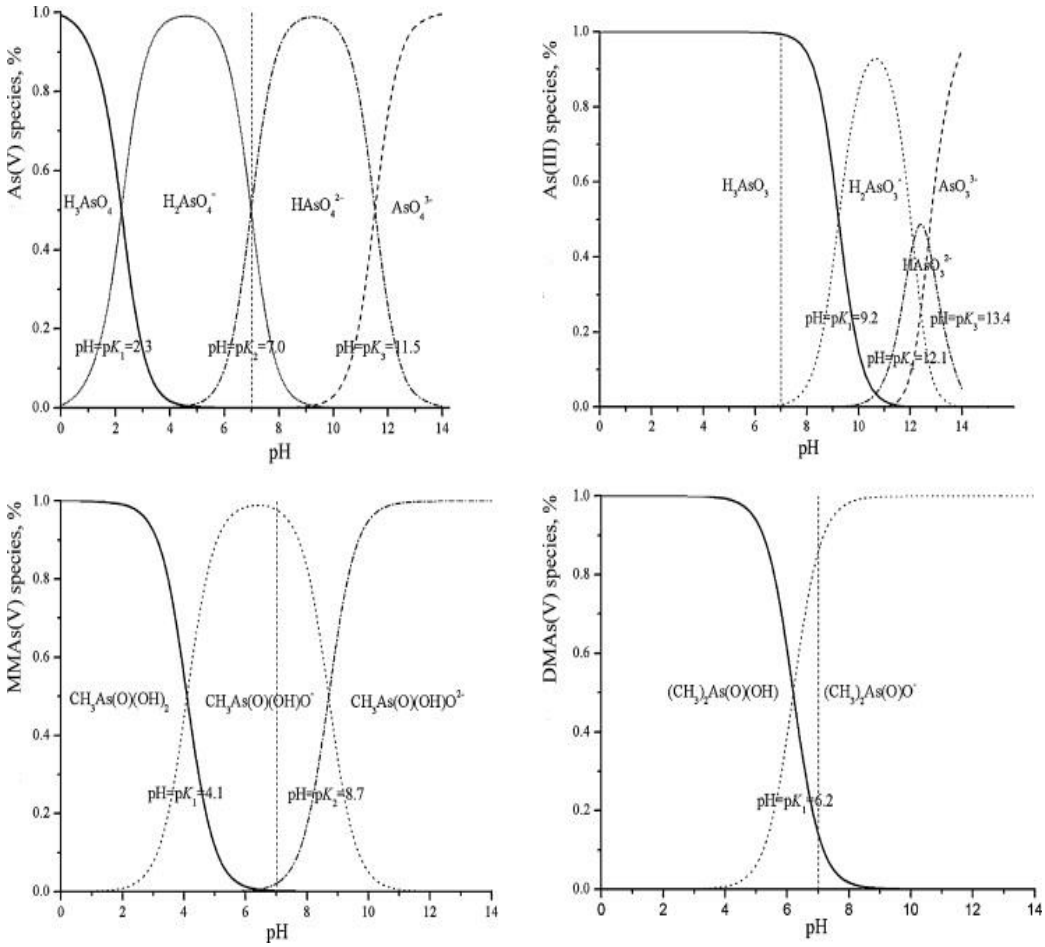

Figure 2-3: The distribution of inorganic arsenic and organic arsenic species as a function of pH values of water (Issa et al., 2011b).

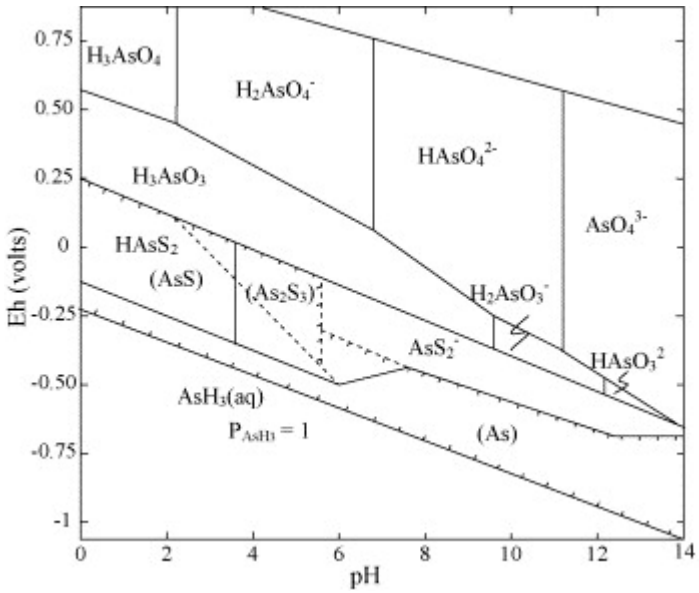

Figure 2-4: The Eh-pH diagram for arsenic at 25ºC and 101.3 kPa (Wang and Mulligan, 2006) .

Arsenic speciation is controlled by redox potential (Eh) and pH. From Fig. 2-4, $H_2AsO_4^-$ dominates at low pH (less than pH 6.9), $HAsO_4^{2-}$ at higher pH, $H_3AsO_{4,}^0$ in strong acid conditions and AsO_4^{3-} present in strong base conditions (Mohan and Pittman Jr., 2007). Successive acid dissociation constants (pK_a) values of As (III) at 25 ^oC are 9.2, 12.1 and 13.4 whereas for As (V), pK_a values are 2.3, 7.0 and 11.5. For the organoarsenicals, pK_a values for MMA (V) are 4.1 and 8.7 and for DMA (V), pKa value of 6.2 exists as neutral species (Issa et al., 2010; Rahman et al., 2011; Xiong et al., 2008). Deprotonation of arsenious acid (H_3AsO_3) and arsenic (H_3AsO_4) in terms of pK_a is shown in Fig. 2-5.

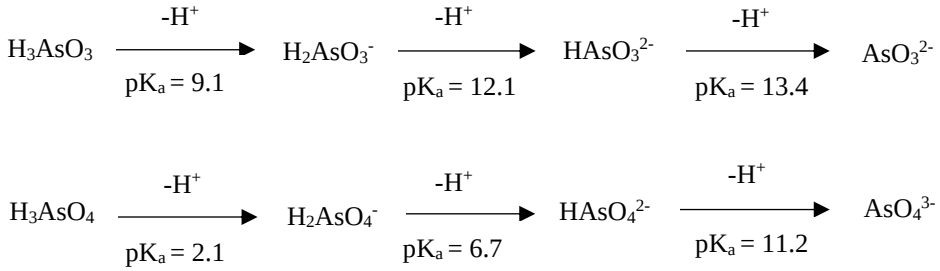

Figure 2-5: Dissociation of As (V) (Mohan and Pittman Jr, 2007) .

Arsenic bearing organic and inorganic chemicals with boiling points below 150 ^oC at atmospheric pressure are known as volatile arsenic compounds. Volatile arsenic compounds include: arsine (AsH_3), As (III) chloride ($AsCl_3$), As (III) fluoride (A_3F_3), As (V) fluoride (AsF_5), monomethylarsonous acid (MMA(III), $(CH_3)As(OH)_2$), dimethylarsinous acid (DMA(III), $(CH_3)_2As(OH)$), trimethylarsine $(CH_3)_3As$), and trimethylarsine oxide ($(CH_3)_3AsO$) (Henke, 2009). Arsenic can also exist in organic form (containing arsenic – carbon bonds) known as organoarsenic. Organic forms of arsenic found in natural waters are monomethylarsonic acid (MMA (V)) and dimethylarsinic acid (DMA (V)). Other more complex organoarsenicals found mostly in tissues of marine biota include arsenobetaine, AB and arsenosugars (Fig. 2-6). Many organisms contains arsenic in the form of As (III) attached to glutathione (GSH) compounds which serve as intracellular metal binding thiol ligands. Likewise, under metal stress, phytochelatins (PCs) which are groups of peptide, are usually found in plants (Nearing et al., 2014).

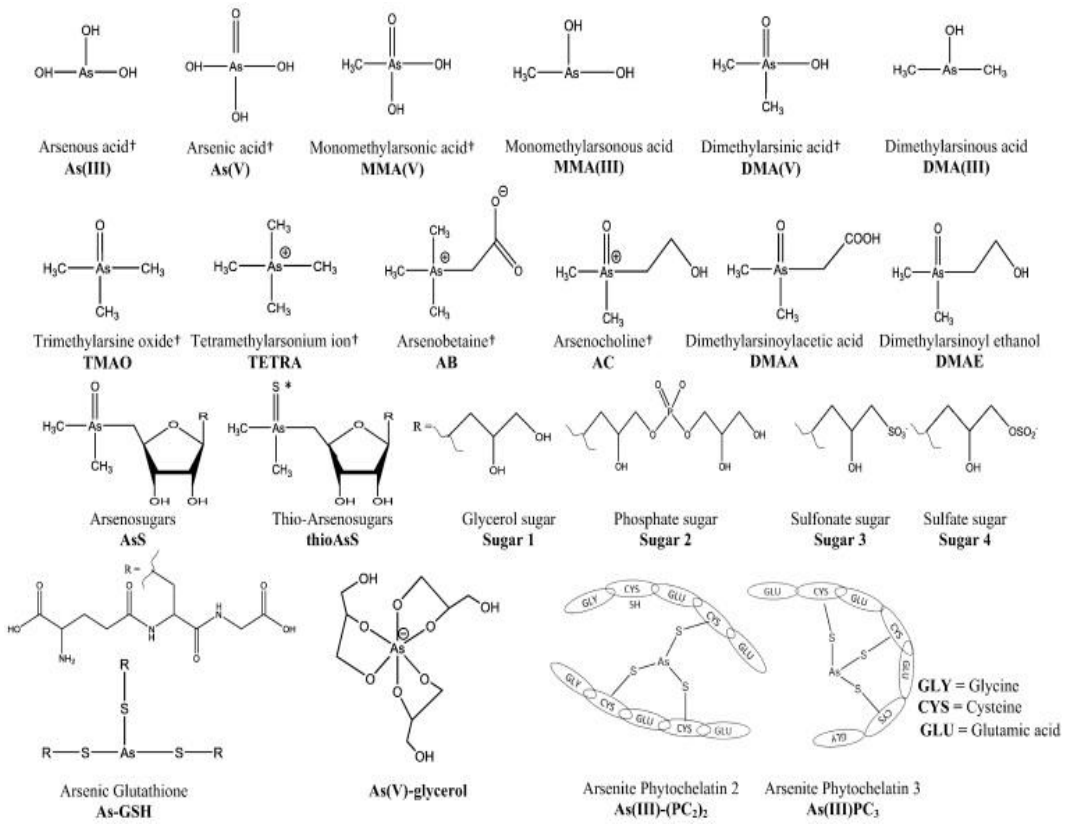

Figure 2-6: Structure and abbreviations for various arsenic compounds. * indicates where an oxygen (O) is replaced with a sulphur (S). + indicates arsenic compound is commercially available (Nearing et al., 2014).

2.4 Arsenic in Waikato River

The Waikato River is located in the North Island of New Zealand. It is the most utilized and longest river in New Zealand (425 km). The source of the water is from the volcanic region of central plateau, and thereafter flows through the largest lake in the country, Lake Taupo. It flows in a northward direction for 385 km passing through Tokoroa, Cambridge and Mercer. From there, the river flows westward for a further 40 km and discharges into the Tasman sea at Port Waikato (McLaren and Kim, 1995; Robinson et al., 1995). The Waikato River also passes through several geothermal fields (Wairakei, Broadlands, Orakei Korako and Atiamuri). The river supports eight hydroelectric power stations, two geothermal power stations (Wairakei and Ohaaki) and one thermal power station (Huntly) (McLaren and Kim, 1995; Robinson et al., 1995).

Table 2-1 shows the amount of arsenic input from different geothermal sources into the Waikato River. Arsenic is released into the Waikato River by natural fluid

discharges from both geothermal power stations. Reay (1973), Aggett and Aspell (1978) and Liddle (1982) are in total agreement with the above statement suggesting that the majority of arsenic originates from geothermal sources (natural and from geothermal power stations). McLaren (1994) said the occurrence of auriferous quartz lodged in the Hauraki goldfield is another source of arsenic contamination of the Waikato River.

Table 2-1: Estimates of arsenic inputs (tonnes/yr) into the Waikato River from geothermal area (Robinson et al., 1995)

Geothermal source	Input (tonnes/yr)
Lake Taupo	30
Wairakei field	22
Ohaaki pool	0.5
Orakei Korako	8 – 13
Waiotapu/Reporoa Valley	1 – 2
Total natural sources	61 – 67
Wairakei Power Station	190

From Fig. 2-7, the amount of arsenic was higher upstream compared to downstream in the Waikato River. Discharge of effluents containing high amounts of arsenic from geothermal power stations and geothermal springs themselves were the reasons for higher incidence upstream (Robinson et al., 1995). Robinson et al. (1995) suggested a few causes that contributed to the lowering of the amount of arsenic downstream in the Waikato River. This may be the result of precipitation of the arsenic into sediments of the dam and riverbed, removal of arsenic by biological activities, dilution by rain and lower arsenic tributaries to the Waikato. Webster-Brown and Lane (2005) identified the chemical forms of arsenic, mechanisms of arsenic retention and removal in the river system and seasonal changes in arsenic concentrations. It was discovered that the arsenic in the Waikato River is dominated by the pentavalent form of inorganic arsenic. The conversion of pentavalent form to trivalent form of arsenic usually occurs in summer months and likely it is more prevalent in the upper catchment area than the lower catchment area (Webster-Brown and Lane, 2005).

Figure 2-7: Arsenic in the Waikato River (Te Ara, New Zealand)

In the 1970s, arsenic was a major topic of interest with respect to the Waikato River and the environmental issues it posed as Auckland city looked into the possibility of it becoming a source of water. Aggett and Aspell (1980) researched the levels of arsenic in various water samples of the Waikato River including sediments, lake weeds and soils. They revealed that inorganic As (V) was the dominant form in the river although the presence of inorganic As (III) was quite significant. Meanwhile, the amount of arsenic in lake weeds varies from 0.1 to 1 mg/g mainly as arsenite and 0.15 to 1 mg/g arsenate in sediments. Additionally, 7 – 8 % of the arsenic entering the river system was being absorbed onto the sediments (Aggett and Aspell, 1980). The percentage of arsenic removed from the Hamilton water treatment plant increased from 80.6 % in 1993 – 1994 to 90.4 % in the year 2002 as shown in Table 2-2.

Table 2-2: Arsenic in the Waikato River and Hamilton drinking water treatment efficiency for 1993-1994 and 2002 (Waikato Regional Council).

Monitoring Year	**1993-1994[a]**	**2002[b]**
River concentration (µg/L)	32	23
Treated water concentration (µg/L)	6.2	2.2
Percent removal (%)	80.6	90.4

Groundwater samples from 302 sites (farms, schools, domestic and community supplies) spread across the Waikato region were analysed for arsenic concentrations by Environment Waikato (2006). Geometric mean and median groundwater depths were 4.42 m and 3.61 m respectively. From Table 2-3, it shows that across the Waikato region, 10 % of groundwater samples exceeded the PMAV of 10 µg/L. The figures showing sampling sites and concentrations of arsenic in Waikato groundwater samples can be seen in Appendix 2A.

Table 2-3: Percentage of groundwater samples exceeding 10 µg/L and 5 µg/L in the Waikato region (Waikato Regional Council).

Area	**Percent exceeding PMAV**	**Percent exceeding half PMAV**
Reporoa Basin	33 %	41 %
North eastern Taupo	12 %	28 %
Coromandel Peninsula	9 %	24 %
Rest of Waikato	2 %	7 %
Overall Waikato average	10 %	19 %

2.5 Arsenic exposure and health effects

Arsenic is a metalloid having several physical and chemical properties of metals and humans are exposed to it through natural and anthropogenic sources. Arsenic in the past and currently has found applications in the production of pesticides, wood preservatives, munitions, semiconductors, and anticancer agents. Arsenic contamination of natural waters have been reported in countries such as USA, New Zealand, Chile, Taiwan, Mexico, Poland, Canada, India, Bangladesh and China (Mohan and Pittman Jr., 2007). More than 200 million people (Table 2-4) worldwide might have been exposed to drinking water with arsenic concentrations above the recommended 10 µg/L (Naujokas Marisa F. et al., 2013).

Table 2-4: Arsenic exposure concerns worldwide reproduced from (Naujokas Marisa F. et al., 2013; Rahman et al., 2018).

Country	Estimated exposed population (millions)[a]	Arsenic concentration in drinking water (µg/L)
Argentina	2.0	<1 – 7550
Bangladesh	35 – 77	<10 to >2500
Chile	0.4	600 – 800
China	0.5 – 2.0	<50 – 4400
Ghana	<0.1	<2 – 175
India	>1.0	<10 to >800
Mexico	0.4	5 – 43
Taiwan	NA	<1 to > 3000
USA	>3.0	<1 to >3100
Vietnam	>3.0	<0.1 - 810

Note: NA = Not available; NRDC = National Resources Defence Council;

[a] estimated number of persons exposed to > 10 µg/L arsenic in drinking water.

In Bangladesh, between 35 and 77 million of its population are at risk of arsenic poisoning from contaminated drinking water (Rahman et al., 2018). According to a United Nations report in 2010, 1.8 % of Nepal's wells have arsenic contamination exceeding the Nepal standard of 50 µg/L and additional 5.6 % exceed WHO standard of 10 µg/L. According to Cable News Network (CNN, 2017), more than 10 million people in the state of Bihar are affected with arsenic poisoning from contaminated water. Likewise, in Pakistan, up to 60 million people living in Pakistan's Indus Plain are at risk of being affected by high levels of arsenic in the region's groundwater supply (CNN, 2017).

Arsenic ranked as the highest chemical on the current U.S. Agency for Toxic Substances and Disease Registry, 2017 (ATSDR) substance priority list (SPL) as shown in Appendix 2B. Arsenic has been defined as a Group 1 human carcinogen by International Agency for Research on Cancer (IARC) and they suggest that human body systems are exposed to potential harm (IARC, 2004). Humans are exposed to arsenic contamination from natural and anthropogenic sources. Fig. 2-8 shows the different pathways of arsenic exposure to humans, which include plant media (rice and vegetable, animal source foods, water, air and soil). Some of the crucial routes of arsenic entering the human body are inhalation, ingestion and skin absorption. Pentavalent and trivalent arsenic compounds are both absorbed from the gastrointestinal tract (Mohammed Abdul et al., 2015). The rate of sodium arsenate absorption is higher while that of inorganic tetravalent arsenic is lower. Meanwhile, lead arsenate and arsenic trisulfide have a low rate of oral absorption (Ueki et al., 2004). Inhalation of arsenic depends mostly on its molecular size. Sodium arsenate, sodium arsenite and arsenic trioxide rate of absorption through inhalation are higher than arsenic sulfide and lead arsenate. Trivalent compounds are more soluble in water and thus more toxic in nature than pentavalent compounds (Mohammed Abdul et al., 2015; Ueki et al., 2004). Arsenic distribution in the body is widely distributed in organs such as kidneys, lungs, liver and skin (Hong et al., 2014).

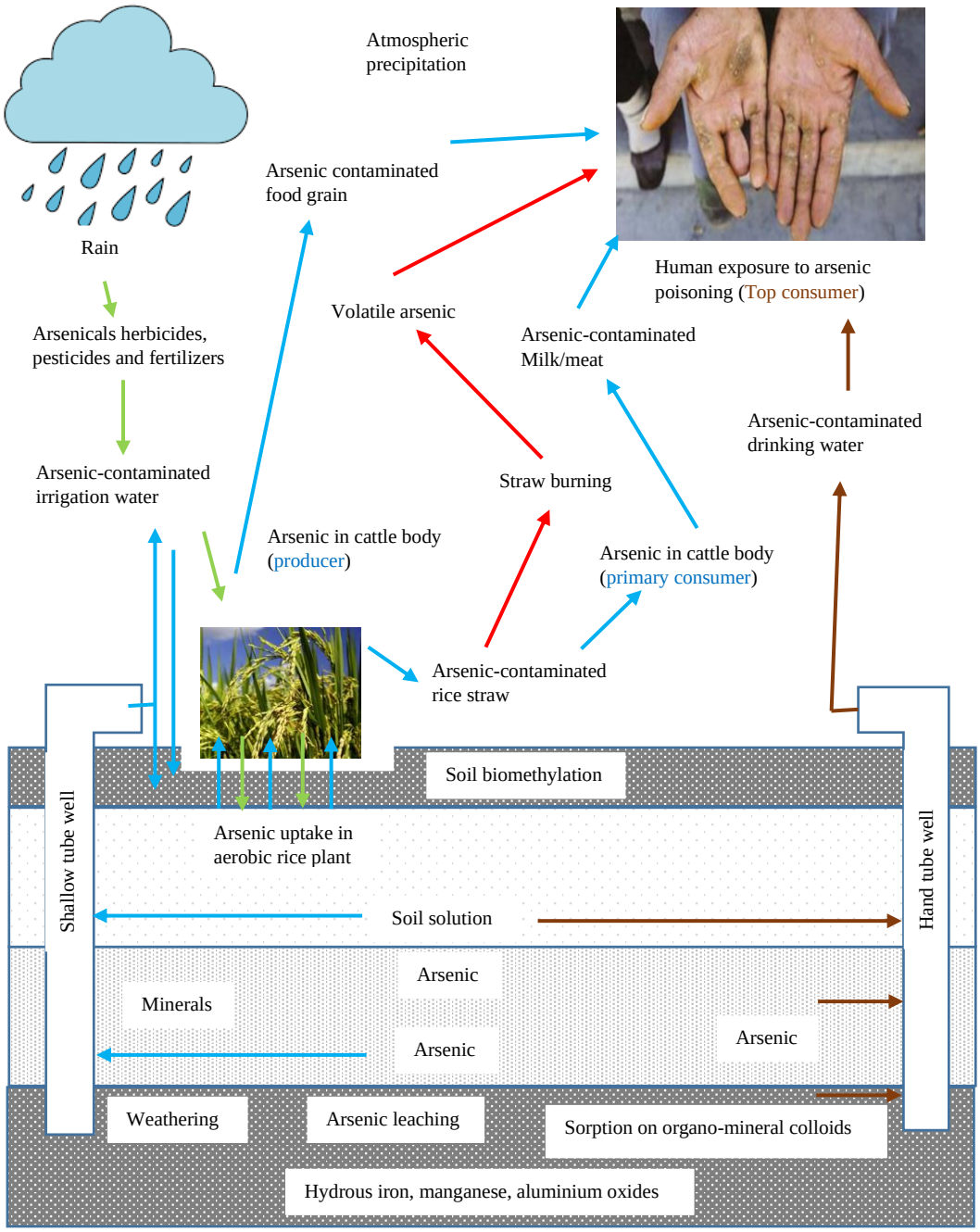

Figure 2-8: Different exposure pathways of arsenic to human (Azizur Rahman et al., 2008).

Effects of arsenic exposure are divided into four stages namely preclinical, clinical, internal complication and malignancy stages (Mohammed Abdul et al., 2015):

(a) ***Preclinical stage*** – this follows the intake of arsenic contaminated water/food, body tissue (hair, nail) and urine shows high arsenic metabolite levels (dimethylarsenic acid and trimethylarsenic acid) with no clinical

symptoms. However, in this stage withdrawal of arsenic contaminated water/food intake leads to no detection of arsenic metabolites in urine.

(b) ***Clinical stage*** – confirmed detection of arsenic toxicity based on analysing external (hairs, nails and skin scales) and other body parts. Major dermatological detections are melanosis, spotted keratosis, Leucomelanosis, spotted palmoplantar keratosis. Minor dermatological detections are mucus membrane melanosis, non-pitting edema and conjunctival congestion.

(c) ***Internal complication stage*** – organs such as eyes, liver, lungs and muscles are affected at this stage and appearance of non-dermatological symptoms (organ dysfunction, asthmatic bronchitis, liver and spleen enlargement etc).

(d) ***Malignancy stage*** – development of tumors and other complications in various organs of the body (lungs, lungs, bladder and uterus) eventually causing death.

2.5.1 Effects of arsenic on various organ on human body

2.5.1.1 Skin – Arsenic effect on human skin was first noted by several physicians in the 1800s (Schwartz, 1997). The skin with its attachments such as hairs and nails forms an integumentary system and is commonly described as the largest organ in the body (Mohammed Abdul et al., 2015). The skin is more susceptible to arsenic and shows initial signs of arsenicosis (Rahman et al., 2009). Several studies have shown that men are more likely to develop arsenic-related skin effects than women (Lindberg et al., 2008). Skin lesions such as keratosis, melanosis and pigmentation are some of the key effects of arsenic exposure (Rahman et al., 2009). Jayasumana et al. (2013) conducted a study in Sri Lanka and observed that of the 125 patients studied, 66 (54.4 %) had hyperpigmentation of palms, 49 (39.2 %) had hyperpigmentation of soles, 29 (23.2 %) had keratosis of palms and the remaining 22 (17.6 %) had keratosis of the soles. In southwest Taiwan, the prevalence rate of keratosis and hyperpigmentation was 7 % and 18 % respectively (Tseng et al., 1968).

2.5.1.2 Nervous system – Chronic arsenic exposure targets the brain thereby affecting learning and concentration due to its ability to cross the blood brain barrier easily (Mohammed Abdul et al., 2015; Mundey et al., 2013). Arsenic species occur throughout the brain, however, the highest accumulation occurs in the pituitary gland (Sánchez-Peña et al., 2010). Neurological complications because of acute or

chronic arsenic exposure develop quickly and are reported as symmetrical sensorimotor neuropathy. Motor nerves are less sensitive to arsenic than sensory nerves. Likewise, neurons having long axons are affected more than neutrons with short axons (Mohammed Abdul et al., 2015). In addition, acute arsenic exposure leads to brain disease and malfunction over time (encephalopathy). Other symptoms include headache, seizures, hallucination and coma (Bartolomé et al., 1999). In Bangladesh, Wasserman et al. (2004) reported that Bangladeshi children exposed to drinking water with arsenic concentration > 50 µg/L had decreased intelligence testing scores when compared with children exposed to lower concentrations of arsenic in drinking water.

2.5.1.3 Respiratory system – Respiratory complications may occur because of arsenic exposure in drinking water or from other sources such as industrial activity, cigarette smoking and energy production. Inhalation of arsenic dust during mining or mining of ores often produces respiratory diseases such as laryngitis, bronchitis, chronic cough and rhinitis (Mohammed Abdul et al., 2015; Saha et al., 1999). The process of arsenic adsorption through the respiratory system occurs in two parts namely: (i) particles deposition onto the airways and lung surfaces and (ii) arsenic absorption from deposited particulates (Henke, 2009). Parvez Faruque et al. (2008) in his study showed that the most common observed respiratory symptoms includes chronic cough, shortness of breath, chest sounds, blood in sputum and other breathing problems.

2.5.1.4 Cardiovascular system - Chronic arsenic exposure has been shown to cause cardiovascular diseases (CVD) along with other risk factors (i.e. hypertension, peripheral vascular disease, ischemic heart disease (IHD), atherosclerosis, arrhythmic, cerebrovascular disease and diabetes) (Henke, 2009; Mohammed Abdul et al., 2015). Long-time inhalation and exposure of inorganic arsenic shows an increased morbidity and mortality rate due to CVD (States et al., 2009). High arsenic concentration in drinking water has also been reported to negatively affect the cardiovascular system (Rahman et al., 2009). Some of such studies have been conducted in South Western Taiwan (Tseng et al., 1968), Utah, United States (Chen and Karagas, 2013) and Bangladesh (Chen et al., 2011).

2.5.1.5 Endocrine system – Chronic exposure to arsenic is a well-known disruptor of the endocrine system including thyroid, thyroid hormone, gonads, pancreas and hypothalamic-pituitary-adrenal axis (Mohammed Abdul et al., 2015). Gong et al. (2015) in a study showed that a low level of arsenic in groundwater (2 -22 µg/L) was associated with hypothyroidism among 723 participants (118 male and 267 female Hispanics; 108 male and 230 female non-Hispanic whites) living in rural West Texas counties. High arsenic exposure primarily from drinking water has been associated with type 2 Diabetes Mellitus (T2DM) which is characterised by insulin resistance in the body. Several studies have been conducted to show the relationship of high arsenic exposure to risk of T2DM developments in countries such as Mexico (Del Razo et al., 2011), Cyprus (Makris et al., 2012), Bangladesh (Islam et al., 2012), Sweden (Rahman et al., 1996) and the United States (Gribble et al., 2012).

2.6 Arsenic treatment techniques in drinking water

Arsenic contamination may occur in various aqueous solutions such as in surface waters, groundwaters, industrial wastewaters, drinking water or mine drainage leachates from landfills. Groundwater is generally more difficult and expensive to treat due to its accessibility than surface water (Henke, 2009). Due to arsenic toxicity, several organization such as WHO, US EPA and DWSNZ have set 10 µg/L as the MCL in drinking water. However, despite the health problem arsenic poses, some countries (Bangladesh, Argentina, Bahrain, Pakistan, Bolivia, Nepal and Vietnam) still set 50 µg/L as the MCL (Fig. 2-9) (Nidheesh and Singh, 2017). In order to remove or reduce arsenic contamination to the MCL, the contaminated drinking water must be treated. There are several technologies available so far for arsenic removal from contaminated drinking water although they come with some drawbacks and intrinsic by-products which can be a potential source for a secondary pollution (Ghosh (Nath) et al., 2019).

Table 2-5: Examples of health effects across multiple bodily systems in humans for arsenic exposure (Naujokas Marisa F. et al., 2013; Rahman et al., 2018).

Target organs	Health effects on humans
Skin	• Skin lesions • Skin cancer
Developmental processed	• Increased infant mortality • Reduced birth weight • Altered DNA methylation of tumor promoter regions in cord blood and maternal leukocytes • Neurological impairments in children • Early-life exposure associated with increased cancer risk as adults
Nervous system	• Impairment intellectual function in children and adults • Impaired motor function • Neuropathy
Respiratory system	• Increased mortality from pulmonary tuberculosis, bronchiectasis and lung cancer
Cardiovascular system	• Coronary and ischemic heart disease • Acute myocardial infarction • Hypertension
Liver, kidney, and bladder	• Liver cancer • Kidney cancer • Bladder and other urinary cancers
Immune system	• Altered immune-related gene expression and cytokine expression • Inflammation • Increased infant morbidity from infectious diseases
Endocrine system	• Diabetes • Impaired glucose tolerance in pregnant women • Disrupted thyroid hormone, retinoic acid, and glucocorticoid receptor pathways in mice and amphibians

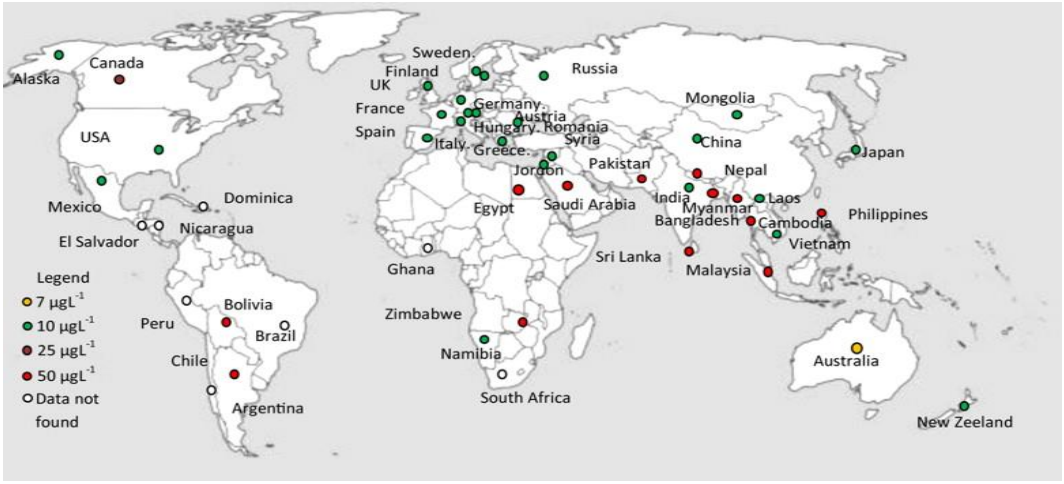

Figure 2-9: Affected countries and their respective MCL (Mondal et al., 2013).

Various conventional and advanced treatment methods for arsenic removal from contaminated drinking water have been proposed under both laboratory and field conditions. These conventional treatment methods can be categorised into physicochemical treatment processes (oxidation, coagulation-flocculation, adsorption, ion exchange, membrane processes, precipitation and coprecipitation), biological processes (biological sorption, treatment of bio-organism), natural remediation and electrocoagulation (Fig. 2-10).

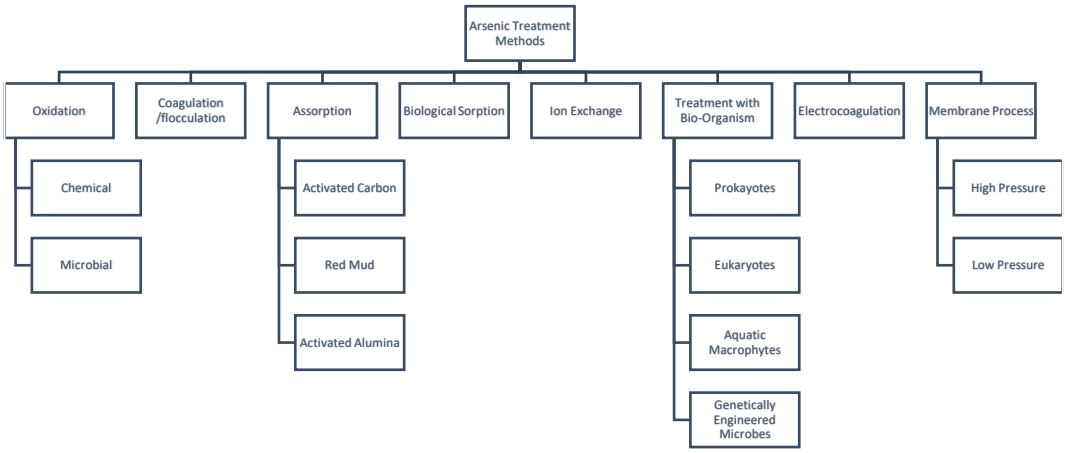

Figure 2-10: Arsenic treatment methods (Ghosh (Nath) et al., 2019).

2.6.1 Adsorption

Adsorption is the attachment of molecules or particles to a surface of a solid materials (adsorbents or sorptions) and is seen as a largely effective, robust, economical and environmentally friendly method in removing heavy metals in

water treatment. Sometimes the adsorbed solute is called the adsorbate and some researchers use the generic term 'sorption' to refer to a process where adsorption and/or absorption are involved or if adsorption and absorption cannot be distinguished (Henke, 2009). The adsorption process can be classified into physical adsorption or van der Waal's adsorption and chemical adsorption or chemisorption (Fig. 2-11). Adsorption processes are flexible in design, operation and produce high quality treated effluent. Adsorbents can also be regenerated in a process called desorption (Fu and Wang, 2011). The adsorption process depends on different factors such as the pH of the solution, arsenic concentration, the temperature and the presence of other competing ions in the solution. Also, the surface area of the adsorbent plays a significant role in the adsorption process as most adsorbent sizes are in nanometres and have large internal pores (Ghosh (Nath) et al., 2019).

2.6.1.1 Interferences

Compared to other treatment processes such precipitation/coprecipitation, adsorbents are more vulnerable to chemical interferences that hinder the removal of arsenic from water. Some ions compete directly for adsorption sites with arsenic species. Two prime examples are phosphate (PO_4^{3-}) and silicate (SiO_4^{4-}) which have the same tetrahedral structure as arsenate (AsO_4^{3-}) (Henke, 2009). Due to these similarities, phosphate and silicate may desorb As (V) from clay, aluminium, iron and other sorbents over a wide pH values or hinder the sorption of As (V) onto these materials (Antonio Violante et al., 2006; D. Smith and Edwards, 2005). Carbonates ($H_2CO_3^0$, HCO^{3-} and/or CO_3^{2-}) present in water have little or no effect on As (V) adsorption, although other evidence suggests that it may interfere with As (III) sorption due to their similar trigonal molecular structure (Stollenwerk, 2003). Dissolved organic materials may also compete with arsenic for a site. Fulvic acid is known to interfere with As (V) adsorption onto aluminium compounds whereas humic acids significantly inhibit As (III) and As (V) on goethite at pH conditions of 6 – 9 and 3 – 8, respectively (Grafe et al., 2001). In contrast, the presence of nitrogen rich humic acid on the surface of kaolinite ($Al_2Si_2O_5(OH)_4$) often improves As (V) sorption from water (Saada et al., 2003).

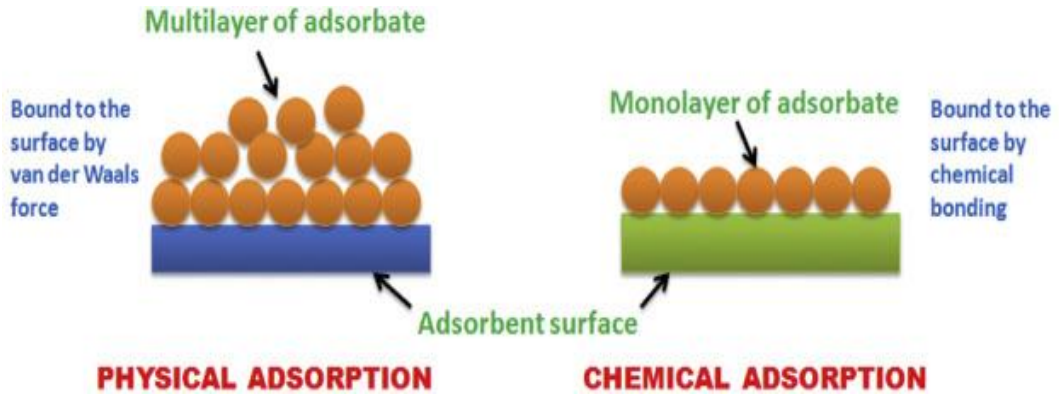

Figure 2-11: Physical and chemical adsorption (Sarkar and Paul, 2016).

2.6.1.2 Adsorption Kinetic Study

The first step in understanding the adsorption process and the foundation for modelling is to depict equilibrium. Thus, the amount of material absorbed onto a media can be expressed in the mass balance shown in Eq. (2.1).

$$\frac{X}{M} = (C_o - C_e)\frac{V}{M} \qquad (2.1)$$

Where *X/M* (usually expressed as mg pollutant/g media) is the mass of pollutant per mass of media, C_o is the initial pollutant concentration in solution, C_e is the concentration of the pollutant in solution after equilibrium has been reached, *V* is the volume of the solution to which the media mass is exposed, and *M* is the mass of the media (Demirbas, 2008).

Several kinetic models have been applied to study the adsorptive kinetics of heavy metals. Panthi and Wareham (2014) use the Lagergren equation, which is a first-order kinetic rate equation for adsorption (Eq. 2.2).

2.6.1.2.1 Pseudo-First-Order Model

The pseudo-first-order equation is given as:

$$\frac{dq_t}{dt} = k_1 (q_e - q_t) \qquad (2.2)$$

Where q_t (mg/g) is the amount adsorbed at time t. q_e (mg/g) is the adsorption capacity at equilibrium, k_1 (1/min) is the pseudo first order rate constant, and *t* is the contact time (min). The integration of (Eq. 2.2) with initial condition (q_t = 0 at *t* = 0) leads to the equation below:

$$\log(q_e - q_t) = \log q_e - \frac{k_1}{2.303} t \quad (2.3)$$

2.6.1.2.2 Pseudo-Second-Order Model

The pseudo-second-order model is represented as:

$$\frac{dq_t}{dt} = k_2(q_e - q_t)^2 \quad (2.4)$$

Where k_2 is the pseudo-second order rate constant (g/mg min). Integrating (Eq. 2.4) and noting that $q_t = 0$ at $t = 0$, the following equation is obtained

$$\frac{t}{q_t} = \frac{1}{k_2 q_e^2} + \frac{1}{q_e} t \quad (2.5)$$

The equilibrium adsorption capacity, q_e is obtained from the slope and k_2 is obtained from the intercept of the linear plot of t/q_t vs t.

2.6.1.2.3 Intra-particle Diffusion Model

The intra-particle diffusion model is a theory proposed by Weber and Morris in identifying the diffusion mechanism by which adsorbate diffuses into the pores of adsorbent which can be the determining step (Weber and Morris, 1963). The intra-particle diffusion model is expressed as:

$$q_t = K_{id}\sqrt{t} + C \quad (2.6)$$

Where K_{id} is the intra-particle diffusion rate constant (mg/g min ^{½}) with C as the intercept along the q_t axis. If a plot of q_t vs $t^{½}$ gives a straight line passing through the origin, the intra-particle diffusion is considered as the rate determining step. If the straight line deviates from the origin, it indicates contributions from film diffusion (Ahamad et al., 2018; Ho and Mckay, 1998). The liquid film diffusion model is given by:

$$\text{In}(1 - F) = -k_{fd}t \quad (2.7)$$

Where, $F = q_t/q_e$ is the fractional attainment of equilibrium, and k_{fd} is the film diffusion rate constant. A linear plot of *In (1 - F)* vs. t with zero intercept and enables k_{fd} to be calculated from the slope.

2.6.1.2.4 Elovich Model

The Elovich Model is an interesting model that has extensively been accepted to describe a chemisorption process (Ahamad et al., 2018; Kaur et al., 2013). The Elovich model equation is expressed as:

$$\frac{dq_t}{dt} = \alpha \exp(-\beta q_t) \quad (2.8)$$

Simplifying the Elovich equation, Chien and Clayton (1980) assumed $\alpha\,\beta >> t$ and by applying the boundary conditions $q_t = 0$ at $t = 0$ and $qt = 0$ at $t = 0$ Eq. (2.8) becomes

$$q_t = \frac{1}{\beta} \text{In}\,(\alpha\beta) + \frac{1}{\beta} \text{In}\,(t) \quad (2.9)$$

Where α (mg/g.min) and β (g/mg) are constants. The constant α is considered as the initial adsorption rate, β is related to the extent of surface coverage and activation energy for chemisorption and q_t (mg/g) is the amount of absorbent absorbed at time t (min). The values of α and β are obtained from a linear plot of qt vs. *In t*.

2.6.1.2.5 Bangham's Model

Bangham's equation has been used to illustrate pore diffusion during the adsorption process and it is expressed as (Aharoni et al., 1979).

$$\text{Log log}\left(\frac{C_0}{C_0} - q_t m\right) = \log\left(\frac{k_0 m}{2.303\,V}\right) + \alpha \log t \quad (2.10)$$

Where C_0 is the initial concentration of the adsorbate in solution (mg/L). V is the volume of the solution (mL), m is the weight of adsorbent (g/L), q_t (mg/g) is the amount of adsorbate retained at time t and α (< 1) and k_o are the constants. A linear plot of (Log log ($C_o/C_o - q_t\,m$) vs. log t demonstrates the diffusion of adsorbate into pores of adsorbents.

2.6.1.3 Adsorption Isotherm

Several mathematical models have been developed to describe experimental data of adsorption isotherms. These models are Langmuir, Freundlich, Dubinin-Radushkevich (D-R), Langmuir – Freundlich (L-F) and Temkin isotherms.

2.6.1.3.1 Langmuir Isotherms

The Langmuir model assumes uniform energies of adsorption onto the surface and is valid for monolayer adsorption containing a finite number of identical sites. It is represented as:

$$q_e = \frac{q_m K_L C_e}{1 + K_L C_e} \quad (2.11)$$

Where q_e is the amount of solute adsorbed per unit weight of adsorbent (mg/g), C_e is the equilibrium concentration of the solute in the solution (mg/L), q_m the maximum adsorption capacity (mg/g), and K_L is the constant related to the free energy of adsorption (L/mg). Table 2-6 below shows the different forms of linearized Langmuir equations and the method to estimate the Langmuir constants q_m and K_L.

Table 2-6: Isotherm models and their linear forms

Isotherms	Equation	Linear Form	Plot
Langmuir 1	$q_e = \frac{q_m K_L C_e}{1 + K_L C_e}$	$\frac{1}{q_e} = \frac{1}{q_m K_L C_e} + \frac{1}{q_m}$	$\frac{1}{q_e}\ vs. \frac{1}{C_e}$
Langmuir 2	$q_e = \frac{q_m K_L C_e}{1 + K_L C_e}$	$\frac{C_e}{q_e} = \frac{1}{q_m}\ C_e + \frac{1}{q_m K_L}$	$\frac{C_e}{q_e}\ vs. C_e$
Langmuir 3	$q_e = \frac{q_m K_L C_e}{1 + K_L C_e}$	$q_e = -\frac{1}{K_L}\frac{q_e}{C_e} + q_m$	$q_e\ vs. \frac{q_e}{C_e}$
Langmuir 4	$q_e = \frac{q_m K_L C_e}{1 + K_L C_e}$	$\frac{q_e}{C_e} = -K_L q_e + q_m K_L$	$\frac{q_e}{C_e}\ vs. q_e$
Langmuir 5	$q_e = \frac{q_m K_L C_e}{1 + K_L C_e}$	$\frac{1}{C_e} = K_L q_m \frac{1}{q_e} - K_L$	$\frac{1}{C_e}\ vs. \frac{1}{q_e}$

2.6.1.3.2 Freundlich Isotherms

This isotherm is an empirical equation used to describe a heterogeneous system. Freundlich equation can be expressed as:

$$q_e = K_F C_e^{\frac{1}{n}} \quad (2.12)$$

The linear form of Freundlich equation can be expressed as:

$$\log q_e = \log K_F + \frac{1}{n}\log C_e \quad (2.13)$$

Where K_F and *1/n* are Freundlich constants. K_F indicates the adsorption capacity and *1/n* is the heterogeneity factor. The values of *n* and K_F are calculated from the slopes and intercepts of the linear plots of log q_e vs. log C_e.

The Langmuir-Freundlich equation can be expressed as:

$$q_e = \frac{K_L q_m C_e^{\frac{1}{n}}}{1 + K_L C_e^{\frac{1}{n}}} \quad (2.14)$$

2.6.1.3.3 Dubinin and Radushkevich (D-R) Isotherm

The D-R isotherm is generally used to describe the sorption of a single solute system. The D-R model is analogous to Langmuir isotherm and it also rejects the homogenous surface or constant adsorption potential (Kaur et al., 2013). It is expressed as:

$$q_e = q_s \exp(-K_{DR}\varepsilon^2) \quad (2.15)$$

$$\varepsilon = RT \ln\left(1 + \frac{1}{C_e}\right) \quad (2.16)$$

Where K_{DR} is D-R isotherm constant (mol^2/KJ^2), ε is the Polanyi potential, q_s is the isotherm saturation capacity (mg/g), *R* is the universal gas constant (8.314 $Jmol^{-1}K^{-1}$) and *T* is the temperature in Kelvin (K).

Eq. (2.15) can be linearized as shown in Eq. (2.17)

$$\ln q_e = \ln q_s - K_{DR}\varepsilon^2 \quad (2.17)$$

2.6.1.3.4 Temkin Isotherm

This model takes into account the interactions between adsorbent – adsorbate. The model suggests that the sorption energy (function of temperature) of all molecules in the layer will decrease linearly rather than logarithmically with coverage (Kaur et al., 2013). The model is given by the following equation:

$$q_e = \frac{RT}{b} \ln (A_T C_e) \quad (2.18)$$

$$q_e = \frac{RT}{b} \ln A_T + \left(\frac{RT}{b}\right) \ln C_e \quad (2.19)$$

$$B = \frac{RT}{b} \quad (2.20)$$

$$q_e = B \ln A_T + B \ln C_e \quad (2.21)$$

Where A_T is the Temkin isotherm equilibrium binding constant (L/g), b is the Temkin isotherm constant, R is the universal gas constant (8.314 J/mol/K), T is the Temperature at 298 K and B is the constant related to heat of sorption (J/mol). The constants A_T and B can be calculated from the linear plot of q_e vs. In C_e.

2.6.1.4 Adsorption column models

The performance of a column is evaluated through breakthrough curves. The effluent adsorbate concentration (C_t) from the column that reaches about 5 % of the influent adsorbate concentration (C_0) is the breakthrough point. The point where the effluent concentration reaches 95 % is called the "point of column exhaustion". The breakthrough curve can be obtained by plotting the dimensionless concentration C_t/C_0 vs t or volume of effluent. The effluent volume, V_{eff} (mL), is calculated from the following equation (Xu et al., 2013):

$$V_{eff} = Q \times t_{total} \quad (2.22)$$

The total mass of adsorbate, q_{total} (mg) adsorbed at specific column parameters can be calculated from the following equation:

$$q_{total} = \frac{Q}{1000} \int_0^{total} C_{ad}\, dt = \frac{Q}{1000} \int_0^{total} (C_0 - C_t)\, dt \quad (2.23)$$

Where Q is the volumetric flowrate (mL/min), t_{total} is the total flow time (min), C_{ad} is adsorbed adsorbate concentration (mg/L). The integral in Eq. (2.23) is equal to the area in the breakthrough curve.

Maximum capacity of the column or equilibrium of adsorbate uptake per unit mass of adsorbent, $q_{eq\,(exp)}$ (mg/g), is calculated as following:

$$q_{eq(exp)} = \frac{q_{total}}{M} \quad (2.24)$$

Where M is the dry weight of resin packed in the column (g).

Total amount of adsorbate passing from the column (W_{total}) and total removal percentage of the adsorbate (Y %) are calculated from the following equation:

$$W_{total} = \frac{C_0 Q t_{total}}{1000} \quad (2.25)$$

$$Y\ (\%) = \frac{q_{total}}{W_{total}}\ X\ 100 \quad (2.26)$$

The empty bed contact time (EBCT) in the column is described as:

$$EBCT\ (min) = \frac{bedvolume\ (mL)}{flowrate\ (mL/min)} \quad (2.27)$$

A successful design of a column adsorption process requires prediction of the concentration-time profile or breakthrough curve for the effluent. Prior to the pilot-scale and industrial applications, lab-scale column studies should first be described and analysed. Over the years, several mathematical models have been developed for predicting the dynamic behaviour of a column namely; Thomas, Yoon-Nelson, Adams-Bohart and Clark models (Xu et al., 2013)

2.6.1.4.1 Thomas Model

The Thomas model is one of the most general and widely used theoretical methods to described column performance (Suksabye et al., 2008). This model behaviour matches the Langmuir kinetics of adsorption – desorption and obeys second-order reversible reaction kinetics. The expression by Thomas for an adsorption column is given below:

$$\frac{C_t}{C_0} = \frac{1}{1+\exp[k_{TH} q_0 x/\upsilon - k_{TH} C_0 t]} \quad (2.28)$$

Where k_{TH} is the Thomas rate constant (mL/mg. min); q_0 is the maximum solid phase concentration (mg/g); x is the amount of adsorbent in the column (g); C_0 and C_t are the inlet and outlet concentrations (mg/L) of the adsorbate at time t respectively; υ is the flowrate (mL/min). The value of t is the flow time (min), ($t = V_{eff}/\upsilon$, V_{eff} is effluent volume at time t).

The linearized form of the Thomas model is as follows:

$$In\left(\frac{C_0}{C_t} - 1\right) = \frac{k_{TH} q_0 x}{\upsilon} - k_{TH} C_0 t \quad (2.29)$$

The values of k_{TH} and q_0 can be obtained by the slope and intercept from plot of $In\ (C_0/C_t - 1)$ *vs.* t

2.6.1.4.2 Yoon – Nelson Model

Yoon and Nelson developed a simple model that is based on the assumption that the rate of decrease in the probability of adsorption of an adsorbate molecule is proportional to the probability of the adsorbate breakthrough on the adsorbent (Ahmad and Hameed, 2010). The Yoon – Nelson equation for a single component system is expressed as (Han et al., 2009):

$$\frac{C_t}{C_0 - C_t} = \exp(k_{YN}\, t - \tau k_{YN}) \tag{2.30}$$

$$\frac{C_t}{C_0} = \frac{1}{1+\exp[K(\tau - t)]} \tag{2.31}$$

The linearized model for Eq. (2.31) can be expressed as:

$$\text{In}\ \frac{C_t}{C_0 - C_t} = k_{YN}\, t - \tau k_{YN} \tag{2.32}$$

Where τ is the time required for 50 % adsorbate breakthrough (min), k_{YN} is the rate constant (1/min) and t is the sampling time (min). The value of k_{YN} and τ can be found by plotting the graph of $In\ (C_t/(C_0 - C_t))$ versus t.

2.6.1.4.3 Adams – Bohart Model

The Adams – Bohart model assumes that the adsorption rate is proportional to both the residual capacity of the adsorbent and the concentration of the adsorbing species. The model is used for the description of the initial part of the breakthrough curve, expressed as (Ahmad and Hameed, 2010):

$$\frac{C_t}{C_0} = \exp\left(k_{AB} C_0 t - k_{AB} N_0 \frac{Z}{F}\right) \tag{2.33}$$

Equation (33) can be linearized as:

$$\text{In}\ \frac{C_t}{C_0} = k_{AB} C_0 t - k_{AB} N_0 \frac{Z}{F} \tag{2.34}$$

Where C_0 and C_t (mg/L) are the inlet and effluent concentration, k_{AB} (L/mg min) is the kinetic constant, F (cm/min) is the linear velocity calculated by dividing the flowrate by the column sectional area, Z (cm) is the bed depth of column and N_0 (mg/L) is the saturation concentration. From this equation, values describing the characteristics operational parameters of the column (k_{AB} and N_0) can be determine from a plot of C_t/C_0 against t.

2.6.1.4.4 Clark Model

The Clark model is based on the use of a mass-transfer concept in combination with Freundlich isotherm (Nouri and Ouederni, 2013). Clark's model can be expressed as:

$$\frac{C_t}{C_0} = \left(\frac{1}{1+Ae^{-rt}}\right)^{1/(n-1)} \quad (2.35)$$

The values of *A* and *r* can be obtained from a nonlinear plot of C_t/C_0 against *t* at a given bed height and flow rate.

The linearized form of the model can be represented as:

$$\text{In}\left[\left(\frac{C_0}{C_t}\right)^{n-1} - 1\right] = -rt + \text{In A} \quad (2.36)$$

Where *n* is the Freundlich parameter, *A* and *r* (1/min) are the Clark constants. *A* and *r* are determined from the slope and the intercept of plot of In $[(C_0/C_t)^{n-1} - 1]$ *vs. t.*

In this review, adsorbents will be classified into three classes: (1) activated carbon adsorbents, (2) carbon nanotubes adsorbents and (3) low-cost adsorbents.

2.6.1.5 Activated carbon adsorbents

Activated carbon is an extremely effective adsorbent widely used to remove heavy metal contaminants in drinking water due to its high surface area resulting from large micropore and mesopore volumes (Fu and Wang, 2011). However, there has been an increase in production price of commercial coal based activated carbon due to depletion of the source. This has raised concern about searching for a cheaper alternative from renewable and cheaper precursors (Demiral and Güngör, 2016). Burdinova et al (2006) also studied arsenic (III) removal from aquatic solutions at different concentrations and pH by using four different activated carbons from solvent extracted olive pulp and olive stone waste materials. Other alternative feedstocks proposed for the preparation of activated carbon are bones, blood, fish, coconut shell, rice hulls, refinery waste leather waste rubber waste etc. Adsorption capacity depends activated carbon properties, adsorbate chemical properties, temperature, pH and ionic strength (Mohan and Pittman Jr., 2007).

2.6.1.6 Carbon nanotubes adsorbents

Carbon nanotubes (CNTs) have been increasingly studied for removing various contaminants from aqueous solutions due to their large surface area, high porosity, low density and hollow structure (Ihsanullah et al., 2016). As a new adsorbent, CNTs have been tested on removing chromium (VI) (Di et al., 2004), lead (II) (Wang et al., 2007) and nickel (Kandah and Meunier, 2007). CNTs are categorized as single-walled nanotubes (SWNTs) and multi-walled nanotubes (MWNTs). The mechanisms by which metal ions are adsorbed onto the CNTs is attributed to chemisorption, physisorption, electrostatic interaction, ion exchange and surface complexation (Fu and Wang, 2011; Ihsanullah et al., 2016). Ntim and Mitra (2012) conducted arsenic removal from water using a multiwall carbon nanotube-zirconia nanohybrid (MWCNT – ZrO_2). The adsorption isotherms fitted both Langmuir and Freundlich isotherms and the maximum adsorption capacity for As (III) and As (V) were 2 mg/g and 5 mg/g respectively. Tawabini et al. (2011) conducted a study to remove As (III) from water using modified multi-walled carbon nanotubes (MCNTs). MCNTs modified with iron oxide (Fe-MCNTs) removed about 77.5 % of As (III) while MCNTs modified with carboxyl group (COOH-MCNTs) removed only 11 % at pH 5.

2.6.1.7 Low-cost adsorbents

Low-cost adsorbents have been studied as a substitute for activated carbon for removing heavy metal ions. Some of the low-cost adsorbents include (1) agricultural product and by-products, (2) industrial by-products/waste, (3) soils and constituents and (4) biosorbents. Agricultural by-products such as untreated rice husk (Agrafioti et al., 2014) and lignite and peat (Allen et al., 1997; Mohan and Chander, 2006) have also been studied. Manning and Goldberg (1996) studied the adsorption of arsenate on kaolinite, montmorillonite and illite. Lastly different forms of inexpensive biosorbents have been studied to remove heavy metals such as chitosan (Elson et al., 1980), fungal organisms (Pokhrel and Viraraghavan, 2006), eggshell (Park et al., 2007) and human hair (Wasiuddin et al., 2002). Biosorption is still in the experimental phase and widely favoured due to low cost and rapid adsorption but separation of the adsorbate is difficult after adsorption (Fu and Wang, 2011).

2.6.1.8 Other commercial adsorbent

2.6.1.8.1 New Zealand Ironsand (NZIS): - is a black, heavy, magnetic iron that originates as crystals within volcanic rocks before being transported to the coast by rivers. In New Zealand, it occurs mainly in the North Island (Panthi and Wareham, 2014). The main iron-based mineral in NZIS is magnetite (Fe_3O_4) and/or titanomagnetite ($Fe_{3-x}Ti_xO_4$ ($0 \leq x \geq 1$), and other minerals include titanium oxide (TiO_2) and vanadium oxide. Panthi and Wareham (2014) and (2011) carried out study on the kinetics and adsorption of arsenic onto New Zealand ironsand. The maximum adsorption capacity for As (III) and As (V) using NZIS was 1.5 mg/g and 0.5 mg/g respectively.

2.6.1.8.2 DMI-65: - is an extremely powerful silica sand based catalytic water filtration media designed for the removal of iron and manganese without the use of potassium permanganate. DMI-65 acts as an oxidation catalyst with immediate oxidation and filtration of the insoluble precipitate derived from this oxidation reaction. It also known to remove arsenic, aluminium and other heavy metals under certain conditions. Other advantages of DMI-65 include operating at a wide pH range (5.8 – 8.6), operating at a temperature up to 45 ^oC, long life and also operating at high flow rates. It found application in mining, protecting reverse osmosis membranes, drinking water applications, arsenic removal, cooling towers and boilers and in industrial applications ("Quantum Filtration Medium," 2019).

2.6.1.8.3 Molecular imprinted polymers (MIPs): - is prepared with a reaction mixture composed of a template, a functional monomer (or two), a cross-linking monomer (or two), and a polymerization initiator in a solvent. During polymerization, there is a complex formation between the template and the functional monomer, and the complex is surrounded by the surplus cross-linking monomer, yielding a three-dimensional polymer network where the template molecules are trapped after completion of polymerization (Cheong et al., 2013). Reaction conditions such as formulation of MIP reaction mixture includes choice of cross-linking monomer, functional monomer, a porogenic solvent, reaction temperature, and time govern the properties, physical appearance, morphology, and performance of MIP. Since MIP was invented in 1972 (Song et al., 2009), it has

found applications in chromatography, sample pre-treatment, purification, catalysts, sensors and drug delivery.

2.6.2 Ion exchange

Ion exchange is a widely known method for removing heavy metals from water/wastewater due to its high adsorption capacity, high removal efficiency, and rapid kinetics (Fu and Wang, 2011; Kang et al., 2004). Ion exchange has three applications in water treatment: (1) softening, (2) specific ion removal, and (3) demineralization. Ion exchange also follows the same principle as adsorption but the difference is that the adsorbate is molecular in the case of adsorption, and ionic in the case of ion exchange. Among the materials used in ion exchange processes, synthetic resins are commonly preferred as they are effective, inexpensive and readily remove heavy metals from the solution (Alyüz and Veli, 2009).

Several media are used in ion exchange such as clays, zeolites and synthetic resin. Ion exchange resins are classified as strong-acid and weak-acid for cation exchanges and strong-base and weak-base for the anion exchangers (Hendricks, 2006). Strong acidic resin with sulfonic acid groups ($-SO_3H$) and weak acid resin with carboxylic acid groups (-COOH) are the most common cation exchangers. Factors affecting the uptake of metal ions by ion exchange resin are temperature, initial metal concentration, pH, and contact time (Gode and Pehlivan, 2006). The process below shows how metal ions are exchanged for hydrogen ions on a resin as a solution containing heavy metal passes through a cation column.

$$nR\text{-}SO_3H + M^{n+} \rightarrow (R\text{-}SO_3\text{-})_nM^{n+} + nH^+$$

$$nR - COOH + M^{n+} \rightarrow (R\text{-}COO^-)_n\, M^{n+} + nH$$

The presence of competing ions such as sulfate (SO_4^{2-}), carbonate (HCO_3^-), and nitrate (NO_3^-) hinder the removal of arsenic because of their high affinity towards the resins (Mondal et al., 2013). Dambies (2005) suggested that the metal loaded polymers can remove both As (III) and As (V) by eliminating the interference of other ions. Table 2-7 shows the adsorption capacity of As (III) and As (V) using different adsorbents.

Table 2-7: Comparative evaluation of activated carbons and various low cost adsorbents for arsenic removal (Mohan and Pittman Jr, 2007).

Adsorbent	Type of water	pH	Concentration/range	Surface area (m^2/g)	Temperature (^oC)	Model used to calculate adsorption capacity	Capacity (mg/g)		References
							As (III)	As (V)	
Activated carbon	Aqueous solution	6.4 – 7.5	157 - 737 mg/L for As (V) and 193 - 992 mg/L for As (III)	43.40	25	-	29.9	30.48	(Pattanayak et al., 2000)
Char carbon	Aqueous solution	2 – 3	157 - 737 mg/l for As (V) and 193 – 992 mg/L for As (III)	36.48	25	-	89.0	34.46	
Iron oxide coated sand	Drinking water	7.6	100 µg/l	10.6	22 ± 2	Langmuir	0.041	0.043	(Thirunavukkarasu et al., 2003)
Red mud	Water (dose: 20g/L)	7.25 for As (III); 3.50 for As (V)	33.37 – 400.4 µmol/L	-	25	Langmuir	0.663	0.514	(Altundoğan et al., 2002)
TiO_2	Drinking water	7.00	-	330	25	Langmuir	59.93	37.46	(Pena et al., 2005)
TiO_2	Ground water	7.00	0.4 – 80 mg/L	251	25	Langmuir	32.4	41.0	(Bang et al., 2005)
Granular ferric hydroxide	Surface and groundwater	7.00	-	226 - 252	24	Freundlich	-	0.004	(Badruzzaman et al., 2004)
Leonardite	Groundwater	7.00		20.64	25	Langmuir	4.46	8.40	(Chammui et al., 2014)
Da –KGM based GO reinforced FMBO	Aqueous solution	7.00	1 – 40 mg/L	-	50	Langmuir	30.21	12.08	(Ye et al., 2017)

Orange juice residue	Wastewater	7 – 11 for As (III) and 2 – 6 for As (V)	-	-	30	Langmuir	70.43	67.43	(Ghimire et al., 2002)
Zirconium loaded activated carbon	Drinking water	8 – 9	5 – 100 mg/L	-	25	Column capacity	-	2.8	(Daus et al., 2004)
Granular ferric hydroxide	Drinking water	8 - 9	5 – 100 mg/L	-	25	Column capacity	-	8.5	(Driehaus et al., 1998)
Coconut husk carbon	Industrial wastewater	12.0	50 – 600 mg/L	206	30	Langmuir	146.30	-	(Manju et al., 1998)
Hematite	Water/ wastewater	4.2	133.49 μmol/L	14.40	30	Langmuir	-	0.20	(Singh et al., 1996)
Feldspar				10.25			-	0.18	
Human hairs	Drinking water	-	90 360 μg/L	-	22	Langmuir	-	0.012	(Wasiuddin et al., 2002)
Zr (IV) – loaded phosphoric acid chelating resin (RPG)	River/ sea water	1.14	2.5 mmol/L	29.2	-	Column capacity	-	49.0	(Zhu and Jyo, 2001)
Molebdate-impregnated chitosan gel beads (MCCB)							-	200	(Dambies et al., 2000)

2.6.3 Coagulation and flocculation

Coagulation and flocculation are essential processes in a number of diverse disciplines including biochemistry, cheese manufacturing, rubber manufacturing and in water and wastewater treatment. In water and wastewater treatment, coagulation and flocculation are extremely important. Historically, most coagulation and flocculation processes are designed for particle and turbidity removal. Traditionally the coagulation process is realized by adding ferric or aluminium ions resulting in the effective removal of wastewater particulates and impurities (Hering et al., 1996). The reactions of metal ions, e.g., Al^{3+} and Fe^{3+} with water results in a variety of products, with species depending on pH, dosage, ionic strength and alkalinity. The two categories of reactions are shown in the equations below (Hendricks, 2006).

1. Complexes

$$Al_2(SO_4)_3 + nH2O \rightarrow 2Al(OH)_n(H_2O)_n^{n+} + H^+ + 3SO_4^{2-}$$

2. Metal ion precipitate

$$Al_2(SO_4)_3 + 6H_2O \rightarrow 2Al(OH)_3 + 6H^+ + 3SO_4^{2-}$$

Coagulation followed by flocculation is a potential way of removing arsenic from groundwater. The mechanism includes destabilization of the stable, charged colloidal particles by neutralizing the charges of the particles. Charge neutralization of the particles eliminates the acting repulsive force and helps the particles to agglomerate, which is then precipitated due to gravity (Ghosh (Nath) et al., 2019). Choong et al. (2007) reported that the positively charged cationic coagulants minimize the negatively charged colloids and as a result, larger particles are formed due to aggregation of particles. Suspended, colloidal or dissolved arsenic can be precipitated in water by applying coagulants and flocculants. This process is usually followed by a filtration process in order to get a clean arsenic free water. Pallier et al. (2010) observed that over 90 % and 77 % of As (V) and As (III) removal was recorded when kaolinite and $FeCl_3$ was used as coagulant/flocculent. The study further revealed that (a) a higher concentration of Fe^{3+} (> 9.2 mg/L) did not result in higher As removal (b) As (V) removal was independent of the concentration of the applied coagulant and (c) As (III) removal was dependent on the coagulant dose as well as the pH of the solution. Hu et al. (2012) studied the effect of aluminium

coagulants (aluminium chloride and two types of polyaluminium chloride) during a coagulation process. The study showed with an initial As (V) concentration of 280 μg/L, all three coagulants reduced As (V) concentration below the MCL recommended by WHO. It further states that aluminium species regulate arsenic removal and thus arsenic removal efficiency can be improved by adjusting the pH. The effect of operational variables such as coagulant dose, As (V) concentration and pH was conducted by Bilici Baskan and Pala (2010). Their findings showed more than 91 % As removal with an initial As (V) concentration of 10 μg/L and an $Al_2(SO_4)_3$ coagulant concentration of 66 mg/L. Likewise almost 100 % removal of As (V) was achieved with an initial As (V) concentration of 500 – 1000 μg/L and a coagulant concentration of 42 – 56 mg/L. The high coagulant dose used in this study can increase the operational cost and generate a secondary waste. Iron (Fe) based coagulants have been used by several authors (Andrianisa et al., 2008; Lacasa et al., 2011; Lakshmanan et al., 2010; Song et al., 2006). Wickramasinghe et al. (2004) use ferric chloride and ferric sulfate as a coagulant to remove arsenic and the study showed that the rate of removal depends on pH adjustment before coagulation and raw water quality.

According to (Ravenscroft et al., 2009), Fe based coagulants are more effective for arsenic treatment than aluminium based coagulants. Aluminium hydroxide (aluminium based coagulant) is stable over a very narrow pH range, whereas iron hydroxides are more stable over a wide pH range (Hering Janet G. et al., 1997). Moreover, iron hydroxides have a high affinity for arsenic and thus, rapid precipitation/co-precipitation of arsenic takes place.

Several tools have been used for coagulation control and effectiveness such as determination of colloid charge, jar testing and pilot plant. Methods for measuring colloid charge include (1) charge titration, (2) zeta-potential and (3) streaming current potential.

There are different types of coagulants and polymers used in the water and wastewater treatment such as metal coagulants, polymers, activated silica and natural polyelectrolytes.

2.6.3.1 Metal coagulants

The commonly used metal coagulants fall into two major categories namely iron and aluminium based. The aluminium based coagulants include aluminium sulfate, aluminium chloride, sodium aluminate, aluminium chlorohydrate (ACH), polyaluminum chloride, polyaluminum sulfate chloride, polyaluminum silicate chloride and forms of polyaluminum chloride with organic polymers. The iron coagulants include ferric sulfate, ferrous sulfate, ferric chloride, ferric chloride sulfate, polyferric sulfate, and ferric salts with organic polymers. The popularity of these metal coagulants arises not only from their effectiveness as coagulants, but also from their ready availability and relatively low cost (Bratby, 2006).

2.6.3.1.1 Aluminium Sulfate: - this is probably the most used coagulant and has been in use for water treatment for several centuries. It is manufactured from the digestion of bauxite ores with sulfuric acid, so that in the final product no free acid is present. Evaporation of water in the process results in the dry product having the approximate formula $Al_2 (SO_4)_3.14H_2O$, with aluminium content ranging from 7.4 to 9.5 % by mass.

2.6.3.1.2 Aluminum Chloride: - this coagulant ($AlCl_3.6H_2O$) is normally supplied in solution form, containing 10.5 % as Al with a pH and density of approximately 2.5 and 1300 kg/m^3, respectively (Bratby, 2006). It is widely used for sludge conditioning.

2.6.3.1.3 Sodium Aluminate: - ($NaAlO_2$) is usually supplied as a viscous, strongly alkaline, and corrosive liquid. The solution strength is usually 13 % as Al. this coagulant differs from alum in that it is alkaline rather than acidic in its reaction. It is rarely used alone, but generally with alum to obtain some special result. $NaAlO_2$ has also been used in the lime-soda softening process as an aid in flocculating the fine precipitates of calcium carbonate and magnesium hydroxide resulting from softening reactions. The reactions of $NaAlO_2$ with $Al_2 (SO_4)_3.14H_2O$ and with free CO_2 produce insoluble aluminium compounds:

$$6NaAlO_2 + Al_2 (SO_4)_3.14H_2O = 8Al(OH)_3 + 3Na_2SO_4 + 2H_2O$$

$$2NaAlO_2 + CO_2 + 3H_2O = Na_2CO_3 + 2Al(OH)_3$$

2.6.3.1.4 Ferric Sulfate: - this coagulant ($Fe_2(SO_4)_3.8H_2O$) is available in both liquid and solid form. In the solid form, the material is granular and free flowing with the following typical specifications: 72 to 75 % $Fe_2(SO_4)_3$ and 20 to 21% Fe^{3+}, by mass. In the liquid form, typical specifications are 40 to 42% $Fe_2(SO_4)_3$ and 21% Fe^{3+}, by mass. Ferric sulfate is particularly used for color removal at low pH values and at high pH values, where it is used for iron and manganese removal and in the softening process.

2.6.3.1.5 Ferrous Sulfate: - this coagulant ($FeSO_4.7H_2O$) is available either as crystals or granules containing 20 % Fe, both of which are readily soluble in water. Ferrous sulfate reacts either with natural alkalinity or added alkalinity to form ferrous hydroxide, $Fe(OH)_2$, but since ferrous hydroxide is relatively soluble, it must be oxidized to ferric hydroxide in order to be useful. The important reactions for ferrous sulfate are:

$$FeSO_4.7H_2O + Ca(OH)_2 = Fe(OH)_2 + CaSO_4 + 7H_2O$$

$$4Fe(OH)_2 + O_2 + 2H_2O = 4Fe(OH)_3$$

2.6.3.1.6 Ferric Chloride: - this coagulant ($FeCl_3$) is available commercially in the liquid, crystal, or anhydrous forms, although the liquid form is by far more common. The liquid and crystal forms are extremely corrosive and must be handled in a similar fashion to hydrochloric acid. The reactions of ferric chloride with natural or added alkalinity may be written as follows:

$$2FeCl_3 + 3Ca(HCO_3)_2 = 2Fe(OH)_3 + 3CaCl_2 + 6CO_2$$

$$2FeCl_3 + 3Ca(OH)_2 = 2Fe(OH)_3 + 3CaCl_2$$

2.6.3.4 Polymers

Polymers refer to a large variety of natural or synthetic, water soluble, macromolecular compounds, which have the ability to destabilize or enhance flocculation of the constituents of a body of water (Bratby, 2006). A polymer may be described as a series of repeating chemical units held together by covalent bonds. If the repeating units are of the same molecular structure, the compound is termed a homopolymer. However, if the molecule is formed from more than one type of repeating chemical unit, it is termed a copolymer.

Polyelectrolytes are special classes of polymers containing certain functional groups along the polymer backbone which may be ionisable. All polyelectrolytes are typical hydrophilic colloids. They have molecular weights generally in the range 10^4 to 10^7 and are soluble in water due to hydration of functional groups. Some types of polyelectrolyte currently in use are discussed below.

2.6.3.5 Activated silica

This is probably the first polyelectrolyte to be used widely in water clarification. In preparing activated silica (which is an anionic polyelectrolyte) commercial sodium silicate solutions (pH approximately 12) at concentrations in excess of 2×10^{-3} M are neutralized with acid reagent (sulfuric acid, chlorine, aluminium sulfate etc.) to a pH less than 9.

2.6.3.6 Natural polyelectrolytes

Coagulation and flocculation could be achieved using either natural coagulants or chemical-based coagulants. Among the two, natural coagulants have long been acknowledged for their application in traditional water purification which is evident from various ancient records (Bratby, 2006). Natural coagulants include starch derivatives which can be natural starches, anionic oxidized starches, or amine treated cationic starches. Other classes include polysaccharides, such as guar gums, tannins, chitosan and the alginates.

2.6.3.6.1 Moringa oleifera seeds: - there are approximately 14 known varieties of moringa oleifera trees around the world, particularly in developing countries. Different varieties appear to have differing coagulating properties that depend on the geographical location, climate, altitude, and soil characteristics. The seed contains up to 40 % by weight of oil. Narasiah et al. (2002) compared the efficiencies of two moringa seed extracts from Burundi, Central Africa, and from Mahajanga, Madagascar on the coagulation of a laboratory prepared kaolin turbid water. In both cases it was found that shelled seeds provide much higher turbidity removal than non-shelled ones and Burundi seeds were superior in quality than those of Madagascar. Ravikumar and Sheeja (2013) use moringa oleifera seed as a coagulant to remove heavy metal from water. The percentage removal by Moringa seeds were 95 % for copper, 93 % for lead, 76 % for cadmium and 70 % for chromium.

2.6.3.6.2 Starches: - polymers may be processed from various sources of starches, including potato, corn, cassava, arrowroot, and yams. Starches are basically highly polymerized carbohydrates. These polymers may be non-ionic, cationic, or anionic depending on the form of processing and the substitutions. Choy et al. (2016) compared turbidity removal efficiency between rice, wheat, corn and potato starches to that of alum and polyaluminium chloride. Using kaolin suspensions, the effects of pH, dosage and need for starch gelatinization was studied.

2.6.3.6.3 Guar Gums: - these are neutral (non-ionic) polysaccharides relatively unaffected by pH and ionic strength. They are subjected to enzymatic degradation on storage, but this may be prevented by addition of citric or oxalic acid. Guar gum has been used in uranium ore processing.

2.6.3.6.4 Tannins: - these are complex polysaccharide tannin derivatives that have been used extensively in potable water, wastewater, and industrial effluent treatment applications. They are generally most effective under acidic conditions. Care must be taken on storage as they are subject to degradation reactions, if left for lengthy periods (Bratby, 2006). Heredia and Martin (2009) tested the effectiveness of a new commercial tannin-based flocculant in order to remove Zn^{2+}, Ni^{2+}, and Cu^{2+} by coagulation-flocculation process.

2.6.3.6.5 Chitosan: - chitin is the skeletal substance of the shells of crustaceans, such as crabs, lobsters, and shrimps and it is described as a high nitrogen containing linear amino-polysaccharide polymer, with a molecular weight of several hundreds of thousands (Bratby, 2006). Chitosan is a cationic polyelectrolyte with a molecular weight of approximately 10^6. Sekine et al. (2006) applied 1.5 mg/L of a commercial chitosan solution directly to the river during a river construction project, to reduce the detrimental ecological effects arising from increased turbidity. Vogelsang et al. (2005) demonstrated the effectiveness of chitosan on the removal of humic substances from Norwegian surface waters. They observed that the highest charged chitosan molecules tested were most effective, indicating that charged neutralization was an important mechanism for the coagulation of the humic matter.

Plant-based natural coagulants are safe, eco-friendly and generally toxin free (Bratby, 2006; Choy et al., 2014). Natural coagulants have been found to generate not only a much smaller sludge volume of up to five times lower but also with a

higher nutritional sludge value (Fig. 2-12). As such, sludge treatment and handling costs are lowered making it a more sustainable option.

2.6.3.7 Synthetic polymers

Although natural polyelectrolyte products have the advantage of being virtually toxic-free, the use of synthetic polyelectrolytes is more widespread. They are, in general, more effective as flocculants principally due to the possibility of controlling properties such as the number and type of charged units and the molecular weight.

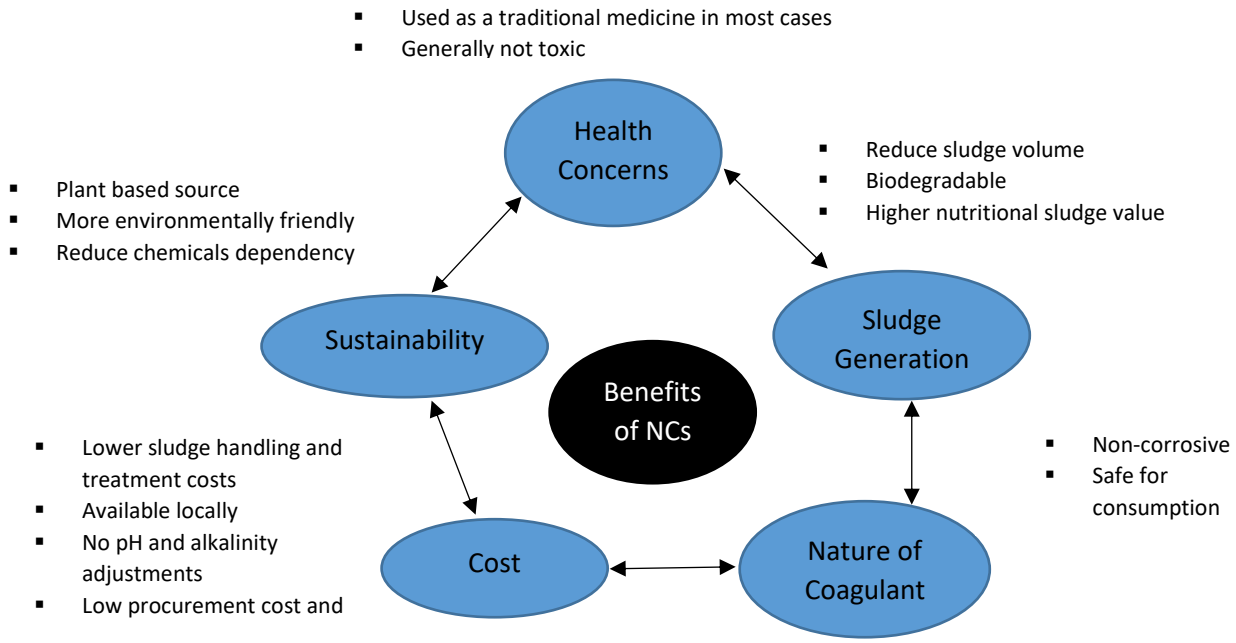

Figure 2-12: Advantages of natural coagulants (NC) over chemical coagulants (Choy et al., 2014).

2.6.3.7.1 polyDADMAC:- poly-diallyldimethylammonium chloride is the most commonly used primary coagulant (Hendricks, 2006). It is prepared by addition polymerization with molecular weights 50,000 – 200,000 being most common for water treatment. These polymers are completely quaternized and are linear in structure with repeating pyrrolidine rings, and they are chlorine resistant (Bratby, 2006). One of the polyDADMAC polymers is manufactured under the trade name "Cat-Floc" and was the first to be approved by the Food and Drug Administration for use in potable water treatment (Hendricks, 2006).

2.6.3.7.2 Epi/DMA: - the epi/DMA group of polymers are used also as primary coagulants (the chemical name of the group is poly-2-hydroxypropyl-N, N-

dimethylammonium chloride). The group is referred to most often as polyamines. Other names include quaternized polyamines, polyquatenary amines, and epi/DMA polymers, with the latter name referring to primary raw materials epichlorohydrin and dimethylamine.

2.6.3.7.3 Polyamines: - this is the third group of primary coagulant polymers, which includes several types. It has a cationic charge which is pH dependent and they are chlorine sensitive; because of these characteristics, they are used less frequently for water treatment than either polyDADMAC or epi/DMA.

2.6.3.7.4 Quaternized Polyamines: - polyamines may be quatenized, which means that all four hydrogens of ammonium, NH_4^+, are replaced by organic groups. Such result makes the monomers more resistant to chlorine; another important characteristic is that their charge does not change with pH (Hendricks, 2006).

2.6.3.8 Electrophoresis measurements and streaming current measurements

Electrophoresis refers to the movement of a charged particle suspended in a fluid induced by an applied electrical force. When a direct-current electric field is applied across a suspension containing particles with a net double layer charge, the particles will migrate to the positive or negative pole depending on whether the particles carry a negative or positive respectively. The mathematical expression for measuring electrophoretic mobility (EM) is:

$$EM = \frac{v}{\delta V/\delta x} \qquad (2.37)$$

In which

EM = electrophoretic mobility (µm/s/volt/cm),

v = velocity of particle in electric field (cm/s),

δV = voltage drop across electrode plates (volts),

δx = distance of separation between electrode plates (m).

Electrophoretic mobility may be converted to zeta potential using an expression related to particle size and electrolyte concentration (Bratby, 2006). However, because of difficulties in assigning values to various terms in the appropriate equations, the calculated zeta potential may differ significantly from the true value.

Therefore, for this reason, many workers express results solely in terms of electrophoretic mobility rather than convert to zeta potential.

When a colloid move in the electric field, some of the counter ions in the ion cloud around the particle move with it. A plane of shear is developed in the diffused layer as shown in Fig. 2-13. The electric potential in volts from the plane of shear to the bulk of the solution is the zeta-potential and is designated with the symbol, ζ, which is a measure of the particle charge causing the motion. The magnitude of the zeta-potential is calculated from measurements of electrophoretic mobility and is measured by a particle charge detector.

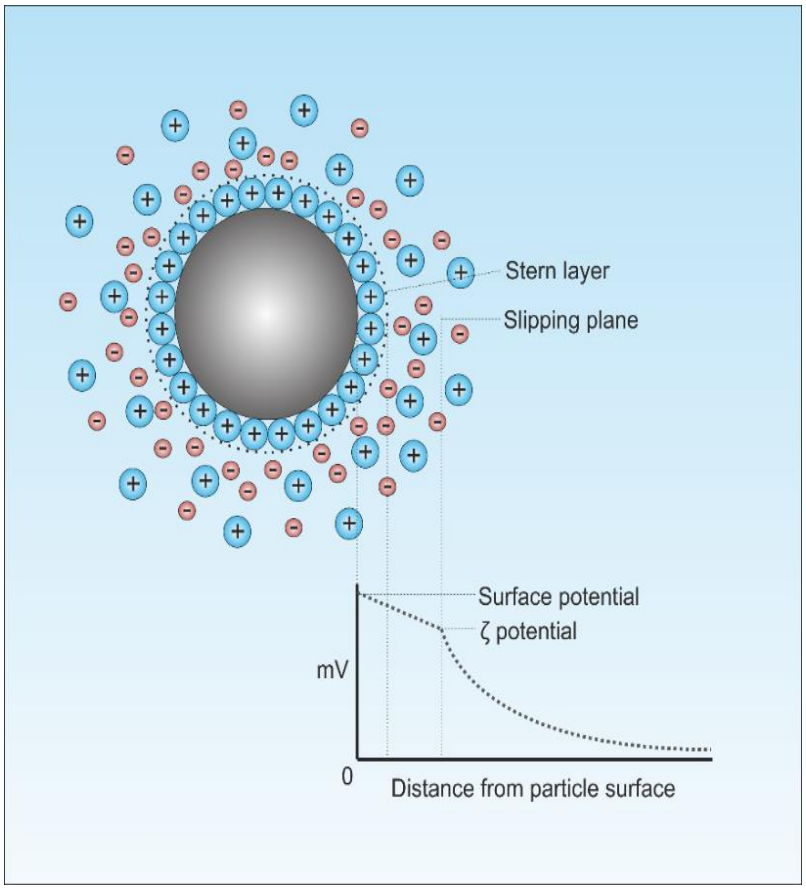

Figure 2-13: Schematic diagram showing the distribution of ions around a charged particle.

The Helmholtz-Smoluchowski equation is the usual equation used to convert EM to zeta potential. The relation is,

$$\zeta = \frac{4\pi\mu}{D} \cdot EM \qquad (2.38)$$

Where

ζ = zeta-potential (mv)

μ = viscosity of water medium (Ns/m^2)

D = dielectric constant for medium (dimensionless)

At the *iso-electric point*, the zeta-potential is zero (Hendricks, 2006). The iso-electric point can be demonstrated by plotting zeta-potential vs coagulant dose or zeta-potential vs pH.

The theory of the zeta-potential is that when the proper dosage of coagulant is added, the zeta-potential should be zero. Thus coagulant dosage can be determined using zeta-potential.

Sharp et al. (2005) investigated the applicability of zeta potential as a control tool on two waters high in natural organic matter (NOM). They found that with both waters, the window of zeta potential for minimum residual dissolved organic carbon (DOC) was approximately -5 to +5 mV. This optimum range was the same for both alum and ferric sulfate used as coagulants. Of the variables that affect zeta-potential, pH and coagulant dosage are very important.

A disadvantage cited of electrophoretic measurements is that they are relatively lengthy and subjective, requiring visual observation and timing of individual particles – although modern instruments do incorporate automatic particle tracking (Bratby, 2006).

Streaming current measurements, on the other hand, have the advantages of speed and are not as subjective as tests of electrophoresis. Furthermore, with the streaming current technique, results obtained are immediately in terms of average for the system. Streaming current devices measure the net residual charge surrounding particles in water. The particles have a net negative surface charge. Coagulant such as alum, ferric salts, or cationic polymers surround the particles with cations or positive charges and reduce or reverse the net surface charge. When in control mode, the streaming current monitor alters the coagulant dose until a preset end point is reached. This set point is determined by jar tests and confirmatory streaming current measurements.

The streaming current is related to zeta potential as follows:

$$i = ZD/N \quad (2.39)$$

Where

i = streaming current

Z = zeta potential

D = dielectric constant

N = viscosity.

2.6.4 Oxidation

2.6.4.1 Chemical oxidation: In an anoxic environment (such as natural groundwater), As (III) is the predominant form of arsenic. Oxidation is mainly used to convert soluble As (III) to As (V), which is then followed by precipitation of As (V) (Masscheleyn et al., 1991). As (V) is less mobile and more easily adsorbed on surfaces than As (III), thus adsorption after oxidation is thought to be effective for arsenic removal (Ghurye and Clifford, 2004; Leupin and Hug, 2005). Oxidants widely used for oxidation of As (III) to As (V) are ozone (O_3), hydrogen peroxide (H_2O_2), chlorine (Cl_2), permanganate, chloramine (NH_2Cl) and Fenton type reagents. Potassium permanganate can be used as an inexpensive reagent for oxidation of As (III) to As (V) in developing countries. One of the most effective oxidants is chlorine but it can produce toxic and carcinogenic trihalomethanes after reacting with organic matter (Ghosh (Nath) et al., 2019). Another option for As (III) to As (V) oxidation is an ultraviolet radiation alone or with a suitable light absorber (e.g. TiO_2) (Litter et al., 2010). The reaction of As (III) and oxidants such as O_3, Cl_2, NH_2Cl, H_2O_2 and ferrate follow the first order kinetics, thus the concentration of As (III) and the oxidants are the most important parameters for effective As removal from aqueous solution (Mondal et al., 2013). The equation below shows the oxidation of As (III) to As (V) (Sharma et al., 2007)

$$As(OH)_3 + H_2O \rightarrow AsO_4^{3-} + 5H^+ + 2e^-$$

$$E^0 = -0.56\ V$$

The oxidation of As (III) to As (V) is very fast for permanganate, chlorine and ozone compared to hydrogen peroxide and chloramine (Dodd et al., 2006; Ghurye and

Clifford, 2004; Lee et al., 2003; Pettine et al., 1999). It is reported that only 54 – 57 % of As (III) can be oxidized to As (V) by using air and pure oxygen but complete oxidation of As (III) can only be achieved with ozone (Kim and Nriagu, 2000). However the process is very expensive as a result of high energy input needed for the reaction (Jiang, 2001). Some of the major challenges of this process is the formation of toxic by-products (especially when the water contains bromide and iodine) and the removal of residual ozone from the water. Manganese dioxide coated sand has been found to be an effective oxidant as well as an adsorbent. It is more effective when combined with Fe containing compounds because the treated products can be filtered out easily (Bajpai Sanjeev and Chaudhuri Malay, 1999). Li et al. (2010) showed that pyrolusite (α-MnO_2) can remove up to 90 % of arsenic at pH 6.0. The reaction can be expressed as:

$MnO_2 + H_3AsO_3 \rightarrow MnHAsO_4 + H_2O$

One of the most effective oxidizing agents in As (III) oxidation is persulphate ($S_2O_8^{2-}$). The process generates highly reactive persulphate radicals which need activation energy. The source of energy can be UV (photochemical) or acoustic (sonochemical) activation (Neppolian et al., 2010). The reactions are as follows:

As (III) + SO_4^{-}* $\rightarrow$ As (IV) + SO_4^{2-}

As (IV) + SO_4^{-}* $\rightarrow$ As (V) + SO_4^{2-}

SO_4^{-}* +$H_2 \rightarrow$ HO* + H^+ + SO_4^{2-}

As (III) + HO* $\rightarrow$ As (IV) + HO^-

The major advantage of the persulfate reaction is the formation of the hydroxyl radical. This OH^-* helps to generate an unstable As (IV) which instantly transforms into As (V). The presence of dissolved oxygen speeds up the reaction whereas the presence of humic acid slows down the reaction by quenching the free radicals (Neppolian et al., 2010). Generally, the persulphate reaction occurs as follows:

As (III) + $S_2O_8^{2-} \rightarrow$ As (V) + $2SO_4^{2-}$

2.6.4.2 Microbiological oxidation : Clark et al. (1918) were first to report bacterial oxidation of As (III) to As (V). There are different microbial organisms available in nature which can oxidize As (III) to As (V) but only few of them can be

considered for the use in drinking water (Kowalski, 2014). One of the most important criterial in bacterial selection is the pathogenicity. Battaglia-Brunet et al. (2002) reported that CASO1 population contains a mixture of organisms such as *Thiomonas* and *Ralstonia pickettii* which are capable of oxidizing As (III) to As (V). They further stated that some of the important characteristics of the mixture are (a) works over a wide pH range, temperature and As (III) concentration, (b) requires low nutrients as it is autotrophic and (c) has high As (III) oxidizing capability. Casiot et al. (2006) reported that organisms such as *Gallionella ferruginea* and *Leptothrix ochracea* also promote As (III) oxidation. Katsoyiannis and Zouboulis (2004) reported that bacteria also help in adsorbing and removing arsenic from contaminated water in addition to their oxidizing capabilities. He further showed the reaction that occurs when an arsenite oxidizing bacteria transform As (III) to As (V) with the help of oxygen. Table 2-8 showed arsenic removal efficient using different oxidants at various operating conditions.

$$H_3AsO_3 + 1/2O_2 \xrightarrow{\text{Bacteria}} H_3AsO_4$$

2.6.5 Flotation

Flotation technology has been used for a long time in ore processing in the mineral industry. Heavy metals are removed from a liquid phase by attaching them to bubbles (Fu and Wang, 2011). There are different types of flotation in which metal ions can be removed from solution such as dissolved air flotation (DAF), ion flotation, electrolytic flotation and precipitation flotation. The flotation method relies on factors such as wetting characteristics and surface properties of particles to separate particles from solution (Al-Zoubi et al., 2015a).

Table 2-8: Different oxidizing agents and their removal efficiencies (Mondal et al., 2013).

Oxidants	Operating pH	Initial As Conc.	Type of water	Remarks	Reference
Free available chlorine ($HOCl + OCl^-$)	7	50 µg/L	Real water	The oxidation of As (III) was very fast and the oxidation of As (III) can be achieved below 1 µg/L within 10 s by using 0.1 mg/l Cl_2 when initial As concentration was 50 µg/L.	(Dodd et al., 2006)
O_3, pure air and oxygen	7.6 – 8.5	46 – 62 µg/L	Groundwater	Oxidation with ozone is faster than by pure oxygen or air >96 % oxidation of As (III) was achieved within 10 min whereas to oxidize >50 % of As (III) by air and pure oxygen, 5 d oxidation is needed.	(Kim and Nriagu, 2000)
MnO_4^-	6.3 – 8.3	50 µg/L	Synthetic water	More than 95 % oxidation was observed in less than 20 s in the presence of three time of stoichiometric amount of MnO_4^-	(Ghurye and
Cl_2O	6.3 – 8.3	50 µg/L	Synthetic water	Not very effective for oxidation but in presence of high ammonia, partial oxidation is possible	Clifford, 2004)
FeO_4^{2-}	8.4 – 12.9	517 µg/L	River water	Total As concentration decreases below 50 µg/L from 517 µg/L due to the oxidation of As (III) by Fe (VI)	(Lee et al., 2003)
H_2O_2	7.5 – 10.3	0.65 µmol/L	Sea and river water	The rate of oxidation increases when the pH increases from 7.5 to 10.3	(Pettine et al., 1999)
Hypochlorite	3 – 8	3 mg/L	Laboratory water	Highest oxidation (100%) achieved at pH 7 by *in situ* hypochlorite generation process (in presence of 125 mg/L chlorine, 0.04 mA/dm^2 current density and 300 K temperature)	(Vasudevan et al., 2006)

MnO_2 coated nanostructured capsule	5.7 – 5.8	0.1 – 1.0 mg/L	Laboratory water	100% oxidation for lower initial As concentration (0.1 and 0.3 mg/L) but for 0.7 and 1.0 mg/L initial As concentration, the maximum oxidation achieved was 90% and 73% even after 24 h	(Criscuoli et al., 2012)
Photocatalytic oxidation					
UV-C/H_2O_2 and UV-A/TiO_2	7	500 µg/L	Ultrapure water (18.2 MΩ cm)	Removal percentage increases after peroxidation and there was no significant difference observed on As removal by Fe (III) or Al (III)	(Yoon and Lee, 2005)
UV light in presence of oxygen and iron	0.5 – 2.5	150 mg/L	Milli Q water	Iron based compounds used as photo-oxidant because the precipitate of iron hydroxides acts as an adsorbent for As (V) and > 0.97 mg/l/min rate of oxidation was achieved in presence of ~800 mg/l iron-complexing anions	(Emett and Khoe, 2001)
Solar light and iron citrate complex	-	2.09 – 5.58 µmol/L	River and synthetic water	Above 90 % total As was removed after 4 h irradiation. However As (III) removal was faster (80% removed in 1 h irradiation) than As (V) (4 h irradiation for 80 % removal)	(Lara et al., 2006)
TiO_2 photo-catalyzed oxidation	4.0 – 9.0	40 – 200 µ M	Laboratory water	This process is able to remove As below 10 µg/L	(Liu et al., 2008)
Photochemical oxidation in ferrioxalate	3 – 7	1.3 – 13,500 µM	Laboratory water	Maximum oxidation achieved at pH 5	(Kocar and Inskeep, 2003)
Photochemical oxidation assisted by peroxydisulfate ions	3	0.07 – 0.675 mM	Milli Q water	UV light intensity and dissolved oxygen are important parameter for oxidation of As (III). Oxidation achieved via sulfate radical	(Neppolian et al., 2008)

Dissolved air flotation was first applied in the processing and dressing of ores at the end of the 19th century and was later introduced to the water industry in the 1920s (Kordmostafapour et al., 2006). Al-Zoubi et al. (2015a) studied the removal of Cd, Ni, Mn, and Pb from wastewater using economic polymeric collectors. Kordmostafapour et al. (2006) also conducted research on arsenic removal from water using DAF where 99 % of arsenic was removed using polyaluminium chloride (PAC) with a flocculation time of 5 to 20 min, coagulant concentration of 40 mg/L and saturation pressure of 4.5 atm.

Ion flotation is another method which is showing great potential in removing heavy metals from drinking water. The process involves the attachment of hydrophilic ions on gas bubbles introduced into the solution and then removal of the ions by bubbles from solution (Hoseinian et al., 2015). Yuan et al. (2008) evaluated the potential of removing Pb, Cu, and Cd from a dilute aqueous solution under different operating parameters such as initial solution pH, the collector to heavy metal ratio and the ionic strength (NaCl). Ion flotation was also applied to removing Ni(II) and Zn(II) ions from low concentration synthetic wastewaters (Hoseinian et al., 2015).

Precipitation is another flotation method based on the formation of a precipitate and subsequent removal by attachment to air bubbles (Fu and Wang, 2011). Stalidis et al. (1989) investigate the selective precipitation and flotation of Cu, Zn, and As from dilute aqueous solution. A laboratory scale investigation was carried out by Medina et al. (2005) to remove Cr (III) by precipitate flotation from dilute aqueous solutions using sodium dodecylsulfate (SDS) as an anionic collector and ethanol as a frother. 96.2 % removal was achieved at pH 8.0.

2.6.5.1 Dissolved air flotation

DAF is a solid-liquid separation process in which nucleated microbubbles are introduced to a suspension comprising flocculated particles. Collision and attachment of bubbles and particles create low density bubble-particle agglomerates which rise to the surface to form a float layer and can be removed mechanically or hydraulically. In water and wastewater treatment plants (WTPs/WWTPs), DAF is used for the removal of low-density contaminants such as algae and natural organic matter (NOM) from reservoir water or waste stabilisation ponds (WSPs). Coagulation-flocculation is conventionally applied to reduce particle and colloid

charge, increase particle sizes, complex with NOM and ensure bubble-particle interactions and subsequent removal efficiencies are optimal (Edzwald, 2010). Below is a typical conventional DAF plant.

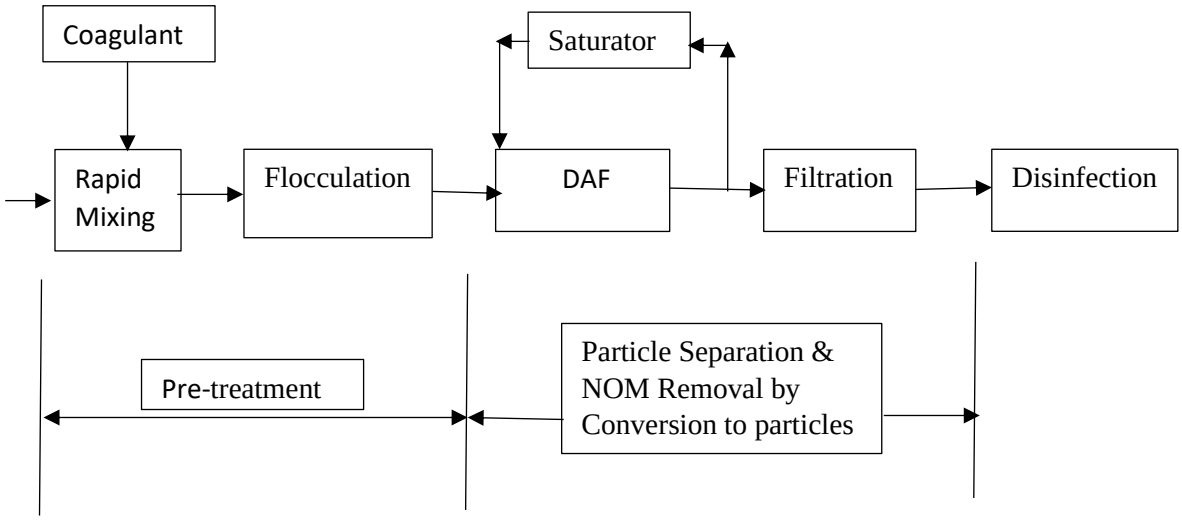

Figure 2-14: A typical water treatment plant with DAF (Edzwald, 2010).

Performance evaluation and operating strategies of DAF systems for treating poultry slaughterhouse wastewater was carried out by (de Nardi et al., 2008). Average removal efficiencies of 43 ± 15 % suspended solids (SS) and 49 ± 8 % oil and grease were achieved by using 24 mg Al^{3+}/L, polyaluminium chloride (PAC) associated with 1.5 mg/L anionic polymer. Coagulation and DAF treatment of semi-aerobic landfill leachate was shown to have optimum operating conditions of 599.22 mg/L of $FeCl_3$ at pH 4.76 and a saturator pressure of 600 kPa, flowrate of 6 L/min and injection time of 101 s (Adlan et al., 2011). Algae removal was conducted at Morton Jaffray water works, Harare, Zimbabwe (Hoko and Makado, 2011) where parameters considered included contact time, coagulant and algaecide doses. It was concluded that algae removal was better at pH 7.0 compared to 7.5 and also algae removal increases with increasing contact times, increasing algaecide dosage and increasing settling. DAF has also been used to remove zinc chloride, lead (II) nitrate, manganese (II) chloride, nickel chloride and cadmium chloride from wastewater with the aid of polymers (polyethylene alcohol, polyethylene glycol and chitosan). The studied heavy metals are (Al-Zoubi et al., 2015b). The results showed that chitosan performed better in affecting removal of Cd (29 %), Ni (27 %), Mn (31 %), and Pb (29 %).

DAF can also be integrated into water treatment. Flotation can be placed above the filter in a vertical arrangement simply called flotation over filtration. It is also abbreviated as DAFF or DAF/F (Edzwald, 2010). This process has a smaller plant footprint thereby reducing the land area, which is important for large cities where land is expensive. It also has the advantage of construction cost savings having one structure for flotation and filtration compared to the conventional plants with a horizontal layout of separate units (Edzwald, 2010). DAF have been used extensively for removing algae, oil and greases and heavy metals from WTPs but not many studies have been carried out on removing the current emerging organic contaminants which can be toxic to humans and animals and also give the drinking water undesirable taste and odour. Table 2-9 shows the applications of dissolved air flotation.

In a DAF tank, the rise rate of an air bubble is a response of two opposing forces. First, the differential densities of air and water generate a net upward buoyant force. Second, the bubble encounters a drag force resisting the upward movement. For a constant rise rate, these forces need to be in balance (Edzwald and Haarhoff, 2012).

$$F_B = F_D \tag{2.40}$$

$$(\rho_w - \rho_b)gV_b = \frac{C_D A_b \rho_w v_b^2}{2} \tag{2.41}$$

Where F_B and F_D are the forces due to buoyancy and drag, respectively; ρ_w and ρ_b are the water and air bubble densities, respectively; V_b is the bubble volume; A_b is the projected area of the bubble in the direction of movement; g is the earth`s gravity acceleration (9.806 m/s^2); v_b is the uniform rise velocity of the bubble; and C_D is the drag coefficient of the rising bubble.

Knowing that DAF bubbles are spheres, V_b is replaced with $(\pi d_b^3)/6$ and A_b with $(\pi d_b^2)/4$. The Reynolds number (Re) for the rising bubble is defined as:

$$Re = \frac{\rho_w v_b d_b}{\mu_w} \tag{2.42}$$

Table 2-9: Dissolved Air Flotation Clarification Applications (Edzwald and Haarhoff, 2012).

Drinking Water Treatment
Clarification in a conventional water treatment plant
Clarification in low-pressure membrane treatment plants and nanotreatment-membrane plants
Clarification in reverse osmosis desalination plants
Clarification in water reclamation/water reuse
Treatment of spent filter backwash water
Municipal Wastewater Treatment
Primary clarification
Secondary clarification
Tertiary treatment: Suspended solids removal, phosphorus removal following chemical precipitation
Combined sewer water and storm water treatment
Wastewater reclamation
Thickening of waste suspensions
Industrial Water Supply and Industrial Wastewater Treatment
Chemical industry
Food waste: Vegetable waste, diaries, meat packing, poultry processing, vegetable oil production
Oil production and refineries
Pharmaceutical plants
Pulp and paper mills
Steel mills
Soap manufacturing
Others
Separation of minerals from ores
Removal of PCBs at hazardous waste sites
In situ treatment of lakes for algae and seawaters for algae and oil spills.

The dynamic viscosity of water is μ_w. Laminar flow is indicated if $Re \leq 1$. For laminar flow, the drag coefficient CD is estimated as a function of Re:

$$C_D = \frac{K}{Re} \qquad (2.43)$$

Separation of particles by flotation adheres to the same laws as sedimentation but in the reverse field of force. The governing equation in air flotation separation, as in all gravity-controlled processes, is Stoke's Law which is used to compute the rise rate of bubble flocs, agglomerates, and bubble-oil aggregation.

For solid spheres, K = 24:

$$v_b = \frac{g(\rho_w - \rho_b)d_b^2}{18\mu_w} \quad (2.44)$$

Key design variables in the system controlling efficiency of removal are as follows:

- Gas input rate and volume of gas entrained per unit volume of liquid
- Bubble-size distribution and degree of dispersion
- Surface properties of the suspended matter
- Hydraulic design of the flotation chamber
- Concentration and type of dissolved materials
- Concentration and type of suspended matter or oils
- Chemicals added
- Temperature
- Residence time
- Recycle ratio
- pH

The key to DAF is the dissolution of air (or other suitable gas) under pressure and the reduction of this pressure to form bubbles. The amount of gas going into solution generally obeys Henry`s Law:

$$p = kC \quad (2.45)$$

Where p = partial pressure of the gas

k = Henry`s Law constant

C = concentration of the gas dissolved in the solution

The most important dependent variable in air flotation systems is bubble size. It affects the performance of collisions and attachment of particles to bubbles and bubble rise velocity. Bubbles are formed from cavitation from the pressure drop in the nozzle or injection device. Bubbles first form nuclei and then grow. For

homogenous nucleation the critical bubble diameter (d_{cb}) is predicted in Eq. (2.46). Where σ is the surface tension of water and ΔP is the pressure difference across the injection device such as the nozzle.

$$d_{cb} = \frac{4\sigma}{\Delta P} \quad (2.46)$$

The actual bubble sizes in DAF are affected by heterogeneous nucleation, bubble growth, the injection flow rate, and the injection device, especially the type of nozzle – these are all important factors affecting bubble size.

Air-solids ratio is another important parameter governing the rise rate of bubble-particle agglomerates in solid-particle DAF systems. Eq. (2.47) indicates that as more air bubbles are incorporated into the aggregate, the aggregates net density decreases, and its rise velocity increases.

$$\frac{A}{S} = \frac{1.3a_s}{S_s}(fP_a - 1) \quad (2.47)$$

Where A/S = air to solids ratio, mg/mg

1.3 = weight constant of air, mg/mL

a_s = air solubility, mL/L

f = fraction of air dissolved at a given pressure usually 0.5

Pa = recycle system pressure, atm

Ss = suspended solids concentration, mg/L

For a system where pressurized recycle is used, Eq. (2.47) is modified as follows:

$$\frac{A}{S} = \frac{1.3a_s}{QS_s}(fP_a - 1)R \quad (2.48)$$

Where R = recycle stream flowrate (m^3/day)

Q = water/wastewater flowrate (m^3/day)

Table 2-10 below shows a typical design and operating parameters for conventional rate DAF plants.

Table 2-10: Design and operating parameters for conventional rate DAF plants (Gregory and Edzwald, 2010).

Item	Values	Comments
Pre-treatment flocculation		
Mean detention time (min)	10 – 20	Some as low as 5 min
Number of stages	2	Some with 3 stages
Mixing intensity (G) (s^{-1})	50 - 100	Some as low as 30 and some as high as 150 sec^{-1}
		Propeller or gate flocculators used
		Some use of tapered flocculation
		Some use of hydraulic flocculation
DAF Tank		
Nominal hydraulic loading rate (m/h)	5 – 15	
Separation zone loading rate (m/h)	6 – 18	Based on the through-put flow and 10% recycle flow, and the separation zone area.
Contact zone detention time (min)	1 – 2.5	
Basin depth (m)	2.0 – 3.5	
Recycle and saturator systems		
Air mass (g/m^3)	6 – 10	10% most typical
Recycle rate (%)	6 – 12	Higher pressures for unpacked saturators
Saturator gauge pressure (kPa)	400 – 600	For saturators with packing, unpacked saturators: 50-70%.
Saturator efficiency (%)	80 - 95	Higher efficiencies for higher temperatures.
Floated sludge		
Hydraulic removal	0.5 – 1 % solids	Some as high as 5%
Chain and flight or reciprocating skimmer	2 – 3 % solids	Also called star wheel, sludge roller, and flipper
Beach drum	1 – 3 % solids	

2.6.6 Membrane processes

Membrane processes are reliable in removing specific ions from groundwater or drinking water production. These membranes are made up of billions of holes which act as selective barriers for filtering arsenic. These barriers are designed in such a way that they allow a selective ion to pass through and reject others (Ghosh (Nath) et al., 2019). Generally, there are two types of pressure driven membrane filtration for treating arsenic contaminated water: high pressure membrane and low-pressure membrane filtration. Microfiltration (MF) and ultrafiltration (UF) are examples of low pressure driven processes while nano-filtration (NF) and reverse osmosis (RO) are examples of high-pressure filtration processes. The separation of contaminants in a high pressure process is achieved via capillary flow or solution diffusion whereas a low pressure driven process is achieved via a mechanical sieve (Shih, 2005).

MF is a low pressure membrane filtration process which has a large pore size wide enough to allow dissolved or colloidal arsenic species to pass through from the feed water (Shih, 2005). The MF process is not very effective in removing arsenic therefore techniques such as coagulation-flocculation are used to increase the molecular weight of the particles (Chwirka et al., 2004; Ghurye and Clifford, 2004). B. Han et al. (2002) used ferric chloride ($FeCl_3$) and ferric sulphate ($Fe_2(SO_4)_3$) as flocculants for removing arsenic species which was dependent on arsenic adsorption onto the Fe (III) complex followed by MF. The study further showed that arsenic removal using flocculation followed by MF performed better than flocculation followed by sedimentation. However, pH of the solution and the presence of other ions also affect the adsorption of arsenic onto the Fe (III) complex.

UF is another low-pressure filtration process which depends on mechanical sieving method. Just like MF, UF alone cannot effectively remove arsenic species from a naturally contaminated water due to its pore size which will allow dissolved arsenic to pass through. However, when UF is combined with other techniques, the removal efficiency depends on several factors which makes optimising the process difficult (Mondal et al., 2013). Brandhuber and Amy (2001) reported the effect of charge on the UF membranes in removing arsenic. The bench scale experiments showed that the neutrally charged UF membranes are less effective than the negatively charged UF membranes. The study showed a rejection of 65 % and 53 % for As (V) and As

(III) respectively. However, arsenic removal was affected by factors such as pH of the solution, initial arsenic concentration and the presence of other ions and organic matter.

NF and RO are high pressure filtration processes deemed to remove dissolved As from water to an appreciable level provided the amount of suspended solids in the feed water is low (Figoli et al., 2010). Waypa et al. (1997) reported that NF and RO can remove up to 99 % of both As (III) and As (V) from water. In terms of energy consumption between NF and RO, NF consumes 21 % less energy than RO and a higher water flux can be achieved at lower transmembrane pressure (Košutić et al., 2005).

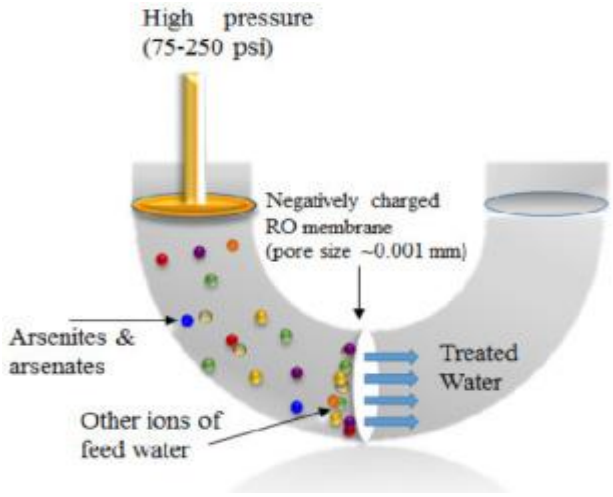

Figure 2-15: Diagram of RO process for arsenic treatment (Ghosh (Nath) et al., 2019).

The RO process occurs at a very high osmotic pressure and low diffusion rate for the water to pass through the membrane (Fig 2-15). These membranes are typically used in a desalination process and more than 99 % (in most cases) rejections of low molecular mass compounds can be achieved (Velizarov et al., 2004). However, one of the major drawbacks for RO is the low rejection of As (III) species compared to As (V). As (V) removal efficiency is ~ 90 % when cellulose-acetate membrane is used compared to a low of 70 % for As (III). Oxidation of As (III) to As (V) is not possible in an RO process as it will only shortened the lifespan of the membrane if there is any possibility of it happening (Geucke et al., 2009; Ghurye and Clifford, 2004; Ning, 2002; Shih, 2005).

Table 2-11: Fate of different constituents of feed raw water in different membrane filtration process (Choong et al., 2007; Ghosh (Nash) et al., 2019; Sarkar and Paul, 2016).

Raw water constituents	Membrane filtration process			
	Microfiltration (membrane pore size 0.1 – 10 mm)	Ultrafiltration (membrane pore size 0.01 – 0.1mm)	Nanofiltration (membrane pore size 0.001 – 0.01 mm)	Reverse osmosis (membrane pore size ~ 0.0001 mm)
Water	Passes through	Passes through	Passes through	Passes through
Monovalent ion/radical	Passes through	Passes through	Passes through	Blocked
Multivalent ion/radical	Passes through	Passes through	Passes through	Blocked
Ions/radical virus	Passes through	Passes through	Partially blocked	Blocked
Bacteria	Passes through	Blocked	Blocked	Blocked
Suspended solids	Blocked	Blocked	Blocked	Blocked

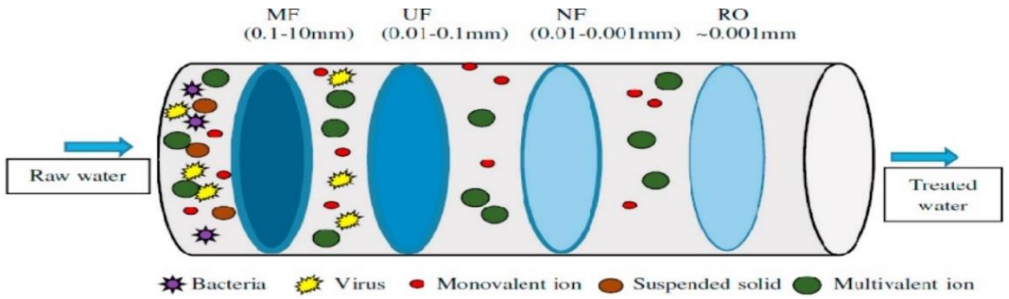

Figure 2-16: Pictorial representation of Table 2.12 (Ghosh (Nath) et al., 2019).

Akin et al. (2011) showed that the feed concentration of arsenic does not affect the rejection rate using RO but the rejection of arsenic species is affected by the pH of the feed water and the operating pressure.

2.6.7 Electro-coagulation (EC)

Electrocoagulation (EC) is an electrochemical process which involves many chemical and physical mechanisms in removing contaminants from water. It is seen as a promising technology and a more acceptable technology than other existing conventional technology (Mollah et al., 2004). Some of the advantages of EC processes are the production of adsorbents within the reactor with less coagulants, less sludge production, less capital costs, less area requirement, sustainable operation in rural areas and relatively low level skills being required (Ghosh (Nath) et al., 2019). EC techniques have been used to remove turbidity (Cañizares et al., 2007), hardness (Malakootian et al., 2010), phosphate (Vasudevan et al., 2009, 2006), fluoride (Vasudevan et al., 2011), copper (Kamaraj et al., 2013; Vasudevan et al., 2012a), mercury (Vasudevan et al., 2012b), lead (Kamaraj et al., 2015; Vasudevan et al., 2012b), cobalt (Vasudevan et al., 2012a), chromium (Vasudevan et al., 2012a), nickel (Vasudevan et al., 2012b), boron (Can et al., 2016; Vasudevan et al., 2013), cadmium (Vasudevan and Lakshmi, 2012, 2011), strontium (Kamaraj and Vasudevan, 2015), cesium (Kamaraj and Vasudevan, 2015), iron (Vasudevan, 2012), oil (Cañizares et al., 2007; Cerqueira et al., 2014) etc. The EC process is also efficient in treating wastewater like textile wastewater (Kobya et al., 2003; M. Kobya et al., 2006; Singh and Ramesh, 2014), oil wastewater (Safari et al., 2016), tannery wastewater (Elabbas et al., 2016), pulp and paper industry effluent (Shankar et al., 2014; Sridhar et al., 2011), poultry slaughterhouse wastewater (Bayramoglu et al., 2006; Mehmet Kobya et al., 2006), dairy wastewater (Sharma, 2014) and paint manufacturing wastewater (Akyol, 2012).

In the EC process, three stages are involved (a) formation of coagulants by electrolytic oxidation of the "*sacrificial electrode"* (b) destabilization of the contaminants, particle suspension, and breaking of emulsions and (c) floc formation from aggregation of destabilized phases (Mollah et al., 2004). The EC process as shown in Fig. 2-17 requires a sacrificial metallic anode, which dissolves into the solution after the application of a direct current (DC). The process uses electrodes like iron, alum, zinc etc. In the anode, the metal dissociates to form di or tri valent

metal ions and in the cathode the water dissociates into H^+ and OH^- ions by water molecules electron interaction. The dissociated H^+ again combines with a free H^+ to form H_2 gas at the cathode (Ghosh (Nath) et al., 2019; Nidheesh and Singh, 2017). The key reactions are as follows:

At the anode:

$M(s) \rightarrow M^{n+}(aq) + ne^-$

$2H_2O \rightarrow 4H^+(aq) + O2(g) + 4e^-$

At the cathode:

$nH_2O + ne^- \rightarrow (n/2)H_2(g) + nOH^-$

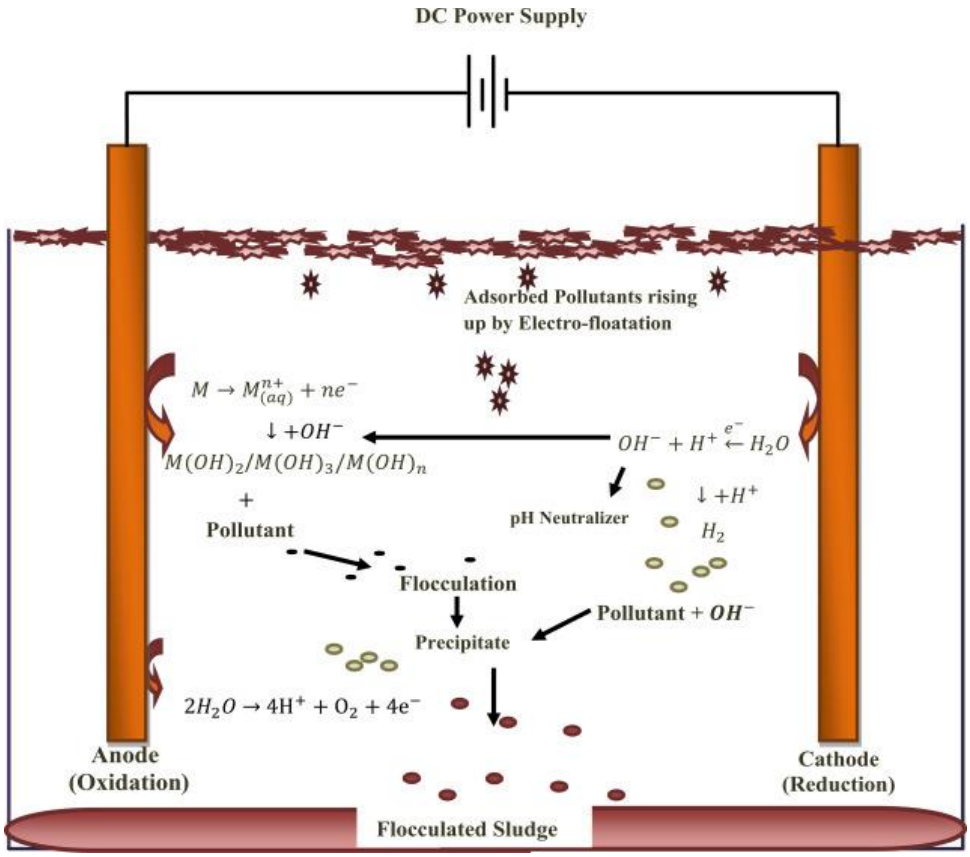

Figure 2-17: Pollutant removal mechanism by electrocoagulation process (Nidheesh and Singh, 2017).

Table 2-12: Summary of recent studies on arsenic removal by EC process.

Arsenic form	Arsenic Concentration	Type of Reactor	Volume of the Reactor	Electrodes used	Optimum condition	Removal Efficiency	Reference
As (III)/(V)	0.05 mg/L	Batch/continuous flow	490 mL	Integrated iron electrode as anode and stainless steel as cathode	As (V): pH 6.5 As (III): pH 8.5	As (V): ~ 99% As (III): ~80%	(Lakshmanan et al., 2010)
As (III)/(V)	0.1 mg/L	Batch Reactor	1000 mL	Fe-Fe	As (III) pH 5 -8 90 min electrolysis As (V) pH 7, 15 min electrolysis	As (III): 99% As (V): 99%	(Wan et al., 2011)
Total As	20 mg/L	Batch reactor with air pumping	1200 mL	Carbon Steel	pH 5.5 – 7	99.7 % with air stripping	(Parga et al., 2005)
Total As	50 μg/L	Continuous reactor	90 mL	Al-Al	pH 8.1, mean linear flow 0.91 cm/s, current density 5 mA/cm^2	More than 99 %	(Flores et al., 2013)
As (V)	20 mg/L	Batch reactor with recirculation	5 L	Iron and Aluminum electrode	Current density 1.0 mA/cm^2	99.99 %	(Lacasa et al., 2013)
As (III)	13.4 mg/L	Batch reactor	250 mL	Al-Al Fe-Fe Al-Fe	pH 2.4, 120 min electrolysis, current density 3mA/cm^2 pH 2.4, 60 min electrolysis, current density 30mA/cm^2	99.3 % 99.6 % 99.6 %	(Gomes et al., 2007)

The dissociated di- or trivalent metallic ions generated combine with the dissociated hydroxyl ions of water at the cathode and form metal hydroxides of the anodic metals. This hydroxide surface is a good adsorbent for the metal ions. These hydroxides act as the adsorbent of arsenic, especially for As (V) species. (Ghosh (Nath) et al., 2019).

Iron and Aluminium are the two most common electrode materials used for the EC process. The use of iron as an anode (for generating iron hydroxide) material is more common than aluminium (for generating aluminium hydroxide) for removing arsenic due to its low cost, easy availability and higher efficiency of these materials (Nidheesh and Singh, 2017). Removal of arsenate is easier than that of arsenite (Table 2-12). Vasudevan et al. (2010) reported complete removal of arsenate from a contaminated water by the EC process. Kobya et al. (2014) tested the eight different electrode combinations (Al-Al-Al-Al; Fe-Fe-Fe-Fe; Fe-Al-Al-Fe; Al-Fe-Fe-Al; Fe-Al-Fe-Al; Al-Fe-Al-Fe; Fe-Al-Al-Al; Al-Fe-Fe-Fe) to test arsenic removal from a contaminated sample with initial concentration 150 μg/L. The results showed that all the different electrode configuration reduced arsenic concentration to less than 10 μg/L within 8 min although the electrode combination of Al-Al-Al-Al took 15 min to reduce arsenic concentration to below 10 μg/L. Other electrodes used in addition to iron and aluminium for arsenic removal are titanium (Ratna Kumar et al., 2004), magnesium (Vasudevan et al., 2012c), zinc (Ali et al., 2013; Maldonado-Reyes et al., 2007), copper (Ali et al., 2013; Maldonado-Reyes et al., 2007), brass (Maldonado-Reyes et al., 2007) etc. Table 2-13 shows the advantages and disadvantages of the different technologies used in removing arsenic from contaminated water.

2.7 Conclusions

The presence of arsenic in surface and/or groundwater is one of the most important environmental problems around the world. The permissible limit of arsenic in drinking water is 10 μg/L and has been set by WHO, US EPA and DWSNZ. A wide range of treatment options such as chemical precipitation, coagulation and flocculation, adsorption, ion exchange, flotation and membrane separation have been used for removing arsenic. The difficulty with coagulation and flocculation techniques is that they remove suspended and dissolved solids as well, resulting in sludge that is contaminated with heavy metals, restricting its use in downstream

applications such as agriculture. The aim of this research is to investigate conditions and methods by which the arsenic can be separated from the bulk of the solids. In this research, individual techniques including adsorption using DMI-65 media, use of different flocculants and coagulants and dissolved air floatation and sedimentation will be investigated to try and preferentially separate the arsenic from the suspended and dissolved solids.

Table 2-13: Advantages and disadvantages of typical arsenic removal methods (Mohan and Pittman Jr., 2007; Mondal et al., 2013; Wang et al., 2019).

Major Oxidation/precipitation technologies	**Removal Efficiency (%)**		**Advantages**	**Disadvantages**
	As (III)	**As (V)**		
Air oxidation	≤ 30	≤ 30	Relatively simple, low cost but slow process; in situ arsenic removal; also oxidizes other inorganic and organic constituents in water	Mainly removes As (V) and accelerates the oxidation process
Chemical oxidation	≤ 30	30 – 60	Oxidizes other impurities and kills microbes; relatively simple and rapid process; minimum residual mass	Efficient control of the pH and oxidation step is needed
Major Coagulation/co-precipitation technologies			Advantages	Disadvantages
Alum coagulation	≤ 30	≥ 90	Durable powder chemicals are available; relatively low capital cost and simple in operation; effective over a wide range of pH	Produces toxic sludges; low removal of arsenic; pre-oxidation may be required
Iron coagulation	60 – 90	≥ 90	Common chemicals are available; more efficient than alum coagulation on weight basis	Medium removal of As (III); sedimentation and filtration needed
Lime softening	30 - 60	≥ 90	Chemicals are available commercially	Readjustment of pH is required

Major sorption and ion-exchange technologies			Advantages	Disadvantages
Activated alumina	60 – 90	≥ 90	Relatively well known and commercially available	Needs replacement after four to five regeneration
Iron coated sand			Cheap; no regeneration is required; removes both As (III) and As (V)	Not standardized; produces toxic solid waste
Ion-exchange resin			Well-defined medium and capacity; pH independent; exclusive ion-specific resin to remove arsenic	High cost medium; high-tech operation and maintenance; regeneration creates a sludge disposal problem; As (III) is difficult to remove; lifespan of resin is limited
Major membrane technologies			Advantages	Disadvantages
Nanofiltration	60 – 90	60 – 90	Well-defined and high-removal efficiency	Very high-capital and running cost, pre-conditioning; high water rejection
			No toxic solid waste is produced	High tech operation and maintenance
Reverse osmosis	60 – 90	60 – 90	Capable of removal of other contaminants	Toxic wastewater produced
Electrodialysis	60 - 90	≥ 90		

References

Addo Ntim, S., Mitra, S., 2012. Adsorption of arsenic on multiwall carbon nanotube–zirconia nanohybrid for potential drinking water purification. J. Colloid Interface Sci. 375, 154–159. https://doi.org/10.1016/j.jcis.2012.01.063

Adlan, M.N., Palaniandy, P., Aziz, H.A., 2011. Optimization of coagulation and dissolved air flotation (DAF) treatment of semi-aerobic landfill leachate using response surface methodology (RSM). Desalination 277, 74–82. https://doi.org/10.1016/j.desal.2011.04.006

Aggett, J., Aspell, A.C., 1980. Arsenic from geothermal sources in the Waikato catchment. New Zealand Journal of Science 1, 77–82.

Agrafioti, E., Kalderis, D., Diamadopoulos, E., 2014. Arsenic and chromium removal from water using biochars derived from rice husk, organic solid wastes and sewage sludge. J. Environ. Manage. 133, 309–314. https://doi.org/10.1016/j.jenvman.2013.12.007

Ahamad, K.U., Singh, R., Baruah, I., Choudhury, H., Sharma, M.R., 2018. Equilibrium and kinetics modeling of fluoride adsorption onto activated alumina, alum and brick powder. Groundw. Sustain. Dev. 7, 452–458. https://doi.org/10.1016/j.gsd.2018.06.005

Aharoni, C., Sideman, S., Hoffer, E., 1979. Adsorption of phosphate ions by collodion-coated alumina. J. Chem. Technol. Biotechnol. 29, 404–412. https://doi.org/10.1002/jctb.503290703

Ahmad, A.A., Hameed, B.H., 2010. Fixed-bed adsorption of reactive azo dye onto granular activated carbon prepared from waste. J. Hazard. Mater. 175, 298–303. https://doi.org/10.1016/j.jhazmat.2009.10.003

Akin, I., Arslan, G., Tor, A., Cengeloglu, Y., Ersoz, M., 2011. Removal of arsenate [As(V)] and arsenite [As(III)] from water by SWHR and BW-30 reverse osmosis. Desalination 281, 88–92. https://doi.org/10.1016/j.desal.2011.07.062

Akyol, A., 2012. Treatment of paint manufacturing wastewater by electrocoagulation. Desalination 285, 91–99. https://doi.org/10.1016/j.desal.2011.09.039

Ali, I., Asim, M., Khan, T.A., 2013. Arsenite removal from water by electro-coagulation on zinc–zinc and copper–copper electrodes. Int. J. Environ. Sci. Technol. 10, 377–384. https://doi.org/10.1007/s13762-012-0113-z

Allen, S.J., Whitten, L.J., Murray, M., Duggan, O., Brown, P., 1997. The Adsorption of Pollutants by Peat, Lignite and Activated Chars. J. Chem. Technol. Biotechnol. 68, 442–452. https://doi.org/10.1002/(SICI)1097-4660(199704)68:4<442::AID-JCTB643>3.0.CO;2-2

Altundoğan, H.S., Altundoğan, S., Tümen, F., Bildik, M., 2002. Arsenic adsorption from aqueous solutions by activated red mud. Waste Manag. 22, 357–363. https://doi.org/10.1016/S0956-053X(01)00041-1

Alyüz, B., Veli, S., 2009. Kinetics and equilibrium studies for the removal of nickel and zinc from aqueous solutions by ion exchange resins. J. Hazard. Mater. 167, 482–488. https://doi.org/10.1016/j.jhazmat.2009.01.006

Al-Zoubi, H., Ibrahim, K.A., Abu-Sbeih, K.A., 2015a. Removal of heavy metals from wastewater by economical polymeric collectors using dissolved air flotation process. J. Water Process Eng. 8, 19–27. https://doi.org/10.1016/j.jwpe.2015.08.002

Al-Zoubi, H., Ibrahim, K.A., Abu-Sbeih, K.A., 2015b. Removal of heavy metals from wastewater by economical polymeric collectors using dissolved air flotation process. J. Water Process Eng. 8, 19–27. https://doi.org/10.1016/j.jwpe.2015.08.002

Andrianisa, H.A., Ito, A., Sasaki, A., Aizawa, J., Umita, T., 2008. Biotransformation of arsenic species by activated sludge and removal of bio-oxidised arsenate from wastewater by coagulation with ferric chloride. Water Res. 42, 4809–4817. https://doi.org/10.1016/j.watres.2008.08.027

Ansari, R., Sadegh, M., 2007. Application of Activated Carbon for Removal of Arsenic Ions from Aqueous Solutions [WWW Document]. J. Chem. https://doi.org/10.1155/2007/829187

Antonio Violante, *, Mariarosaria Ricciardella, Stefania Del Gaudio, and, Pigna, M., 2006. Coprecipitation of Arsenate with Metal Oxides: Nature, Mineralogy, and Reactivity of Aluminum Precipitates [WWW Document]. https://doi.org/10.1021/es052321m

Asmel, N.K., Yusoff, A.R.M., Sivarama Krishna, L., Majid, Z.A., Salmiati, S., 2017. High concentration arsenic removal from aqueous solution using nano-iron ion enrich material (NIIEM) super adsorbent. Chem. Eng. J. 317, 343–355. https://doi.org/10.1016/j.cej.2017.02.039

Azizur Rahman, M., Hasegawa, H., Mahfuzur Rahman, M., Mazid Miah, M.A., Tasmin, A., 2008. Arsenic accumulation in rice (Oryza sativa L.): Human exposure through food chain. Ecotoxicol. Environ. Saf. 69, 317–324. https://doi.org/10.1016/j.ecoenv.2007.01.005

Badruzzaman, M., Westerhoff, P., Knappe, D.R.U., 2004. Intraparticle diffusion and adsorption of arsenate onto granular ferric hydroxide (GFH). Water Res. 38, 4002–4012. https://doi.org/10.1016/j.watres.2004.07.007

Bajpai Sanjeev, Chaudhuri Malay, 1999. Removal of Arsenic from Ground Water by Manganese Dioxide–Coated Sand. J. Environ. Eng. 125, 782–784. https://doi.org/10.1061/(ASCE)0733-9372(1999)125:8(782)

Bang, S., Patel, M., Lippincott, L., Meng, X., 2005. Removal of arsenic from groundwater by granular titanium dioxide adsorbent. Chemosphere 60, 389–397. https://doi.org/10.1016/j.chemosphere.2004.12.008

Barbee, J.Y., Prince, T.S., 1999. Acute respiratory distress syndrome in a welder exposed to metal fumes. South. Med. J. 92, 510–512.

Bartolomé, B., Córdoba, S., Nieto, S., Fernández-Herrera, J., García-Díez, A., 1999. Acute arsenic poisoning: clinical and histopathological features. Br. J. Dermatol. 141, 1106–1109. https://doi.org/10.1046/j.1365-2133.1999.03213.x

Battaglia-Brunet, F., Dictor, M.-C., Garrido, F., Crouzet, C., Morin, D., Dekeyser, K., Clarens, M., Baranger, P., 2002. An arsenic(III)-oxidizing bacterial population: selection, characterization, and performance in reactors. J. Appl. Microbiol. 93, 656–667. https://doi.org/10.1046/j.1365-2672.2002.01726.x

Bayramoglu, M., Kobya, M., Eyvaz, M., Senturk, E., 2006. Technical and economic analysis of electrocoagulation for the treatment of poultry slaughterhouse wastewater. Sep. Purif. Technol. 51, 404–408. https://doi.org/10.1016/j.seppur.2006.03.003

Bektaş, N., Kara, S., 2004. Removal of lead from aqueous solutions by natural clinoptilolite: equilibrium and kinetic studies. Sep. Purif. Technol. 39, 189–200. https://doi.org/10.1016/j.seppur.2003.12.001

Beltrán Heredia, J., Sánchez Martín, J., 2009. Removing heavy metals from polluted surface water with a tannin-based flocculant agent. J. Hazard. Mater. 165, 1215–1218. https://doi.org/10.1016/j.jhazmat.2008.09.104

Bertinato, J., L'Abbé, M.R., 2004. Maintaining copper homeostasis: regulation of copper-trafficking proteins in response to copper deficiency or overload. J. Nutr. Biochem. 15, 316–322. https://doi.org/10.1016/j.jnutbio.2004.02.004

Bilici Baskan, M., Pala, A., 2010. A statistical experiment design approach for arsenic removal by coagulation process using aluminum sulfate. Desalination 254, 42–48. https://doi.org/10.1016/j.desal.2009.12.016

Bonzongo, J.C., Heim, K.J., Warwick, J.J., Lyons, W.B., 1996. Mercury levels in surface waters of the Carson River-Lahontan Reservoir system, Nevada: Influence of historic mining activities. Environ. Pollut. Barking Essex 1987 92, 193–201.

Brandhuber, P., Amy, G., 2001. Arsenic removal by a charged ultrafiltration membrane — influences of membrane operating conditions and water quality on arsenic rejection. Desalination 140, 1–14. https://doi.org/10.1016/S0011-9164(01)00350-2

Bratby, J., 2006. Coagulation and flocculation in water and wastewater treatment, 2nd ed. IWA Publishing, Alliance House, 12 Caxton Street, London SW1H 0QS, UK, United Kingdom.

Budinova, T., Petrov, N., Razvigorova, M., Parra, J., Galiatsatou, P., 2006. Removal of Arsenic(III) from Aqueous Solution by Activated Carbons Prepared from Solvent Extracted Olive Pulp and Olive Stones. Ind. Eng. Chem. Res. 45, 1896–1901. https://doi.org/10.1021/ie051217a

Can, B.Z., Boncukcuoğlu, R., Yılmaz, A.E., Fil, B.A., 2016. Arsenic and Boron Removal by Electrocoagulation with Aluminum Electrodes. Arab. J. Sci. Eng. 41, 2229–2237. https://doi.org/10.1007/s13369-015-1922-4

Can, Ö., Balköse, D., Ülkü, S., 2010. Batch and column studies on heavy metal removal using a local zeolitic tuff. Desalination 259, 17–21. https://doi.org/10.1016/j.desal.2010.04.047

Cañizares, P., Jiménez, C., Martínez, F., Sáez, C., Rodrigo, M.A., 2007. Study of the Electrocoagulation Process Using Aluminum and Iron Electrodes. Ind. Eng. Chem. Res. 46, 6189–6195. https://doi.org/10.1021/ie070059f

Casiot, C., Pedron, V., Bruneel, O., Duran, R., Personné, J.C., Grapin, G., Drakidès, C., Elbaz-Poulichet, F., 2006. A new bacterial strain mediating As oxidation in the Fe-rich biofilm naturally growing in a groundwater Fe treatment pilot unit. Chemosphere 64, 492–496. https://doi.org/10.1016/j.chemosphere.2005.11.072

Cerqueira, A.A., Souza, P.S.A., Marques, M.R.C., 2014. Effects of direct and alternating current on the treatment of oily water in an electroflocculation process. Braz. J. Chem. Eng. 31, 693–701. https://doi.org/10.1590/0104-6632.20140313s00002363

Chammui, Y., Sooksamiti, P., Naksata, W., Thiansem, S., Arqueropanyo, O., 2014. Removal of arsenic from aqueous solution by adsorption on Leonardite. Chem. Eng. J. 240, 202–210. https://doi.org/10.1016/j.cej.2013.11.083

Chen, Y., Graziano, J.H., Parvez, F., Liu, M., Slavkovich, V., Kalra, T., Argos, M., Islam, T., Ahmed, A., Rakibuz-Zaman, M., Hasan, R., Sarwar, G., Levy, D., Geen, A. van, Ahsan, H., 2011. Arsenic exposure from drinking water and mortality from cardiovascular disease in Bangladesh: prospective cohort study. BMJ 342, d2431. https://doi.org/10.1136/bmj.d2431

Chen, Y., Karagas, M.R., 2013. Arsenic and Cardiovascular Disease: New Evidence From the United States. Ann. Intern. Med. https://doi.org/10.7326/0003-4819-159-10-201311190-00720

Cheong, W.J., Yang, S.H., Ali, F., 2013. Molecular imprinted polymers for separation science: A review of reviews. J. Sep. SCI 36, 609–628.

Chien, S.H., Clayton, W.R., 1980. Application of Elovich Equation to the Kinetics of Phosphate Release and Sorption in Soils 1. Soil Sci. Soc. Am. J. 44, 265–268. https://doi.org/10.2136/sssaj1980.03615995004400020013x

Choong, T.S.Y., Chuah, T.G., Robiah, Y., Gregory Koay, F.L., Azni, I., 2007. Arsenic toxicity, health hazards and removal techniques from water: an overview. Desalination 217, 139–166. https://doi.org/10.1016/j.desal.2007.01.015

Choy, S.Y., Prasad, K.M.N., Wu, T.Y., Raghunandan, M.E., Ramanan, R.N., 2014. Utilization of plant-based natural coagulants as future alternatives towards sustainable water clarification. J. Environ. Sci. 26, 2178–2189. https://doi.org/10.1016/j.jes.2014.09.024

Choy, S.Y., Prasad, K.N., Wu, T.Y., Raghunandan, M.E., Ramanan, R.N., 2016. Performance of conventional starches as natural coagulants for turbidity removal. Ecol. Eng. 94, 352–364. https://doi.org/10.1016/j.ecoleng.2016.05.082

Chwirka, J.D., Colvin, C., Gomez, J.D., Mueller, P.A., 2004. Arsenic removal from drinking water using the coagulation/microfiltration process. J. Am. Water Works Assoc. 96, 106–114.

Clark, W.M., Green, F.W., Race, J., 1918. THE DIFFERENTIATION OF BACTERIA OF THE COLON-AEROGENES FAMILY [with DISCUSSION]. J. Am. Water Works Assoc. 5, 26–35.

Criscuoli, A., Majumdar, S., Figoli, A., Sahoo, G.C., Bafaro, P., Bandyopadhyay, S., Drioli, E., 2012. As(III) oxidation by MnO2 coated PEEK-WC nanostructured capsules. J. Hazard. Mater., Nanotechnologies for the Treatment of Water, Air and Soil 211–212, 281–287. https://doi.org/10.1016/j.jhazmat.2011.11.023

D. Smith, S., Edwards, M., 2005. The influence of silica and calcium on arsenate sorption to oxide surfaces. J. Water Supply Res. Technol. - AQUA 54, 201–211. https://doi.org/10.2166/aqua.2005.0019

Dambies, D.L., 2005. Existing and Prospective Sorption Technologies for the Removal of Arsenic in Water. Sep. Sci. Technol. 39, 603–627. https://doi.org/10.1081/SS-120027997

Dambies, L., Guibal, E., Roze, A., 2000. Arsenic(V) sorption on molybdate-impregnated chitosan beads. Colloids Surf. Physicochem. Eng. Asp. 170, 19–31. https://doi.org/10.1016/S0927-7757(00)00484-2

Daus, B., Wennrich, R., Weiss, H., 2004. Sorption materials for arsenic removal from water:: a comparative study. Water Res. 38, 2948–2954. https://doi.org/10.1016/j.watres.2004.04.003

de Nardi, I.R., Fuzi, T.P., Del Nery, V., 2008. Performance evaluation and operating strategies of dissolved-air flotation system treating poultry slaughterhouse wastewater. Resour. Conserv. Recycl. 52, 533–544. https://doi.org/10.1016/j.resconrec.2007.06.005

Del Razo, L.M., García-Vargas, G.G., Valenzuela, O.L., Castellanos, E.H., Sánchez-Peña, L.C., Currier, J.M., Drobná, Z., Loomis, D., Stýblo, M., 2011. Exposure to arsenic in drinking water is associated with increased prevalence of diabetes: a cross-sectional study in the Zimapán and Lagunera regions in Mexico. Environ. Health 10, 73. https://doi.org/10.1186/1476-069X-10-73

Deliyanni, E.A., Peleka, E.N., Matis, K.A., 2007. Removal of zinc ion from water by sorption onto iron-based nanoadsorbent. J. Hazard. Mater. 141, 176–184. https://doi.org/10.1016/j.jhazmat.2006.06.105

Demiral, H., Güngör, C., 2016. Adsorption of copper(II) from aqueous solutions on activated carbon prepared from grape bagasse. J. Clean. Prod. 124, 103–113. https://doi.org/10.1016/j.jclepro.2016.02.084

Demirbas, A., 2008. Heavy metal adsorption onto agro-based waste materials: A review. J. Hazard. Mater. 157, 220–229. https://doi.org/10.1016/j.jhazmat.2008.01.024

Di, Z.-C., Li, Y.-H., Luan, Z.-K., Liang, J., 2004. Adsorption of Chromium(VI) Ions from Water by Carbon Nanotubes. Adsorpt. Sci. Technol. 22, 467–474. https://doi.org/10.1260/0263617042879537

Dieter, H.H., Bayer, T.A., Multhaup, G., 2005. Environmental Copper and Manganese in the Pathophysiology of Neurologic Diseases (Alzheimer's Disease and Manganism). Acta Hydrochim. Hydrobiol. 33, 72–78. https://doi.org/10.1002/aheh.200400556

Dionex, 1996. Dionex, Determination of Cr(VI) in water, wastewater and solid waste extracts,.

Dodd, M.C., Vu, N.D., Ammann, A., Le, V.C., Kissner, R., Pham, H.V., Cao, T.H., Berg, M., von Gunten, U., 2006. Kinetics and Mechanistic Aspects of As(III) Oxidation by Aqueous Chlorine, Chloramines, and Ozone: Relevance to Drinking Water Treatment. Environ. Sci. Technol. 40, 3285–3292. https://doi.org/10.1021/es0524999

Driehaus, W., Jekel, M., Hildebrandt, U., 1998. Granular ferric hydroxide—a new adsorbent for the removal of arsenic from natural water. J. Water Supply Res. Technol.-Aqua 47, 30–35. https://doi.org/10.2166/aqua.1998.0005

Edzwald, J.K., 2010. Dissolved air flotation and me. Water Res. 44, 2077–2106. https://doi.org/10.1016/j.watres.2009.12.040

Edzwald, J.K., Haarhoff, J., 2012. Dissolved Air Flotation for Water Clarification. McGraw Hill, New York.

Elabbas, S., Ouazzani, N., Mandi, L., Berrekhis, F., Perdicakis, M., Pontvianne, S., Pons, M.-N., Lapicque, F., Leclerc, J.-P., 2016. Treatment of highly concentrated tannery wastewater using electrocoagulation: Influence of the quality of aluminium used for the electrode. J. Hazard. Mater., SI: Honoring Brillas & Oturan 319, 69–77. https://doi.org/10.1016/j.jhazmat.2015.12.067

Elson, C.M., Davies, D.H., Hayes, E.R., 1980. Removal of arsenic from contaminated drinking water by a chitosan/chitin mixture. Water Res. 14, 1307–1311. https://doi.org/10.1016/0043-1354(80)90190-6

Emett, M.T., Khoe, G.H., 2001. Photochemical oxidation of arsenic by oxygen and iron in acidic solutions. Water Res. 35, 649–656. https://doi.org/10.1016/S0043-1354(00)00294-3

Figoli, A., Cassano, A., Criscuoli, A., Mozumder, M.S.I., Uddin, M.T., Islam, M.A., Drioli, E., 2010. Influence of operating parameters on the arsenic removal by nanofiltration. Water Res. 44, 97–104. https://doi.org/10.1016/j.watres.2009.09.007

Flores, O.J., Nava, J.L., Carreño, G., Elorza, E., Martínez, F., 2013. Arsenic removal from groundwater by electrocoagulation in a pre-pilot-scale continuous filter press reactor. Chem. Eng. Sci. 97, 1–6. https://doi.org/10.1016/j.ces.2013.04.029

Fu, F., Wang, Q., 2011. Removal of heavy metal ions from wastewaters: A review. J. Environ. Manage. 92, 407–418. https://doi.org/10.1016/j.jenvman.2010.11.011

Geucke, T., Deowan, S.A., Hoinkis, J., Pätzold, C., 2009. Performance of a small-scale RO desalinator for arsenic removal. Desalination 239, 198–206. https://doi.org/10.1016/j.desal.2008.03.018

Ghimire, K.N., Inoue, K., Makino, K., Miyajima, T., 2002. Adsorptive Removal of Arsenic Using Orange Juice Residue. Sep. Sci. Technol. 37, 2785–2799. https://doi.org/10.1081/SS-120005466

Ghosh (Nath), S., Debsarkar, A., Dutta, A., 2019. Technology alternatives for decontamination of arsenic-rich groundwater—A critical review. Environ. Technol. Innov. 13, 277–303. https://doi.org/10.1016/j.eti.2018.12.003

Ghurye, G., Clifford, D., 2004. As(III) oxidation using chemical and solid-phase oxidants. J. Am. Water Works Assoc. - J AMER WATER WORK ASSN 96, 84–96. https://doi.org/10.1002/j.1551-8833.2004.tb10536.x

Gode, F., Pehlivan, E., 2006. Removal of chromium(III) from aqueous solutions using Lewatit S 100: The effect of pH, time, metal concentration and temperature. J. Hazard. Mater. 136, 330–337. https://doi.org/10.1016/j.jhazmat.2005.12.021

Gomes, J.A.G., Daida, P., Kesmez, M., Weir, M., Moreno, H., Parga, J.R., Irwin, G., McWhinney, H., Grady, T., Peterson, E., Cocke, D.L., 2007. Arsenic removal by electrocoagulation using combined Al–Fe electrode system and characterization of products. J. Hazard. Mater. 139, 220–231. https://doi.org/10.1016/j.jhazmat.2005.11.108

Gong, G., Basom, J., Mattevada, S., Onger, F., 2015. Association of hypothyroidism with low-level arsenic exposure in rural West Texas. Environ. Res. 138, 154–160. https://doi.org/10.1016/j.envres.2015.02.001

Grafe, M., Eick, M.J., Grossl, P.R., 2001. Adsorption of Arsenate (V) and Arsenite (III) on Goethite in the Presence and Absence of Dissolved Organic Carbon. Soil Sci. Soc. Am. J. 65, 1680–1687. https://doi.org/10.2136/sssaj2001.1680

Gribble, M.O., Howard, B.V., Umans, J.G., Shara, N.M., Francesconi, K.A., Goessler, W., Crainiceanu, C.M., Silbergeld, E.K., Guallar, E., Navas-Acien, A., 2012. Arsenic Exposure, Diabetes Prevalence, and Diabetes Control in the Strong Heart Study. Am. J. Epidemiol. 176, 865–874. https://doi.org/10.1093/aje/kws153

Han, B., Runnells, T., Zimbron, J., Wickramasinghe, R., 2002. Arsenic removal from drinking water by flocculation and microfiltration. Desalination 145, 293–298. https://doi.org/10.1016/S0011-9164(02)00425-3

Han, R., Wang, Yu, Zhao, X., Wang, Yuanfeng, Xie, F., Cheng, J., Tang, M., 2009. Adsorption of methylene blue by phoenix tree leaf powder in a fixed-bed column:

experiments and prediction of breakthrough curves. Desalination, Engineering with Membranes 2008 245, 284–297. https://doi.org/10.1016/j.desal.2008.07.013

Hendricks, D., 2006. Water treatment Unit Processes Physical and Chemical. Taylor & Francis Group.

Henke, K.R., 2009. Arsenic - Environmental Chemistry, Health Threats and Waste Treatment, 1st Edition. ed. John Wiley & Sons Ltd.

Hering Janet G., Chen Pen-Yuan, Wilkie Jennifer A., Elimelech Menachem, 1997. Arsenic Removal from Drinking Water during Coagulation. J. Environ. Eng. 123, 800–807. https://doi.org/10.1061/(ASCE)0733-9372(1997)123:8(800)

Hering, J.G., Pen-Yuan, C., Wilkie, J.A., Elimelech, M., Sun, L., 1996. Arsenic removal by ferric chloride. Am. Water Works Assoc. J. 88, 155.

Ho, Y.S., Mckay, G., 1998. The kinetics of sorption of basic dyes from aqueous solution by sphagnum moss peat. Can. J. Chem. Eng. 76, 822–827. https://doi.org/10.1002/cjce.5450760419

Hoko, Z., Makado, P.K., 2011. Optimization of algal removal process at Morton Jaffray water works, Harare, Zimbabwe. Phys. Chem. Earth Parts ABC, 11th WaterNet/WARFSA/GWP-SA Symposium: IWRM for National and Regional Integration through Science, Policy and Practice 36, 1141–1150. https://doi.org/10.1016/j.pce.2011.07.074

Hong, Y.-S., Song, K.-H., Chung, J.-Y., 2014. Health Effects of Chronic Arsenic Exposure. J. Prev. Med. Pub. Health 47, 245–252. https://doi.org/10.3961/jpmph.14.035

Hoseinian, F.S., Irannajad, M., Nooshabadi, A.J., 2015. Ion flotation for removal of Ni(II) and Zn(II) ions from wastewaters. Int. J. Miner. Process. 143, 131–137. https://doi.org/10.1016/j.minpro.2015.07.006

http://www.coriolis-pharma.com/contract-analytical-services/zeta-potential/, n.d.

Hu, C., Liu, H., Chen, G., Qu, J., 2012. Effect of aluminum speciation on arsenic removal during coagulation process. Sep. Purif. Technol. 86, 35–40. https://doi.org/10.1016/j.seppur.2011.10.017

Hu, J., Chen, C., Zhu, X., Wang, X., 2009. Removal of chromium from aqueous solution by using oxidized multiwalled carbon nanotubes. J. Hazard. Mater. 162, 1542–1550. https://doi.org/10.1016/j.jhazmat.2008.06.058

Ihsanullah, Abbas, A., Al-Amer, A.M., Laoui, T., Al-Marri, M.J., Nasser, M.S., Khraisheh, M., Atieh, M.A., 2016. Heavy metal removal from aqueous solution by advanced carbon nanotubes: Critical review of adsorption applications. Sep. Purif. Technol. 157, 141–161. https://doi.org/10.1016/j.seppur.2015.11.039

Ihsanullah, Al-Khaldi, F.A., Abusharkh, B., Khaled, M., Atieh, M.A., Nasser, M.S., laoui, T., Saleh, T.A., Agarwal, S., Tyagi, I., Gupta, V.K., 2015. Adsorptive removal of cadmium(II) ions from liquid phase using acid modified carbon-based adsorbents. J. Mol. Liq. 204, 255–263. https://doi.org/10.1016/j.molliq.2015.01.033

Islam, M.R., Khan, I., Hassan, S.M.N., McEvoy, M., D'Este, C., Attia, J., Peel, R., Sultana, M., Akter, S., Milton, A.H., 2012. Association between type 2 diabetes and chronic arsenic exposure in drinking water: A cross sectional study in Bangladesh. Environ. Health 11, 38. https://doi.org/10.1186/1476-069X-11-38

Issa, N.B., Rajaković-Ognjanović, V.N., Jovanović, B.M., Rajaković, L.V., 2010. Determination of inorganic arsenic species in natural waters—Benefits of separation and preconcentration on ion exchange and hybrid resins. Anal. Chim. Acta 673, 185–193. https://doi.org/10.1016/j.aca.2010.05.027

Issa, N.B., Rajaković-Ognjanović, V.N., Marinković, A.D., Rajaković, L.V., 2011a. Separation and determination of arsenic species in water by selective exchange and hybrid resins. Anal. Chim. Acta 706, 191–198. https://doi.org/10.1016/j.aca.2011.08.015

Issa, N.B., Rajaković-Ognjanović, V.N., Marinković, A.D., Rajaković, L.V., 2011b. Separation and determination of arsenic species in water by selective exchange and hybrid resins. Anal. Chim. Acta 706, 191–198. https://doi.org/10.1016/j.aca.2011.08.015

Järup, L., 2003. Hazards of heavy metal contamination. Br. Med. Bull. 68, 167–182.

Jayasumana, M. a. C.S., Paranagama, P.A., Amarasinghe, M.D., Wijewardane, K.M.R.C., Dahanayake, K.S., Fonseka, S.I., Rajakaruna, K.D.L.M.P., Mahamithawa, A.M.P., Samarasinghe, U.D., Senanayake, V.K., 2013. Possible link of Chronic arsenic toxicity with Chronic Kidney Disease of unknown etiology in Sri Lanka.

Jiang, J.-Q., 2001. Removing arsenic from groundwater for the developing world - a review. Water Sci. Technol. 44, 89–98. https://doi.org/10.2166/wst.2001.0348

Jovanovic, D., Jakovljević, B., Rašić-Milutinović, Z., Paunović, K., Peković, G., Knezević, T., 2011. Arsenic occurrence in drinking water supply systems in ten municipalities in Vojvodina Region, Serbia. Environ. Res., Fire Effects on Soil Properties: Forest Fires and Prescribed Fires 111, 315–318. https://doi.org/10.1016/j.envres.2010.11.014

Kamaraj, R., Ganesan, P., Lakshmi, J., Vasudevan, S., 2013. Removal of copper from water by electrocoagulation process—effect of alternating current (AC) and direct current (DC). Environ. Sci. Pollut. Res. 20, 399–412. https://doi.org/10.1007/s11356-012-0855-7

Kamaraj, R., Ganesan, P., Vasudevan, S., 2015. Removal of lead from aqueous solutions by electrocoagulation: isotherm, kinetics and thermodynamic studies. Int. J. Environ. Sci. Technol. 12, 683–692. https://doi.org/10.1007/s13762-013-0457-z

Kamaraj, R., Vasudevan, S., 2015. Evaluation of electrocoagulation process for the removal of strontium and cesium from aqueous solution. Chem. Eng. Res. Des. 93, 522–530. https://doi.org/10.1016/j.cherd.2014.03.021

Kandah, M.I., Meunier, J.-L., 2007. Removal of nickel ions from water by multi-walled carbon nanotubes. J. Hazard. Mater. 146, 283–288. https://doi.org/10.1016/j.jhazmat.2006.12.019

Kang, S.-Y., Lee, J.-U., Moon, S.-H., Kim, K.-W., 2004. Competitive adsorption characteristics of Co2+, Ni2+, and Cr3+ by IRN-77 cation exchange resin in synthesized wastewater. Chemosphere 56, 141–147. https://doi.org/10.1016/j.chemosphere.2004.02.004

Katsoyiannis, I.A., Zouboulis, A.I., 2004. Application of biological processes for the removal of arsenic from groundwaters. Water Res. 38, 17–26. https://doi.org/10.1016/j.watres.2003.09.011

Kaur, S., Rani, S., Mahajan, R.K., 2013. Adsorption Kinetics for the Removal of Hazardous Dye Congo Red by Biowaste Materials as Adsorbents [WWW Document]. J. Chem. https://doi.org/10.1155/2013/628582

Kim, M.-J., Nriagu, J., 2000. Oxidation of arsenite in groundwater using ozone and oxygen. Sci. Total Environ. 247, 71–79. https://doi.org/10.1016/S0048-9697(99)00470-2

Knight, C., Kaiser, J., Lalor, G.C., Robotham, H., Witter, J.V., 1997. Heavy metals in surface water and stream sediments in Jamaica. Environ. Geochem. Health 19, 63–66. https://doi.org/10.1023/A:1018442219943

Kobya, M., Akyol, A., Demirbas, E., Oncel, M.S., 2014. Removal of arsenic from drinking water by batch and continuous electrocoagulation processes using hybrid Al-Fe plate electrodes. Environ. Prog. Sustain. Energy 33, 131–140. https://doi.org/10.1002/ep.11765

Kobya, M., Can, O.T., Bayramoglu, M., 2003. Treatment of textile wastewaters by electrocoagulation using iron and aluminum electrodes. J. Hazard. Mater. 100, 163–178. https://doi.org/10.1016/S0304-3894(03)00102-X

Kobya, M., Demirbas, E., Can, O.T., Bayramoglu, M., 2006. Treatment of levafix orange textile dye solution by electrocoagulation. J. Hazard. Mater. 132, 183–188. https://doi.org/10.1016/j.jhazmat.2005.07.084

Kobya, Mehmet, Senturk, E., Bayramoglu, M., 2006. Treatment of poultry slaughterhouse wastewaters by electrocoagulation. J. Hazard. Mater. 133, 172–176. https://doi.org/10.1016/j.jhazmat.2005.10.007

Kocar, B.D., Inskeep, W.P., 2003. Photochemical Oxidation of As(III) in Ferrioxalate Solutions. Environ. Sci. Technol. 37, 1581–1588. https://doi.org/10.1021/es020939f

Kordmostafapour, F., Pourmoghadas, H., Shahmansouri, M.R., Parvaresh, A., 2006. Arsenic Removal by Dissolved Air Flotation. J. Appl. Sci. 6, 1153–1158.

Košutić, K., Furač, L., Sipos, L., Kunst, B., 2005. Removal of arsenic and pesticides from drinking water by nanofiltration membranes. Sep. Purif. Technol. 42, 137–144. https://doi.org/10.1016/j.seppur.2004.07.003

Kowalski, K.P., 2014. Advanced Arsenic Removal Technologies Review. Chem. Adv. Environ. Purif. Process. Water.

Krishna, M.V.B., Chandrasekaran, K., Karunasagar, D., Arunachalam, J., 2001. A combined treatment approach using Fenton's reagent and zero valent iron for the removal of arsenic from drinking water. J. Hazard. Mater. 84, 229–240. https://doi.org/10.1016/S0304-3894(01)00205-9

Lacasa, E., Cañizares, P., Sáez, C., Fernández, F.J., Rodrigo, M.A., 2011. Removal of arsenic by iron and aluminium electrochemically assisted coagulation. Sep. Purif. Technol. 79, 15–19. https://doi.org/10.1016/j.seppur.2011.03.005

Lacasa, E., Sáez, C., Cañizares, P., Fernández, F.J., Rodrigo, M.A., 2013. Arsenic Removal from High-Arsenic Water Sources by Coagulation and Electrocoagulation. Sep. Sci. Technol. 48, 508–514. https://doi.org/10.1080/01496395.2012.690806

Lakshmanan, D., Clifford, D.A., Samanta, G., 2010. Comparative study of arsenic removal by iron using electrocoagulation and chemical coagulation. Water Res., Groundwater Arsenic: From Genesis to Sustainable Remediation 44, 5641–5652. https://doi.org/10.1016/j.watres.2010.06.018

Lara, F., Cornejo, L., Yáñez, J., Freer, J., Mansilla, H.D., 2006. Solar-light assisted removal of arsenic from natural waters: effect of iron and citrate concentrations. J. Chem. Technol. Biotechnol. 81, 1282–1287. https://doi.org/10.1002/jctb.1547

Lee, Y., Um, I., Yoon, J., 2003. Arsenic(III) Oxidation by Iron(VI) (Ferrate) and Subsequent Removal of Arsenic(V) by Iron(III) Coagulation. Environ. Sci. Technol. 37, 5750–5756. https://doi.org/10.1021/es034203+

Leupin, O.X., Hug, S.J., 2005. Oxidation and removal of arsenic (III) from aerated groundwater by filtration through sand and zero-valent iron. Water Res. 39, 1729–1740. https://doi.org/10.1016/j.watres.2005.02.012

Li, Q., Wu, S., Liu, G., Liao, X., Deng, X., Sun, D., Hu, Y., Huang, Y., 2004. Simultaneous biosorption of cadmium (II) and lead (II) ions by pretreated biomass of Phanerochaete chrysosporium. Sep. Purif. Technol., A selection of papers on Environmental Technologies and Membrane Separation presented at the 17th International Symposium on Chemical Reaction Engineering 34, 135–142. https://doi.org/10.1016/S1383-5866(03)00187-4

Li, X., Liu, Cheng-shuai, Li, F., Li, Y., Zhang, L., Liu, Chuan-ping, Zhou, Y., 2010. The oxidative transformation of sodium arsenite at the interface of α-MnO2 and water. J. Hazard. Mater. 173, 675–681. https://doi.org/10.1016/j.jhazmat.2009.08.139

Lièvremont, D., Bertin, P.N., Lett, M.-C., 2009. Arsenic in contaminated waters: Biogeochemical cycle, microbial metabolism and biotreatment processes. Biochimie, Metals in health 91, 1229–1237. https://doi.org/10.1016/j.biochi.2009.06.016

Lindberg, A.-L., Rahman, M., Persson, L.-Å., Vahter, M., 2008. The risk of arsenic induced skin lesions in Bangladeshi men and women is affected by arsenic metabolism and the age at first exposure. Toxicol. Appl. Pharmacol. 230, 9–16. https://doi.org/10.1016/j.taap.2008.02.001

Litter, M.I., Morgada, M.E., Bundschuh, J., 2010. Possible treatments for arsenic removal in Latin American waters for human consumption. Environ. Pollut. 158, 1105–1118. https://doi.org/10.1016/j.envpol.2010.01.028

Liu, G., Zhang, X., Talley, J.W., Neal, C.R., Wang, H., 2008. Effect of NOM on arsenic adsorption by TiO2 in simulated As(III)-contaminated raw waters. Water Res. 42, 2309–2319. https://doi.org/10.1016/j.watres.2007.12.023

Liu, S.S., Chen, Y.Z., De Zhang, L., Hua, G.M., Xu, W., Li, N., Zhang, Y., 2011. Enhanced removal of trace Cr(VI) ions from aqueous solution by titanium oxide–Ag composite adsorbents. J. Hazard. Mater. 190, 723–728. https://doi.org/10.1016/j.jhazmat.2011.03.114

Loubières, Y., de Lassence, A., Bernier, M., Vieillard-Baron, A., Schmitt, J.M., Page, B., Jardin, F., 1999. Acute, fatal, oral chromic acid poisoning. J. Toxicol. Clin. Toxicol. 37, 333–336.

Makris, K.C., Christophi, C.A., Paisi, M., Ettinger, A.S., 2012. A preliminary assessment of low level arsenic exposure and diabetes mellitus in Cyprus. BMC Public Health 12, 334. https://doi.org/10.1186/1471-2458-12-334

Malakootian, M., Mansoorian, H.J., Moosazadeh, M., 2010. Performance evaluation of electrocoagulation process using iron-rod electrodes for removing hardness from drinking water. Desalination 255, 67–71. https://doi.org/10.1016/j.desal.2010.01.015

Maldonado-Reyes, A., Montero-Ocampo, C., Solorza-Feria, O., 2007. Remediation of drinking water contaminated with arsenic by the electro-removal process using different metal electrodes. J. Environ. Monit. 9, 1241–1247. https://doi.org/10.1039/B708671G

Mandal, B.K., Suzuki, K.T., 2002. Arsenic round the world: a review. Talanta 58, 201–235.

Manju, G.N., Raji, C., Anirudhan, T.S., 1998. Evaluation of coconut husk carbon for the removal of arsenic from water. Water Res. 32, 3062–3070. https://doi.org/10.1016/S0043-1354(98)00068-2

Manning, B.A., Goldberg, S., 1996. Modelling arsenate competitive adsorption on kaolinite, montmorillonite and illite. Clays Clay Miner. 609–623.

Masscheleyn, P.H., Delaune, R.D., Patrick, W.H., 1991. Effect of redox potential and pH on arsenic speciation and solubility in a contaminated soil. Environ. Sci. Technol. 25, 1414–1419. https://doi.org/10.1021/es00020a008

McLaren, S.J., Kim, N.D., 1995. Evidence for a seasonal fluctuation of arsenic in New Zealand's longest river and the effect of treatment on concentrations in drinking water. Environ. Pollut. 90, 67–73. https://doi.org/10.1016/0269-7491(94)00092-R

Medina, B.Y., Torem, M.L., de Mesquita, L.M.S., 2005. On the kinetics of precipitate flotation of Cr III using sodium dodecylsulfate and ethanol. Miner. Eng., Reagents '04 18, 225–231. https://doi.org/10.1016/j.mineng.2004.08.018

Mohammed Abdul, K.S., Jayasinghe, S.S., Chandana, E.P.S., Jayasumana, C., De Silva, P.M.C.S., 2015. Arsenic and human health effects: A review. Environ. Toxicol. Pharmacol. 40, 828–846. https://doi.org/10.1016/j.etap.2015.09.016

Mohan, D., Chander, S., 2006. Removal and recovery of metal ions from acid mine drainage using lignite—A low cost sorbent. J. Hazard. Mater. 137, 1545–1553. https://doi.org/10.1016/j.jhazmat.2006.04.053

Mohan, D., Pittman Jr., C.U., 2007. Arsenic removal from water/wastewater using adsorbents—A critical review. J. Hazard. Mater. 142, 1–53. https://doi.org/10.1016/j.jhazmat.2007.01.006

Mohan, D., Pittman Jr., C.U., 2006. Activated carbons and low cost adsorbents for remediation of tri- and hexavalent chromium from water. J. Hazard. Mater. 137, 762–811. https://doi.org/10.1016/j.jhazmat.2006.06.060

Mohan, D., Singh, K.P., Singh, V.K., 2006. Trivalent chromium removal from wastewater using low cost activated carbon derived from agricultural waste material and activated carbon fabric cloth. J. Hazard. Mater. 135, 280–295. https://doi.org/10.1016/j.jhazmat.2005.11.075

Mollah, M.Y.A., Morkovsky, P., Gomes, J.A.G., Kesmez, M., Parga, J., Cocke, D.L., 2004. Fundamentals, present and future perspectives of electrocoagulation. J. Hazard. Mater. 114, 199–210. https://doi.org/10.1016/j.jhazmat.2004.08.009

Mondal, P., Bhowmick, S., Chatterjee, D., Figoli, A., Van der Bruggen, B., 2013. Remediation of inorganic arsenic in groundwater for safe water supply: A critical assessment of technological solutions. Chemosphere 92, 157–170. https://doi.org/10.1016/j.chemosphere.2013.01.097

Morselli, L., Olivieri, P., Brusori, B., Passarini, F., 2003. Soluble and insoluble fractions of heavy metals in wet and dry atmospheric depositions in Bologna, Italy. Environ. Pollut. 124, 457–469. https://doi.org/10.1016/S0269-7491(03)00013-7

Mortada, W.I., Sobh, M.A., El-Defrawy, M.M., Farahat, S.E., 2001. Study of lead exposure from automobile exhaust as a risk for nephrotoxicity among traffic policemen. Am. J. Nephrol. 21, 274–279. https://doi.org/46261

Muhammad, S., Shah, M.T., Khan, S., 2011. Health risk assessment of heavy metals and their source apportionment in drinking water of Kohistan region, northern Pakistan. Microchem. J. 98, 334–343. https://doi.org/10.1016/j.microc.2011.03.003

Mundey, M.K., Roy, M., Roy, S., Awasthi, M.K., Sharma, R., 2013. Antioxidant potential of Ocimum sanctum in arsenic induced nervous tissue damage. Braz. J. Vet. Pathol. 6, 95–101.

Narasiah, K.S., Vogel, A., Kramadhati, N.N., 2002. Coagulation of turbid waters using Moringa oleifera seeds from two distinct sources. Water Sci. Technol. Water Supply 2, 83–88.

Naujokas Marisa F., Anderson Beth, Ahsan Habibul, Aposhian H. Vasken, Graziano Joseph H., Thompson Claudia, Suk William A., 2013. The Broad Scope of Health Effects from Chronic Arsenic Exposure: Update on a Worldwide Public Health Problem. Environ. Health Perspect. 121, 295–302. https://doi.org/10.1289/ehp.1205875

Nearing, M.M., Koch, I., Reimer, K.J., 2014. Complementary arsenic speciation methods: A review. Spectrochim. Acta Part B At. Spectrosc. 99, 150–162. https://doi.org/10.1016/j.sab.2014.07.001

Neppolian, B., Celik, E., Choi, H., 2008. Photochemical Oxidation of Arsenic(III) to Arsenic(V) using Peroxydisulfate Ions as an Oxidizing Agent. Environ. Sci. Technol. 42, 6179–6184. https://doi.org/10.1021/es800180f

Neppolian, B., Doronila, A., Ashokkumar, M., 2010. Sonochemical oxidation of arsenic(III) to arsenic(V) using potassium peroxydisulfate as an oxidizing agent. Water Res. 44, 3687–3695. https://doi.org/10.1016/j.watres.2010.04.003

Nidheesh, P.V., Singh, T.S.A., 2017. Arsenic removal by electrocoagulation process: Recent trends and removal mechanism. Chemosphere 181, 418–432. https://doi.org/10.1016/j.chemosphere.2017.04.082

Ning, R.Y., 2002. Arsenic removal by reverse osmosis. Desalination 143, 237–241. https://doi.org/10.1016/S0011-9164(02)00262-X

Nouri, H., Ouederni, A., 2013. Modeling of the Dynamics Adsorption of Phenol from an Aqueous Solution on Activated Carbon Produced from Olive Stones. J. Chem. Eng. Process Technol. 4, 254–261. https://doi.org/10.4172/2157-7048.C1.003

Ouyang, Y., Higman, J., Thompson, J., O'Toole, T., Campbell, D., 2002. Characterization and spatial distribution of heavy metals in sediment from Cedar and Ortega rivers subbasin. J. Contam. Hydrol. 54, 19–35. https://doi.org/10.1016/S0169-7722(01)00162-0

Pallier, V., Feuillade-Cathalifaud, G., Serpaud, B., Bollinger, J.-C., 2010. Effect of organic matter on arsenic removal during coagulation/flocculation treatment. J. Colloid Interface Sci. 342, 26–32. https://doi.org/10.1016/j.jcis.2009.09.068

Panthi, S.R., Wareham, D.G., 2014. Kinetic study of adsorption of arsenic onto New Zealand Ironsand (NZIS). J. Environ. Sci. Health Part A Tox. Hazard. Subst. Environ. Eng. 49, 1474–1480. https://doi.org/10.1080/10934529.2014.937161

Panthi, S.R., Wareham, D.G., 2011. Removal of arsenic from water using the adsorbent: New Zealand iron-sand. J. Environ. Sci. Health Part A Tox. Hazard. Subst. Environ. Eng. 46, 1533–1538. https://doi.org/10.1080/10934529.2011.609376

Parga, J.R., Cocke, D.L., Valenzuela, J.L., Gomes, J.A., Kesmez, M., Irwin, G., Moreno, H., Weir, M., 2005. Arsenic removal via electrocoagulation from heavy metal contaminated groundwater in La Comarca Lagunera México. J. Hazard. Mater. 124, 247–254. https://doi.org/10.1016/j.jhazmat.2005.05.017

PARK, H.J., JEONG, S.W., YANG, J.K., KIM, B.G., LEE, S.M., 2007. Removal of heavy metals using waste eggshell. J. Environ. Sci. 19, 1436–1441. https://doi.org/10.1016/S1001-0742(07)60234-4

Parvez Faruque, Chen Yu, Brandt-Rauf Paul W., Bernard Alfred, Dumont Xavier, Slavkovich Vesna, Argos Maria, D'Armiento Jeanine, Foronjy Robert, Hasan M. Rashidul, Eunus HEM Mahbubul, Graziano Joseph H., Ahsan Habibul, 2008. Nonmalignant Respiratory Effects of Chronic Arsenic Exposure from Drinking Water among Never-Smokers in Bangladesh. Environ. Health Perspect. 116, 190–195. https://doi.org/10.1289/ehp.9507

Pattanayak, J., Mondal, K., Mathew, S., Lalvani, S.B., 2000. A parametric evaluation of the removal of As(V) and As(III) by carbon-based adsorbents. Carbon 38, 589–596. https://doi.org/10.1016/S0008-6223(99)00144-X

Paulino, A.T., Minasse, F.A.S., Guilherme, M.R., Reis, A.V., Muniz, E.C., Nozaki, J., 2006. Novel adsorbent based on silkworm chrysalides for removal of heavy metals from wastewaters. J. Colloid Interface Sci. 301, 479–487. https://doi.org/10.1016/j.jcis.2006.05.032

Pena, M.E., Korfiatis, G.P., Patel, M., Lippincott, L., Meng, X., 2005. Adsorption of As(V) and As(III) by nanocrystalline titanium dioxide. Water Res. 39, 2327–2337. https://doi.org/10.1016/j.watres.2005.04.006

Pettine, M., Campanella, L., Millero, F.J., 1999. Arsenite oxidation by H2O2 in aqueous solutions. Geochim. Cosmochim. Acta 63, 2727–2735. https://doi.org/10.1016/S0016-7037(99)00212-4

Pichel, N., Vivar, M., Fuentes, M., 2019. The problem of drinking water access: A review of disinfection technologies with an emphasis on solar treatment methods. Chemosphere 218, 1014–1030. https://doi.org/10.1016/j.chemosphere.2018.11.205

Pokhrel, D., Viraraghavan, T., 2006. Arsenic removal from an aqueous solution by a modified fungal biomass. Water Res. 40, 549–552. https://doi.org/10.1016/j.watres.2005.11.040

Quantum Filtration Medium, 2019.

Radovic, L.., Moreno Castilla, C., Rivera-Utrilla, J., 2000. Carbon materials as adsorbents in aqueous solutions. New York.

Rahman, I.M.M., Begum, Z.A., Nakano, M., Furusho, Y., Maki, T., Hasegawa, H., 2011. Selective separation of arsenic species from aqueous solutions with immobilized macrocyclic material containing solid phase extraction columns. Chemosphere 82, 549–556. https://doi.org/10.1016/j.chemosphere.2010.10.045

Rahman, M., Wingren, G., Axelson, O., 1996. Diabetes mellitus among Swedish art glass workers--an effect of arsenic exposure? Scand. J. Work. Environ. Health 22, 146–149.

Rahman, M.A., Rahman, A., Khan, M.Z.K., Renzaho, A.M.N., 2018. Human health risks and socio-economic perspectives of arsenic exposure in Bangladesh: A scoping review. Ecotoxicol. Environ. Saf. 150, 335–343. https://doi.org/10.1016/j.ecoenv.2017.12.032

Rahman, M.M., Ng, J.C., Naidu, R., 2009. Chronic exposure of arsenic via drinking water and its adverse health impacts on humans. Environ. Geochem. Health 31, 189–200. https://doi.org/10.1007/s10653-008-9235-0

Ratna Kumar, P., Chaudhari, S., Khilar, K.C., Mahajan, S.P., 2004. Removal of arsenic from water by electrocoagulation. Chemosphere 55, 1245–1252. https://doi.org/10.1016/j.chemosphere.2003.12.025

Ravenscroft, P., Brammer, H., Richards, K., 2009. Arsenic Pollution: A Global Synthesis. Wiley-Blackwell, Oxford, UK.

Ravikumar, K., Sheeja, A., K., 2013. Heavy metal removal from water using Moringa oleifere seed coagulant and double filtration. Int. J. Sci. Eng. Res. 4, 10–13.

Robinson, B., Outred, H., Brooks, R., Kirkman, J., 1995. The distribution and fate of arsenic in the Waikato River system, North Island, New Zealand. Chem. Speciat. Bioavailab. 7, 89–96. https://doi.org/10.1080/09542299.1995.11083250

Saada, A., Breeze, D., Crouzet, C., Cornu, S., Baranger, P., 2003. Adsorption of arsenic (V) on kaolinite and on kaolinite-humic acid complexes - Role of humic acid nitrogen groups. Chemosphere 51, 757–63. https://doi.org/10.1016/S0045-6535(03)00219-4

Safari, S., Azadi Aghdam, M., Kariminia, H.-R., 2016. Electrocoagulation for COD and diesel removal from oily wastewater. Int. J. Environ. Sci. Technol. 13, 231–242. https://doi.org/10.1007/s13762-015-0863-5

Saha, J.C., Dikshit, A.K., Bandyopadhyay, M., Saha, K.C., 1999. A Review of Arsenic Poisoning and its Effects on Human Health. Crit. Rev. Environ. Sci. Technol. 29, 281–313. https://doi.org/10.1080/10643389991259227

Sánchez-Peña, L.C., Petrosyan, P., Morales, M., González, N.B., Gutiérrez-Ospina, G., Del Razo, L.M., Gonsebatt, M.E., 2010. Arsenic species, AS3MT amount, and AS3MT gen expression in different brain regions of mouse exposed to arsenite. Environ. Res., 2nd International Congress, As 2008: Arsenic from Nature to Humans (Valencia, Spain, May 21-23) 110, 428–434. https://doi.org/10.1016/j.envres.2010.01.007

Sarkar, A., Paul, B., 2016. The global menace of arsenic and its conventional remediation - A critical review. Chemosphere 158, 37–49. https://doi.org/10.1016/j.chemosphere.2016.05.043

Schwartz, R.A., 1997. Arsenic and the skin. Int. J. Dermatol. 36, 241–250. https://doi.org/10.1046/j.1365-4362.1997.00101.x

Sekine, M., Takeshita, A., Oda, N., Ukita, M., Imai, T., Higuchi, T., 2006. On-site treatment of turbid river water using chitosan, a natural organic polymer coagulant. Water Sci. Technol. J. Int. Assoc. Water Pollut. Res. 53, 155–161.

Shankar, S., Shanker, U., Shikha, 2014. Arsenic Contamination of Groundwater: A Review of Sources, Prevalence, Health Risks, and Strategies for Mitigation [WWW Document]. Sci. World J. https://doi.org/10.1155/2014/304524

Sharma, D., 2014. Treatment of dairy waste water by electro coagulation using aluminum electrodes and settling, filtration studies. Int. J. ChemTech Res. 6, 591–599.

Sharma, V.K., Dutta, P.K., Ray, A.K., 2007. Review of kinetics of chemical and photocatalytical oxidation of Arsenic(III) as influenced by pH. J. Environ. Sci. Health Part A 42, 997–1004. https://doi.org/10.1080/10934520701373034

Sharp, E.L., Banks, J., Billica, J.A., Gertig, K.R., Henderson, R., Parsons, S.A., Wilson, D., Jefferson, B., 2005. Application of zeta potential measurements for coagulation control: pilot-plant experiences from UK and US waters with elevated organics. Water Sci. Technol. Water Supply 5, 49–56.

Shih, M.-C., 2005. An overview of arsenic removal by pressure-drivenmembrane processes. Desalination 172, 85–97. https://doi.org/10.1016/j.desal.2004.07.031

Singh, D.B., Prasad, G., Rupainwar, D.C., 1996. Adsorption technique for the treatment of As(V)-rich effluents. Colloids Surf. Physicochem. Eng. Asp. 111, 49–56. https://doi.org/10.1016/0927-7757(95)03468-4

Singh, T.S.A., Ramesh, S.T., 2014. An experimental study of CI Reactive Blue 25 removal from aqueous solution by electrocoagulation using Aluminum sacrificial electrode: kinetics and influence of parameters on electrocoagulation performance. Desalination Water Treat. 52, 2634–2642. https://doi.org/10.1080/19443994.2013.794714

Song, S., Lopez-Valdivieso, A., Hernandez-Campos, D.J., Peng, C., Monroy-Fernandez, M.G., Razo-Soto, I., 2006. Arsenic removal from high-arsenic water by enhanced coagulation with ferric ions and coarse calcite. Water Res. 40, 364–372. https://doi.org/10.1016/j.watres.2005.09.046

Song, X., Wang, J., Zhu, jin, 2009. Effect of porogenic Solvent on Selective Performance of Molecurlarly Imprinted polymer for Quercetin. Materials Research 12, 299–304.

Sridhar, R., Sivakumar, V., Prince Immanuel, V., Prakash Maran, J., 2011. Treatment of pulp and paper industry bleaching effluent by electrocoagulant process. J. Hazard. Mater. 186, 1495–1502. https://doi.org/10.1016/j.jhazmat.2010.12.028

Srivastava, N.K., Majumder, C.B., 2008. Novel biofiltration methods for the treatment of heavy metals from industrial wastewater. J. Hazard. Mater. 151, 1–8. https://doi.org/10.1016/j.jhazmat.2007.09.101

Stalidis, G.A., Matis, K.A., Lazaridis, N.K., 1989. Selective Separation of Cu, Zn, and As from Solution by Flotation Techniques. Sep. Sci. Technol. 24, 97–109. https://doi.org/10.1080/01496398908049754

States, J.C., Srivastava, S., Chen, Y., Barchowsky, A., 2009. Arsenic and Cardiovascular Disease. Toxicol. Sci. 107, 312–323. https://doi.org/10.1093/toxsci/kfn236

Stollenwerk, K.G., 2003. Geochemical Processes Controlling Transport of Arsenic in Groundwater. Arsen. Ground Water.

Suksabye, P., Thiravetyan, P., Nakbanpote, W., 2008. Column study of chromium(VI) adsorption from electroplating industry by coconut coir pith. J. Hazard. Mater. 160, 56–62. https://doi.org/10.1016/j.jhazmat.2008.02.083

Tawabini, B.S., Al-Khaldi, S.F., Khaled, M.M., Atieh, M.A., 2011. Removal of arsenic from water by iron oxide nanoparticles impregnated on carbon nanotubes. J. Environ. Sci. Health Part A Tox. Hazard. Subst. Environ. Eng. 46, 215–223. https://doi.org/10.1080/10934529.2011.535389

Thirunavukkarasu, O.S., Viraraghavan, T., Subramanian, K.S., 2003. Arsenic removal from drinking water using iron-oxide coated sand. Water. Air. Soil Pollut. 142, 95–111. https://doi.org/10.1023/A:1022073721853

Tseng, W.P., Chu, H.M., How, S.W., Fong, J.M., Lin, C.S., Yeh, S., 1968. Prevalence of skin cancer in an endemic area of chronic arsenicism in Taiwan. J. Natl. Cancer Inst. 40, 453–463.

Ueki, K., Kondo, T., Tseng, Y.-H., Kahn, C.R., 2004. Central role of suppressors of cytokine signaling proteins in hepatic steatosis, insulin resistance, and the metabolic syndrome in the mouse. Proc. Natl. Acad. Sci. 101, 10422–10427. https://doi.org/10.1073/pnas.0402511101

Varol, M., 2011. Assessment of heavy metal contamination in sediments of the Tigris River (Turkey) using pollution indices and multivariate statistical techniques. J. Hazard. Mater. 195, 355–364. https://doi.org/10.1016/j.jhazmat.2011.08.051

Vasudevan, S., 2012. Effects of alternating current (AC) and direct current (DC) in electrocoagulation process for the removal of iron from water. Can. J. Chem. Eng. 90, 1160–1169. https://doi.org/10.1002/cjce.20625

Vasudevan, S., Kannan, B.S., Lakshmi, J., Mohanraj, S., Sozhan, G., 2011. Effects of alternating and direct current in electrocoagulation process on the removal of fluoride from water. J. Chem. Technol. Biotechnol. 86, 428–436. https://doi.org/10.1002/jctb.2534

Vasudevan, S., Lakshmi, J., 2012. Effect of alternating and direct current in an electrocoagulation process on the removal of cadmium from water. Water Sci. Technol. 65, 353–360. https://doi.org/10.2166/wst.2012.859

Vasudevan, S., Lakshmi, J., 2011. Effects of alternating and direct current in electrocoagulation process on the removal of cadmium from water – A novel approach. Sep. Purif. Technol. 80, 643–651. https://doi.org/10.1016/j.seppur.2011.06.027

Vasudevan, S., Lakshmi, J., Jayaraj, J., Sozhan, G., 2009. Remediation of phosphate-contaminated water by electrocoagulation with aluminium, aluminium alloy and mild steel anodes. J. Hazard. Mater. 164, 1480–1486. https://doi.org/10.1016/j.jhazmat.2008.09.076

Vasudevan, S., Lakshmi, J., Sozhan, G., 2013. Electrochemically assisted coagulation for the removal of boron from water using zinc anode. Desalination, Removal of Boron

from Seawater, Geothermal Water and Wastewater 310, 122–129. https://doi.org/10.1016/j.desal.2012.01.016

Vasudevan, S., Lakshmi, J., Sozhan, G., 2012a. Simultaneous removal of Co, Cu, and Cr from water by electrocoagulation. Toxicol. Environ. Chem. 94, 1930–1940. https://doi.org/10.1080/02772248.2012.742898

Vasudevan, S., Lakshmi, J., Sozhan, G., 2012b. Optimization of electrocoagulation process for the simultaneous removal of mercury, lead, and nickel from contaminated water. Environ. Sci. Pollut. Res. 19, 2734–2744. https://doi.org/10.1007/s11356-012-0773-8

Vasudevan, S., Lakshmi, J., Sozhan, G., 2012c. Studies on the removal of arsenate from water through electrocoagulation using direct and alternating current. Desalination Water Treat. 48, 163–173. https://doi.org/10.1080/19443994.2012.698809

Vasudevan, S., Lakshmi, J., Sozhan, G., 2010. Studies Relating to Removal of Arsenate by Electrochemical Coagulation: Optimization, Kinetics, Coagulant Characterization. Sep. Sci. Technol. 45, 1313–1325. https://doi.org/10.1080/01496391003775949

Vasudevan, S., Mohan, S., Sozhan, G., Raghavendran, N.S., Murugan, C.V., 2006. Studies on the Oxidation of As(III) to As(V) by In-Situ-Generated Hypochlorite. Ind. Eng. Chem. Res. 45, 7729–7732. https://doi.org/10.1021/ie060339f

Velizarov, S., Crespo, J.G., Reis, M.A., 2004. Removal of inorganic anions from drinking water supplies by membrane bio/processes. Rev. Environ. Sci. Biotechnol. 3, 361–380. https://doi.org/10.1007/s11157-004-4627-9

Vogelsang, C., Andersen, D.O., Hey, A., Håkonsen, T., Jantsch, T.G., Müller, E.D., Pedersen, M.A., Vårum, K.M., 2005. Removal of humic substances by chitosan. Water Sci. Technol. Water Supply 4, 121–129.

Vojoudi, H., Badiei, A., Bahar, S., Mohammadi Ziarani, G., Faridbod, F., Ganjali, M.R., 2017. Post-modification of nanoporous silica type SBA-15 by bis(3-triethoxysilylpropyl)tetrasulfide as an efficient adsorbent for arsenic removal. Powder Technol. 319, 271–278. https://doi.org/10.1016/j.powtec.2017.06.028

Wan, W., Pepping, T.J., Banerji, T., Chaudhari, S., Giammar, D.E., 2011. Effects of water chemistry on arsenic removal from drinking water by electrocoagulation. Water Res. 45, 384–392. https://doi.org/10.1016/j.watres.2010.08.016

Wang, C., Luan, J., Wu, C., 2019. Metal-organic frameworks for aquatic arsenic removal. Water Res. https://doi.org/10.1016/j.watres.2019.04.043

Wang, H., Zhou, A., Peng, F., Yu, H., Yang, J., 2007. Mechanism study on adsorption of acidified multiwalled carbon nanotubes to Pb(II). J. Colloid Interface Sci. 316, 277–283. https://doi.org/10.1016/j.jcis.2007.07.075

Wang, S., Mulligan, C.N., 2006. Occurrence of arsenic contamination in Canada: sources, behavior and distribution. Sci. Total Environ. 366, 701–721. https://doi.org/10.1016/j.scitotenv.2005.09.005

Wasiuddin, N.M., Tango, M., Islam, M.R., 2002. A Novel Method for Arsenic Removal at Low Concentrations. Energy Sources 24, 1031–1041. https://doi.org/10.1080/00908310290086914

Wasserman, G.A., Liu, X., Parvez, F., Ahsan, H., Factor-Litvak, P., van Geen, A., Slavkovich, V., Lolacono, N.J., Cheng, Z., Hussain, I., Momotaj, H., Graziano, J.H., 2004. Water Arsenic Exposure and Children's Intellectual Function in Araihazar, Bangladesh. Environ. Health Perspect. 112, 1329–1333. https://doi.org/10.1289/ehp.6964

Wasserman, G.A., Liu, X., Parvez, F., Ahsan, H., Levy, D., Factor-Litvak, P., Kline, J., van Geen, A., Slavkovich, V., LoIacono, N.J., Cheng, Z., Zheng, Y., Graziano, J.H., 2006. Water manganese exposure and children's intellectual function in Araihazar, Bangladesh. Environ. Health Perspect. 114, 124–129.

Waypa, J.J., Elimelech, M., Hering, J.G., 1997. Arsenic removal by RO and NF membranes. J. - Am. Water Works Assoc. 89, 102–114. https://doi.org/10.1002/j.1551-8833.1997.tb08309.x

Weber, W.J., Morris, J.C., 1963. Kinetics of adsorption on carbon from solution. Kinet. Adsorpt. Carbon Solut.

Webster-Brown, J., Lane, V., 2005. The Environmental Fate of Geothermal Arsenic in a Major River System, New Zealand, in: Proceedings World Geothermal Congress. Antalya, Turkey, pp. 1–7.

Wickramasinghe, S.R., Han, B., Zimbron, J., Shen, Z., Karim, M.N., 2004. Arsenic removal by coagulation and filtration: comparison of groundwaters from the United States and Bangladesh. Desalination 169, 231–244. https://doi.org/10.1016/j.desal.2004.03.013

Xiong, C., He, M., Hu, B., 2008. On-line separation and preconcentration of inorganic arsenic and selenium species in natural water samples with CTAB-modified alkyl silica microcolumn and determination by inductively coupled plasma-optical emission spectrometry. Talanta 76, 772–779. https://doi.org/10.1016/j.talanta.2008.04.031

Xu, X., Gao, B., Tan, X., Zhang, X., Yue, Q., Wang, Y., Li, Q., 2013. Nitrate adsorption by stratified wheat straw resin in lab-scale columns. Chem. Eng. J. 226, 1–6. https://doi.org/10.1016/j.cej.2013.04.033

Yang, S., Li, J., Shao, D., Hu, J., Wang, X., 2009. Adsorption of Ni(II) on oxidized multi-walled carbon nanotubes: Effect of contact time, pH, foreign ions and PAA. J. Hazard. Mater. 166, 109–116. https://doi.org/10.1016/j.jhazmat.2008.11.003

Ye, S., Jin, W., Huang, Q., Hu, Y., Li, Y., Li, J., Li, B., 2017. Da-KGM based GO-reinforced FMBO-loaded aerogels for efficient arsenic removal in aqueous solution. Int. J. Biol. Macromol. 94, Part A, 527–534. https://doi.org/10.1016/j.ijbiomac.2016.10.059

Yoon, S.-H., Lee, J.H., 2005. Oxidation Mechanism of As(III) in the UV/TiO2 System: Evidence for a Direct Hole Oxidation Mechanism. Environ. Sci. Technol. 39, 9695–9701. https://doi.org/10.1021/es051148r

Yuan, X.Z., Meng, Y.T., Zeng, G.M., Fang, Y.Y., Shi, J.G., 2008. Evaluation of tea-derived biosurfactant on removing heavy metal ions from dilute wastewater by ion flotation. Colloids Surf. Physicochem. Eng. Asp. 317, 256–261. https://doi.org/10.1016/j.colsurfa.2007.10.024

Zaw, M., Emett, M.T., 2002. Arsenic removal from water using advanced oxidation processes. Toxicol. Lett. 133, 113–118.

Zhu, X., Jyo, A., 2001. Removal of Arsenic(v) by Zirconium(iv)-Loaded Phosphoric Acid Chelating Resin. Sep. Sci. Technol. 36, 3175–3189. https://doi.org/10.1081/SS-100107766

CHAPTER THREE

Kinetic and isotherms studies on adsorption of arsenic using silica based catalytic media

Published in

Journal of Water Process Engineering

Abstract

This study investigates the removal of arsenic (both As (III) and As (V)) from drinking water using a silica based catalytic media (DMI-65). In this study, BET, FTIR, XRD, SEM and XRF were used to characterize the adsorbent before and after contact with As (III) and As (V). Batch experiments were performed to evaluate the adsorption kinetics at different pH (5, 6, 7 and 8.5). The kinetic study showed that a contact time of 6 hours was needed to reach equilibrium and the experimental data were best fitted to the pseudo second-order kinetic model for both As (III) and As (V). Several batch tests were conducted with different concentration of arsenic at different pH conditions (5, 6, 7 and 8.5). During the adsorption test, the maximum adsorption of As (III) occurred at pH 5, while As (V) adsorption reached its maximum at pH 8.5. The adsorption data showed a good fit to Langmuir isotherm models and the maximum adsorption capacity of the silica based catalytic media for As (III) and As (V) were estimated to be 0.318 mg/g and 0.237 mg/g respectively.

3.1 Introduction

Arsenic is known as one of the most toxic and carcinogenic elements worldwide (Roghani et al., 2016). Arsenic contamination of drinking water has been reported in several countries including India, China, USA, Taiwan, Vietnam, Chile, Argentina, Canada and New Zealand. Arsenic in surface and groundwater originates from both natural and anthropogenic sources. It is released into water bodies from sedimentary rocks, weathered volcanic rocks and from geothermal water. Human activities such as mining, metallurgy, chemical manufacturing, and pesticide application also release arsenic into water bodies (Budinova et al., 2009; Harvey et al., 2002; López-Muñoz et al., 2017). Arsenic is known to cause skin diseases, cancer, diabetes and vascular diseases (Banerji and Chaudhari, 2016; El-Moselhy et al., 2017; Mohan and Pittman Jr., 2007; Sigdel et al., 2016).

Arsenic occurs in both organic and inorganic forms in natural waters and exists in the -3, 0, +3, +5 oxidation states. The -3 and 0 elemental states are extremely rare, whereas the +3 and +5 oxidation states are commonly found in drinking water sources in the form of arsenite (AsO_3^{3-}) and arsenate (AsO_4^{3-}) (Yazdani et al., 2016). The dominant species in natural surface water bodies is As (V) while As (III) mainly exists in anoxic environments such as groundwater. As (III) is usually more toxic and more difficult to remove from water than As (V) (Song et al., 2006). Depending on pH, As (III) may mainly exist as $H_3AsO_3^0$, $H_2AsO_3^-$, $HAsO_3^{2-}$ and AsO_3^{3-} whereas As (V) typically occurs as $H_3AsO_{4,}^0$ $H_2AsO_4^-$, $HAsO_4^{2-}$, and AsO_4^{3-} (Ansari and Sadegh, 2007; Asmel et al., 2017; Vojoudi et al., 2017).

The World Health Organization (WHO), United States Environmental Protection Agency (US. EPA) and the Drinking Water Standards for New Zealand (DWSNZ 2005 (revised 2008)) have set the maximum contamination level (MCL) or maximum acceptable concentration (MAC) at 10 µg/L for arsenic in drinking water (WHO, 2017; US EPA, 2017; DWSNZ, 2018). To meet the standard, a more efficient method of arsenic removal from drinking water is required. Over the last decade, several methods have evolved to effectively remove arsenic from drinking water such as precipitation, membrane processes, ion exchange, coagulation followed by filtration and adsorption (Choong et al., 2007; Litter et al., 2010; Villaescusa and Bollinger, 2008). Some of the factors that should be considered

before selecting a particular treatment method include: treatment cost, arsenic disposal, operational complexity of the technology and skill required to operate the technology (Çiftçi and Henden, 2015).

The Waikato River is located in the North Island of New Zealand and it is the longest river in New Zealand (425 km) and the most utilized river in New Zealand. The source of the water is from the volcanic region of the central plateau, and thereafter flows through the largest lake in the country, Lake Taupo (McLaren and Kim, 1995). Arsenic concentration in the Waikato River is more than the recommended value of 10 µg/L mostly from geothermal source (natural and geothermal power stations) (Robinson et al., 1995).

Adsorption is used as an alternative to conventional removal techniques because it is considered to be relatively simple, efficient, cheap, more convenient for rural application and for regeneration (Babel and Kurniawan, 2003; Bhat et al., 2015; Chammui et al., 2014; Lee and Davis, 2001). Several adsorbents have been studied to remove arsenic from drinking water such as feldspars (Yazdani et al., 2016), molecular imprinted polymers (Önnby et al., 2012), amine doped acrylic ion exchange fibres (Lee et al., 2017), nanoparticle coated resins (Çiftçi and Henden, 2015), New Zealand Iron Sand (Panthi and Wareham, 2014), biochar (Zhu et al., 2016) and multi carbon nanotubes (Addo Ntim and Mitra, 2012).

Silica based catalytic media (DMI-65) is a dark brown to black coloured granular material which facilitates an oxidation-precipitation-filtration process and was primarily designed to remove iron and manganese. The surface of DMI-65 contains manganese and oxygen sites for iron adsorption present in water. Insoluble ferric hydroxide which precipitates in crystalline form is removed via filtration through the media surface as the reaction of ferrous bicarbonate and NaOCl oxidizes by giving up OH^- (Eq. 3.1) and the redox reaction is shown in Fig. 3-1a. The reaction mechanism of manganese removal (Fig. 3-1b) is shown in Eq. (3.2) below:

$$2Fe(HCO_3)_2 + NaOCl + H_2O \Rightarrow 2Fe(OH)_3 + 2CO_2 + NaCl \quad (3.1)$$

$$Mn(HCO_3)_2 + NaOCl \Rightarrow MnO(OH)_2 + NaCl + 2CO_2 \quad (3.2)$$

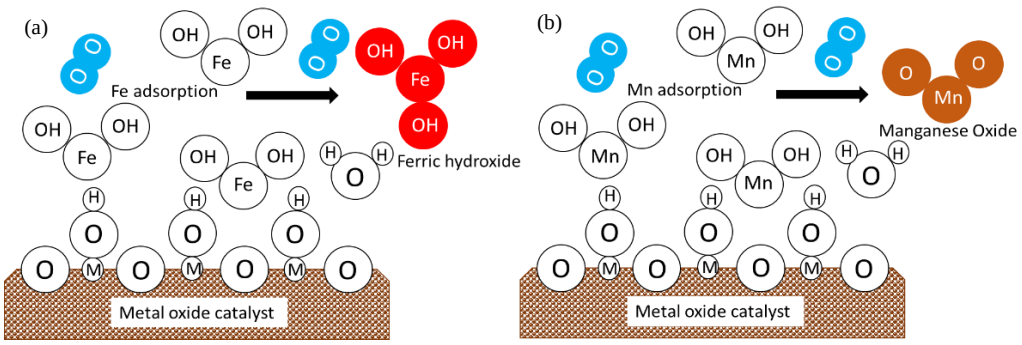

Figure 3-1: (a) Iron oxidation at catalytic surface (b) Manganese oxidation at catalytic surface (Quantum Filtration Medium, 2018).

Where M: (Mn+);n = 1,2…metal ion in the catalytic surface lattice, O = oxygen atom or ion (O^-), Fe= iron atom or ion (Fe^{2+}, Fe^{3+}), H = hydrogen atom or ion (H^+), OH = hydroxide, or hydroxyl anion (OH^-), H_20 = water molecule, $Fe(OH)_2$ = ferrous hydroxide, $Fe(OH)_3$ = ferric hydroxide , O_2 = oxygen molecule, MnO_2 = manganese oxide. The preferred oxidant is chlorine (fed as sodium hypochlorite (NaOCl) or bleach (12.5% NaOCl) because of its availability, low cost and effectiveness. Chlorine also keeps the media free of bacterial growth. Other oxidants that can be used are hydrogen peroxide (H_2O_2), chlorine oxide (ClO_2) and ozone (Quantum Filtration Medium, 2018).

DMI-65 was traditionally designed to remove iron and manganese from raw water; it has not been trialled for arsenic removal. In this study, the effectiveness of DMI-65 for As (III) and As (V) removal was explored. The effect of pH of the aqueous solution, adsorption time, temperature and initial concentration of As (III) and As (V) were evaluated to find the optimum adsorption conditions.

3.2 Experimental

3.2.1 Materials and chemicals

DMI-65 is a dark odourless granule obtained from Quantum Filtration Medium Property Ltd, Australia and was activated using NaOCl prior to use for the adsorption study. All chemicals and reagents used were of analytical grade. A stock solution of 100 mg/L As (III) and As (V) were prepared by dissolving As_2O_3 (Sigma-Aldrich, 99%) and As_2O_5 (Sigma-Aldrich, 99%) in deionized water (18.2 MΩ cm-1; Barnstead, EASYpure) respectively. The stock solution was diluted with distilled water to obtain the required As (III) and As (V) concentrations used in this study. A stock solution of 50 g/L ferric chloride ($FeCl_3$) and 50 mg/L NaOCl were

prepared in a volumetric flask and diluted to the required concentrations of 50 mg/l $FeCl_3$ and 5 mg/L NaOCl. The pH adjustments were performed using 0.1M hydrochloric acid (HCl) and 0.1M sodium hydroxide (NaOH) solutions. Other chemicals used were nitric acid (70 % HNO_3) and ethanol (70 % C_2H_5OH). All chemicals were supplied by Merck KGaA, Darmstadt, Germany unless stated otherwise.

3.2.2 Instrumentation

A pH meter (Eutech pH150 pH/temperature meter) and a fixed temperature shaker (Ratek orbital) were utilized in this study. The pH meter was calibrated prior to use using 4.01, 7.01 and 10.04 pH buffers (Merck KGaA, Darmstadt, Germany). Total arsenic concentration was measured by an inductively coupled plasma mass – spectrometry (ICP-MS). Quality control employed for ICP-MS measurements are shown in APPENDIX 2BA. Palintest Photometer 7100 was used to measure the free chlorine and manganese concentration during the activation process.

3.2.3 DMI-65 activation

In the batch adsorption experiments, 15 mL Falcon tubes containing 1 g of DMI-65 were prepared. All the samples were soaked with 5 mL of 12.5 % NaOCl. After 24 hours, the media was washed repeatedly until the free chlorine residual in the solution dropped to 0.1 – 0.3 ppm and manganese concentration dropped to 0.15 ppm. Activation process is necessary so that the catalytic surface of the media is kept clean and available to ions from water to contact, and the use of distilled water or water known to be strongly corrosive to metals should not be used for the activation process.

3.2.4 Characterization of adsorbent (Silica based catalytic media)

Porosity and surface characteristics were measured by N_2 (0.162 nm^2) adsorption using a NOVA-2000E (Quantachrome, USA) surface area analyzer. Brunauer-Emmertt-Teller (BET) surface area, pore volume and pore size of the adsorbent were determined by multipoint BET analysis of adsorption data points. Fourier transform infrared spectroscopy (FTIR PerkinElmer Spectrum 100) was used to detect the surface functional groups at a spectral range of 450 – 4000 cm^{-1} at 25 ^oC with a resolution of 4 cm^{-1}. X-ray diffraction (XRD) patterns of DMI-65 were measured using X – ray diffractometer (PANalytical Empyrean) with Ni filter Cu

Kα (λ = 0.154 nm) radiation operated at 40 kV and 40 mA. X-ray diffraction patterns were recorded in the range of 2θ = 4 – 80°. The surface morphology and chemical composition of the DMI-65 were investigated using a scanning electron microscopy coupled with energy dispersive spectroscopy (SEM-EDX, HITACHI S-4700) and X–ray fluorescence (XRF, S8 TIGER Series 2 WDXRF) respectively. The samples were coated with platinum to improve conductivity and to obtain good images. Elemental analysis was done by EDX operating at an accelerating voltage of 5 kV. The average particle size of DMI-65 was determined by Malvern Mastersizer 3000.

3.2.5 Adsorption experiments

All batch experiments were conducted by adding 1g of DMI-65 to 50 mL of As (III) and As (V) solution (20 g/L) in a 100 mL Erlenmeyer conical flask and agitating at 130 rpm on an orbital shaker at room temperature (19 ± 2 °C). In addition, 0.25 mg/L of $FeCl_3$ and 0.4 mg/L NaOCl were also added to the solution. The initial pH was adjusted with 0.1M NaOH and 0.1M HCl. After a predetermined contact time, media samples were filtered through Whatman-42 filter papers (0.45 μm) and the arsenic concentration in the filtrate was measured using ICP-MS.

Adsorption kinetics experiments were conducted by shaking 1 g of activated DMI-65 with 50 mL of As (III) or As (V) solution containing 0.06 mg/L As (V) at different pH (5, 6, 7 and 8.5). The sorption amount of As (III)/As (V) was measured at different time intervals. The mixture was agitated at 130 rpm on an orbital shaker at room temperature for 24 hour to reach equilibrium conditions.

Adsorption isotherm experiments were conducted as follows: 1 g of activated DMI-65 was mixed with 50 mL As (III) and As (V) solution with concentrations (0.03 – 20 mg/l) for As (III) and (0.03 – 30 mg/L) for As (V) at different pH (5, 6, 7 and 8.5). The mixture containing different As (III) or As (V) concentrations was agitated at 130 rpm in an orbital shaker at room temperature for 24 hour to reach equilibrium. All adsorption experiments were performed in duplicate.

The amount of As (III)/As (V) adsorbed, q_t (mg/g) at time *t*, was calculated according to equation (3):

$$q_t = \frac{[(C_o - C_t)V]}{W} \quad (3.3)$$

Where C_o and C_t (mg/L) are the liquid phase concentrations of As (III)/As (V) at initial time zero and time *t* respectively, V is the volume of the arsenic solution (L), and W is the mass (g) of DMI-65 used for As (III)/As (V) adsorption.

The percentage of arsenic removal was calculated according to Eq. (3.4):

$$R\ \% = \left[\frac{C_o - C_e}{C_o}\right] X\ 100 \quad (3.4)$$

Where C_e is the equilibrium concentration in the solution (mg/L).

3.2.6 Thermodynamics experiments

The effect of temperature (283, 288, 293 and 298 K) on adsorption processes was carried out to determine the values of enthalpy (ΔH^o), entropy (ΔS^o) and Gibbs free energy (ΔG^o). 1 g of activated DMI-65 was mixed with 50 ml As (III) and As (V) solutions at pH 7. The mixture containing different As (III)/As (V) concentrations was agitated at 130 rpm in an orbital shaker at 283, 288, 293 and 298 K for 24 hour to reach equilibrium.

3.3 Results and discussion

3.3.1 Characterization of silica based catalytic media

The results obtained for elemental composition of raw DMI-65 using XRF are shown in Table 3-1. The elemental analysis showed that the main constituent of DMI-65 is SiO_2 (96.55 %) by mass. Procedure is shown in Appendix 3L.

Table 3-1: Chemical composition of DMI-65 using XRF

Constituent	SiO_2	Al_2O_3	TiO_2	Fe_2O_3	MgO	K_2O	CaO	P_2O_5	CO_2
Before Activation (%)	96.55	1.16	0.046	0.116	0.074	0.867	0.47	0.082	0.54
After Activation (%)	97.52	0.97	0.048	0.115	0.075	0.620	0.42	0.049	0.21
After Contact As (III) (%)	97.04	1.15	0.057	0.165	0.066	0.760	0.44	0.048	0.17
After Contact As (V) (%)	97.15	1.09	0.046	0.145	0.071	0.705	0.47	0.049	0.13

Constituent	Sc	Cr	Co	Ni	Cu	MnO	S	Cl
Before Activation (ppm)	3.00	44.00	202.00	13.00	5.00	6519.00	3,015.00	1680.00
After Activation (ppm)	3.00	9.00	121.00	10.00	5.00	4104.00	nd	67.00
After Contact As (III) (ppm)	3.00	31.00	110.00	10.00	2.00	3839.00	nd	48.00
After Contact As (V) (ppm)	3.00	20.00	118.00	10.00	2.00	3916.00	nd	46.00

nd = Not detected

The following minor components Al_2O_3, K_2O, CaO and Fe_2O_3 are the most prominent and also include trace elements such as Co, Cu, Ni, S, Sc, Cr, Cl and MnO (ppm). It was observed that the amount of Fe_2O_3 increases after contact with As (III) and As (V). This is probably due to the addition of $FeCl_3$ during the adsorption tests. Also Sulphur in the media before activation (3015 ppm) was completely removed during the activation process and the amount of Cl reduced significantly after activating the media.

Particle size distribution by volume was analysed using Malvern mastersizer as shown in Fig. 3-2 to evaluate any changes in the media before and after activating the media. The D10, D50 and D90 values for the distribution before activation are 469, 742 and 1170 µm respectively. After activation, the values are D10 (484 µm), D50 (726 µm) and D90 (1100µm). The volume mean diameter D[4,3] and surface mean D[3,2] before activation are 783 µm and 700 µm respectively whereas D[4,3] and D[3,2] after activation are 765 µm and 695 µm respectively. The reduction in D90 after activation is due to some loss of particle surface during the activation process as some particulates were observed after the media had been removed from solution.

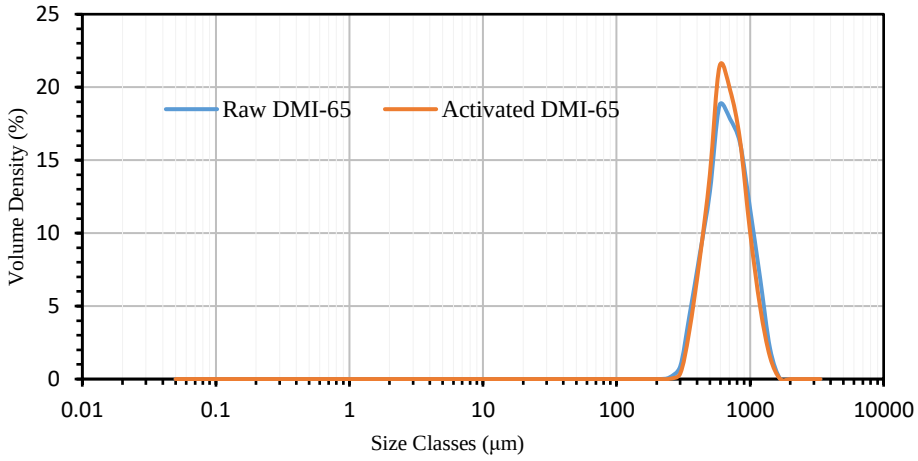

Figure 3-2: Particle size distribution by volume of DMI-65 before and after activation

The adsorption/desorption experiments using nitrogen gas (N_2) is a standard procedure for determining surface area, pore size and pore volume of samples using multipoint BET method and it was repeated four times. The BET surface area of DMI-65 increased from 0.50 m^2/g to 5.24 m^2/g after activation with NaOCl (Table

3-2). There was also an increase in pore volume and pore size after activation. However there was reduction in surface area, pore volume and pore size after contact with As (III) and As (V) under the same operating conditions (contact time: 24 h; agitation speed: 130 rpm, initial pH 7 ± 0.2; dosage 20 g/L and As (III) and As (V) 0.06 mg/L). The obvious reduction in surface area and pore volume suggest the successful adsorption of arsenic onto the media. (Appendix 3A -3D)

Table 3-2: Surface areas, pore volume and pore size of DMI-65 before activation, after activation and after contact with As (III) and As (V) (Appendix 3K)

	Surface Area (m^2/g)	Pore volume (cm^3/g)	Pore size (nm)
Before activation	0.50 ± 0.03	0.00013	2.13 ± 0.15
After activation	5.24 ± 0.36	0.00139	1.16 ± 0.21
After contact with As (III)	3.89 ± 0.41	0.00106	1.24 ± 0.92
After contact with As (V)	3.88 ± 0.09	0.00107	1.24 ± 0.15

The surface morphology and EDX analysis of all the DMI-65 samples before activation, before and after adsorption with As (III) and As (V) were observed by scanning electron microscopy (SEM) and is shown in Fig. 3-3 (a-d). The surface of the inactivated DMI-65 was rough due to the presence of sulphur with traces of chlorine and potassium on the surface with cavities present (Fig. 3-3a) whereas after activation, the sulphur coatings had reduced significantly in size and shape resulting in a relatively smooth surface. The reduction in size and shape can be attributed to the washing of the DMI-65 as part of the activation process. As illustrated in Fig. 3-3c and d, there is a remarkable change in the morphology and surface of DMI-65 after contact with As (III) and As (V). The micrograph shows surface heterogeneity and crystals embedded on the surface of the adsorbent resulting from adsorption of As (III) and As (V). EDX spectra from Fig. 3-3 (a-d) showed an abundance of silica in the adsorbent with an elevated amount of silica observed after activation. Other elements present are Mn, Cl, O, S and K and the high oxygen content in the EDX analyses shows the presence of oxyhydroxides and oxides. However the presence of arsenic was not observed by the SEM-EDX due to the low concentration of arsenic used in this study and thus difficult to see (Appendix 3F – 3J).

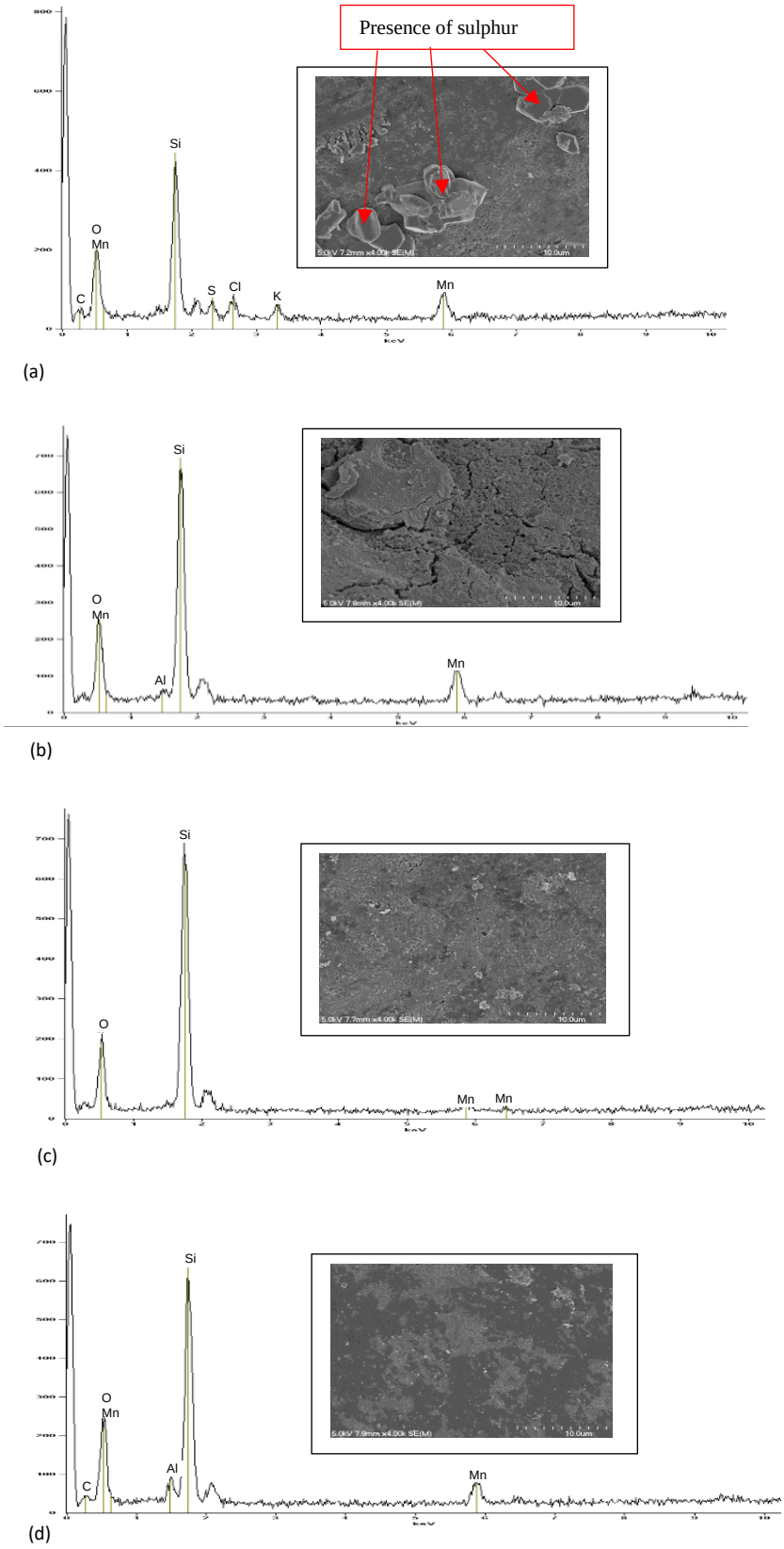

Figure 3-3: SEM images and EDX surface analysis of DMI-65 (a) raw DMI-65; (b) activated DMI-65; (c) after contact with As (III); (d) after contact with As (V) (adsorbent dosage = 20 g/L, initial concentration = 0.06 mg/L, contact time = 24 hours, agitation speed = 130 rpm, pH 7 ± 0.2).

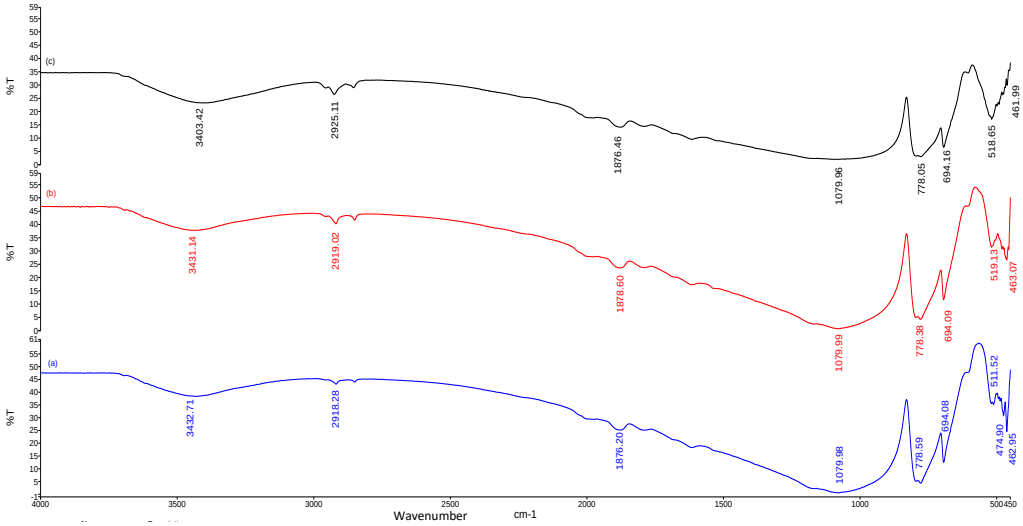

Figure 3-4: FTIR spectra for DMI-65 at 4000 – 450 cm^{-1} (a) raw DMI-65, (b) after contact with As (III) and (c) after contact with As (V). (Procedure = Appendix 3M)

The FTIR spectra of samples before and after adsorption with As (III) and As (V) were investigated (Fig. 3-4) to determine the functional groups and structure of the material. The spectra were measured across the 4000 – 450 cm^{-1} range. The broad peak at wavelength of 3100 – 3700 cm^{-1} corresponds to the stretching vibrations of functional group –OH which indicates the presence of water molecules forming a hydrogen bond to the inorganic structure (Ahmed et al., 2016). The presence of a strong and broad absorption band at 1083.87 cm^{-1} is attributed to asymmetrical stretch vibration of Si-O-Si from silica quartz in the media whereas the peaks at 797.25 cm^{-1} and 462.73 cm^{-1} are symmetric stretching vibration and bending vibration of Si-O-Si bond respectively (Hadizade et al., 2017; Wang et al., 2018). The band at 1619.26 cm^{-1} is due to the bending vibration mode of free water molecules while the band at 581.05 cm^{-1} is probably an indication of the presence of Fe-O from hematite and an additional Cu-O bonding at 694.48 cm^{-1} (Lin and Wang, 2014). The 1877.59 band is the C=O stretch characteristic for a non-conjugated strong carbonyl group (CO_2 in DMI 65) from calcite in the DMI media. The peak at 3472.71 shifted to 3403.42 after contact with As (V) whereas there is a shift in peaks at 511.52 for both As (III) and As (V) to 519.13 and 518.65 respectively. This indicates an interaction of both As (III) and As (V) and Fe-O.

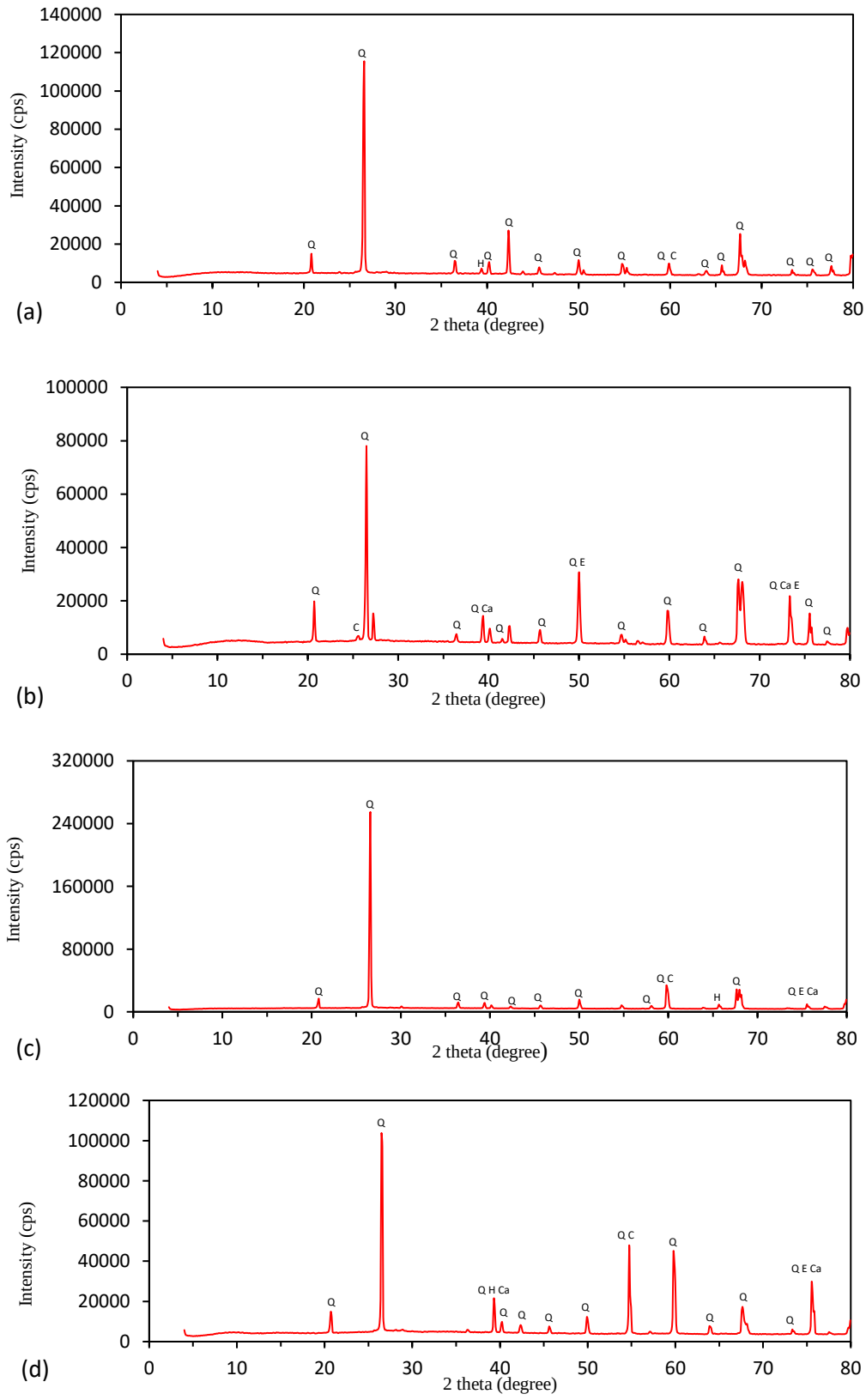

Figure 3-5: XRD pattern of DMI-65 (a) before activation, (b) after activation, (c) after contact with As (III) and (d) after contact with As (V). (Q: Quartz; C: Corundum; Ca: Calcite; E: Eskolaite; H: Hematite).

The X-ray diffraction (XRD) patterns for DMI-65 shown in Fig. 3-5 revealed that quartz (SiO_2) is the major constituent before activation and after contact with arsenic with traces of hematite and corundum (JCPDS 46-1045). This is in agreement with analysis from XRF which show SiO_2 to be the major composition of DMI 65. Diffraction peaks were observed at 2θ = 20.852, 26.649, 36.458, 40.283, 42.466, 45.809, 50.143, 55.327, 59.951, 65.761, 68.131, 73.459, 75.673 and 77.665 which were corresponding to 100, 101, 110, 111, 200, 201, 112, 103, 211, 300, 301, 104, 301 and 220 planes respectively. After activation, there is a significant increase in intensity for all the planes and traces of calcite and eskolaite. After adsorption with As (III), a sharp increase in intensity was observed at 2θ = 26.456 (101) and a reduction in intensity in other angles whereas after adsorption with As (V), an increase in intensity was observed in most angles.

3.3.2 Effect of pH and adsorption kinetics

The effect of pH which is an important parameter controlling the adsorption of arsenic (Fig. 3-6) both in the acidic and alkaline range was examined. The dominant form of As (III) in natural waters exist in solution as H_3AsO_3 at pH 0-9 while $H_2AsO_3^-$, $HAsO_3^{2-}$ and AsO_3^{3-} ions exist as stable forms at pH 10-12, 13 and 14 respectively whereas the dominant form of As (V) in natural waters exist in solution as $H_3AsO_4^0$ (pH < 2), $H_2AsO_4^-$ (pH 3-6), $HAsO_4^{2-}$ (pH 7-11) and AsO_4^{3-} (pH 12-14) respectively (Lin and Wang, 2014; Wang et al., 2018). The pH range of 5 – 8.5 was chosen for this study due to the fact that DMI-65 is known to perform satisfactorily at a certain pH range (5.8 – 8.6). The percentage of As (III) removal did not change significantly with increase in pH which might be due to the presence of undissociated As (III) species in the aqueous solution (Youngran et al., 2007). The removal of As (V) decreases from pH 5 - 8.5. The decrease is due to competition with OH^- for active sites as lower pH range favoured the protonation of the adsorbent surface. This reduction in As (V) adsorption might also be due to reduction of electrostatic attraction between surface and $H_2AsO_4^-$ anions. This decrease might also be due to strong electrostatic repulsion between the negatively charged sites on the surface and $H_2AsO_4^-$ anion (Chaudhry et al., 2017; Elizalde-González et al., 2001). The equilibrium pH after the adsorption process is in the range of 6.51 – 6.93 for both As (III) and As (V) as shown in Fig. 3-6.

From Fig. 3-7, more than 93 % of As (III) in the solution was removed for all the pH considered after a contact time of 24 hours. The maximum As (III) removal was found to 96.55 % at pH 5. The maximum percentage of As (V) removal was 90.4 % at pH 5 whereas 89.30 %, 87.49 % and 86.56 % of As (V) were removed after a contact time of 24 hours at pH 5, 6 and 7 respectively. This result shows that more than 86 % of the initial arsenic concentration was removed for all the pH values considered in this study and are below the MAV of 0.010 mg/L.

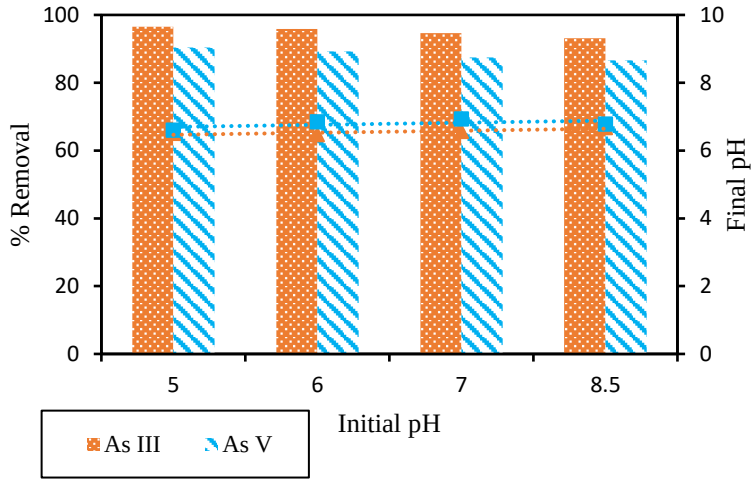

Figure 3-6: Effect of pH on As (III) and As (V) removal by DMI-65 (adsorbent dosage = 20 g/L, initial concentration = 0.06 mg/L, contact time = 24 hours, agitation speed = 130 rpm) and also showing the final pH at equilibrium (dotted lines = Final pH).

Three different kinetic models were applied to determine the kinetic data for arsenic adsorption and to select the most suitable model for defining the experimental q_e value. The three models are pseudo first-order, pseudo second-order and Elovich kinetic models. The pseudo first-order non-linear model can be expressed as shown in Eq. (3.5):

$$q_t = q_e(1 - \exp^{-K_1 t}) \quad (3.5)$$

Eq. (3.5) can further be linearized by the following equation:

$$\log(q_e - q_t) = \log q_e - \frac{K_1 t}{2.303} \quad (3.6)$$

The non-linear form of pseudo second-order model is given as:

$$q_t = \frac{K_2 q_e^2 t}{(1 + q_e K_2 t)} \quad (3.7)$$

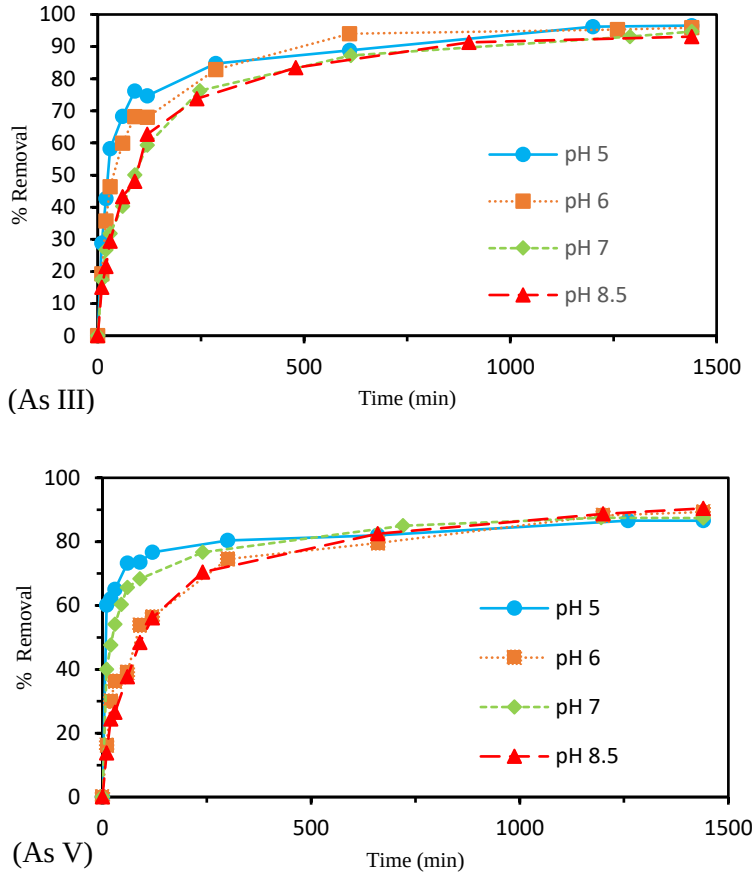

Figure 3-7: Effect of contact time on As (III) and As (V) removal by DMI-65 (adsorbent dosage = 20 g/L, initial concentration = 0.06 mg/L, contact time = 24 hours, temperature = 19 ± 2 ºC, agitation speed = 130 rpm, pH (5, 6, 7 and 8.5)

Eq. (3.7) can further be linearly expressed by the following equation:

$$\frac{t}{q_t} = \frac{1}{K_2 q_e^2} + \frac{t}{q_e} \qquad (3.8)$$

Where K_1 and K_2 is the pseudo first-order (min^{-1}) and pseudo second-order (g/mg.min) rate constants respectively, t is the time (min), q_e and q_t represent the quantity of As (III)/As (V) adsorbed (mg/g) on the surface of DMI-65 at equilibrium and at time t (min) respectively (Gulnaz et al., 2005).

The Elovich kinetic model can be expressed as:

$$q_t = \left(\frac{1}{\beta}\right) \text{In } (\alpha\beta) + \left(\frac{1}{\beta}\right) \text{In } (t) \qquad (3.9)$$

Where α (mg/g min) and β (g/mg) are the initial adsorption rate constant and the Elovich adsorption constant respectively (Sen Gupta and Bhattacharyya, 2011).

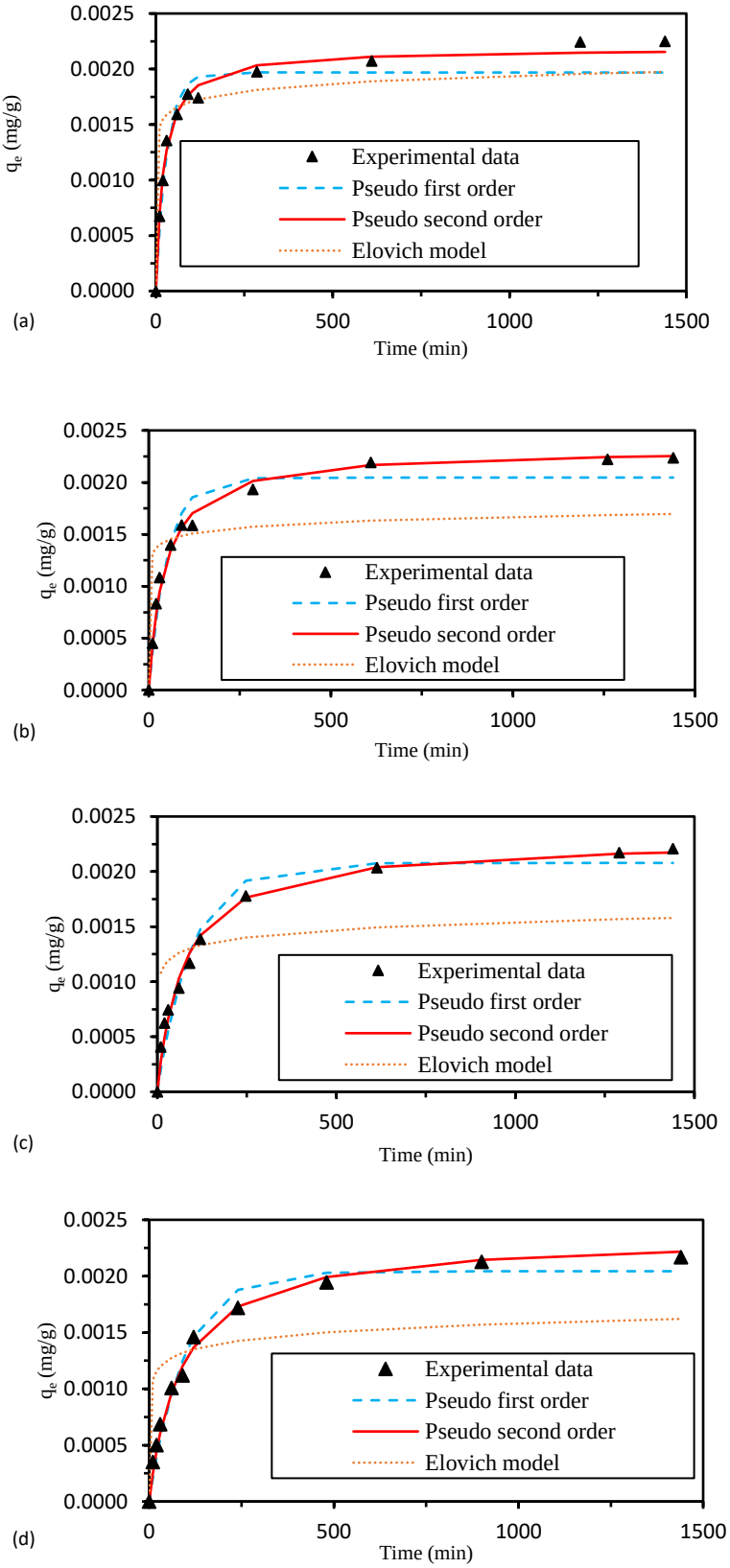

Figure 3-8: Adsorption kinetic plots for As (III) (adsorbent dosage = 20 g/L, initial concentration = 0.06 mg/L, contact time = 24 hours, temperature = 19 ± 2 ºC, agitation speed = 130 rpm. (a) pH 5, (b) pH 6, (c) pH 7 and (d) pH 8.5.

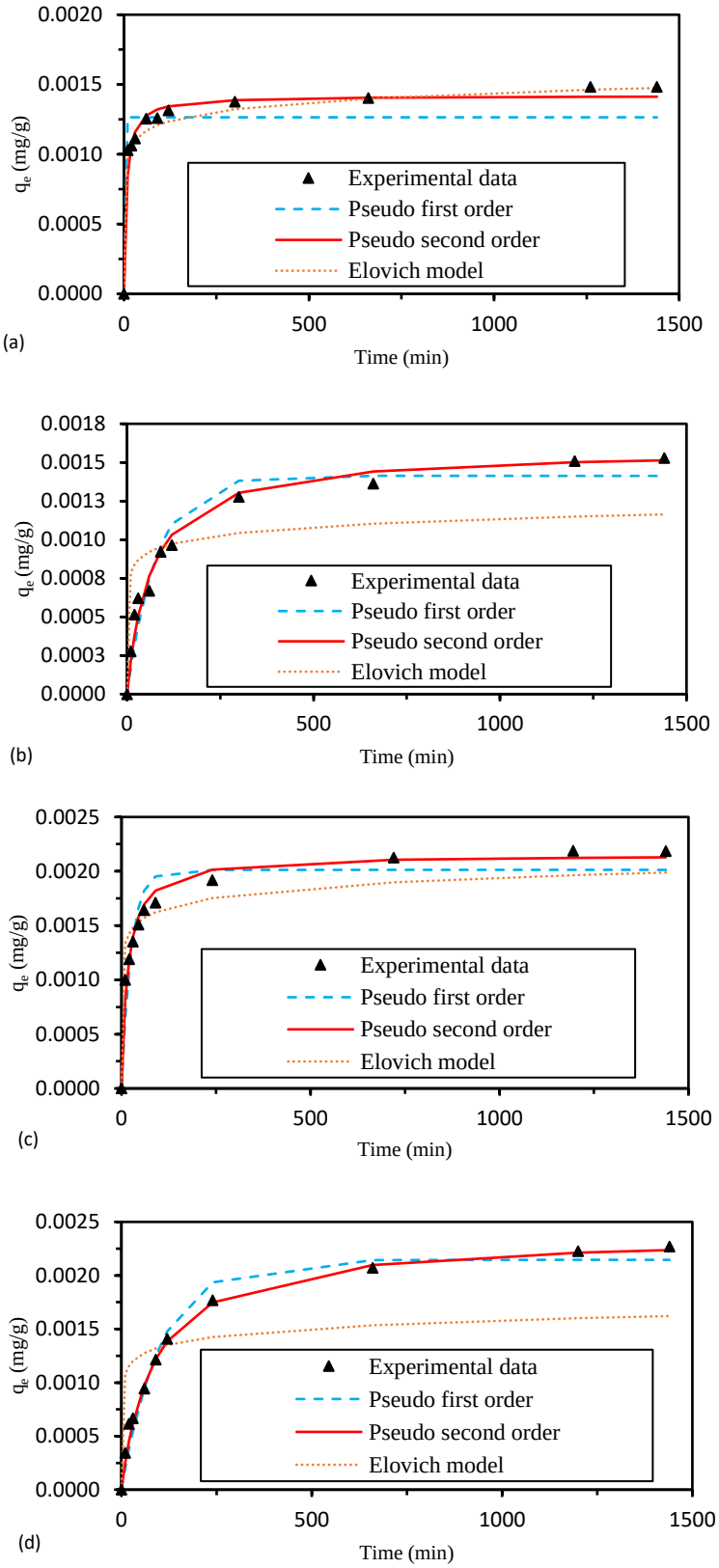

Figure 3-9: Adsorption kinetic plots for As (V) (adsorbent dosage = 20 g/L, initial concentration = 0.06 mg/L, contact time = 24 hours, temperature = 19 ± 2 ºC, agitation speed = 130 rpm. (a) pH 5, (b) pH 6, (c) pH 7 and (d) pH 8.5.

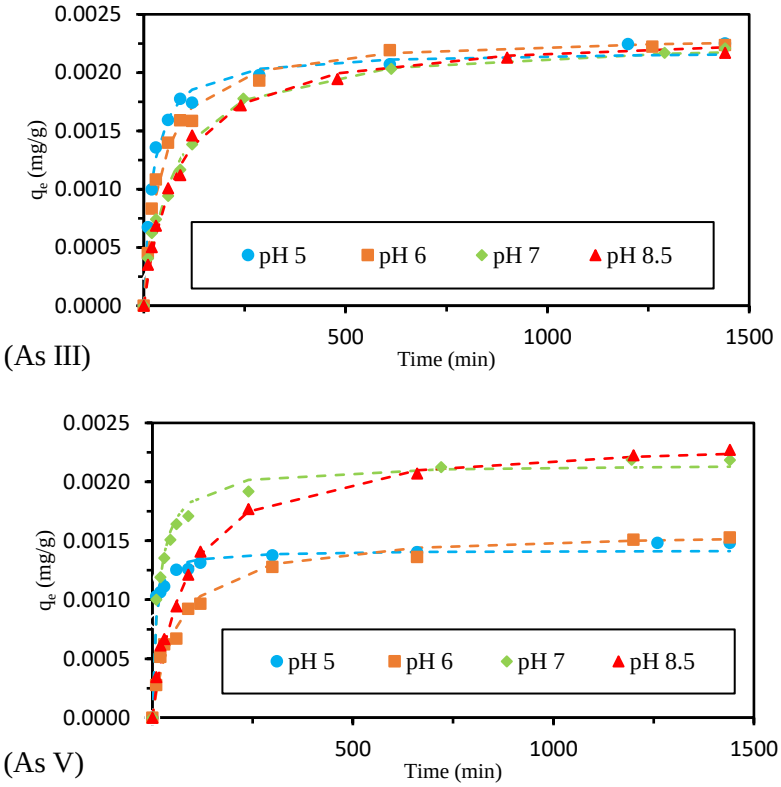

Figure 3-10: Pseudo-second-order-rate kinetics model for As (III) and As (V) removal by DMI 65 (adsorbent dose = 20 g/L, initial concentration = 0.06 mg/L, contact time = 24 hours, temperature = 19 ± 2 °C, agitation speed = 130 rpm, pH (5, 6, 7 and 8.5).

Pseudo first-order, pseudo second-order and Elovich kinetic models were employed to analyse the kinetic data. The kinetic plots for As (III) and As (V) adsorption onto DMI-65 at different pHs are shown in Fig. 3-8 and 3-9. The rate of As (V) adsorption was rapid in the first 20 min for pH 5 and pH 7 whereas at pH 6 and 8.5, a gradual adsorption process occurs before reaching equilibrium. The rate of As (III) adsorption showed a gradual increase in the first 7 hours for all the different pH considered in this study.

The kinetic parameters were determined by fitting the experimental data to non-linear kinetic models as presented in Table 3-3. According to the correlation factor (R^2), the pseudo second-order model (Fig. 3-10) fitted the experimental data better than pseudo first-order and Elovich models for As (III) and As (V) adsorption onto DMI-65 (Appendix 3N and 3O).

The adsorption of As (V) onto DMI-65, the values of q_e obtained from the non - linear pseudo second-order model are close to experimental values of q_e (0.00142, 0.00158, 0.00215 and 0.00235 mg/g) for pH 5, 6, 7 and 8.5 respectively. Likewise,

the values of q_e for As (III) adsorption are much closer to the experimental values (0.00225, 0.00224, 0.00221 and 0.00217) for pH 5, 6, 7 and 8.5 respectively. These show that the kinetics of As (III) and As (V) adsorption onto DMI-65 fit very well with the pseudo second-order rate kinetic model, which might suggest that the adsorption process is chemisorption which involves exchange/sharing of electrons between DMI-65 and As (III) and As (V) as covalent forces and ion exchange (Sherlala et al., 2019). The supremacy of pseudo second-order model over the pseudo first-order and Elovich models has been reported in other studies (Asmel et al., 2017; Bhaumik et al., 2015; Çiftçi and Henden, 2015). Comparison between As (III) and As (V) adsorption kinetics (pseudo-second order kinetic) is shown in Appendix 3P.

3.3.3 Adsorption isotherm studies

The Langmuir, Freundlich, Langmuir-Freundlich (L-F) and Dubinin-Radushkevich (D-R) models (Gimenez et al., 2007; Mandal et al., 2013) were used in this study to explain the interaction between arsenic and the DMI-65 media (Fig. 3-11 and 3-12).

The Langmuir equation can be expressed as:

$$q_e = \frac{K_L q_m C_e}{1 + K_L C_e} \tag{3.10}$$

Where q_e is the amount of As (III)/As (V) adsorbed at equilibrium (mg/g), C_e represents the equilibrium concentration of As (III)/As (V) in the aqueous solution (mg/L), q_m is the maximum adsorption capacity (mg/g) and K_L is the Langmuir constant (L/mg).

Eq. (3.10) can further be linearized as shown in Eq. (3.11)

$$\frac{C_e}{q_e} = \frac{1}{q_m K_L} + \frac{C_e}{q_m} \tag{3.11}$$

The Freundlich equation can be expressed as:

$$q_e = K_F C_e^{\frac{1}{n}} \tag{3.12}$$

Where K_F is the Freundlich constant (mg/g) and 1/n is a constant related to the adsorption intensity.

Table 3-3: Pseudo first-order, Pseudo second-order and Elovich models for As (III) and As (V) adsorption on DMI-65 at different initial pH conditions.

Model	pH 5		pH 6		pH 7		pH 8.5	
	As (III)	As (V)	As (III)	As (V)	As (III)	As (V)	As (III)	As (V)
Pseudo first-order kinetic model								
K_1 (min^{-1})	0.0328	0.8999	0.0198	0.0126	0.0021	0.0388	0.0105	0.0086
$q_{e,\ experimental}$ (mg/g)	0.00225	0.00148	0.00224	0.00153	0.00221	0.00153	0.00217	0.00227
$q_{e,\ model}$ (mg/g)	0.00197	0.00127	0.00205	0.00141	0.00208	0.00201	0.00204	0.00215
R^2	0.950	0.857	0.956	0.944	0.966	0.921	0.977	0.975
Pseudo second-order kinetic model								
K_2 (g/mg.min)	21.15	104.67	9.90	9.90	6.00	28.47	4.95	4.95
q_e (mg/g)	0.00219	0.00142	0.00232	0.00158	0.00228	0.00215	0.00234	0.00235
R^2	0.991	0.971	0.990	0.978	0.989	0.983	0.986	0.993
Elovich kinetic model								
α (mg/g)	26.0	0.301	247.015	0.226	0.500	0.334	0.224	0.222
β (g/mg.min)	9999.0	10389.2	13126.1	13126.2	10001	7600.0	9189.7	9189.8
R^2	0.711	0.852	0.555	0.531	0.475	0.793	0.507	0.492

Eq. (3.12) can further be linearized as shown in Eq. (3.13)

$$\log q_e = \log K_F + \frac{1}{n}\log C_e \qquad (3.13)$$

The Langmuir-Freundlich equation can be expressed as:

$$q_e = \frac{K_L q_m C_e^{\frac{1}{n}}}{1 + K_L C_e^{\frac{1}{n}}} \quad (3.14)$$

Table 3-4: Estimated isotherms parameters for adsorption using DMI-65

Model	pH 5		pH 6		pH 7		pH 8.5	
	As (III)	As (V)	As (III)	As (V)	As (III)	As (V)	As (III)	As (V)
Langmuir								
q_m (mg/g)	0.318	0.131	0.269	0.122	0.270	0.170	0.291	0.224
K_L (L/mg)	0.774	1.981	1.389	2.146	1.093	1.297	0.890	0.901
R^2	0.992	0.993	0.994	0.991	0.990	0.990	0.994	0.991
Freundlich								
K_F (mg/g)	0.141	0.072	0.141	0.071	0.135	0.083	0.134	0.095
n	3.409	3.383	3.962	3.214	3.778	2.540	3.481	2.226
R^2	0.960	0.895	0.925	0.934	0.940	0.961	0.953	0.985
Langmuir-Freundlich								
q_m (mg/g)	0.248	0.125	0.254	0.123	0.240	0.165	0.239	0.203
K_L (L/mg)	1.101	1.342	1.125	1.310	1.116	1.001	1.101	0.908
n	2.355	2.116	2.696	2.289	2.577	2.527	2.466	2.428
R^2	0.980	0.961	0.981	0.986	0.989	0.961	0.988	0.979
Dubinin-Radushkevich								
q_s (mg/g)	0.273	0.113	0.248	0.114	0.244	0.146	0.257	0.174
K_{DR} (mol^2/KJ^2)	0.261	0.069	0.162	0.080	0.202	0.117	0.251	0.127
R^2	0.951	0.989	0.969	0.960	0.961	0.951	0.962	0.934

The Dubinin - Radushkevich equation can be expressed as:

$$q_e = q_s \exp(-K_{DR}\varepsilon^2) \quad (3.15)$$

$$\varepsilon = RT \ln\left(1 + \frac{1}{C_e}\right) \quad (3.16)$$

Where K_{DR} is D-R isotherm constant (mol^2/KJ^2), ε is the Polanyi potential, q_s is the isotherm saturation capacity (mg/g), R is the universal gas constant (8.314 $Jmol^{-1}K^{-1}$) and T is the temperature in Kelvin (K).

Eq. (3.15) can be linearized as shown in Eq. (3.17)

$$\ln q_e = \ln q_s - K_{DR}\varepsilon^2 \quad (3.17)$$

Isotherm parameters were obtained using non-linear regression to fit the models to experimental data at different pH (5, 6, 7 and 8.5) for As (III) and As (V) (Fig. 3-11 and 3-12) using Excel-solver (Table 3-4).

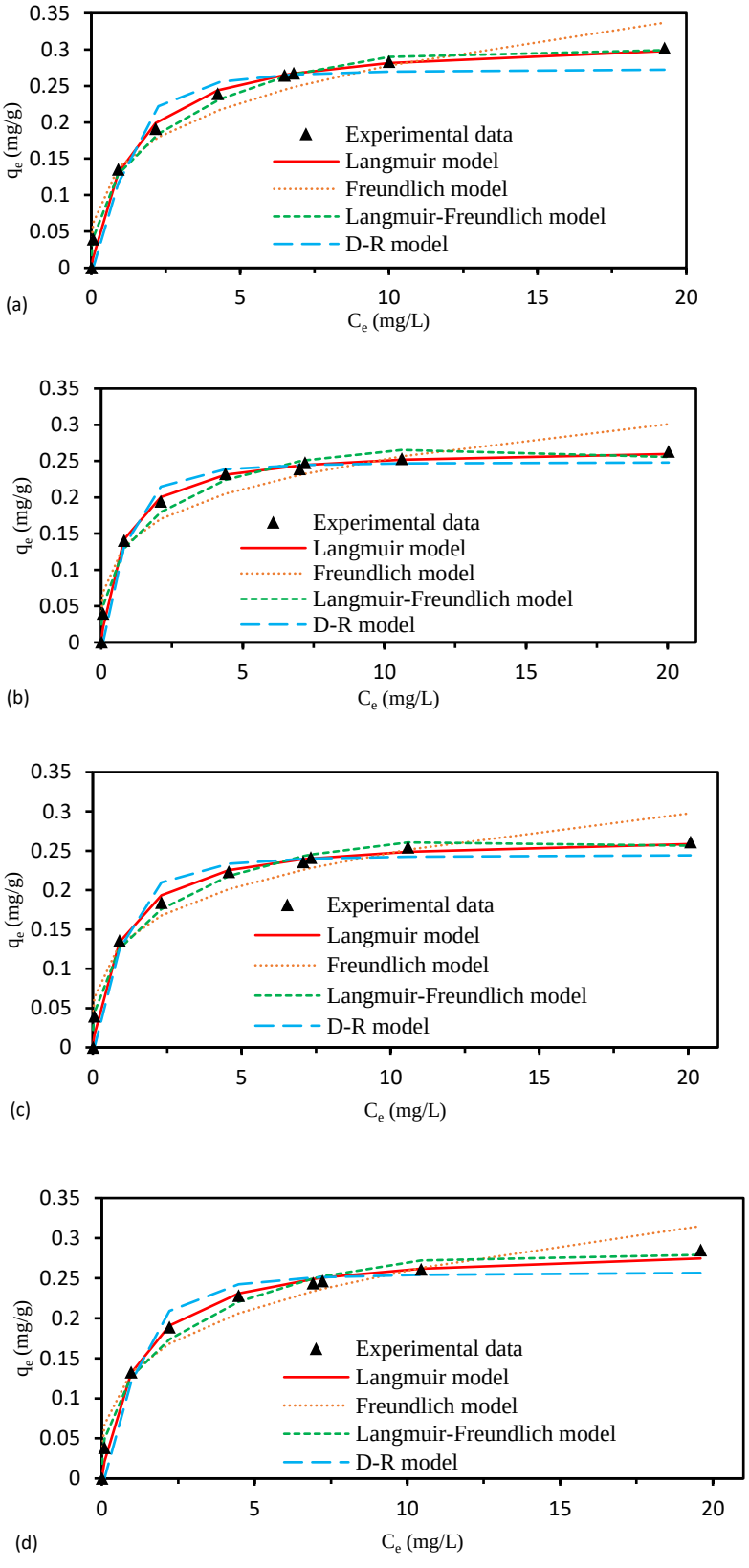

Figure 3-11: Adsorption isotherms of As (III) on DMI-65 (adsorbent dosage = 20 g/L), contact time = 24 hours, temperature = 19 ± 2 ºC, agitation speed = 130 rpm. (a) pH 5, (b) pH 6, (c) pH 7 and (d) pH 8.5.

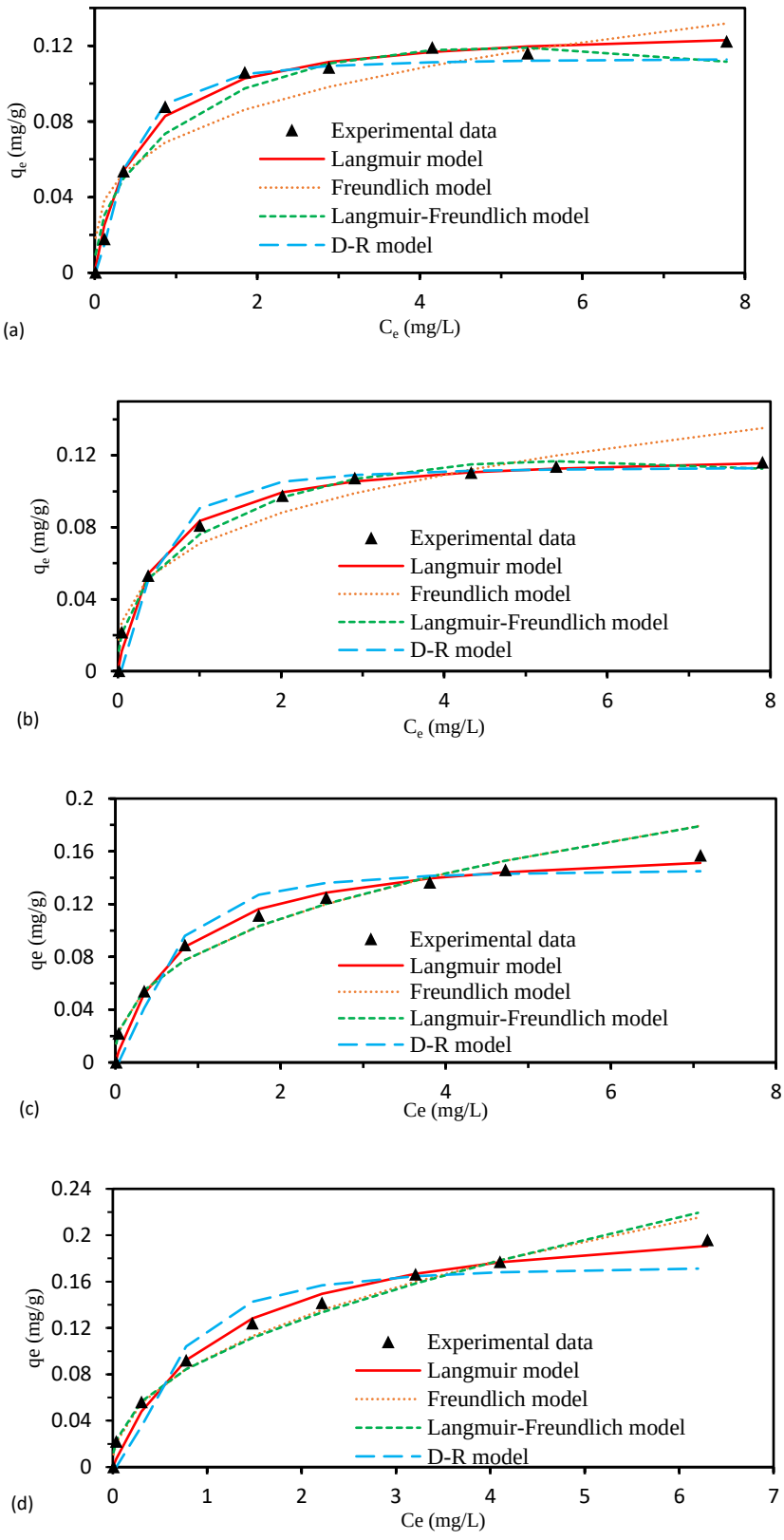

Figure 3-12: Adsorption isotherms of As (V) on DMI-65 (adsorbent dosage = 20 g/L), contact time = 24 hours, temperature = 19 ± 2 ºC, agitation speed = 130 rpm. (a) pH 5, (b) pH 6, (c) pH 7 and (d) pH 8.5.

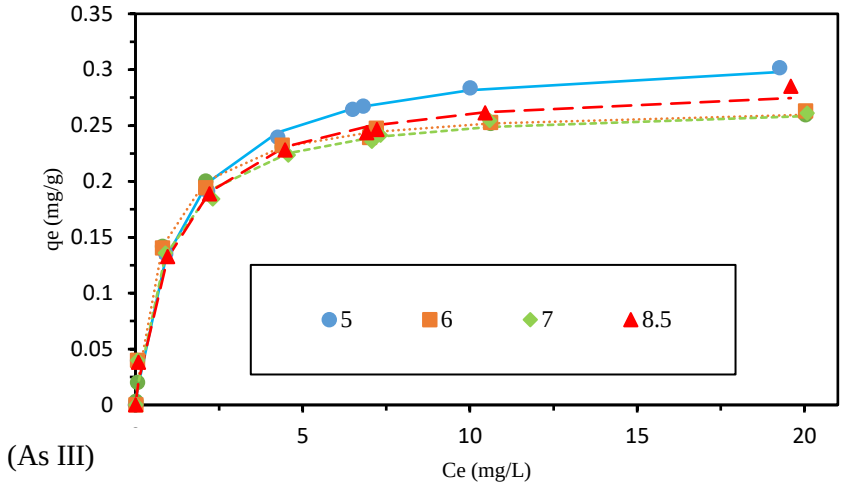

(As III)

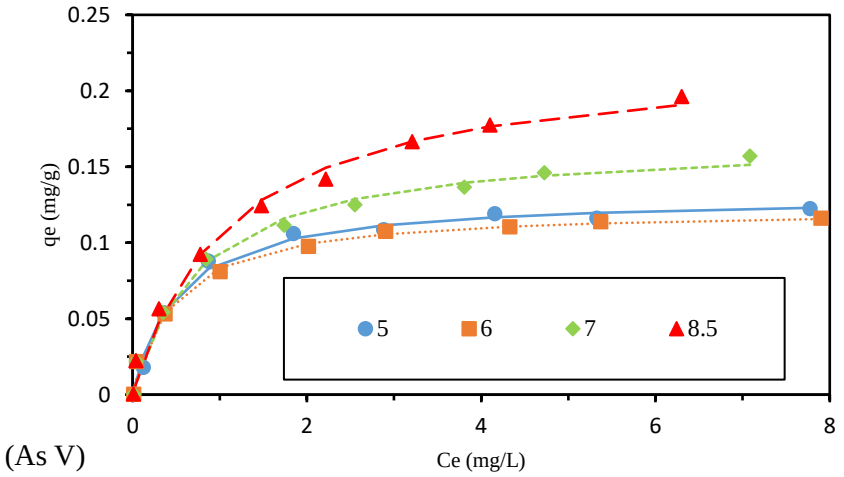

(As V)

Figure 3-13: Langmuir adsorption isotherm study of arsenic adsorption onto DMI-65 (adsorbent dosage = 20 g/L), contact time = 24 hours, agitation speed = 130 rpm. (a) As (III) and (b) As (V).

The regression coefficient (R^2) for the Langmuir model was larger than that for Freundlich, Langmuir – Freundlich and D–R models, suggesting that Langmuir isotherm was more suitable for describing the adsorption behaviour (Fig. 3-13). The maximum adsorption capacity of As (III) was found to be 0.315 mg/g at pH 5, while that of As (V) was found to be 0.224 mg/g at pH 8.5 using the Langmuir isotherm (Appendix 3Q and 3R). A comparison of the results obtained in this study with those reported in previous works are shown in Table 3-5.

Table 3-5: Comparison of adsorption capacities of some adsorbent used for removing arsenic

Adsorbent	q_m (mg/g)		References
	As(III)	As(V)	
ZrPACM-43	0.200	-	(Mandal et al., 2013)
Goethite	-	0.380	(Gimenez et al., 2007)
Hematite	-	0.260	(Gimenez et al., 2007)
Iron oxide coated sand	0.041	0.043	(Thirunavukkarasu et al., 2003)
Iron oxide coated zeolite	-	0.680	(Jeon et al., 2009)
Nano sized iron oxide-coated perlite	-	0.390	(Mostafa et al., 2011)
Al-HDTMA-sericite, (AA)	0.338	0.433	(Tiwari and Lee, 2012)
New Zealand Iron sand	1.250	0.500	(Panthi and Wareham, 2011)
Clay	0.004	0.004	(Mishra and Mahato, 2016)
FePILC	0.017	0.026	(Mishra and Mahato, 2016)
MnPILC	0.026	0.026	(Mishra and Mahato, 2016)
DMI-65	0.315	0.224	This study

3.3.4 Thermodynamic studies

Thermodynamic parameters such as changes in free energy (ΔG^o), enthalpy (ΔH^o) and entropy (ΔS^o) were determined using Eq. (3.18) and Eq. (3.19) (Chaudhry et al., 2017; Jain and Agarwal, 2017) and shown in Table 3-6.

$$\Delta G^o = -RTInK_c \quad (3.18)$$

$$\Delta G^o = \Delta H^o - T\Delta S^o \quad (3.19)$$

Where T is the solution temperature (K), R is the gas constant (8.314 J/mol K) and Kc (L/mg) can be obtained from either the Langmuir or Freundlich isotherms model (Tran et al., 2017). The Langmuir isotherm gave a better fit and thus it was used in calculating the value of Kc which is a dimensionless value as shown in Eq. (20) (Velazquez-Jimenez et al., 2018; Zhou and Zhou, 2014).

$$K_c = M_w \, x \, 55.5 \, x \, 1000 \, x \, K_L \quad (3.20)$$

Where M_w is the molecular weight of the adsorbate and 55.5 is the number of moles of pure water per liter (1,000 g/L divided by 18 g/mol). The values of ΔS^o and ΔH^o are determined from Van`t Hoff equation (Appendix 3S).

$$In\ K_c = \frac{\Delta S^o}{R} - \frac{\Delta H^o}{RT} \quad (3.21)$$

The plot of In K_c versus I/T for As (III) and As (V) adsorption is linear (Fig. 3-14a) with the intercept and the slope giving the values of ΔS^o and ΔH^o. The negative values of free energy change ΔG^o demonstrate the spontaneous nature of the adsorption process for both As (III) and As (V) by DMI-65. The positive values of ΔH^o indicate an endothermic nature of the adsorption process for both As (III) and As (V). The obvious decrease in the negative values of ΔG^o with increase in temperature shows that adsorption became more favourable at higher temperature. This means that adsorption would increase with increasing temperature and is also in accordance with the trend observed for K_c. The enthalpy change due to physisorption is less than 42 kJ/mol while the enthalpy change due to chemisorption generally falls between 40 – 200 kJ/mol. The values of ΔH^o for both As (III) and As (V) are 3.021 and 6.156 kJ/mol respectively therefore the adsorption process can be attributed to physisorption which is a result of van der Waals interaction at the surface of the adsorbent (Duan et al., 2017; Yazdani et al., 2016). The positive value of ΔS^o for both As (III) and As (V) indicates the increased randomness at the solid/solution interface during the sorption of arsenic onto DMI-65. It also shows that during the adsorption process, adsorption is likely to be driven by changes in the microstructure of adsorbate or adsorbent (Bulut et al., 2008; Xie et al., 2019).

Table 3-6: Parameters of Langmuir isotherms and thermodynamics of As (III) and As (V) adsorption

	Temperature	Langmuir parameters			Thermodynamics		
		q_m	K_L	R^2	ΔG^o	ΔS^o	ΔH^o
	(K)	(mg/g)	(L/mg)		(kJ/mol)	(J/mol K)	(kJ/mol)
As (III)	283	0.253	1.285	0.993	-36.449		
	288	0.263	1.323	0.991	-37.162	139.492	3.021
	293	0.270	1.342	0.994	-37.842		
	298	0.286	1.374	0.994	-38.547		
As (V)	283	0.154	2.966	0.974	-38.417		
	288	0.167	3.169	0.986	-39.254	157.584	6.156
	293	0.170	3.294	0.995	-40.030		
	298	0.192	3.388	0.999	-40.783		

The adsorption capacity and arsenic removal percentage using DMI-65 increased with increasing temperatures as shown in Fig. 3-14 (b) which may be due to the increase in movement of arsenic species in the solution or as a result of decrease in solution viscosity. Also, increasing the temperature may produce a swelling effect

on the internal structure of the media to enable arsenic to penetrate further (Ghodbane et al., 2008; Mahmoodi et al., 2011).

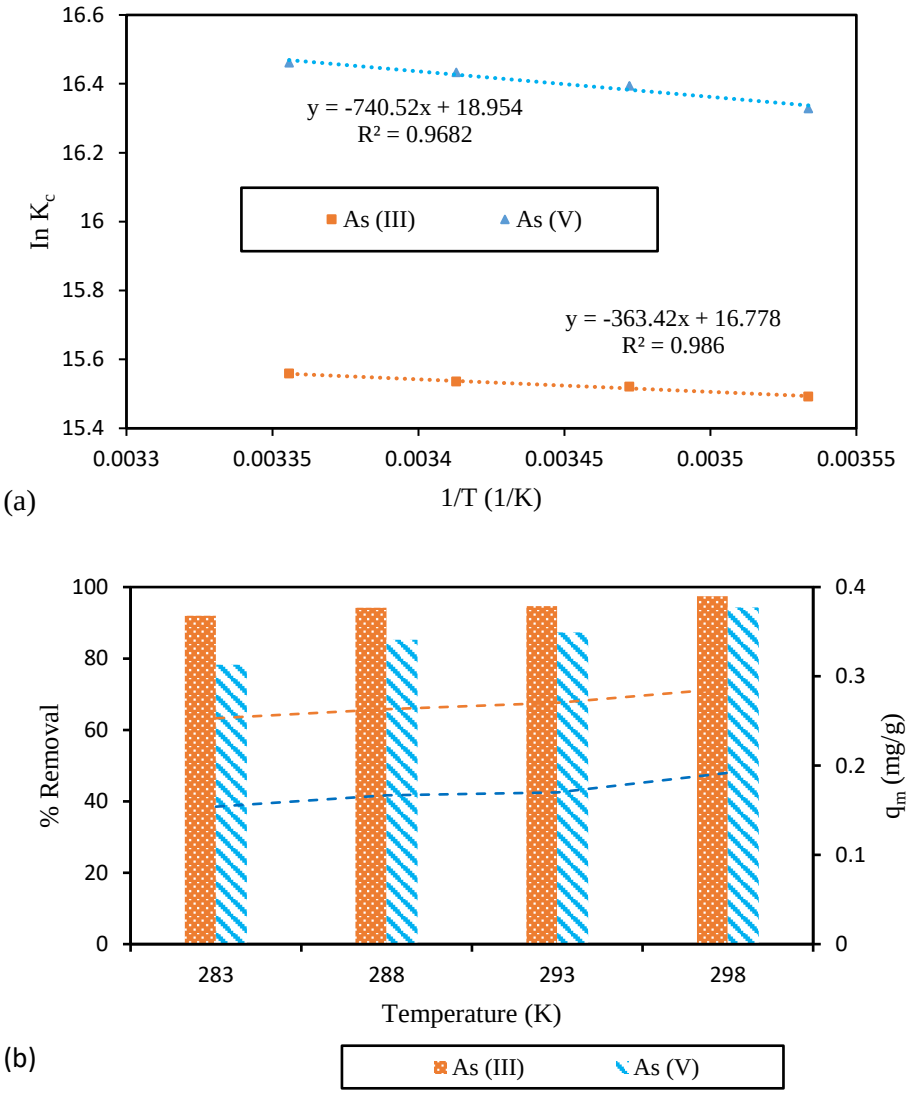

Figure 3-14: (a) Van`t Hoff plot for the removal of As (III) and As (V) by DMI-65 (b) Effect of temperature on % removal and adsorption capacity.

3.3.5 Regeneration studies

Regeneration studies were carried out in order to know the reusability of DMI-65 in removing As (III) and As (V). Reusability of a media is an important economic factor. Likewise, a good media should be stable and able to maintain its adsorption capacity after undergoing several cycles. DMI-65 was activated using NaOCl and investigated after over 5 cycles of adsorption. The adsorbent was regenerated after each cycle using 0.1M NaOH by agitating for 3 hr at a speed of 130 rpm, rinsed with deionised water and dried in an oven.

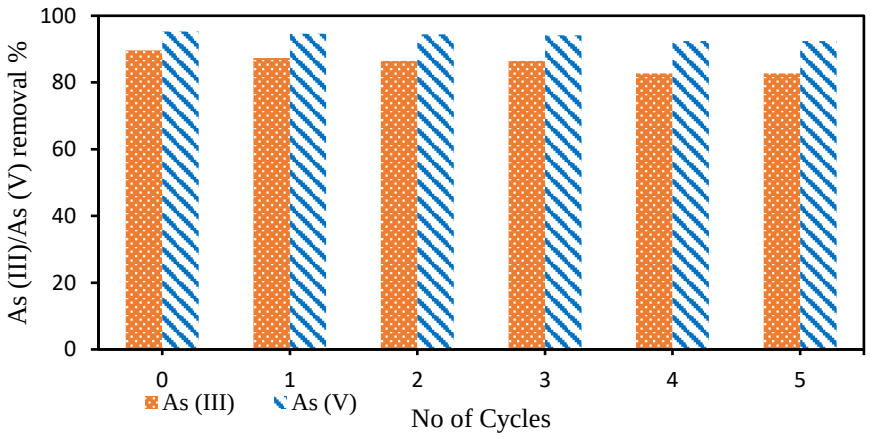

Figure 3-15: Removal of As (III) and As (V) by DMI-65 during 5 regeneration cycles (adsorbent dosage – 20 g/L, initial concentration – As (III) = 30 µg/L, As (V) = 15 µg/L; Temperature = 20 ± 2 ºC; agitation speed = 130 rpm; pH = 7.0 ± 0.2; contact time = 20 hrs).

The initial concentrations of As (III) and As (V) are 30 µg/L and 15 µg/L respectively. Fig. 3-15 shows the adsorption efficiency over the 5 cycles. There is a gradual decrease in both As (III) and As (V) removal over the cycles. For As (III), the removal efficiency decreased from 89.59 % to 82.68 % while for As (V), the removal efficiency decreased from 95.32 % to 92.44 % at the end of the fifth cycle. This decrease in removal efficiency can be considered low after 5 cycles and thus demonstrates an excellent reusability and can be used for practical applications.

3.4 Conclusions

In this study, DMI-65 which is a silica based catalytic media was used to investigate the feasibility of removing As (III) and As (V) from synthetic water in a batch experiment. Activating the DMI-65 revealed an increase in the surface area, pore volume and pore size. The kinetics of the experimental data for removing As (III) and As (V) fitted with the pseudo second-order model and equilibrium was reached after 5 h and 6 h for As (III) and As (V) removal respectively. The pH of the arsenic solution had little effect on the removal efficiency and adsorption capability. The maximum removal efficiency for As (III) was 96.55 % at pH 5 and 90.40 % for As (V) at pH 8.5. The results of adsorption isotherms are best fitted to Langmuir model which shows that the maximum adsorption capacity of As (III) and As (V) to be 0.315 mg/g and 0.224 mg/g respectively. Thermodynamic parameters show that the adsorption process for As (III) and As (V) is a spontaneous process. The positive values for ΔS^o and ΔH^o for both As (III) and As (V) indicate an increased

randomness at the solid/liquid interface and the endothermic nature of the adsorption process respectively. The regeneration studies showed that DMI-65 can be regenerated using NaOH solution and reused for several cycles.

DMI-65 was primarily designed to remove iron and manganese in drinking water. The level of As (III) and As (V) in this study was reduced from a high of 0.06 mg/L to 0.0058 mg/L for As (V) at pH 5 and from 0.06 mg/L to 0.0016 mg/L for As (III) at pH 5. These values are below the level recommended by WHO, US EPA and DWSNZ (10 µg/L). Furthermore, DMI-65 operates over a wide pH range thereby making it potentially suitable for removing arsenic in drinking water.

References

Addo Ntim, S., Mitra, S., 2012. Adsorption of arsenic on multiwall carbon nanotube–zirconia nanohybrid for potential drinking water purification. J. Colloid Interface Sci. 375, 154–159. https://doi.org/10.1016/j.jcis.2012.01.063

Ahmed, K., Rehman, F., Pires, C.T.G.V.M.T., Rahim, A., Santos, A.L., Airoldi, C., 2016. Aluminum doped mesoporous silica SBA-15 for the removal of remazol yellow dye from water. Microporous Mesoporous Mater. 236, 167–175. https://doi.org/10.1016/j.micromeso.2016.08.040

Ansari, R., Sadegh, M., 2007. Application of Activated Carbon for Removal of Arsenic Ions from Aqueous Solutions [WWW Document]. J. Chem. https://doi.org/10.1155/2007/829187

Asmel, N.K., Yusoff, A.R.M., Sivarama Krishna, L., Majid, Z.A., Salmiati, S., 2017. High concentration arsenic removal from aqueous solution using nano-iron ion enrich material (NIIEM) super adsorbent. Chem. Eng. J. 317, 343–355. https://doi.org/10.1016/j.cej.2017.02.039

Babel, S., Kurniawan, T.A., 2003. Low-cost adsorbents for heavy metals uptake from contaminated water: a review. J. Hazard. Mater. 97, 219–243. https://doi.org/10.1016/S0304-3894(02)00263-7

Banerji, T., Chaudhari, S., 2016. Arsenic removal from drinking water by electrocoagulation using iron electrodes- an understanding of the process parameters. J. Environ. Chem. Eng. 4, 3990–4000. https://doi.org/10.1016/j.jece.2016.09.007

Bhat, A., Megeri, G.B., Thomas, C., Bhargava, H., Jeevitha, C., Chandrashekar, S., Madhu, G.M., 2015. Adsorption and optimization studies of lead from aqueous solution using γ-Alumina. J. Environ. Chem. Eng. 3, 30–39. https://doi.org/10.1016/j.jece.2014.11.014

Bhaumik, M., Noubactep, C., Gupta, V.K., McCrindle, R.I., Maity, A., 2015. Polyaniline/Fe0 composite nanofibers: An excellent adsorbent for the removal of arsenic from aqueous solutions. Chem. Eng. J. 271, 135–146. https://doi.org/10.1016/j.cej.2015.02.079

Budinova, T., Savova, D., B.Tsyntsarski, Ania, C.O., Cabal, B., Parra, J.B., Petrov, N., 2009. Biomass waste-derived activated carbon for the removal of arsenic and manganese ions from aqueous solutions. Appl. Surf. Sci. 255, 4650–4657. https://doi.org/10.1016/j.apsusc.2008.12.013

Bulut, E., Özacar, M., Şengil, İ.A., 2008. Adsorption of malachite green onto bentonite: Equilibrium and kinetic studies and process design. Microporous Mesoporous Mater. 115, 234–246. https://doi.org/10.1016/j.micromeso.2008.01.039

Chammui, Y., Sooksamiti, P., Naksata, W., Thiansem, S., Arqueropanyo, O., 2014. Removal of arsenic from aqueous solution by adsorption on Leonardite. Chem. Eng. J. 240, 202–210. https://doi.org/10.1016/j.cej.2013.11.083

Chaudhry, S.A., Khan, T.A., Ali, I., 2017. Zirconium oxide-coated sand based batch and column adsorptive removal of arsenic from water: Isotherm, kinetic and thermodynamic studies. Egypt. J. Pet. 26, 553–563. https://doi.org/10.1016/j.ejpe.2016.11.006

Choong, T.S.Y., Chuah, T.G., Robiah, Y., Gregory Koay, F.L., Azni, I., 2007. Arsenic toxicity, health hazards and removal techniques from water: an overview. Desalination 217, 139–166. https://doi.org/10.1016/j.desal.2007.01.015

Çiftçi, T.D., Henden, E., 2015. Nickel/nickel boride nanoparticles coated resin: A novel adsorbent for arsenic(III) and arsenic(V) removal. Powder Technol. 269, 470–480. https://doi.org/10.1016/j.powtec.2014.09.041

Duan, X., Zhang, C., Srinivasakannan, C., Wang, X., 2017. Waste walnut shell valorization to iron loaded biochar and its application to arsenic removal. Resour.-Effic. Technol. 3, 29–36. https://doi.org/10.1016/j.reffit.2017.01.001

Elizalde-González, M.P., Mattusch, J., Einicke, W.-D., Wennrich, R., 2001. Sorption on natural solids for arsenic removal. Chem. Eng. J. 81, 187–195. https://doi.org/10.1016/S1385-8947(00)00201-1

El-Moselhy, M.M., Ates, A., Çelebi, A., 2017. Synthesis and characterization of hybrid iron oxide silicates for selective removal of arsenic oxyanions from contaminated water. J. Colloid Interface Sci. 488, 335–347. https://doi.org/10.1016/j.jcis.2016.11.003

Ghodbane, I., Nouri, L., Hamdaoui, O., Chiha, M., 2008. Kinetic and equilibrium study for the sorption of cadmium(II) ions from aqueous phase by eucalyptus bark. J. Hazard. Mater. 152, 148–158. https://doi.org/10.1016/j.jhazmat.2007.06.079

Gimenez, J., Martinez, M., Depablo, J., Rovira, M., Duro, L., 2007. Arsenic sorption onto natural hematite, magnetite, and goethite. J. Hazard. Mater. 141, 575–580. https://doi.org/10.1016/j.jhazmat.2006.07.020

Gulnaz, O., Saygideger, S., Kusvuran, E., 2005. Study of Cu(II) biosorption by dried activated sludge: effect of physico-chemical environment and kinetics study. J. Hazard. Mater. 120, 193–200. https://doi.org/10.1016/j.jhazmat.2005.01.003

Hadizade, G., Binaeian, E., Emami, M.R.S., 2017. Preparation and characterization of hexagonal mesoporous silica/polyacrylamide nanocomposite capsule (PAM-HMS) for dye removal from aqueous solutioxns. J. Mol. Liq. 238, 499–507. https://doi.org/10.1016/j.molliq.2017.05.026

Harvey, C.F., Swartz, C.H., Badruzzaman, A.B.M., Keon-Blute, N., Yu, W., Ali, M.A., Jay, J., Beckie, R., Niedan, V., Brabander, D., Oates, P.M., Ashfaque, K.N., Islam, S., Hemond, H.F., Ahmed, M.F., 2002. Arsenic mobility and groundwater extraction in Bangladesh. Science 298, 1602–1606. https://doi.org/10.1126/science.1076978

Jain, A., Agarwal, M., 2017. Kinetic equilibrium and thermodynamic study of arsenic removal from water using alumina supported iron nano particles. J. Water Process Eng. 19, 51–59. https://doi.org/10.1016/j.jwpe.2017.07.001

Jeon, C.-S., Baek, K., Park, J.-K., Oh, Y.-K., Lee, S.-D., 2009. Adsorption characteristics of As(V) on iron-coated zeolite. J. Hazard. Mater. 163, 804–808. https://doi.org/10.1016/j.jhazmat.2008.07.052

Lee, C.-G., Alvarez, P.J.J., Nam, A., Park, S.-J., Do, T., Choi, U.-S., Lee, S.-H., 2017. Arsenic(V) removal using an amine-doped acrylic ion exchange fiber: Kinetic, equilibrium, and regeneration studies. J. Hazard. Mater. 325, 223–229. https://doi.org/10.1016/j.jhazmat.2016.12.003

Lee, S.M., Davis, A.P., 2001. Removal of cu(II) and cd(II) from aqueous solution by seafood processing waste sludge. Water Res. 35, 534–540. https://doi.org/10.1016/S0043-1354(00)00284-0

Lin, J.-Y., Wang, B.-X., 2014. Room-Temperature Voltage Stressing Effects on Resistive Switching of Conductive-Bridging RAM Cells with Cu-Doped SiO_2 Films. Adv. Mater. Sci. Eng. 2014, 1–6. https://doi.org/10.1155/2014/594516

Litter, M.I., Morgada, M.E., Bundschuh, J., 2010. Possible treatments for arsenic removal in Latin American waters for human consumption. Environ. Pollut. 158, 1105–1118. https://doi.org/10.1016/j.envpol.2010.01.028

López-Muñoz, M.J., Arencibia, A., Segura, Y., Raez, J.M., 2017. Removal of As(III) from aqueous solutions through simultaneous photocatalytic oxidation and adsorption by TiO2 and zero-valent iron. Catal. Today, Environmental Applications of Advanced Oxidation Processes – EAAOP4 280, 149–154. https://doi.org/10.1016/j.cattod.2016.05.043

Mahmoodi, N.M., Hayati, B., Arami, M., Lan, C., 2011. Adsorption of textile dyes on Pine Cone from colored wastewater: Kinetic, equilibrium and thermodynamic studies. Desalination 268, 117–125. https://doi.org/10.1016/j.desal.2010.10.007

Mandal, S., Sahu, M.K., Patel, R.K., 2013. Adsorption studies of arsenic(III) removal from water by zirconium polyacrylamide hybrid material (ZrPACM-43). Water Resour. Ind. 4, 51–67. https://doi.org/10.1016/j.wri.2013.09.003

McLaren, S.J., Kim, N.D., 1995. Evidence for a seasonal fluctuation of arsenic in New Zealand's longest river and the effect of treatment on concentrations in drinking water. Environ. Pollut. 90, 67–73. https://doi.org/10.1016/0269-7491(94)00092-R

Mishra, T., Mahato, D.K., 2016. A comparative study on enhanced arsenic(V) and arsenic(III) removal by iron oxide and manganese oxide pillared clays from ground water. J. Environ. Chem. Eng. 4, 1224–1230. https://doi.org/10.1016/j.jece.2016.01.022

Mohan, D., Pittman Jr., C.U., 2007. Arsenic removal from water/wastewater using adsorbents—A critical review. J. Hazard. Mater. 142, 1–53. https://doi.org/10.1016/j.jhazmat.2007.01.006

Mostafa, M.G., Chen, Y.-H., Jean, J.-S., Liu, C.-C., Lee, Y.-C., 2011. Kinetics and mechanism of arsenate removal by nanosized iron oxide-coated perlite. J. Hazard. Mater. 187, 89–95. https://doi.org/10.1016/j.jhazmat.2010.12.117

Önnby, L., Pakade, V., Mattiasson, B., Kirsebom, H., 2012. Polymer composite adsorbents using particles of molecularly imprinted polymers or aluminium oxide nanoparticles for treatment of arsenic contaminated waters. Water Res. 46, 4111–4120. https://doi.org/10.1016/j.watres.2012.05.028

Panthi, S.R., Wareham, D.G., 2014. Kinetic study of adsorption of arsenic onto New Zealand Ironsand (NZIS). J. Environ. Sci. Health Part A Tox. Hazard. Subst. Environ. Eng. 49, 1474–1480. https://doi.org/10.1080/10934529.2014.937161

Panthi, S.R., Wareham, D.G., 2011. Removal of arsenic from water using the adsorbent: New Zealand iron-sand. J. Environ. Sci. Health Part A 46, 1533–1538. https://doi.org/10.1080/10934529.2011.609376

Robinson, B., Outred, H., Brooks, R., Kirkman, J., 1995. The distribution and fate of arsenic in the Waikato River system, North Island, New Zealand. Chem. Speciat. Bioavailab. 7, 89–96. https://doi.org/10.1080/09542299.1995.11083250

Roghani, M., Nakhli, S.A.A., Aghajani, M., Rostami, M.H., Borghei, S.M., 2016. Adsorption and oxidation study on arsenite removal from aqueous solutions by polyaniline/polyvinyl alcohol composite. J. Water Process Eng. 14, 101–107. https://doi.org/10.1016/j.jwpe.2016.10.012

Sen Gupta, S., Bhattacharyya, K.G., 2011. Kinetics of adsorption of metal ions on inorganic materials: A review. Adv. Colloid Interface Sci. 162, 39–58. https://doi.org/10.1016/j.cis.2010.12.004

Sherlala, A.I.A., Raman, A.A.A., Bello, M.M., Buthiyappan, A., 2019. Adsorption of arsenic using chitosan magnetic graphene oxide nanocomposite. J. Environ. Manage. 246, 547–556. https://doi.org/10.1016/j.jenvman.2019.05.117

Sigdel, A., Park, J., Kwak, H., Park, P.-K., 2016. Arsenic removal from aqueous solutions by adsorption onto hydrous iron oxide-impregnated alginate beads. J. Ind. Eng. Chem. 35, 277–286. https://doi.org/10.1016/j.jiec.2016.01.005

Song, S., Lopez-Valdivieso, A., Hernandez-Campos, D.J., Peng, C., Monroy-Fernandez, M.G., Razo-Soto, I., 2006. Arsenic removal from high-arsenic water by enhanced coagulation with ferric ions and coarse calcite. Water Res. 40, 364–372. https://doi.org/10.1016/j.watres.2005.09.046

Thirunavukkarasu, O.S., Viraraghavan, T., Subramanian, K.S., 2003. Arsenic removal from drinking water using iron-oxide coated sand. Water. Air. Soil Pollut. 142, 95–111. https://doi.org/10.1023/A:1022073721853

Tiwari, D., Lee, S.M., 2012. Novel hybrid materials in the remediation of ground waters contaminated with As(III) and As(V). Chem. Eng. J. 204–206, 23–31. https://doi.org/10.1016/j.cej.2012.07.086

Tran, H.N., You, S.-J., Hosseini-Bandegharaei, A., Chao, H.-P., 2017. Mistakes and inconsistencies regarding adsorption of contaminants from aqueous solutions: A critical review. Water Res. 120, 88–116. https://doi.org/10.1016/j.watres.2017.04.014

Velazquez-Jimenez, L.H., Arcibar-Orozco, J.A., Rangel-Mendez, J.R., 2018. Overview of As(V) adsorption on Zr-functionalized activated carbon for aqueous streams remediation. J. Environ. Manage. 212, 121–130. https://doi.org/10.1016/j.jenvman.2018.01.072

Villaescusa, I., Bollinger, J.-C., 2008. Arsenic in drinking water: sources, occurence and health effects (a review). Rev Env. Sci Biotechnol 7, 307–323.

Vojoudi, H., Badiei, A., Bahar, S., Mohammadi Ziarani, G., Faridbod, F., Ganjali, M.R., 2017. Post-modification of nanoporous silica type SBA-15 by bis(3-triethoxysilylpropyl)tetrasulfide as an efficient adsorbent for arsenic removal. Powder Technol. 319, 271–278. https://doi.org/10.1016/j.powtec.2017.06.028

Wang, B., Zhou, Y., Li, L., Xu, H., Sun, Y., Wang, Y., 2018. Novel synthesis of cyano-functionalized mesoporous silica nanospheres (MSN) from coal fly ash for removal of toxic metals from wastewater. J. Hazard. Mater. 345, 76–86. https://doi.org/10.1016/j.jhazmat.2017.10.063

Xie, F., Dai, Z., Zhu, Y., Li, G., Li, H., He, Z., Geng, S., Wu, F., 2019. Adsorption of phosphate by sediments in a eutrophic lake: Isotherms, kinetics, thermodynamics and the influence of dissolved organic matter. Colloids Surf. Physicochem. Eng. Asp. 562, 16–25. https://doi.org/10.1016/j.colsurfa.2018.11.009

Yazdani, M. (Roza), Tuutijärvi, T., Bhatnagar, A., Vahala, R., 2016. Adsorptive removal of arsenic(V) from aqueous phase by feldspars: Kinetics, mechanism, and thermodynamic aspects of adsorption. J. Mol. Liq. 214, 149–156. https://doi.org/10.1016/j.molliq.2015.12.002

Youngran, J., Fan, M., Van Leeuwen, J., Belczyk, J.F., 2007. Effect of competing solutes on arsenic(V) adsorption using iron and aluminum oxides. J. Environ. Sci. 19, 910–919. https://doi.org/10.1016/S1001-0742(07)60151-X

Zhou, Xueyong, Zhou, Xin, 2014. The Unit Problem in the Thermodynamic Calculation of Adsorption Using the Langmuir Equation. Chem. Eng. Commun. 201, 1459–1467. https://doi.org/10.1080/00986445.2013.818541

Zhu, N., Yan, T., Qiao, J., Cao, H., 2016. Adsorption of arsenic, phosphorus and chromium by bismuth impregnated biochar: Adsorption mechanism and depleted adsorbent utilization. Chemosphere 164, 32–40. https://doi.org/10.1016/j.chemosphere.2016.08.036

CHAPTER FOUR

Continuous fixed-bed column study and adsorption modelling: Arsenic removal from contaminated drinking water using silica based catalytic media.

Content to be submitted to

Journal of Water Process Engineering

Abstract

A continuous adsorption study in a fixed-bed column was carried out by using DMI-65 as an adsorbent for removing arsenic from a Waikato River water sample. The effect of flowrate (10, 12.5 and 20 mL/min) and pH (5, 7 and 9) on the adsorption characteristics of DMI-65 was investigated. Results from this study show that the breakthrough curves were highly influenced by process variables like pH and flowrate. The following kinetic models (Thomas, Yoon-Nelson, Adams-Bohart and Clark model) were applied to predict the breakthrough curve using nonlinear regression analysis. The dynamic adsorption capacity and 0.5 breakthrough time was well predicted by Thomas and Yoon-Nelson models respectively. The maximum adsorption capacity of column was found to be 11.96 mg/g using DMI-65 as adsorbent for initial concentration, flowrate and pH of ~ 13.00 – 20.00 µg/L, 20 mL/min and 5, respectively. Based on error analyses and coefficient correlation R^2, the Yoon-Nelson and Thomas model fitted better than Adams-Bohart and Clark models using a nonlinear regression analysis and were in good agreement with the experimental value. The study concluded that DMI-65 is an effective adsorbent for removing arsenic from contaminated water using fixed-bed adsorption column.

4.1 Introduction

Arsenic is classified as a carcinogen for both humans and animals despite having applications in medicine, industry and in agriculture (Palma-Lara et al., 2020) Arsenic is the number 1 element listed on ATSDR priority list in 2017 (Appendix 2B) which is a list based on frequency, toxicity and potential for human exposure. It is estimated that more than 100 million people worldwide are exposed to drinking water contaminated with arsenic with an estimated 35 to 77 million exposed in Bangladesh (Reddy et al., 2020). Prolonged exposure to arsenic can cause serious health problems such as various types of cancer (Argos et al., 2010; Dhar et al., 1997; Karim, 2000; Smith et al., 2000) and cardiovascular disease (Chen et al., 2011).

Arsenic has been removed from aqueous solution using different conventional treatment methods such as adsorption, precipitation, coagulation and flocculation, membrane filtration, ion exchange and bio-sorption (Sun et al., 2019). Adsorption is considered as the most favourable treatment option due to its availability, cost and simplicity (Jian et al., 2015; Jiang et al., 2019; Wang et al., 2018).

Several studies have been conducted on the use of various adsorbents for the removal of arsenic, but most of them used batch experiments (Mondal and Garg, 2017). Few studies have been conducted in dynamic column experiments for arsenic removal in a column such as Iron-impregnated granular activated carbon (Kalaruban et al., 2019), activated siderite-hematite (Guo et al., 2008), iron oxide nanoneedle array-decorated biochar fibers (Wei et al., 2019), fungal strains (Jaiswal et al., 2018), magnetic binary oxide particles (MBOP) (Dhoble et al., 2017) and nanomaterials (Hristovski et al., 2007).

In designing an adsorption process system, continuous adsorption studies allow us to know and evaluate several parameters that will influence the operation of the process such as the effect of feed concentration, contact time, pH of the solution, mass of the adsorbent and bed depth (Aichour et al., 2019). Two factors are mainly responsible for the performance of adsorbent media in a fixed-bed column namely: the adsorption capacity of the media and its mass transport kinetics (Hristovski et al., 2007). The continuous adsorption process is usually characterized by using the breakthrough curves; which is the pollutant effluent concentration versus time in a

fixed-bed column. Designing and optimizing the fixed-bed column usually involved the use of mathematical models for the breakthrough curves. information from both the descriptive and predictive data are useful in scale-up and design purposes (de Franco et al., 2018).

In this study, the effect of operational parameters such as flowrate and pH were investigated in removing arsenic from the Waikato River in a fixed-bed column. The batch adsorption of arsenic from a synthetic water using DMI-65 has been explored in previous work (Aremu et al., 2019). The adsorption kinetics were studied using four well known kinetic models (i.e., Adams-Bohart, Clark, Thomas and Yoon-Nelson model) to predict the column performance using the solver add-in with Microsoft`s spreadsheet, Excel 2006 (Microsoft Corporation). Dynamic behaviour of a fixed-bed column was described in terms of a breakthrough curve. Error analysis was carried out to test the accuracy and adequacy of the model equations.

4.2 Experimental

4.2.1 Materials and methods

DMI-65 is a dark odourless granule obtained from Quantum Filtration Medium Property Ltd, Australia and was activated using NaOCl (Damar Industries Ltd, Rotorua, New Zealand) prior to use for the adsorption study. All chemicals and reagents used were of analytical grade (Merck KGaA, Darmstadt, Germany). A stock solution of 50 mg/L NaOCl were prepared in a volumetric flask and diluted to the required concentrations of 5 mg/L NaOCl. The pH adjustments were performed using 0.1M hydrochloric acid (HCl) and 0.1M sodium hydroxide (NaOH) solutions. Other chemicals used were nitric acid (70 % HNO_3) and ethanol (70 % C_2H_5OH). The characteristics of the water sample (Waikato River) used in the experiments are presented in Table 4-1.

4.2.2 Instrumentation

A pH meter (Eutech pH150 pH/temperature meter) was utilized in this study to measure the pH and temperature of samples. The pH meter was calibrated prior to use using 4.01, 7.01 and 10.04 pH buffers (Merck KGaA, Darmstadt, Germany). A HACH 2100P turbidimeter was used to measure turbidity. The meter was calibrated

with 10, 20 and 100 NTU turbidity standards (HACH Turbidity Standard kit model 2100P) before use. Total arsenic concentration was measured by inductively coupled plasma mass – spectrometry (ICP-MS). Quality control employed for ICP-MS measurements are shown in APPENDIX 2BA. Palintest Photometer 7100 was used to measure the free chlorine and manganese concentration during the activation process.

Table 4-1: Characteristics of Waikato River water sample

Properties	**Values**
pH	7.48 ± 0.5
Turbidity (NTU)	3.12 ± 1.11
Alkalinity (mg $CaCO_3$/L)	20 ± 2
As (mg/L)	0.016 ± 0.003
DO (mg/L)	2.33 ± 1.01
UV_{254nm} (cm^{-1})	0.059 ± 0.016
Temperature (^oC)	22.2 ± 2.2
Nitrate (mg/L N)	1.34 ± 0.2
Phosphate (mg/L PO_4)	0.38 ± 0.03
Conductivity (µS/cm)	139 ± 5

4.2.3 DMI-65 activation

In the column adsorption experiments, 100 g of DMI-65 samples were soaked with 50 mL of 12.5 % NaOCl. After 24 hours, the media was carefully put in a column and washed by backwashing tap water through the column at 100 mL/min until the free chlorine residual in the solution dropped to 0.1 – 0.3 ppm and manganese concentration dropped to 0.15 ppm. Activation process is necessary so that the catalytic surface of the media is kept clean and available to ions from water to contact - and the use of distilled water or water known to be strongly corrosive to metals should not be used for the activation process.

4.2.4 DMI-65 Characterization

The DMI-65 used in this study has been characterized and the detailed physical and chemical properties can be seen in Chapter 3. XRF and XRD analysis showed that silica (SiO_2) is the main component of DMI-65. The surface area, pore volume and

pore size of DMI-65 after activation are 5.24 m^2/g, 0.00139 cm^3/g and 1.16 nm respectively. The particle size distribution showed that the volume mean diameter and surface mean of DMI-65 after activation are 765 µm and 695 µm. The surface of DMI-65 is rough, and it is composed of other elements such as Mn, Cl, O, S and K in addition to Si. The FT-IR spectra of DMI-65 is composed of the peaks of OH-, Fe-O, Cu-O, C=O and an asymmetrical stretch vibration of Si-O-Si from the silica quartz (Section 3.3.1).

4.2.5 Fixed-bed column studies

A Plexiglass column with an internal diameter of 20 mm and a height of 20 cm was used in the column study as fixed bed down flow reactor. Effect of flowrates (10, 12.5 and 20 mL/min) and pH (5, 7 and 9) on column adsorption were investigated. A peristaltic pump (Masterflex ® L/S ®) was used to maintain the desired flowrate. On the bottom side 3 mm thick glass fiber was placed to prevent any loss of adsorbent and to also give a mechanical support to the adsorbent bed. Experiments were carried out at room temperature 20 ± 2 ^oC and samples were collected at regular time intervals from the bottom of the column and tested to measure arsenic concentration, turbidity and UV_{254nm}.

4.2.6 Column modelling

The breakthrough curve plays a vital role in determining the performance and operation of a column (Aksu and Gönen, 2004; Ang et al., 2020). The column performance was investigated by calculating the breakthrough time and adsorption capacity (Fig. 4-1).

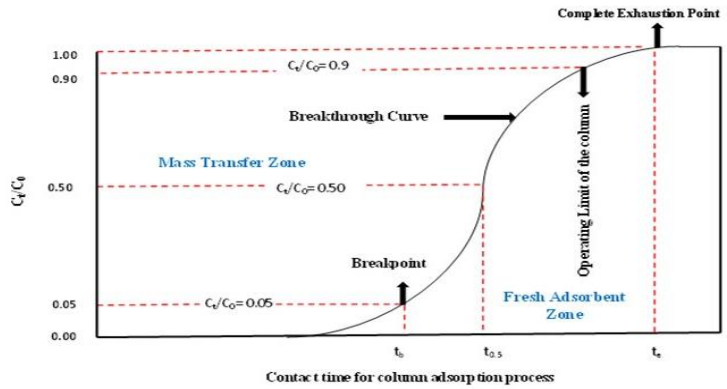

Figure 4-1: Breakthrough curve characteristics in the fixed bed column adsorption process with respect to time.

The breakthrough curve showed the loading performance of arsenic to be adsorbed from the solution in a column reactor and it is typically written as (C_{ad} = inlet As content (C_o) – Outlet As content (C_t)). C_t/C_o was drawn against time (x-axis) to create a breakthrough curve. The optimum column capacity, q_{total} (mg), for a specific influent content and flowrate is equivalent to the area of plot for adsorbed arsenic content C_{ad} versus effluent time (t, min) and is quantified as shown in Eq. (4.1)

$$q_{total} = \frac{QA}{1000} = \frac{Q}{1000} \int_{t=0}^{t= t_{total}} C_{ad} dt \quad (4.1)$$

Where, q_{total}, A and Q represent the total flowrate time (min), the area under the breakthrough curve, and volumetric flowrate (mL/min), respectively. The equilibrium uptake (q_{eq}), the amount of arsenic adsorbed by unit dry mass of the adsorbent (mg/g) in the column reactor was determined from Eq. (4.2) as shown below:

$$q_{eq} = \frac{q_{total}}{m} \quad (4.2)$$

Where m (g) is the total weight of DMI-65 in the column reactor. The total quantity of arsenic as influent (W_{total}) was calculated by Eq. (4.3).

$$W_{total} = \frac{C_o Q t_{total}}{1000} \quad (4.3)$$

Total arsenic removal efficiency (Y) is the proportion of the quantity of the arsenic adsorbed (q_{total}) to the total quantity of arsenic directed to the column (W_{total}), and it is calculated as shown in Eq. (4.4).

$$Y = \left(\frac{q_{total}}{W_{total}}\right) \text{ x } 100 \quad (4.4)$$

Arsenic uptake at equilibrium (q_{eq}) in the column reactor is shown by Eq. (4.5) which is the total quantity of arsenic adsorbed in 100 g of adsorbed (q_{total}) per gram of sorbent (X) after total flow time.

$$q_{eq} = \frac{q_{total}}{X} \quad (4.5)$$

The empty bed contact time (EBCT) in the column is described as:

$$\text{EBCT (min)} = \frac{\text{bedvolume (mL)}}{\text{flowrate (mL/min)}} \quad (4.6)$$

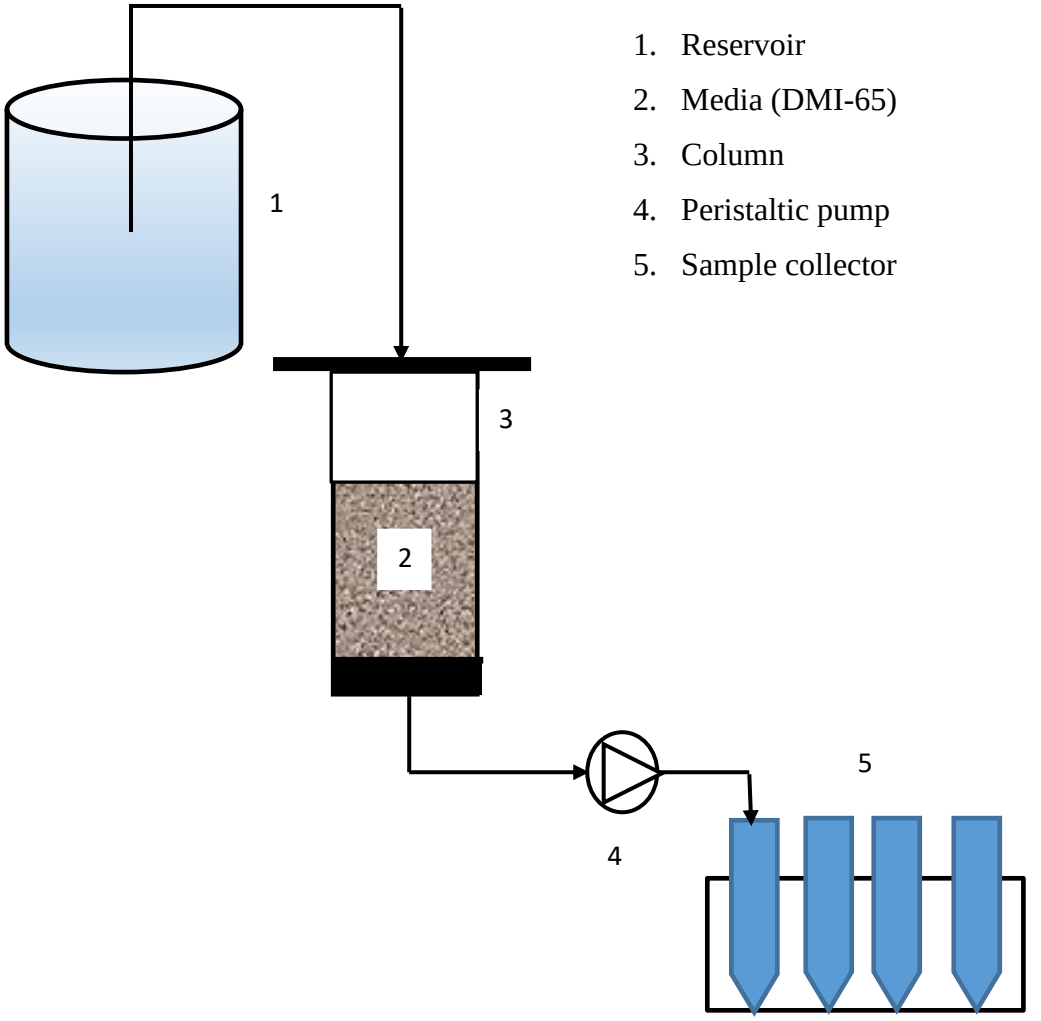

Figure 4-2: Flowchart of down flow packed bed column for fixed bed studies

4.2.7 Kinetic modelling

The appropriate design of column performance requires a good prediction of the breakthrough curve for the effluent. There are several models used to predict the breakthrough curve as discussed in Chapter 2, but the Thomas model is commonly applied; this is due to its accuracy and simplicity (Han et al., 2007, 2009; Xu et al., 2013). These models have been used to investigate column performance in removing organic and inorganic contaminants (Charola et al., 2018; de Franco et al., 2018; Gupta and Garg, 2019; Sheng et al., 2018; Vieira et al., 2018). Fig. 4-2 showed a flowchart of the fixed bed adsorption column used in this study. Below are the mathematical expressions of the models used in this study (Bohart and Adams, 1920; Clark, 1987; Thomas, 1948; Yoon and Nelson, 1984):

Thomas model

The equation for the Thomas model for adsorption column reactor is given below in Eq. (4.7).

$$\frac{C_t}{C_0} = \frac{1}{1+\exp[k_{TH}q_0x/Q - k_{TH}C_0t]} \quad (4.7)$$

Where k_{TH} is the Thomas rate constant (mL/mg. min); q_0 is the maximum solid phase concentration (mg/g); x is the amount of adsorbent in the column (g); C_0 and C_t are the inlet and outlet concentrations (mg/L) of the adsorbate at time t respectively; Q is the flowrate (mL/min). The value of t is the flow time (min, $t = V_{eff}/v$, V_{eff} is effluent volume at time t).

The linearized form of the Thomas model is as follows:

$$\text{In}\left(\frac{C_0}{C_t} - 1\right) = \frac{k_{TH}q_0x}{Q} - k_{TH}C_0t \quad (4.8)$$

The values of k_{TH} and q_0 can be obtained by the slope and intercept from plot of $In\ (C_0/C_t - 1)$ *vs.* t

Yoon-Nelson Model

The Yoon-Nelson equation can be expressed as shown in Eq. (4.9) below:

$$\frac{C_t}{C_0 - C_t} = \exp(k_{YN}\,t - \tau k_{YN}) \quad (4.9)$$

$$\frac{C_t}{C_0} = \frac{1}{1+\exp[K(\tau - t)]} \quad (4.10)$$

The linearized model for Eq. (4.9) can be expressed as:

$$\text{In}\,\frac{C_t}{C_0 - C_t} = k_{YN}\,t - \tau k_{YN} \quad (4.11)$$

Where τ is the time required for 50 % adsorbate breakthrough (min), k_{YN} is the rate constant (1/min) and t is the sampling time (min). The value of k_{YN} and τ can be found by plotting the graph between $In\ (C_t/(C_0 - C_t))$ and t.

Adams – Bohart Model

The Adams – Bohart model can be expressed as shown in Eq. (4.12) below:

$$\frac{C_t}{C_0} = \exp\left(k_{AB}C_0t - k_{AB}N_0\frac{Z}{F}\right) \quad (4.12)$$

Eq. (4.12) can be linearized as:

$$\text{In}\ \frac{C_t}{C_0} = k_{AB}C_0 t - k_{AB}N_0\frac{Z}{F} \quad (4.13)$$

Where C_0 and C_t (mg/L) are the inlet and effluent concentration, k_{AB} (L/mg min) is the kinetic constant, F (cm/min) is the linear velocity calculated by dividing the flowrate by the column sectional area, Z (cm) is the bed depth of column and N_0 (mg/L) is the saturation concentration. From this equation, values describing the characteristic operational parameters of the column (k_{AB} and N_0) can be determined from a plot of C_t/C_0 against t.

Clark Model

This model which is based on mass transfer is expressed in Eq. (4.14) as shown below:

$$\frac{C_t}{C_0} = \left(\frac{1}{1+Ae^{-rt}}\right)^{1/(n-1)} \quad (4.14)$$

The values of A and r can be obtained from a nonlinear plot of C_t/C_0 against t at a given bed height and flow rate.

The linearized form of the model can be represented as:

$$\text{In}\left[\left(\frac{C_0}{C_t}\right)^{n-1} - 1\right] = -rt + \text{In A} \quad (4.15)$$

Where n is the Freundlich parameter, and A and r (1/min) are the Clark constants. A and r are determined from the slope and the intercept of plot of In $[(C_0/C_t)^{n-1} - 1]$ *vs.* t.

4.2.8 The error analysis

In order to confirm the best fit model for a column adsorption model, it is necessary to analyse the data using the error analysis and by combining the values of determined correlation coefficient (R^2) from regression analysis. In this study, a nonlinear regressive method was used as it gives a better option in avoiding errors (Han et al., 2007; Ho et al., 2005). The nonlinear error functions employed in this study are as follows (Kundu and Gupta, 2006):

1. The sum of the squares of the errors (SSE):

$$SSE = \sum_{i=1}^{n}\left(q_{e,calc} - q_{e,exp}\right)_i^2 \quad (4.16)$$

2. The Sum of the absolute errors (SAE):

$$SAE = \sum_{i=1}^{n}\left|q_{e,calc} - q_{e,exp}\right|_i \quad (4.17)$$

3. The average relative error (ARE):

$$ARE = \frac{100}{n}\sum_{i=1}^{n}\left|\frac{q_{e,exp} - q_{e,calc}}{q_{e,exp}}\right|_i \quad (4.18)$$

4. The hybrid fractional error function (HYBRID):

$$HYBRID = \frac{100}{n-p}\sum_{i=1}^{n}\left[\frac{\left(q_{e,exp} - q_{e,cal}\right)^2}{q_{e,exp}}\right]_i \quad (4.19)$$

5. Marquardt`s percent standard deviation (MPSD)

$$MPSD = 100\sqrt{\frac{1}{n-p}\sum_{i=1}^{n}\left(\frac{q_{e,exp} - q_{e,calc}}{q_{e,exp}}\right)_i^2} \quad (4.20)$$

Where $q_{e,exp}$ is the adsorption capacity found from the experimental (mg/g), $q_{e,cal}$ is adsorption capacity calculated from models, n is the number of experimental data points and p is the number of parameters in the models. Lower value of SSE, HYBRID and MPSD and higher value of R^2 are the indication of best-fit model.

4.3 Results and discussion

4.3.1 The effect of flowrate on breakthrough curve

Flowrate is one of the key factors for determining the effectiveness of adsorbents in a large scale continuous fixed-bed adsorption (Charola et al., 2018). To investigate the effect of flowrate on arsenic adsorption, the influent of arsenic concentration and pH was held constant at ~ 0.0135 mg/L and 7 respectively. The experiments were conducted at bed depth of 20 cm with flowrate ranging from 10 mL/min to 20 mL/min. In this study, the breakthrough and the exhaustion concentrations were set at 50 % and 95 % of the input concentration, respectively. The breakthrough curves are shown in Fig. 4-3 (plot of C_t/C_o vs t). Fig. 4-3 indicates that the both breakthrough and exhaustion point occur faster with higher flowrate than with a lower one (López-Cervantes et al., 2017; Wu et al., 2012). This can be

attributed to insufficient residence time of arsenic in the fixed-bed column to allow for diffusion of arsenic into the pores of the DMI-65 (Salman et al., 2011; Zou et al., 2013). As the flowrate was increased from 10 to 20 mL/min, the EBCT decreased from 25.1 min to 12.57 min in a DMI-65 fixed-bed column. The time it took to reach breakthrough point, t_b for 10, 12.5 and 20 mL/min are 96.27, 57.50 and 22.83 hours respectively. Whereas the time it took to exhaustion point, t_e for 10, 12.5 and 20 mL/min are 8.02, 6.31 and 2.0 days respectively (Appendix 4A).

From Table 4.2, arsenic uptakes at different flowrates (10, 12.5 and 20 mL/min) were 0.0043, 0.0027 and 0.0016 mg/g, respectively. The adsorption capacity is lower at a higher flowrate due to insufficient residence time between arsenic and the DMI-65 in the fixed-bed column (Xu et al., 2013). The results presented in Table 4-2 indicated that the fixed-bed column had a better performance at a lower flowrate if a high percentage removal was required. However, the overall processing time increased at lower flowrates which will not be favourable in large-volume applications.

Table 4-2: Parameters in fixed-bed column for arsenic adsorption by the DMI-65

C_o (mg/L)	Q (mL/min)	Z (cm)	pH	t_{total} (min)	m_{total} (mg)	q_{total} (mg)	q_{eq} (mg/g)	V_{eff} (mL)	Y (%)
0.01305	10	20	7	5776	0.754	0.426	0.0043	57760	56.54
0.01305	12.5	20	7	3450	0.563	0.273	0.0027	43125	48.55
0.01305	20	20	7	1370	0.358	0.157	0.0016	27400	43.98
0.01852	20	20	5	3050	1.129	0.664	0.0066	61000	58.75
0.01987	20	20	9	615	0.244	0.080	0.0008	12300	32.84

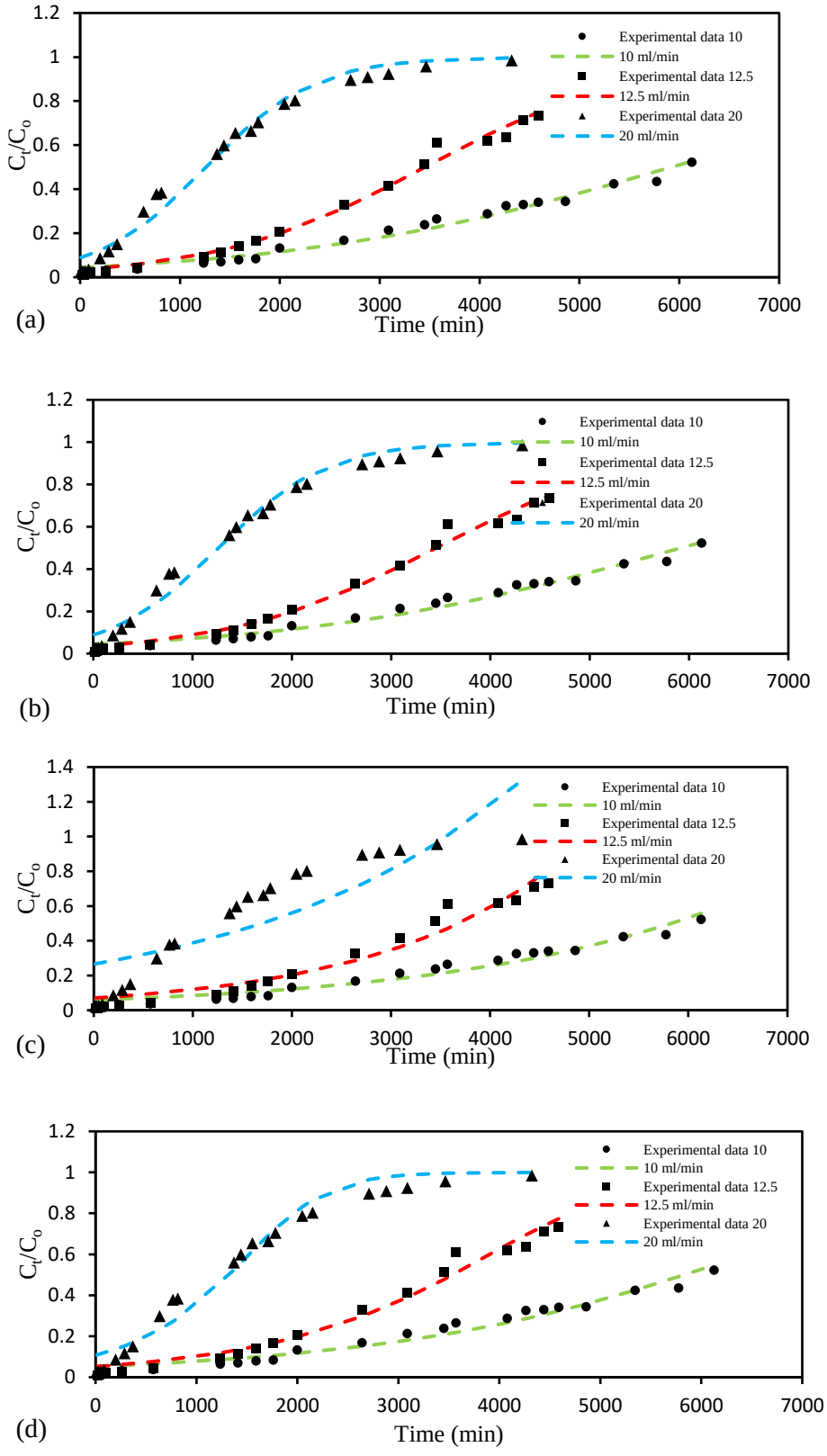

Figure 4-3: Breakthrough curves of the effect of flowrate on arsenic adsorption onto DMI-65 (a) Thomas model (b) Yoon-Nelson model (c) Adam`s – Bohart model (d) Clark model.

From Fig. 4-5a, turbidity removal at 10 mL/min performed better for most part of the experiments followed by 12.5 mL/min flowrate. Overall, up to 60 % turbidity removal was recorded and an average of 50 % removal was recorded for 20 mL/min flowrate. UV_{254nm} removal (%) reduces with increase in flowrate and tends to reduce with time for all the flowrates (10, 12.5 and 20 mL/min). Arsenic removal (%) reduces also with increase in flowrate and time as shown in Fig. 4-5. Fouling of the column is a problem encountered at lower flowrates (10 and 12.5 mL/min) as shown in Fig. 4-4 and that resulted in pressure drop in the column.

(a)

(b)

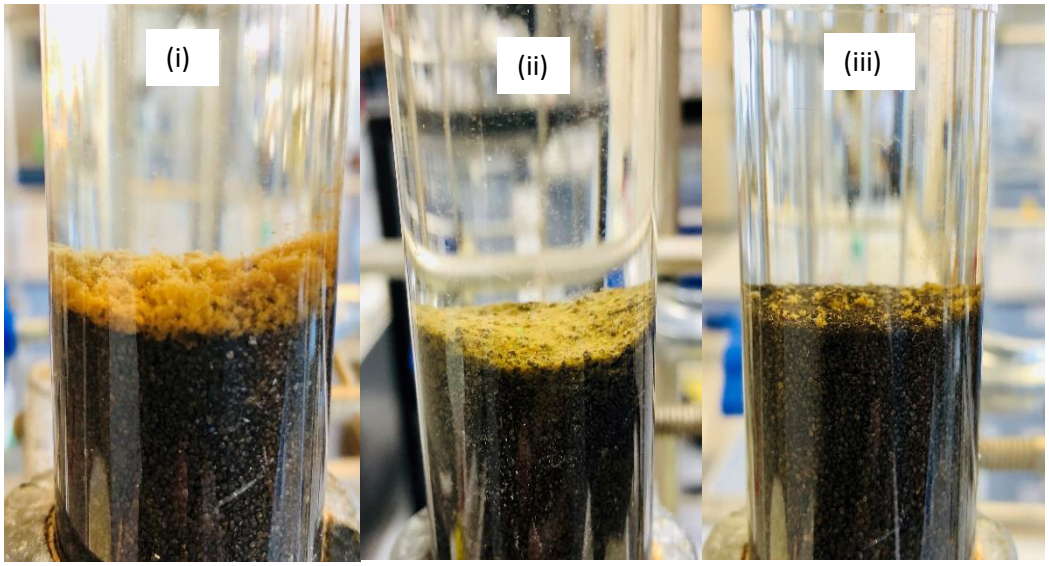

Figure 4-4: (a) Experimental set-up of the adsorption column experiment (b) fouling in the column at different flowrates (i) 10 mL/min (ii) 12.5 mL/min and (iii) 20 mL/min.

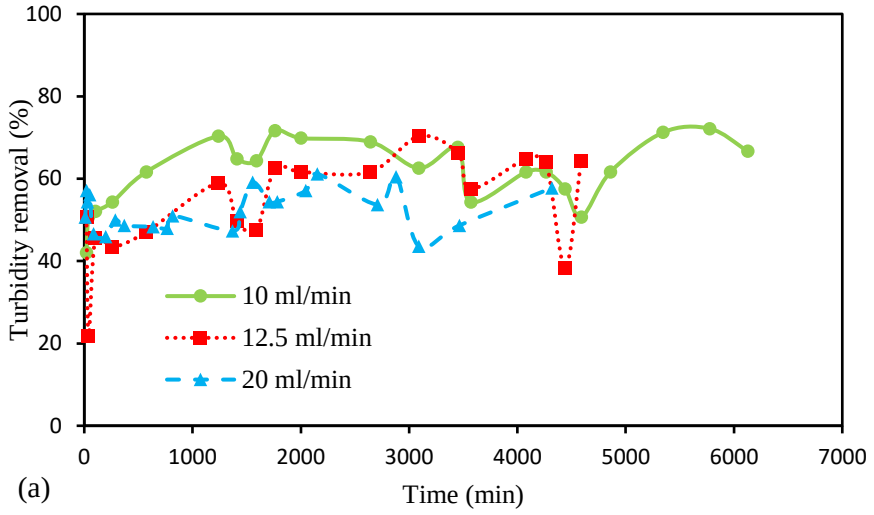

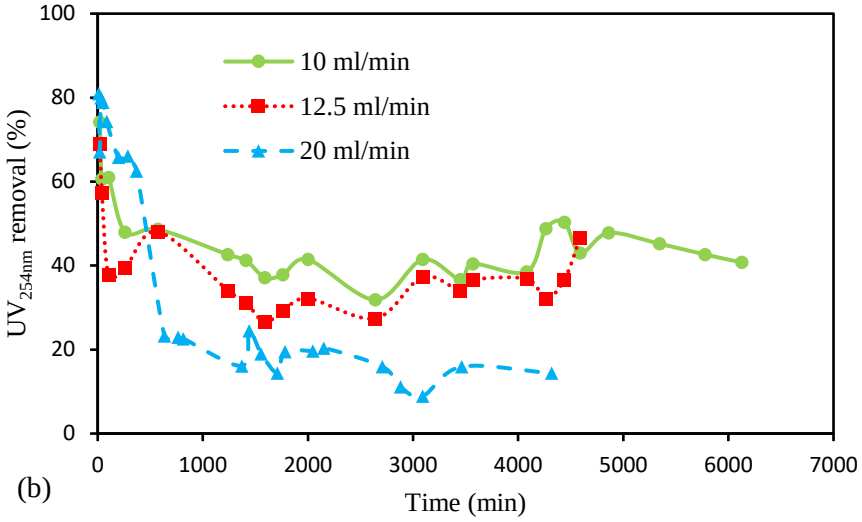

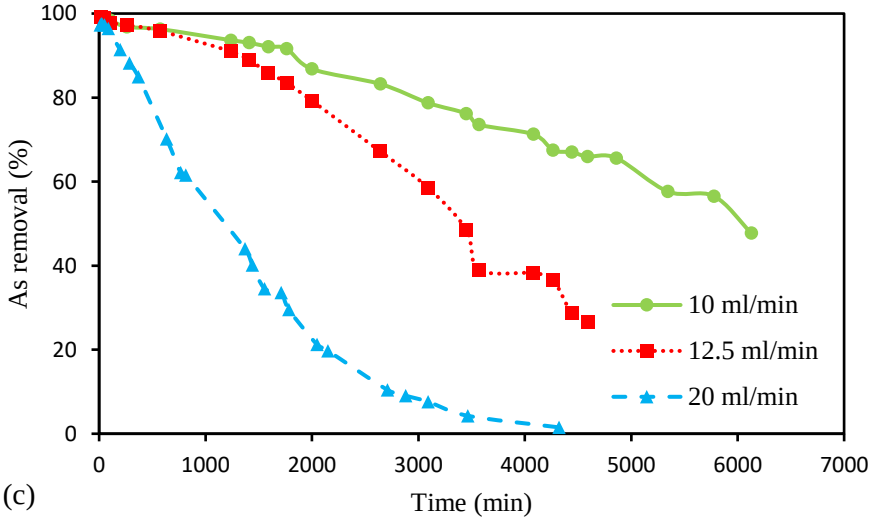

Figure 4-5: Effect of flowrate on (a) turbidity (b) UV_{254nm} and (c) arsenic removal in a fixed-bed column.

Fouling occurred most at the lower flowrates (10 and 12.5 mL/min) as a result of suspended particles not being able to pass through the pore space of the DMI-65 (which in this case also act as a filter) but improves turbidity and UV_{254nm} removal.

4.3.2 The effect of pH on breakthrough curve

The influent pH is an important factor which does not only affect adsorption capacity but also plays a major role in determining the adsorption mechanisms. The pH of the solution also reflects the nature of the physico-chemical interactions between the compounds in solution and binding sites of the adsorbent (Gupta and Garg, 2019). The breakthrough curve (C_t/C_o versus breakthrough time) for the arsenic uptake at different influent pH (5, 7 and 9) by DMI-65 is presented in Fig. 4-5. In these experiments, the initial concentration of As, flow rate and the mass of the adsorbent were fixed (C_o = 18.52 µg/L (pH 5); C_o = 19.87 µg/L (pH 9) Q = 20 mL/min, m = 100 g).

Arsenic uptakes at different influent pH (5.0, 7.0 and 9.0) were 0.0066, 0.0043 and 0.0008 mg/g, respectively. It is apparent that arsenic adsorption capacity decreases with increase in pH influent condition. The lower arsenic adsorption at higher pH may be explained by the increased electrostatic repulsion due to the increased negative charge on the surface of DMI-65 (Sellner et al., 2019). Thus when the pH was increased from 5 to 9, the DMI-65 became more negatively charged due to the presence of more OH^- and HCO_3^- (Sheng et al., 2018; Xu et al., 2013). It can be seen from Fig. 4-5 that when the pH value increases from 5 to 9, the breakthrough time and exhaustion point decrease from 50.83 hours to 10.25 hours and from 4.17 days to 1.39 days, respectively. From Fig. 4-6, As, turbidity and UV_{254nm} removal performed better at pH 5 than at pH 7 and 9 throughout the time considered in this study (Appendix 4B).

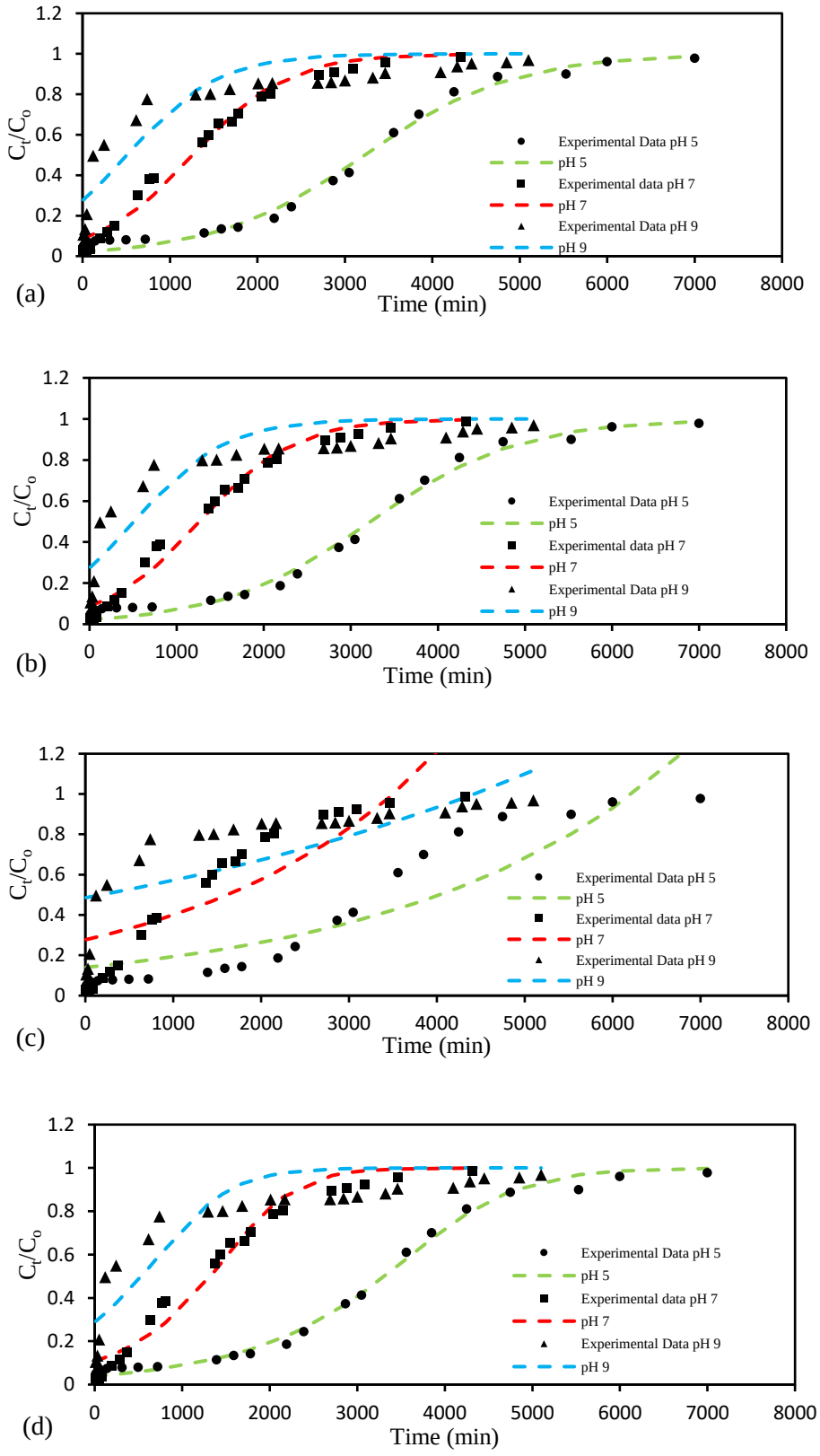

Figure 4-6: Breakthrough curves of the effect of pH on arsenic adsorption onto DMI-65 (a) Thomas model (b) Yoon-Nelson model (c) Adam`s – Bohart model (d) Clark model.

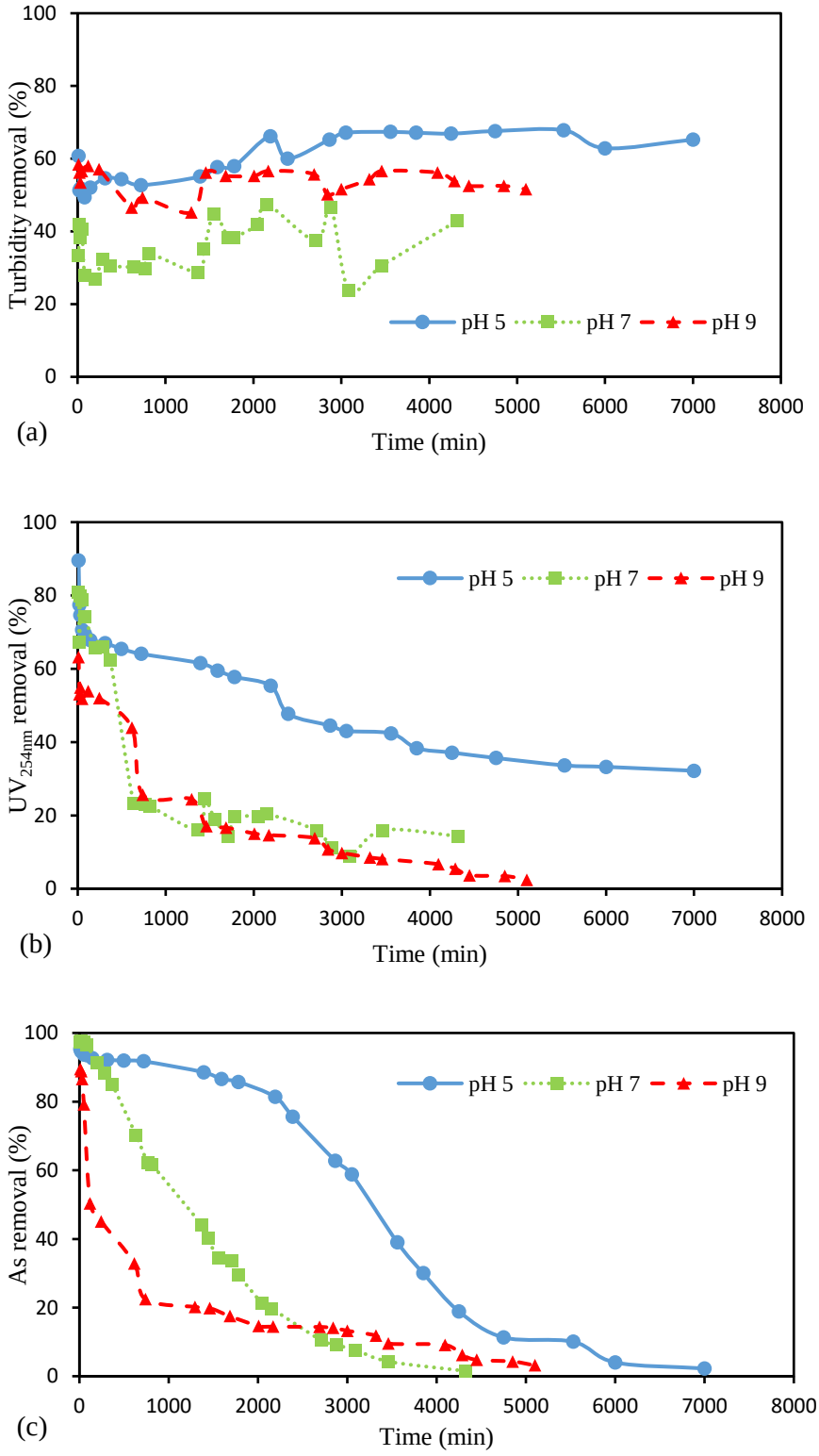

Figure 4-7: Effect of flowrate on (a) turbidity (b) UV_{254nm} and (c) arsenic removal in a fixed bed column.

4.3.3 Dynamic modelling of fixed-bed column

Successful design of a column adsorption process requires prediction of the concentration-time or breakthrough curve for the effluent (Han et al., 2009). Mathematical models have been developed and used over the years for describing and analysing the lab-scale column studies for the purpose of industrial applications (Chen et al., 2012; Han et al., 2009; Kumar and Chakraborty, 2009; Vinodhini and Das, 2010). In this study, four models, Thomas, Yoon-Nelson, Adams-Bohart and Clark were used to identify the best model for predicting the dynamic behaviour of the column.

4.3.3.1 Thomas model:

The column data were fitted to the nonlinear regression analysis of the Thomas model as shown in Eq. (4.7) to determine the Thomas rate constant (k_{TH}) and equilibrium arsenic uptake (q_e) by DMI-65. The model parameters (k_{TH} and q_e) and the correlation coefficient (R^2) for all the experimental breakthrough curves are presented in Table 4-3. The rate constant increased with increase of flowrate and increase from pH 5 to pH 7. With flowrate and pH increasing, the value of qe decreased. Analysis of the regression coefficients indicated that the regressed lines provided a good fit to the experimental data with R^2 values ranging from 0.977 – 0.989 and 0.835 – 0.991 for effect of flowrate and pH respectively. The values of q_e parameters estimated by the Thomas model for the breakthrough curves were close to experimental value. So the Thomas model can be used to predict the adsorption process, which is an indication that the internal and external diffusions were not the limiting steps (Han et al., 2009; Xu et al., 2013).

4.3.3.2 Yoon-Nelson model

The Yoon-Nelson model is a simple theoretical model developed to investigate the breakthrough behaviour of arsenic on DMI-65 (Han et al., 2009). A nonlinear regression analysis as shown in Eq. (4.10) was used to determine the values of k_{YN} (a rate constant) and τ (the time required for 50 % arsenic breakthrough). The values of k_{YN} and τ are presented in Table 4.4. As seen from Table 4-4, the rate constant k_{YN} increased and the 50 % breakthrough time τ decreased with both increasing flowrate and pH. The τ values in Table 4-4 are close to experimental results as shown in Fig. 4-2 and 4-5 and the correlation coefficients R^2 were > 0.963. This

model fit well with the experimental results indicating that this model can be used to describe the fixed-bed adsorption process. A comparison of the R^2 values indicates that the Yoon-Nelson and Thomas model better fit the experimental data than Adams-Bohart and Clark models.

4.3.3.3 Adams-Bohart model

The Adams-Bohart adsorption model was applied to describe the initial part of the breakthrough curve. The values of k_{AB} and N_0 for all the breakthrough curves were presented in Table 4-5. The value of k_{AB} did not show any particular trend with increase in flowrate. However, the value of N_0 decreased with increase in flowrate. Additionally, the value of N_0 decreased with increase in pH but no particular trend was observed in the value of k_{AB} with increase in pH. The correlation coefficients (R^2) were found to be between 0.572 – 0.953 for the adsorption process and is not a good fit with the experimental breakthrough curve.

4.3.3.4 Clark model

From Chapter 3, it was found out that the Freundlich model for As (V) adsorption was approximately valid for the adsorption of As (V) on DMI-65 in batch adsorption (Aremu et al., 2019). The Freundlich constant *n* (3.2) obtained in a batch experiment (Table 3-4) was used to calculate the parameters in the Clark model. The values of A and r in the Clark model were determined using Eq. (4.14) by nonlinear regression analysis and are shown in Table 4-6.

As seen from Table 4-6, as flowrate increased, the value of *r* increased. These results are similar to those found by other researchers working on different adsorbent-adsorbate systems (Ayoob and Gupta, 2007; Han et al., 2009). The experimental results and calculated data from the regression analysis showed that the Clark model provided good correlation on the effect of flowrate (R^2 = 0.963 – 0.977) and pH (R^2 = 0.812 – 0.995).

4.3.4 Non-linear error function analysis

The conventional method of selecting the best-fit model based on the regression coefficient (R^2) is not always the appropriate method of choosing the best model. Error measurements can be used to obtain better fits for any mathematic model by using nonlinear adsorption models.

Table 4-3: Model parameters by nonlinear regression analysis with the Thomas model for adsorption of arsenic unto DMI-65

C_o (mg/L)	*v* (mL/min)	Z, cm	pH	k_{TH} (mL/min mg)	$q_{o,cal}$ (mg/g)	SSE	SAE	ARE	HYBRID	MPSD	R^2
0.0131	10	20	7	0.0398	7.733	0.0118	0.1051	0.1344	3.9556	99.443	0.977
0.0131	12.5	20	7	0.0736	5.638	0.0137	0.1146	0.1512	2.7576	103.789	0.989
0.0131	20	20	7	0.1412	3.304	0.0529	0.3750	0.1478	6.2416	118.967	0.981
0.0185	20	20	5	0.0632	11.955	0.0229	0.2720	0.5155	0.6316	37.847	0.991
0.0198	20	20	9	0.0958	2.028	0.3084	1.1512	0.0780	1.4571	57.483	0.835

Table 4-4: Yoon-Nelson parameters at different conditions using nonlinear regression analysis

C_o (mg/L)	*v* (mL/min)	Z, cm	pH	K_{YN} (1/min)	τ (min)	SSE	SAE	ARE	HYBRID	MPSD	R^2
0.0131	10	20	7	0.00052	5922.50	0.0118	0.1051	0.1344	3.9556	99.443	0.977
0.0131	12.5	20	7	0.00096	3453.98	0.0137	0.1146	0.1512	2.7576	103.789	0.989
0.0131	20	20	7	0.00184	1265.12	0.0529	0.3750	0.1478	6.2416	118.967	0.994
0.0185	20	20	5	0.00117	3227.57	0.0229	0.2720	0.5155	0.6316	37.847	0.997
0.0198	20	20	9	0.00190	510.34	0.3084	1.1512	0.0780	1.4571	57.483	0.963

Table 4-5: Adams-Bohart parameters at different conditions using nonlinear regression analysis

C_o (mg/L)	*v* (mL/min)	Z, cm	pH	K_{AB} (L/mg/min)	No (mg/L)	SSE	SAE	ARE	HYBRID	MPSD	R^2
0.0131	10	20	7	0.0281	16.788	0.0246	0.1617	0.1604	8.557	146.263	0.953
0.0131	12.5	20	7	0.0409	10.836	0.0587	0.2505	0.2172	15.693	247.589	0.952
0.0131	20	20	7	0.0284	7.757	0.7808	0.4636	0.1575	84.050	436.565	0.725
0.0185	20	20	5	0.0170	19.214	0.4340	0.3542	0.2129	3.966	94.839	0.837
0.0198	20	20	9	0.0082	14.635	0.7994	0.0979	0.0252	7.053	126.467	0.572

Table 4-6: Clark parameters at different conditions using nonlinear regression analysis

C_o (mg/L)	*v* (mL/min)	Z, cm	pH	A	r (1/min)	SSE	SAE	ARE	HYBRID	MPSD	R^2
0.0131	10	20	7	618.63	0.000895	0.0194	0.1216	0.1439	6.214	124.642	0.963
0.0131	12.5	20	7	649.92	0.001477	0.0289	0.2061	0.1933	7.710	173.536	0.977
0.0131	20	20	7	133.98	0.002734	0.0920	0.5535	0.1612	10.225	152.268	0.967
0.0185	20	20	5	1232.35	0.001763	0.0142	0.0403	0.1446	0.1855	20.513	0.995
0.0198	20	20	9	14.34	0.002594	0.3521	1.3179	0.0864	1.6959	62.013	0.812

n=3.2 (From Table 3-4, Freundlich equation). n is used in Clark model.

Depending on R^2 value, the Thomas and Yoon-Nelson models were found as the well-fitting models. According to Biswas and Mishra (2015), error function analysis is the most suitable optimization method to evaluate the best fitted model for the experimental data. Therefore, lower value of SSE, HYBRID and MPSD and higher R^2 are indications of the best-fitted model. Results of the error analysis illustrated in Table 4-3 – 4-6 showed that both Thomas and Yoon-Nelson models were the best-fitted models for the adsorption of arsenic on DMI-65.

Hamilton water treatment plant processes 90 million L of water daily during peak period of the summer months of December - February. To remove 50 % of the arsenic, 148 tonnes of DMI-65 in total would be required for two adsorption columns, each having a volume of 101 m^3. It is recommended to have three adsorption columns, one as a back up while another is being cleaned, each having a packed bed height of 4.5 m and a diameter of 4 m (Appendix 4C). Each column can be run for 47 hours with 1 hour for backwashing. Futher work on pilot scale systems would be required to determine the pressure drop during operation through the columns and extent of fouling if it was installed prior to flocculation and clarification. Different modes of operation could be investigated such as upflow expanded bed adsorption to reduce fouling issues, otherwise if flocculation and clarifications were able to be developed by which the solids could be removed without the arsenic, the columns could be installed between the sand filters and the activated carbon filters. Alternatively, the DMI-65 media could also be used in the filter beds.

4.4 Conclusion

This study demonstrated the performance of DMI-65 for removing arsenic from Waikato River water sample in a fixed-bed adsorption column. Based on the results from this study, the following conclusion can be drawn:

(a) DMI-65 can be used as an adsorbent in removing arsenic from a contaminated drinking water in a fixed-bed adsorption process.
(b) The adsorption performance was dependent on volumetric flowrate and pH.
(c) The Yoon-Nelson and Thomas models appeared to be the most suited for the prediction of the breakthrough characteristics of the adsorption process.

The models have a high correlation coefficient (R^2) and recorded low value of SSE, HYBRID and MPSD. The Yoon-Nelson model estimated the 50 % breakthrough time of the adsorption process and the Thomas model predicted the saturated adsorption capacity.

(d) The maximum adsorption capacity of DMI-65 was found to be 11.96 mg/g for removing arsenic from a contaminated drinking water under the following operating parameters (arsenic concentration = ~13.10 – 20 µg/L, bed height = 20 cm, flowrate = 20 mL/min and pH = 5).

(e) When the flowrate increased from 10 to 20 mL/min, the removal percentage of arsenic reduced from 56.56 to 43.98 % (breakthrough point of C_t/C_o = 0.5).

(f) The findings showed that both Yoon-Nelson and Thomas models could be applied for improving the design, scaling up and optimising the performance of a continuous fixed-bed adsorption process.

Appendix 4. Supplementary data

- This contains experimental data for both effect of flowrate and pH on adsorption of arsenic onto DMI-65.
- Linear plots of Thomas, Yoon-Nelson, Adams-Bohart and Clark model

Declaration of Competing Interest

None

References

Aichour, A., Zaghouane-Boudiaf, H., Mohamed Zuki, F.B., Kheireddine Aroua, M., Ibbora, C.V., 2019. Low-cost, biodegradable and highly effective adsorbents for batch and column fixed bed adsorption processes of methylene blue. J. Environ. Chem. Eng. 7, 103409. https://doi.org/10.1016/j.jece.2019.103409

Aksu, Z., Gönen, F., 2004. Biosorption of phenol by immobilized activated sludge in a continuous packed bed: prediction of breakthrough curves. Process Biochem. 39, 599–613. https://doi.org/10.1016/S0032-9592(03)00132-8

Ang, T.N., Young, B.R., Taylor, M., Burrell, R., Aroua, M.K., Baroutian, S., 2020. Breakthrough analysis of continuous fixed-bed adsorption of sevoflurane using activated carbons. Chemosphere 239, 124839. https://doi.org/10.1016/j.chemosphere.2019.124839

Aremu, J.O., Lay, M., Glasgow, G., 2019. Kinetic and isotherm studies on adsorption of arsenic using silica based catalytic media. J. Water Process Eng. 32, 100939. https://doi.org/10.1016/j.jwpe.2019.100939

Argos, M., Kalra, T., Rathouz, P.J., Chen, Y., Pierce, B., Parvez, F., Islam, T., Ahmed, A., Rakibuz-Zaman, M., Hasan, R., Sarwar, G., Slavkovich, V., van Geen, A., Graziano, J., Ahsan, H., 2010. Arsenic exposure from drinking water, and all-cause and chronic-disease mortalities in Bangladesh (HEALS): a prospective cohort study. The Lancet 376, 252–258. https://doi.org/10.1016/S0140-6736(10)60481-3

Ayoob, S., Gupta, A.K., 2007. Sorptive response profile of an adsorbent in the defluoridation of drinking water. Chem. Eng. J. 133, 273–281. https://doi.org/10.1016/j.cej.2007.02.013

Biswas, S., Mishra, U., 2015. Continuous Fixed-Bed Column Study and Adsorption Modeling: Removal of Lead Ion from Aqueous Solution by Charcoal Originated from Chemical Carbonization of Rubber Wood Sawdust [WWW Document]. J. Chem. https://doi.org/10.1155/2015/907379

Bohart, G.S., Adams, E.Q., 1920. SOME ASPECTS OF THE BEHAVIOR OF CHARCOAL WITH RESPECT TO CHLORINE.1. J. Am. Chem. Soc. 42, 523–544. https://doi.org/10.1021/ja01448a018

Charola, S., Yadav, R., Das, P., Maiti, S., 2018. Fixed-bed adsorption of Reactive Orange 84 dye onto activated carbon prepared from empty cotton flower agro-waste. Sustain. Environ. Res. 28, 298–308. https://doi.org/10.1016/j.serj.2018.09.003

Chen, S., Yue, Q., Gao, B., Li, Q., Xu, X., Fu, K., 2012. Adsorption of hexavalent chromium from aqueous solution by modified corn stalk: A fixed-bed column study. Bioresour. Technol., Special issue on the Challenges in Environmental Science and Engineering 113, 114–120. https://doi.org/10.1016/j.biortech.2011.11.110

Chen, Y., Graziano, J.H., Parvez, F., Liu, M., Slavkovich, V., Kalra, T., Argos, M., Islam, T., Ahmed, A., Rakibuz-Zaman, M., Hasan, R., Sarwar, G., Levy, D., Geen, A. van, Ahsan, H., 2011. Arsenic exposure from drinking water and mortality from cardiovascular disease in Bangladesh: prospective cohort study. BMJ 342. https://doi.org/10.1136/bmj.d2431

Clark, R.M., 1987. Evaluating the cost and performance of field-scale granular activated carbon systems. Environ. Sci. Technol. 21, 573–580. https://doi.org/10.1021/es00160a008

de Franco, M.A.E., de Carvalho, C.B., Bonetto, M.M., de Pelegrini Soares, R., Féris, L.A., 2018. Diclofenac removal from water by adsorption using activated carbon in batch mode and fixed-bed column: Isotherms, thermodynamic study and breakthrough curves modeling. J. Clean. Prod. 181, 145–154. https://doi.org/10.1016/j.jclepro.2018.01.138

Dhar, R.K., Biswas, B.K., Samanta, G., Mandal, B.K., Chakraborti, D., Roy, S., Jafar, A., Islam, A., Ara, G., Kabir, S., Khan, A.W., Ahmed, S.A., Hadi, S.A., 1997. Groundwater arsenic calamity in Bangladesh. Curr. Sci. 73, 48–59.

Dhoble, R.M., Maddigapu, P.R., Rayalu, S.S., Bhole, A.G., Dhoble, A.S., Dhoble, S.R., 2017. Removal of arsenic(III) from water by magnetic binary oxide particles (MBOP): Experimental studies on fixed bed column. J. Hazard. Mater. 322, 469–478. https://doi.org/10.1016/j.jhazmat.2016.09.075

Guo, H., Stüben, D., Berner, Z., Kramar, U., 2008. Adsorption of arsenic species from water using activated siderite–hematite column filters. J. Hazard. Mater. 151, 628–635. https://doi.org/10.1016/j.jhazmat.2007.06.035

Gupta, A., Garg, A., 2019. Adsorption and oxidation of ciprofloxacin in a fixed bed column using activated sludge derived activated carbon. J. Environ. Manage. 250, 109474. https://doi.org/10.1016/j.jenvman.2019.109474

Han, R., Wang, Yi, Zou, W., Wang, Yuanfeng, Shi, J., 2007. Comparison of linear and nonlinear analysis in estimating the Thomas model parameters for methylene blue adsorption onto natural zeolite in fixed-bed column. J. Hazard. Mater. 145, 331–335. https://doi.org/10.1016/j.jhazmat.2006.12.027

Han, R., Wang, Yu, Zhao, X., Wang, Yuanfeng, Xie, F., Cheng, J., Tang, M., 2009. Adsorption of methylene blue by phoenix tree leaf powder in a fixed-bed column: experiments and prediction of breakthrough curves. Desalination, Engineering with Membranes 2008 245, 284–297. https://doi.org/10.1016/j.desal.2008.07.013

Ho, Y.-S., Chiu, W.-T., Wang, C.-C., 2005. Regression analysis for the sorption isotherms of basic dyes on sugarcane dust. Bioresour. Technol. 96, 1285–1291. https://doi.org/10.1016/j.biortech.2004.10.021

Hristovski, K., Baumgardner, A., Westerhoff, P., 2007. Selecting metal oxide nanomaterials for arsenic removal in fixed bed columns: From nanopowders to aggregated nanoparticle media. J. Hazard. Mater. 147, 265–274. https://doi.org/10.1016/j.jhazmat.2007.01.017

Jaiswal, V., Saxena, S., Kaur, I., Dubey, P., Nand, S., Naseem, M., Singh, S.B., Srivastava, P.K., Barik, S.K., 2018. Application of four novel fungal strains to remove arsenic from contaminated water in batch and column modes. J. Hazard. Mater. 356, 98–107. https://doi.org/10.1016/j.jhazmat.2018.04.053

Jian, M., Liu, B., Zhang, G., Liu, R., Zhang, X., 2015. Adsorptive removal of arsenic from aqueous solution by zeolitic imidazolate framework-8 (ZIF-8) nanoparticles. Colloids Surf. Physicochem. Eng. Asp. 465, 67–76. https://doi.org/10.1016/j.colsurfa.2014.10.023

Jiang, Q., Xie, W., Han, S., Wang, Y., Zhang, Y., 2019. Enhanced adsorption of Pb(II) onto modified hydrochar by polyethyleneimine or H3PO4: An analysis of surface property and interface mechanism. Colloids Surf. Physicochem. Eng. Asp. 583, 123962. https://doi.org/10.1016/j.colsurfa.2019.123962

Kalaruban, M., Loganathan, P., Nguyen, T.V., Nur, T., Hasan Johir, M.A., Nguyen, T.H., Trinh, M.V., Vigneswaran, S., 2019. Iron-impregnated granular activated carbon for arsenic removal: Application to practical column filters. J. Environ. Manage. 239, 235–243. https://doi.org/10.1016/j.jenvman.2019.03.053

Karim, M.M., 2000. Arsenic in groundwater and health problems in Bangladesh. Water Res. 34, 304–310. https://doi.org/10.1016/S0043-1354(99)00128-1

Kumar, P.A., Chakraborty, S., 2009. Fixed-bed column study for hexavalent chromium removal and recovery by short-chain polyaniline synthesized on jute fiber. J. Hazard. Mater. 162, 1086–1098. https://doi.org/10.1016/j.jhazmat.2008.05.147

Kundu, S., Gupta, A.K., 2006. Arsenic adsorption onto iron oxide-coated cement (IOCC): Regression analysis of equilibrium data with several isotherm models and their optimization. Chem. Eng. J. 122, 93–106. https://doi.org/10.1016/j.cej.2006.06.002

López-Cervantes, J., Sánchez-Machado, D.I., Sánchez-Duarte, R.G., Correa-Murrieta, M.A., 2017. Study of a fixed-bed column inthe adsorption of an azo dye from an aqueous medium using a chitosan–glutaraldehyde biosorbent. Adsorpt Sci Technol 1–18.

Mondal, M.K., Garg, R., 2017. A comprehensive review on removal of arsenic using activated carbon prepared from easily available waste materials. Environ. Sci. Pollut. Res. 24, 13295–13306. https://doi.org/10.1007/s11356-017-8842-7

Palma-Lara, I., Martínez-Castillo, M., Quintana-Pérez, J.C., Arellano-Mendoza, M.G., Tamay-Cach, F., Valenzuela-Limón, O.L., García-Montalvo, E.A., Hernández-Zavala, A., 2020. Arsenic exposure: A public health problem leading to several cancers. Regul. Toxicol. Pharmacol. 110, 104539. https://doi.org/10.1016/j.yrtph.2019.104539

Reddy, R.R., Rodriguez, G.D., Webster, T.M., Abedin, M.J., Karim, M.R., Raskin, L., Hayes, K.F., 2020. Evaluation of arsenic field test kits for drinking water: Recommendations for improvement and implications for arsenic affected regions such as Bangladesh. Water Res. 170, 115325. https://doi.org/10.1016/j.watres.2019.115325

Salman, J.M., Njoku, V.O., Hameed, B.H., 2011. Batch and fixed-bed adsorption of 2,4-dichlorophenoxyacetic acid onto oil palm frond activated carbon. Chem. Eng. J. 174, 33–40. https://doi.org/10.1016/j.cej.2011.08.024

Sellner, B.M., Hua, G., Ahiablame, L.M., 2019. Fixed bed column evaluation of phosphate adsorption and recovery from aqueous solutions using recycled steel byproducts. J. Environ. Manage. 233, 595–602. https://doi.org/10.1016/j.jenvman.2018.12.070

Sheng, L., Zhang, Y., Tang, F., Liu, S., 2018. Mesoporous/microporous silica materials: Preparation from natural sands and highly efficient fixed-bed adsorption of methylene blue in wastewater. Microporous Mesoporous Mater. 257, 9–18. https://doi.org/10.1016/j.micromeso.2017.08.023

Smith, A.H., Lingas, E.O., Rahman, M., 2000. Contamination of drinking-water by arsenic in Bangladesh: A public health emergency. Bull. World Health Organ. 78, 1093–1103.

Sun, X., Huang, H., Zhu, Y., Du, Y., Yao, L., Jiang, X., Gao, P., 2019. Adsorption of Pb2+ and Cd2+ onto Spirulina platensis harvested by polyacrylamide in single and binary solution systems. Colloids Surf. Physicochem. Eng. Asp. 583, 123926. https://doi.org/10.1016/j.colsurfa.2019.123926

Thomas, H.C., 1948. Chromatography: A Problem in Kinetics. Ann. N. Y. Acad. Sci. 49, 161–182. https://doi.org/10.1111/j.1749-6632.1948.tb35248.x

Vieira, M.L.G., Martinez, M.S., Santos, G.B., Dotto, G.L., Pinto, L.A.A., 2018. Azo dyes adsorption in fixed bed column packed with different deacetylation degrees chitosan coated glass beads. J. Environ. Chem. Eng. 6, 3233–3241. https://doi.org/10.1016/j.jece.2018.04.059

Vinodhini, V., Das, N., 2010. Packed bed column studies on Cr (VI) removal from tannery wastewater by neem sawdust. Desalination 264, 9–14. https://doi.org/10.1016/j.desal.2010.06.073

Wang, M., Li, X., Zhang, T., Deng, L., Li, P., Wang, X., Hsiao, B.S., 2018. Eco-friendly poly(acrylic acid)-sodium alginate nanofibrous hydrogel: A multifunctional platform for superior removal of Cu(II) and sustainable catalytic applications. Colloids Surf. Physicochem. Eng. Asp. 558, 228–241. https://doi.org/10.1016/j.colsurfa.2018.08.074

Wei, Y., Wei, S., Liu, C., Chen, T., Tang, Y., Ma, J., Yin, K., Luo, S., 2019. Efficient removal of arsenic from groundwater using iron oxide nanoneedle array-decorated biochar fibers with high Fe utilization and fast adsorption kinetics. Water Res. 167, 115107. https://doi.org/10.1016/j.watres.2019.115107

Wu, X., Wu, D., Fu, R., Zeng, W., 2012. Preparation of carbon aerogels with different pore structures and their fixed bed adsorption properties for dye removal. Dyes Pigments 95, 689–694. https://doi.org/10.1016/j.dyepig.2012.07.001

Xu, X., Gao, B., Tan, X., Zhang, X., Yue, Q., Wang, Y., Li, Q., 2013. Nitrate adsorption by stratified wheat straw resin in lab-scale columns. Chem. Eng. J. 226, 1–6. https://doi.org/10.1016/j.cej.2013.04.033

YOON, Y.H., NELSON, J.H., 1984. Application of Gas Adsorption Kinetics I. A Theoretical Model for Respirator Cartridge Service Life. Am. Ind. Hyg. Assoc. J. 45, 509–516. https://doi.org/10.1080/15298668491400197

Zou, W., Zhao, L., Zhu, L., 2013. Adsorption of uranium(VI) by grapefruit peel in a fixed-bed column: Experiments and prediction of breakthrough curves. J. Radioanal. Nucl. Chem. 295, 717–727. https://doi.org/10.1007/s10967-012-1950-4

CHAPTER FIVE

Arsenate removal from contaminated drinking water: Comparative study between dissolved air flotation and sedimentation

Abstract

Coagulation/flocculation/sedimentation (C/F/S) and coagulation / flocculation /dissolved air flotation (C/F/DAF) were performed using natural water spiked with arsenate to evaluate the influence of coagulants, coagulant dose and pH on arsenate (As (V)) removal. Two types of coagulants were used in this study namely Polydiallyldimethylammonium chloride (polyDADMAC) and Chitosan from crab shell. The results showed that 49.43 % of As (V) was removed in the C/F/DAF process using chitosan compared to 22.06 % As (V) removal using polyDADMAC. Lower As (V) removal was recorded for both chitosan (39.59 %) and polyDADMAC (35.91 %) in the C/F/S process. Higher turbidity removal (> 70 %) was recorded using both coagulants and processes considered in this study. C/F/DAF recorded a better performance than C/F/S using Chitosan across the pHs (4 – 9) in removing As (V). However, C/F/S performed better than C/F/DAF using polyDADMAC in removing As (V) across the pH range (4 – 9) studied with maximum As (V) removal (< 40 %). Overall, results showed that both Chitosan and polyDADMAC performed poorly in removing As (V) using both processes but recorded higher turbidity removal.

5.1 Introduction

Polymers have found extensive usage in water and wastewater treatment (Amin et al., 2014; Manhokwe and Zvidzai, 2019). This increase in use is due to to their ability to produce better water quality, a lower sludge volume and a better sludge quality (Mahvi and Razavi, 2005). There are two types of organic polymers used in water and wastewater treatment namely: natural and synthetic polymers (Zahrim et al., 2011). Two important properties used in characterising synthetic polymers are molecular mass and charge density (Bolto and Gregory, 2007; Zahrim et al., 2011). Polydiallyldimethylammonium chloride (polyDADMAC) is one of the most extensively used synthetic polyelectrolytes used in industry (Razali et al., 2011). PolyDADMAC was the first polymer to be permitted for use in drinking water treatment by the Food and Drug Administration of U.S.A (Letterman and Pero, 1990). Likewise, about 75 % of flocculants used in water treatment processes in South Africa are polyDADMAC and epichlorohydrin-dimethylamine (epi-DMA) (Majam et al., 2004). PolyDADMAC molecules have a strong cationic group in its structure (Fig. 5-1). Its ability to neutralise or reduce electric charges on the surface of suspended particles makes it suitable for flocculation processes (Kleimann et al., 2005; Manhokwe and Zvidzai, 2019; Razali et al., 2011).

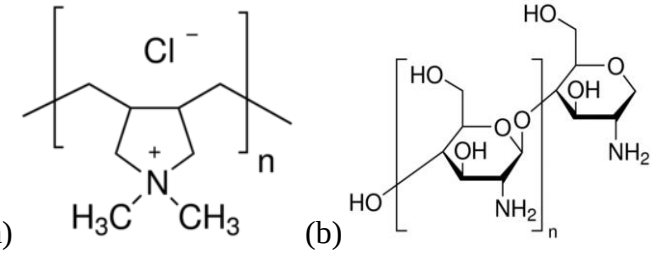

Figure 5-1: Structure of (a) polyDADMAC and (b) Chitosan from crab shell (Source: Sigma Aldrich, New Zealand).

The Polymer-assisted (soluble and insoluble) removal process has been studied for the removal of arsenic. The quaternary amine group in particular have been shown to effectively remove As (V) during a membrane assisted study (Pirgalıoğlu et al., 2015; Pookrod et al., 2004; Rivas et al., 2007, 2003). Rivas et al. (2010) reported the use of various water soluble plymers combined with ultra-filtration to remove arsenic using the $(R)_4N^+X^-$ group.

Chitosan is a family of linear polysaccharides with repeated units of glucosamine and N-acetyl-glucosamine obtained from the exoskeletons of marine crustaceans such as crabs (Samrot et al., 2018), shrimps (Teli and Sheikh, 2012), lobsters (Ilangumaran et al., 2017), prawns (Mohammed et al., 2013) and fungi (Logesh et al., 2012; Zamani et al., 2007). Chitosan along with its derivatives has excellent biological properties including wound healing (Dai et al., 2011), bioadhesion (Chuah et al., 2013), biocompatibility, biodegradability, high drug holding ability and non-toxicicity (Huang et al., 2019; Samrot et al., 2018). Therefore chitosan and its derivatives have wide application in medicinal fields, the chemical industry, food industry, textiles, cosmetics, wastewater treatment plants, etc. (Chiang et al., 2012). However, its poor solubility in water limits its application in food and biomedical fields (Affes et al., 2019).

Chitosan is effective in removing transition metals via adsorption due to the presence of amino ($-NH_3$) and hydroxyl (-OH) groups on chitosan chains, which serve as coordination and electrostatic interaction sites respectively (Guibal et al., 1994; López-León et al., 2005; Sheng et al., 2004). Yee et al. (2019) used chitosan-coated bentonite as an adsorbent in removing arsenate from a contaminated ground water (Initial As (V) concentration = 50.99 µg/L; maximum adsorption capacity = 1.47 mg/g).

The main objective of this study was to investigate the performance of C/F/S and C/F/DAF under various operating counditions in removing arsenic from a contaminated water. The effect of type of coagulant (polyDADMAC and Chitosan from crab shell), coagulant dosage and pH (4 – 9) was studied. The turbidity, arsenate and UV_{254nm} concentrations were used as the evaluating parameters. The dissolved air flotation experiments were performed for comparison purposes.

5.2 Materials and methods

5.2.1 Natural water samples

The raw water employed in this work was collected from Lady Goodfellow Chapel Lake ($37^0$47’17.7”S $175^0$18’53.1”E) located on the University of Waikato, Hamilton, New Zealand Campus. It has an area of 0.44 ha and a maximum depth of 1.8 m. The water sample was collected in June, 2018 and was spiked with As (V)

prior to the experiments. The characteristics of the contaminated water are shown in Table 5-1.

5.2.2 Chemicals

All chemicals used were analytical reagent grade (AR) unless otherwise stated. Arsenic (V) oxide hydrate (As_2O_5, 99%), concentrated nitric acid (HNO_3, 70 %), hydrochloric acid (HCl, 36-38%), acetic acid, sodium hydroxide (NaOH) and chitosan from crab shell were bought from Sigma Aldrich (New Zealand). The other coagulant used is PolyDADMAC (10 wt % Al_2O_3) with stock solution of 1g/L. Distilled water was used in preparing all the solutions used in this experiment: As (V) (100 mg/L), 0.1M HCl and 0.1M NaOH. Chitosan from crab shell was prepared by dissolving 1 g in 900 mL of distilled water contanining 10 mL of acetic acid with the aid of a magnetic stirrer until it was fully dissolved. All chemicals were supplied by Merck KGaA, Darmstadt, Germany unless stated otherwise.

5.2.3 Analytical techniques

Arsenate concentration in the solution was measured using inductive coupled plasma mass spectrometry (ICP-MS). Quality control employed for ICP-MS measurements are shown in APPENDIX 2BA. Prior to arsenate analysis, 10 mL of sample was filtered through 0.45 µm membrane filter and 200 µL HNO_3 was added. pH of the solutions were measured using a Eutech pH150/temperature meter. The pH meter was calibrated prior to use using 4.01, 7.01 and 10.04 pH buffers (Merck KGaA, Darmstadt, Germany). A HACH 2100P turbidimeter was used to measure turbidity. The meter was calibrated with 10, 20 and 100 NTU turbidity standards (HACH Turbidity Standard kit model 2100P) before use. A PharmaSpec UV 1700 spectrophotometer (SHIMADZU) was used to measure UV_{254nm} absorbance by a direct reading method. Eutech instruments, CyberScan DO 300 and CyberScan 100 were used to measure dissolved oxygen (DO) and conductivity respectively. The concentrations of NO_3, PO_4 and alkalinity were measured using a Palintest photometer 7100.

5.2.4 Coagulation/flocculation/sedimentation experiments

Two different coagulants are used in these experiments namely chitosan from crab shell and PolyDADMAC. The different concentration ranges used for the two different coagulants are 2.0 – 3.0 mg/L for PolyDADMAC and 0.2 – 1.0 mg/L for

Chitosan from crab shell. The point zero charge of the contaminated water was determined using a Mutek PCD 03 particle charge detector and titrating using 1 g/L chitosan and 1 g/L polyDADMAC. Coagulation/flocculation/sedimentation (C/F/S) experiments were performed on 1 L samples at room temperature (23 ± 2 ^{o}C) using a jar tester (Boltac Industries, Hamilton, New Zealand). The pH of the contaminated water sample (pH 4 – pH 9) was adjusted using 0.1M HCl and 0.1 MNaOH solutions. The C/F/S process consisted of 3 minutes of rapid mixing (100 revolutions per minute (rpm)) slow mixing for 10 minutes (30 rpm) and sedimentation for 10 minutes.

Table 5-1: Characteristics of water sample

pH	6.88 (± 0.03)
DO (mg/L)	6.90 (± 0.03)
Turbidity (NTU)	11.3 (± 2.1)
Spiked As (V) (µg/L)	26.5 (± 0.08)
UV_{254nm} (cm^{-1})	0.255 (± 0.002)
Temperature (^{o}C)	20.7 (± 0.8)
Conductivity (µS/cm)	41.6 (± 0.8)
Alkalinity (mg/L $CaCO_3$)	50 (± 3.0)
Nitrate (mg/L N)	0.006 (± 0.02)
Phosphate (mg/L PO_4)	0.06 (± 0.04)

5.2.5 Coagulation/flocculation/DAF experiments

Coagulation/flocculation/DAF experiments were performed using two coagulants (PolyDADMAC and Chitosan from crab shell) at room temperature (23 ± 2 ^{o}C). Bubbles were generated in a laboratory-made saturator (10 L) filled with tap water (pH 7.2 and turbidity of 0.8 NTU) pressurised to 4 bar using industrial grade air. The coagulation/flocculation/DAF process consisted of 3 minutes rapid mix (100 rpm) followed by slow mixing for 10 minutes (30 rpm) and 10 minutes of flotation using a 20 % recycle ratio. The pH of the contaminated water sample was adjusted prior to the C/F/DAF process using 0.1M HCl and 0.1M NaOH solutions. Experiments were carried out in duplicate and for computing the removal of all parameters in the clarified water, removal (%) = $[(1 – C_f /C_i)]$ X 100 was used where C_f and C_i are the final and initial concentrations.

5.3 Results and discussion

5.3.1 Use of PolyDADMAC

5.3.1.1 Effect of polyDADMAC dose.

The value of point zero charge from the particle charge detector is 2.2 mg/L at pH 6.88. Fig. 5-2 shows the effect of polyDADMAC dose from the range of 2.0 – 3.0 mg/L was examined at pH 7.0 to remove As (V), turbidity and UV_{254nm} by using a C/F/S and C/F/DAF process. There was no significant difference on As (V) removal in both the C/F/S and C/F/DAF process though it was observed that the sedimentation process removes more As (V) than the DAF process at all the coagulant doses considered in this study (Appendix 5A). The maximum As (V) removal using C/F/S process was 35.91 % at 2.2 mg/L coagulant dose while the 22.87 % was the maximum As (V) removal using the C/F/DAF process at 2.0 mg/L coagulant dose.

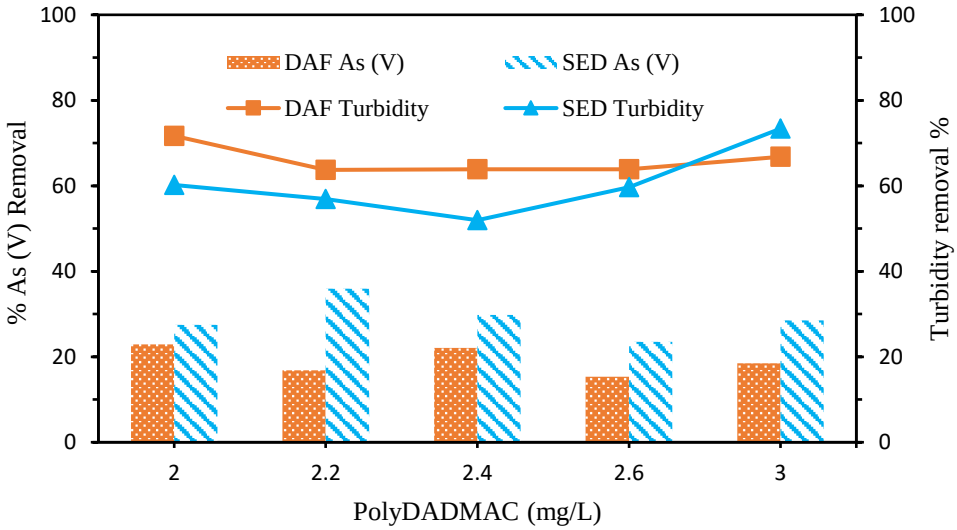

Figure 5-2: Comparative results of As (V) and turbidity removal from C/F/S and C/F/DAF experiments (initial pH = 7.0).

Turbidity removal using the C/F/S reduces from 60.18 % at a coagulant dose of 2.0 mg/L to 51.64 % at a coagulant dose of 2.4 and thereafter starts to increase to a high of 73.36 % at a dose of 3.0 mg/L. Turbidity removal using the C/F/DAF process showed a similar pattern to the C/F/DAF process with the highest turbidity removal of 71.00 % at 2.0 mg/L and a low of 63.89 at pH 2.4 mg/L coagulant dose. Overall, the C/F/DAF process preforms at a higher turbidity removal than the C/F/S process at all the coagulant doses with the exception of 3.0 mg/L.

Fig. 5-3 shows the percentage removal of UV_{254nm} at the investigated coagulant doses using both C/F/S and C/F/DAF processes. The DAF process showed a higher UV_{254nm} removal than the sedimentation process with both showing similar removal patterns. The results showed a reduction in UV_{254nm} from 53.16 % at a coagulant dose of 2.0 mg/L to 39.47 % at a coagulant dose of 2.4 mg/L before showing a higher UV_{254nm} removal efficiency of 52.63 % at 3.0 mg/L coagulant dosage for the C/F/S process. In the C/F/DAF process, increasing coagulant dose (2.0 mg/L to 2.6 mg/L) reduces UV_{254nm} removal efficiency from 64.74 % to 51.05 % and starts to increase at a coagulant dose of 3.0 mg/L to 54.21 %. Likewise, the final pH of the two processes considered in this study (C/F/S and C/F/DAF) are all in the range of 7.06 – 7.69 with the flotation process showing a little higher final pH than the sedimentation. The high turbidity, UV_{254nm} removal and final pH in the C/F/DAF process might be attributed to a clean tap water (turbidity = 0.8 NTU, pH = 7.3) that was used in the saturator during the flotation process.

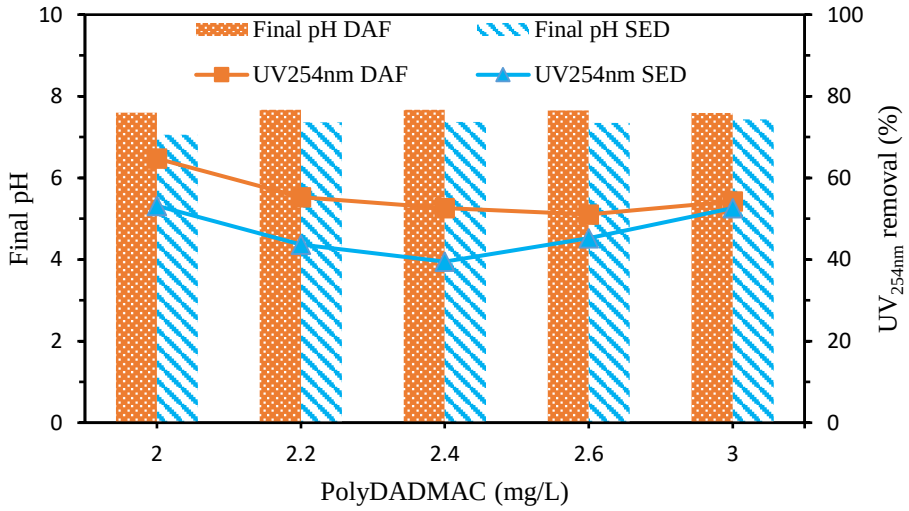

Figure 5-3: Comparative results from C/F/S and C/F/DAF experiments on UV_{254nm} percent removal and final pH value.

Generally, As (V) removal using both C/F/S and C/F/DAF is low with the highest removal percentage recoreded at 35.91 % at a coagulant dose of 2.2 mg/L polyDADMAC using the sedimentation process at pH 7.0. However, the flotation process showed a higher turbidity and UV_{254nm} removal than the sedimentation process for all the coagulant doses (2.0 mg/L – 3.0 mg/L) with the exception of coagulant dose at 3.0 mg/L where sedimentation performs slightly better than the flotation process.

5.3.1.2 Effect of pH

To determine the optimum pH value for polyDADMAC, a fixed coagulant dose of 2.2 mg/L was used. The pH range of 4 – 9 was used throughout this experiment.

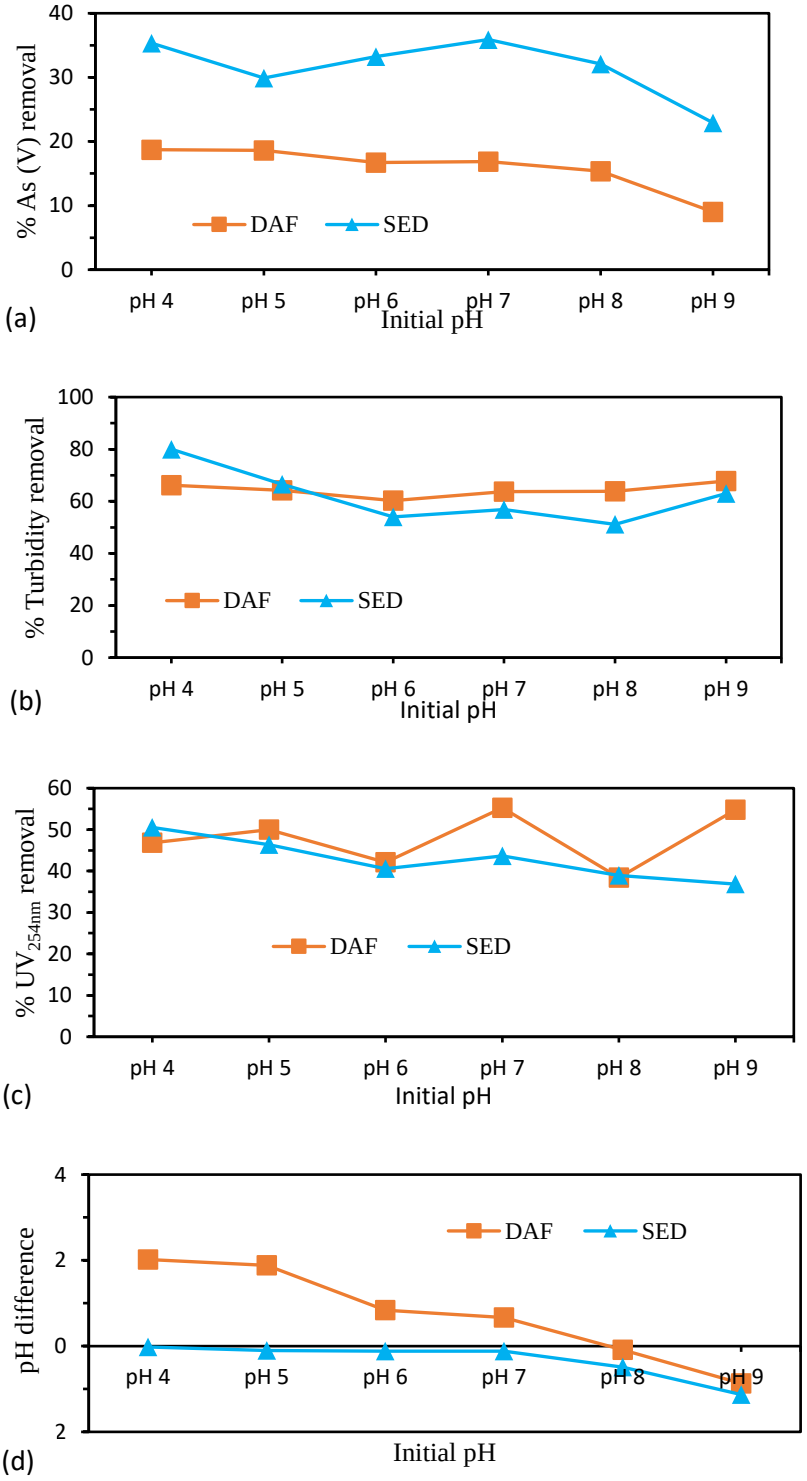

Figure 5-4: Effect of pH on (a) As (V) removal, (b) turbidity removal (c) UV_{254nm} removal and (d) pH difference (coagulant dose = 2.2 mg/L).

It can be seen from Fig. 4a that the percentage removal of As (V) reduces from pH 4 (35.32 %) to pH 5 (29.91 %) and gradually increases to a maximum 35.91 % at pH 7 using a C/F/S process. In the C/F/DAF process, there is almost a gradual decrease in As (V) removal from pH 4 to pH 9 with the maximum removal percentage recorded at pH 5 (22.12 %). Across the pH range (4 – 9), C/F/S performs better than the C/F/DAF in removing As (V) from a contaminated water. The highest turbidity removal from Fig. 4b is 80.0 % at pH 4 in the C/F/S process while turbidity removal from the C/F/DAF process is lowest at pH 6 (60.27 %) and maximum at pH 9 (67.79 %).

UV_{254nm} removal showed a gradual reduction from pH 4 (50.52 %) to pH 9 (36.84 %) in the C/F/S process while a maximum UV_{254nm} removal in the C/F/DAF process occurred at pH 7 (55.26 %). A pH decrease was observed in the solution after adding polyDADMAC across all the pHs in the C/F/DAF with a high pH difference of 1.18 recorded at pH 9. In the C/F/DAF process, the final solution pH was higher than the initial pH from pH 4 – pH 7 and thereafter decreased to 0.87 at pH 9. The increase in pH in the C/F/DAF process can be attributed to the pH of water (pH = 7.3) used in the saturator.

5.3.2 Use of Chitosan from crab shell

5.3.2.1 Effect of Chitosan dose.

To find the optimum chitosan dose, different doses ranging from 0.2 – 1.0 mg/L were tested to remove As (V), turbidity and UV_{254nm} using a C/F/S and C/F/DAF process at pH 7.0. The effect of a chitosan dose on As (V) removal is presented in Fig. 5-5. When the chitosan dose was increased from 0.2 to 0.6 mg/L in the C/F/DAF process, there was little difference with an average removal efficiency of 47.83 % and with increase in dosage of 0.8 to 1.0 mg/L, As (V) removal decreased further to an average of 40.98 %. For the C/F/S process, there was an increase in As (V) removal from 31.48 5 to 39.50 % at coagulant dose of 0.2 mg/L to 0.6 mg/L respectively. At a coagulant dose of 0.8 mg/L and 1.0 mg/L, As (V) removal percentage reduces to 37.21 % and 37.38 % respectively. Turbidity removal increases from 47.52 % to 71.06 % with increase in coagulant dose from 0.2 mg/L to 0.8 mg/L using the C/F/S process but increasing the dose to 1.0 mg/L reduces turbidity removal to 64.69 %. Likewise, the same turbidity removal pattern was

observed in the C/F/DAF process with the highest removal turbidity recorded at 75.75 %.

Fig. 5-6 illustrates that UV_{254nm} removal increases as chitosan dosage is increased, and starts to decrease after reaching the optimum value at 0.6 mg/L. It is noted that the highest UV_{254nm} removal percentage at the optimum dose using C/F/S process is 43.68 %. For the C/F/DAF process, UV_{254nm} removal percentage follows the same pattern with the C/F/S process (Appendix 5B).

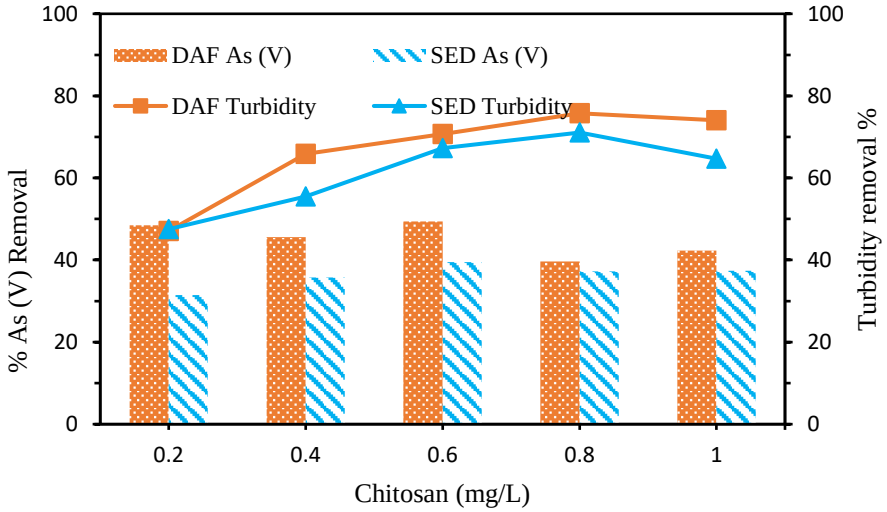

Figure 5-5: Comparative results of As (V) and turbidity removal from C/F/S and C/F/DAF experiments (initial pH = 7.0).

The highest UV_{254nm} removal was recorded at the optimal dose of 0.6 mg/L (50.53%). There is a gradual decrease in final pH from 5.5 (0.2 mg/L) to 4.4 (1.0 mg/L) using the C/F/S and a gradual decrease in final pH from 6.4 (0.2 mg/L) to 4.7 (1.0 mg/L) using the C/F/DAF process. The higher final pH recorded at C/F/DAF process might be due to the tap water (turbidity = 0.8 NTU, pH = 7.3) in the saturator during the flotation process. Likewise, the tap water might also be responsible for the higher UV_{254nm} and turbidity removal recorded at all the dosage levels considered in this study.

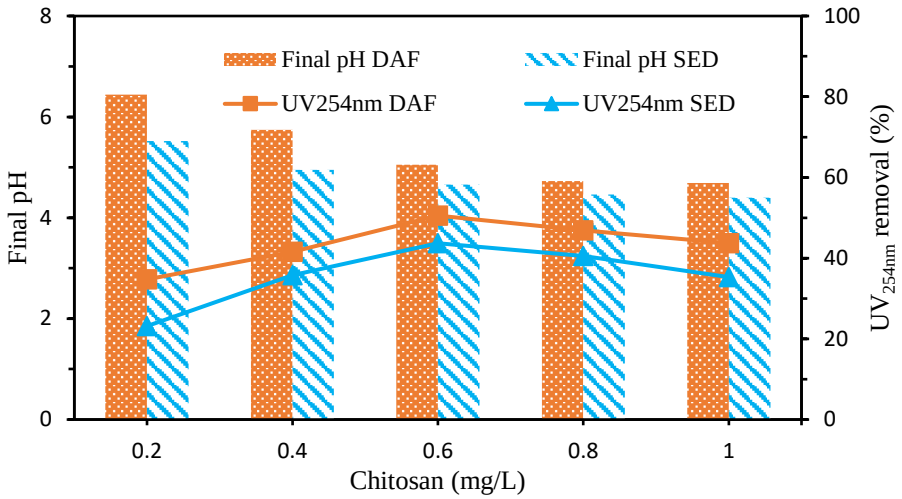

Figure 5-6: Comparative results from C/F/S and C/F/DAF experiments on UV_{254nm} percent removal and final pH value.

Overall, the C/F/DAF process performed better than the C/F/S process in As (V), turbidity and UV_{254nm} removal at all the coagulant dosage (0.2 – 1.0 mg/L). The maximum removal efficiency of As (V) was achieved at coagulant dose of 0.6 mg/L (49.43 %), turbidity removal at coagulant dose of 0.8 mg/L (75.75 %) and UV_{254nm} removal at coagulant dose of 0.6 mg/L (50.52%).

5.3.2.2 Effect of pH

To determine the optimum pH value for chitosan from crab shell, a pH range of 4 – 9 was evaluated at a fixed coagulant dose equivalent to 0.6 mg/L. Fig. 5-7a-c show the C/F/S and C/F/DAF performance (in terms of As (V), turbidity and UV_{254nm} removal) on the clarification of contaminated drinking water. Results showed that there is an increase in As (V) removal in the C/F/S process with increase in pH with the maximum removal rate obtained at pH 9 (39.34 %) whereas the maximum As (V) removal in the C/F/DAF process also is at pH 9 (53.15 %). Overall, the C/F/DAF process performed better at removing As (V) across pH 4 – pH 9 than C/F/S. There is little difference in turbidity removal across the pH considered in the C/F/DAF process as shown in Fig. 5-4b with the maximum turbidity removal observed at pH 9 (70.80 %). A similar pattern was observed in the C/F/S process with the highest turbidity observed at pH 9 (57.17 %). UV_{254nm} removal reduced from pH 4 (40.52 %) to pH 6 (36.84 %) and increased to 43.68 % at pH 7 where the maximum removal was recorded. The same pattern was observed using the C/F/S process although UV_{254nm} removal was less than the C/F/DAF process throughout the pH considered in this experiment.

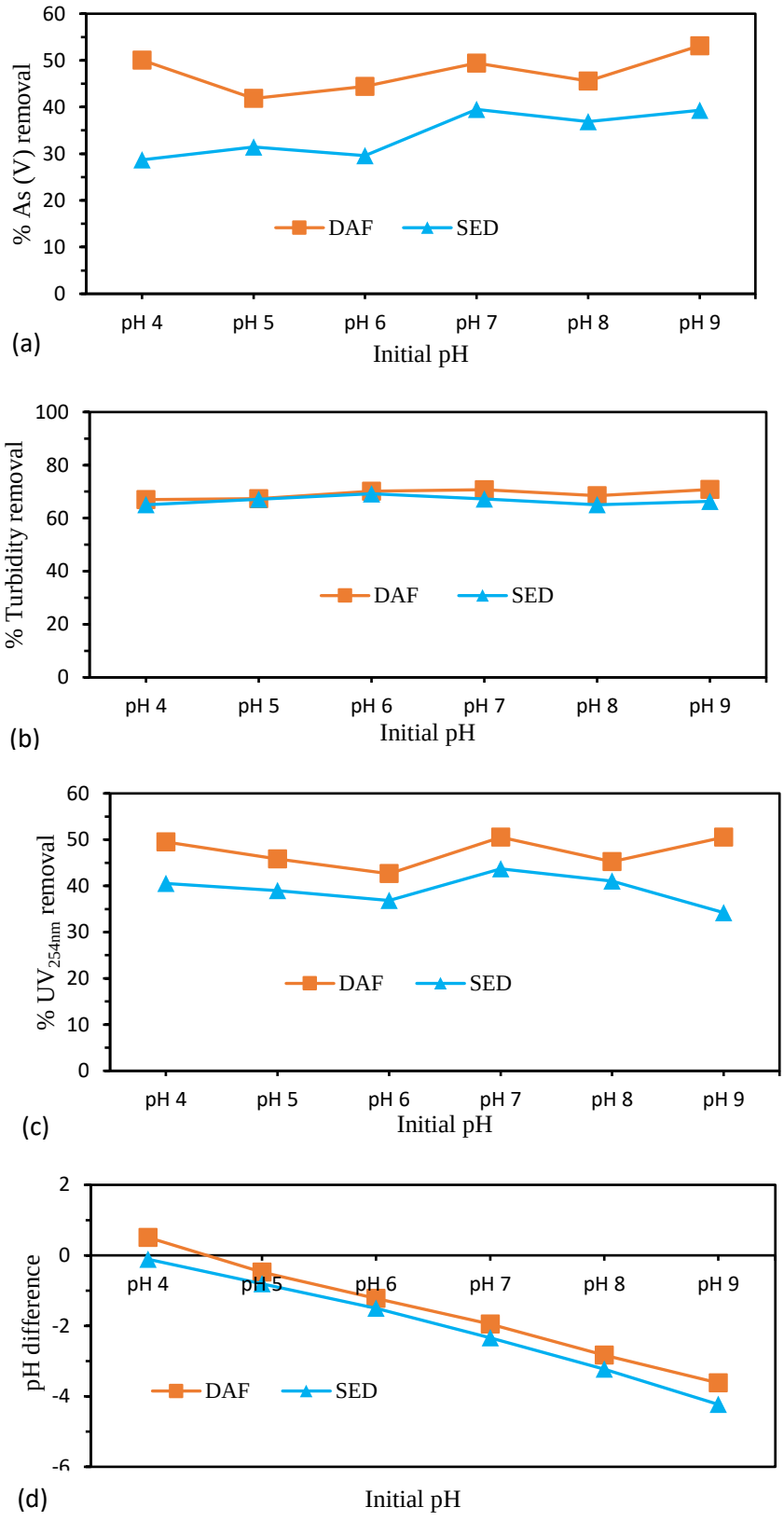

Figure 5-7: Effect of pH on (a) As (V) removal, (b) turbidity removal (c) UV_{254nm} removal and (d) final pH (coagulant dose = 0.6 mg/L)

From Fig. 5-4d, a drop in pH was observed in the solution after adding coagulant in the C/F/DAF process. As the pH increases, there is also a corresponding increase in the difference between the initial pH and the final pH of the solution in both C/F/DAF and C/F/S processes. The final pH shows that the solution is more acidic after using chitosan from crab shell as a coagulant.

5.4 Conclusions

This study compared the performance of C/F/S and C/F/DAF to remove As (V), turbidity and UV_{254nm} under different pH and coagulant doses. Two different coagulants namely polyDADMAC and chitosan from crab shell were used in both processes. The results showed that:

(1) Coagulation/flocculation/sedimentation (C/F/S) process using polyDADMAC (2.0 – 3.0 mg/L) and chitosan from crab shell (0.2 – 1 mg/L) achieved As (V) removal efficiencies of 35.91 % (2.2 mg/L) and 39.59 % (0.4 mg/L) respectively. Corresponding turbidity removal values were 73.36 % (3.0 mg/L) and 71.06 % (0.8 mg/L) respectively. Maximum UV_{254nm} removal using polyDADMAC and chitosan are 53.16 % (2.0 mg/L) and 43.68 % (0.6 mg/L) respectively.

(2) Coagulation/flocculation/dissolved air flotation (C/F/DAF) process showed that chitosan from crab shell removed higher As (V) (49.43 % at 0.6 mg/L) as compared to polyDADMAC (22.06 % at 2.4 mg/L). In addition, both coagulants showed high turbidity removal with polyDADMAC (71.68 % at 2.0 mg/L) and chitosan (75.75 % at 0.8 mg/L). Also, UV_{254nm} removal was 64.74 % using polyDADMAC and 50.53 % using chitosan from crab shell.

(3) The effect of pH using polyDADMAC showed that C/F/S performed better that C/F/DAF across the pH ranges (4 – 9) although the maximum As (V) removal is less than 40 %. Turbidity removal is highest at pH 4 using C/F/S process at 80.0 % whereas maximum UV_{254nm} removal was recorded at pH 7 (55.26 %) using C/F/DAF. The final pH in the C/F/S process is a little lower than the initial starting pH whereas for the C/F/DAF process, there was an increase in final pH value upto pH 7 and thereafter a decrease in final pH was observed.

(4) The effect of pH using chitosan showed a different performance to using polyDADMAC in terms of As (V) removal where C/F/DAF removes more As (V) across the pH than C/F/S. Turbidity removal was similar for both processes. With increase in pH, there is little improvement in turbidity removal. The difference in pH after chitosan addition showed a reduction in pH except for pH 4.

These results showed that neither polyDADMAC nor chitosan from crab shell is good in removing arsenic from a contaminated water. The two processes considered showed > 40 % arsenic removal efficiency. Both polyDADMAC and chitosan recorded high turbidity removal at all the pH investigated in this study and would find application in removing turbidity in contaminated water. One of the challenges of using chitosan is its inability to dissolve readily in water, which will make its application on a large-scale process complicated.

Conflict of interest

None

Appendix 5. Supplementary data

Contains supplementary data related to this Chapter

References

Affes, S., Aranaz, I., Hamdi, M., Acosta, N., Ghorbel-Bellaaj, O., Heras, Á., Nasri, M., Maalej, H., 2019. Preparation of a crude chitosanase from blue crab viscera as well as its application in the production of biologically active chito-oligosaccharides from shrimp shells chitosan. Int. J. Biol. Macromol. 139, 558–569. https://doi.org/10.1016/j.ijbiomac.2019.07.116

Amin, M.F.M., Heijman, S.G.J., Rietveld, L.C., 2014. The potential use of polymer flocculants for pharmaceuticals removal in wastewater treatment. Environ. Technol. Rev. 3, 61–70. https://doi.org/10.1080/21622515.2014.966784

Bolto, B., Gregory, J., 2007. Organic polyelectrolytes in water treatment. Water Res. 41, 2301–2324. https://doi.org/10.1016/j.watres.2007.03.012

Chiang, Z.-C., Yu, S.-H., Chao, A.-C., Dong, G.-C., 2012. Preparation and characterization of dexamethasone-immobilized chitosan scaffold. J. Biosci. Bioeng. 113, 654–660. https://doi.org/10.1016/j.jbiosc.2012.01.002

Chuah, L.H., Billa, N., Roberts, C.J., Burley, J.C., Manickam, S., 2013. Curcumin-containing chitosan nanoparticles as a potential mucoadhesive delivery system to the colon. Pharm. Dev. Technol. 18, 591–599. https://doi.org/10.3109/10837450.2011.640688

Dai, T., Tanaka, M., Huang, Y.-Y., Hamblin, M.R., 2011. Chitosan preparations for wounds and burns: antimicrobial and wound-healing effects. Expert Rev. Anti Infect. Ther. 9, 857–879. https://doi.org/10.1586/eri.11.59

Guibal, E., Saucedo, I., Jansson-Charrier, M., Delanghe, B., Le Cloirec, P., 1994. Uranium and vanadium sorption by chitosan and derivatives. Water Sci. Technol. 30, 183–190.

Huang, L., Bi, S., Pang, J., Sun, M., Feng, C., Chen, X., 2019. Preparation and characterization of chitosan from crab shell (Portunus trituberculatus) by NaOH/urea solution freeze-thaw pretreatment procedure. Int. J. Biol. Macromol. https://doi.org/10.1016/j.ijbiomac.2019.10.059

Ilangumaran, G., Stratton, G., Ravichandran, S., Shukla, P.S., Potin, P., Asiedu, S., Prithiviraj, B., 2017. Microbial Degradation of Lobster Shells to Extract Chitin Derivatives for Plant Disease Management. Front. Microbiol. 8. https://doi.org/10.3389/fmicb.2017.00781

Kleimann, J., Gehin-Delval, C., Auweter, H., Borkovec, M., 2005. Super-Stoichiometric Charge Neutralization in Particle−Polyelectrolyte Systems. Langmuir 21, 3688–3698. https://doi.org/10.1021/la046911u

Letterman, R.D., Pero, R.W., 1990. Contaminants in polyelectrolytes used in water treatment. J. Am. Water Works Assoc. 82, 87–97.

Logesh, A., Thillaimaharani, K., Sharmila, K., Kalaiselvam, M., Raffi, S., 2012. Production of chitosan from endolichenic fungi isolated from mangrove environment and its antagonistic activity. Asian Pac. J. Trop. Biomed. 2, 140–143. https://doi.org/10.1016/S2221-1691(11)60208-6

López-León, T., Carvalho, E.L.S., Seijo, B., Ortega-Vinuesa, J.L., Bastos-González, D., 2005. Physicochemical characterization of chitosan nanoparticles: electrokinetic and stability behavior. J. Colloid Interface Sci. 283, 344–351. https://doi.org/10.1016/j.jcis.2004.08.186

Mahvi, A.H., Razavi, M., 2005. Application of Polyelectrolyte in Turbidity Removal from Surface Water.

Majam, S., Jonnalagadda, S.B., Thompson, P., 2004. Development of analytical methods for organic polymer determination used in water treatment, in: Proceedings of Environmental Science and Technology. Presented at the Water Institute of South African (WISA) Biannual Conference, Cape Town, South Africa, pp. 62–67.

Manhokwe, S., Zvidzai, C., 2019. Post-treatment of yeast processing effluent from a bioreactor using aluminium chlorohydrate polydadmac as a coagulant. Sci. Afr. 6, e00125. https://doi.org/10.1016/j.sciaf.2019.e00125

Mohammed, M.H., Williams, P.A., Tverezovskaya, O., 2013. Extraction of chitin from prawn shells and conversion to low molecular mass chitosan. Food Hydrocoll. 31, 166–171. https://doi.org/10.1016/j.foodhyd.2012.10.021

Pirgalıoğlu, S., Özbelge, T.A., Özbelge, H.Ö., Bicak, N., 2015. Crosslinked polyDADMAC gels as highly selective and reusable arsenate binding materials. Chem. Eng. J. 262, 607–615. https://doi.org/10.1016/j.cej.2014.10.015

Pookrod, P., Haller, K.J., Scamehorn, J.F., 2004. Removal of Arsenic Anions from Water Using Polyelectrolyte-Enhanced Ultrafiltration. Sep. Sci. Technol. 39, 811–831.

Razali, M.A.A., Ahmad, Z., Ahmad, M.S.B., Ariffin, A., 2011. Treatment of pulp and paper mill wastewater with various molecular weight of polyDADMAC induced flocculation. Chem. Eng. J. 166, 529–535. https://doi.org/10.1016/j.cej.2010.11.011

Rivas, B.L., Aguirre, M. del C., Pereira, E., 2007. Cationic water-soluble polymers with the ability to remove arsenate through an ultrafiltration technique. J. Appl. Polym. Sci. 106, 89–94. https://doi.org/10.1002/app.26499

Rivas, B.L., Pereira, E.D., Moreno-Villoslada, I., 2003. Water-soluble polymer–metal ion interactions. Prog. Polym. Sci. 28, 173–208. https://doi.org/10.1016/S0079-6700(02)00028-X

Rivas, B.L., Sánchez, J., Pooley, S.A., Basaez, L., Pereira, E., Bucher, C., Royal, G., Aman, E.S., Moutet, J.-C., 2010. Water-Soluble Polyelectrolytes with Ability to Remove Arsenic. Macromol. Symp. 296, 416–428. https://doi.org/10.1002/masy.201051057

Samrot, A.V., Burman, U., Philip, S.A., N, S., Chandrasekaran, K., 2018. Synthesis of curcumin loaded polymeric nanoparticles from crab shell derived chitosan for drug delivery. Inform. Med. Unlocked 10, 159–182. https://doi.org/10.1016/j.imu.2017.12.010

Sheng, P.X., Ting, Y.-P., Chen, J.P., Hong, L., 2004. Sorption of lead, copper, cadmium, zinc, and nickel by marine algal biomass: characterization of biosorptive capacity and investigation of mechanisms. J. Colloid Interface Sci. 275, 131–141. https://doi.org/10.1016/j.jcis.2004.01.036

Teli, M.D., Sheikh, J., 2012. Extraction of chitosan from shrimp shells waste and application in antibacterial finishing of bamboo rayon. Int. J. Biol. Macromol. 50, 1195–1200. https://doi.org/10.1016/j.ijbiomac.2012.04.003

Yee, J.-J., Arida, C.V.J., Futalan, C.M., de Luna, M.D.G., Wan, M.-W., 2019. Treatment of Contaminated Groundwater via Arsenate Removal Using Chitosan-Coated Bentonite. Molecules 24. https://doi.org/10.3390/molecules24132464

Zahrim, A.Y., Tizaoui, C., Hilal, N., 2011. Coagulation with polymers for nanofiltration pre-treatment of highly concentrated dyes: A review. Desalination 266, 1–16. https://doi.org/10.1016/j.desal.2010.08.012

Zamani, A., Edebo, L., Sjöström, B., Taherzadeh, M.J., 2007. Extraction and Precipitation of Chitosan from Cell Wall of Zygomycetes Fungi by Dilute Sulfuric Acid. Biomacromolecules 8, 3786–3790. https://doi.org/10.1021/bm700701w

CHAPTER SIX

Effect of competing anions on arsenate removal from a contaminated water using batch dissolved air flotation

Content to be submitted to

Separation and Purification Technology Journal

Abstract

Arsenic compounds are carcinogenic to humans and are typically removed from contaminated water through various conventional treatment technologies such as adsorption, coagulation/flocculation and ion exchange Flotation technology is a solid-liquid separation technique originating from the field of mineral processing and it has found wide applications, particularly in industrial wastewater treatment. Ionic composition plays an important role in arsenic removal efficiency. The effects of sulfate (SO_4^{2-}), phosphate ($H_2PO_4^-$), nitrate (NO_3^-) and carbonate (CO_3^{2-}) on removing arsenate from contaminated water was evaluated using batch coagulation/flocculation/dissolved air flotation (C/F/DAF) with polyaluminium chloride (PAC) used as coagulant. The batch process was carried out at three competing ion concentrations levels (1, 5 and 10 mM), in the pH range of 5 – 9, and at a saturated pressure of 4 bar. The flotation process showed that using 10 mM of phosphate anions at pH 6 resulted in removals 78.94 % turbidity, 76.36 % UV_{254nm}, and 5.42 % As (V). Arsenate removal was inhibited by the four anions with phosphate ion exerting the maximum inhibition among the anions at each pH level. Overall, the inhibitory effect of added ions on arsenate removal using a batch coagulation/flocculation/dissolved air flotation (C/F/DAF) process was in the sequence of $H_2PO_4^- > CO_3^{2-} > NO_3^- > SO_4^{2-}$.

Keywords

Arsenate, competing anions, coagulation and flocculation, dissolved air flotation (DAF)

6.1 Introduction

Arsenic contamination of drinking water has become a major environmental problem in the 21st century due to its high toxicity to animals, humans and plants and can exist in four valency states:-3, 0, +3 and +5 (Mohan and Pittman Jr., 2007). Contamination of drinking water by arsenic has been reported in several countries (USA, China, India, Pakistan, Vietnam, Bangladesh, Argentina, Canada, Taiwan) and over the last decades, there has been an increase in the number of studies investigating the removal of arsenic from drinking water due to the health challenge it poses to the ecosystem (Chaudhry et al., 2017; Manna and Ghosh, 2007; Podder and Majumder, 2016). Long-term exposure to arsenic in drinking water can cause several diseases such as hypertension, keratosis, cancer of the liver, brain, kidney and stomach (Chammui et al., 2014; Saha et al., 1999; Smith A H et al., 1992). Arsenic in surface and groundwater originates from anthropogenic activities such as smelting of metal ores, petroleum refining, gold mining, combustion of fossil fuel and herbicide and pesticide application (Lee et al., 2017; Mandal et al., 2013; Mondal et al., 2006) as well as through natural processes such as natural weathering processes, biological and geothermal activities (Biswas et al., 2008; Podder and Majumder, 2018). In natural water, arsenic usually occurs in inorganic form as arsenite (As (III)) and arsenate (As (V)) with arsenite 20 to 60 times more toxic than arsenate in the environment (Podder and Majumder, 2018; Sigdel et al., 2016). The dominant species in reducing anaerobic environments is As (III) while As (V) is found to be more abundant in surface water (Roghani et al., 2016). Also As (III) can be converted to As (V) by oxygen, permanganate, hypochlorite and ozone (Kofa et al., 2015). World health organization (WHO), United States environmental protection agency (USEPA) and Drinking water standards for New Zealand (DWSNZ 2005 (revised 2008)) have set the maximum contamination level (MCL) or maximum acceptable level (MAC) at 10 µg/L for arsenic in drinking water due to the severe impacts on people`s health (DWSNZ, 2008; U.S.EPA, 2016; WHO, 2011).

Several conventional methods used to remove arsenic from drinking water include precipitation, adsorption, ion exchange, membranes, filtration and flotation (Choong et al., 2007; Litter et al., 2010; Villaescusa and Bollinger, 2008). In choosing a treatment technique for arsenic removal, some factors considered

include treatment cost, operational complexity of technology, skills required in operating the treatment technology, arsenic speciation, volume to be treated, hardness and the presence of other chemical species (such as silica, phosphate, nitrate, sulfate, carbonate, chloride and iron) (Çiftçi and Henden, 2015; Hernández-Flores et al., 2018; Hua, 2018). Coagulation/flocculation is one of the most practised technologies in achieving an efficient solid-liquid separation in water treatment and it is widely employed in many industries such as pulp and paper production, food, tannery, pharmaceutical, cosmetics, oil extraction and mining (Ahmad et al., 2008; Roussy et al., 2005; Sher et al., 2013; Yang et al., 2016). The efficiency of the coagulation/flocculation process depends largely on the selected coagulants/flocculants, dosage, pH value, temperature and ionic strength (Domínguez et al., 2007; Sher et al., 2013; Wei et al., 2018). Coagulation/flocculation as one of the methods used for arsenic removal involves three main mechanisms namely (a) adsorption involving the formulation of surface complexes between soluble arsenic and active sites of formed hydroxides; (b) co-precipitation with incorporation of soluble arsenic species into a growing hydroxide phase by inclusion and (c) precipitation and formation of insoluble compounds (Pallier et al., 2010).

Flotation technology has been used for a long time in ore processing and has found application in removing heavy metals from a liquid phase using bubble attachment originating from mineral processing (Fu and Wang, 2011). There are different types of flotation in which metal ions can be removed from solution: dissolved air flotation (DAF), ion flotation, electrolytic flotation and precipitate flotation. Flotation methods rely on factors such as wetting characteristics and surface properties to separate particles from solution (Al-Zoubi et al., 2015). DAF is a well-known technology which has been used for decades in many solid-liquid separation processes. It has found application in water treatment and in recent years, it has been used to efficiently remove pollutants such as microorganisms, proteins, bacteria, viruses, oil and heavy metals (Amaral Filho et al., 2016; Edzwald, 2010; Karhu et al., 2014; Teixeira and Rosa, 2007). The DAF process also has some advantages/disadvantages as compared to the conventional sedimentation process. Some of the advantages are high loading rate, shorter hydraulic retention time, smaller flocculation tank and high metal selectivity. However, the disadvantages

are that DAF processes have high maintenance and operation costs and is not suitable for raw water with high-density suspended solids (Edzwald, 2010; Fu and Wang, 2011; Ihsanullah et al., 2016; Kurniawan et al., 2006).

The DAF process uses a variety of coagulants which are mostly inorganic salts such as aluminium based products (aluminium sulfate (alum), polyaluminium chloride, polyaluminium sulfate, aluminium chlorohydrate), ferric chloride, ferrous sulfate and ferric chlorosulfate. Other types of coagulants used are organic polymers such as polyamines, polyvinylamides, polyacrylamides and poly diallyl-dimethyammonium chloride (PolyDADMAC) (Ghafari et al., 2010; Miranda et al., 2013). Polyaluminum chloride (PAC), a pre-hydrolysed coagulant is becoming increasingly popular in water and wastewater treatment due to the advantages it has over conventional hydrolysed aluminium or iron salt. The advantages are better performance at low temperature, low sludge volume, little effect on the pH of the water, less residual aluminium and more rapid flocculation (Aguilar et al., 2002; Duan and Gregory, 2003; Van Benschoten and Edzwald, 1990; Wei et al., 2015; Yang et al., 2011; Yu et al., 2007). The following steps are involved in removing arsenic from solution: (i) deprotonation of the aluminium clusters during coagulation, (ii) adsorption of arsenic to the coagulant by inner-sphere and outer-sphere complexation (iii) formation of flocs and (iv) formation of precipitates resulting from the formation of amorphous solid (Mertens et al., 2012).

Several studies have looked into the effect of competing ions on arsenic adsorption onto Maghemite (Tuutijärvi et al., 2012), iron and aluminium oxides (Youngran et al., 2007a), zerovalent iron (Su and Puls, 2001) and goethite (Deng et al., 2018). Most of the competing ligands in natural waters are in the form of organic anions: nitrate, silicate, sulfate, bicarbonate and phosphate. These anions are known to compete with arsenic for adsorption sites and the results are also influenced by solution pH, anion concentrations and intrinsic binding affinities (Guan et al., 2009).

The drinking water industry is faced with more stringent regulations nowadays, not only in providing quality drinking water but also in producing a sludge that can find application in agriculture with low concentration of arsenic in the biosolids. The aim of this research is to investigate the effect of pH, added anionic species (nitrate, carbonate, sulfate and phosphate) and ionic strength to remove arsenate from a

contaminated drinking water using a batch C/F/DAF process. PAC was used as the coagulant and the performance of the process was compared through achieved removal of turbidity, arsenic, UV_{254nm} and final pH.

6.2 Materials and methods

6.2.1 Water sample

The experimental water sample was collected from Oranga Lake (one of three lakes located on the University of Waikato Hamilton, New Zealand campus) with an area of 0.69 ha and a maximum depth of 0.6 m. The contaminated water was spiked with As (V) prior to the experiments. Table 6-1 shows the average composition of the spiked contaminated water used in the experiment.

Table 6-1: Characteristics of water sample

pH	6.78
DO (mg/L)	6.33 (±0.03)
Turbidity (NTU)	16.1 (±2.1)
Spiked As (V) (µg/L)	23.5 (±0.08)
UV_{254nm} (cm^{-1})	0.313 (±0.002)
Temperature (^oC)	14.7 (±0.8)
Zeta potential (µS/cm)	130.6 (±0.8)
Alkalinity (mg/L $CaCO_3$)	105 (±3.0)
Nitrate (mg/L N)	0.017 (±0.02)
Phosphate (mg/L PO_4)	0.44 (±0.04)

6.2.2 Chemicals

All chemicals used were analytical grade, unless stated otherwise. All standard solutions were prepared by dilution with distilled water. Coagulant PAC used was a commercially available product purchased from IXOM Operations Pty Ltd, Melbourne, Australia (23.5 % w/w as Al_2O_3, Basicity of 83 % w/w, specific gravity (SG) = 1.34, pH =3.5 and Freezing point of < 0 ^oC). Sodium nitrate ($NaNO_3$), sodium sulfate (Na_2SO_4), sodium carbonate (Na_2CO_3) and sodium dihydrogen phosphate (NaH_2PO_4) were purchased from Sigma Aldrich (New Zealand). Other

chemicals used are arsenic (V) oxide hydrate (As_2O_5, 99%) concentrated nitric acid (HNO_3, 70 % Merck KGaA, Darmstadt, Germany), hydrochloric acid (HCl, 36-38% Merck KGaA, Darmstadt, Germany) and sodium hydroxide (NaOH Merck KGaA, Darmstadt, Germany).

6.2.3 Experimental procedure

The experimental procedure for the batch C/F/DAF test was performed at room temperature (25 ± 2 ^oC) as illustrated in Fig. 6-1. A jar test was performed with the conventional jar apparatus (Boltac Industries, New Zealand) using 23.5 mg/L PAC from the prepared stock solution (0.235 g/L). The pH of the sample water was adjusted using 0.1M HCl and 0.1M NaOH solutions before addition of competing anions. Three concentrations (1, 5 and 10 mM) of competing anions ($H_2PO_4^-$, CO_3^{2-}, NO_3^- and SO_4^{2-}) were added to the sample water before addition of PAC. The Coagulation/flocculation process consisted of 3 minutes rapid mix (100 revolutions per minutes (rpm)) followed by slow mixing for 10 min (30 rpm). This was followed by 10 min flotation period by adding 20 % of tap water (with pH 7.2 and turbidity of 0.8 NTU) to a well-designed saturator as shown in Fig 6.2. Industrial grade air was used to pressure the saturator to 4 bar which was the pressure used throughout this experiment. Experiments were conducted in duplicate and for computing the removal of all parameters in the clarified water, removal (%) = [(1 – C_f /C_i)] X 100 was used where C_f and C_i are the final and initial concentrations.

6.2.4 Analytical techniques

Samples were analysed for pH, turbidity, UV_{254nm} and As (V) concentration. As (V) analysis was done using inductive coupled plasma mass spectrometry (ICP-MS) after sample filtration on a 0.45 µm membrane filter and addition of 200 µl of HNO_3 to 10 mL of filtered sample. Quality control employed for ICP-MS measurements are shown in APPENDIX 2BA. A pH meter (Eutech pH150/temperature meter) was used to measure the pH of solutions before and after addition of coagulation and competing anions during the batch DAF process. The pH meter was calibrated prior to use using 4.01, 7.01 and 10.04 pH buffers (Merck KGaA, Darmstadt, Germany). Turbidity was measured using a turbidimeter (HACH 2100P turbidimeter) and UV_{254nm} was measured using a PharmaSpec UV 1700 Spectrophotometer (SHIMADZU). A HACH 2100P turbidimeter was used to measure turbidity. The meter was calibrated with 10, 20 and 100 NTU turbidity

standards (HACH Turbidity Standard kit model 2100P) before use. Other instruments used are Eutech instrument CyberScan DO 300 and Eutech instrument CyberScan 100 to measure dissolved oxygen (DO) and conductivity respectively. The concentrations of NO_3, PO_4 and alkalinity were measured using a Palintest photometer 7100.

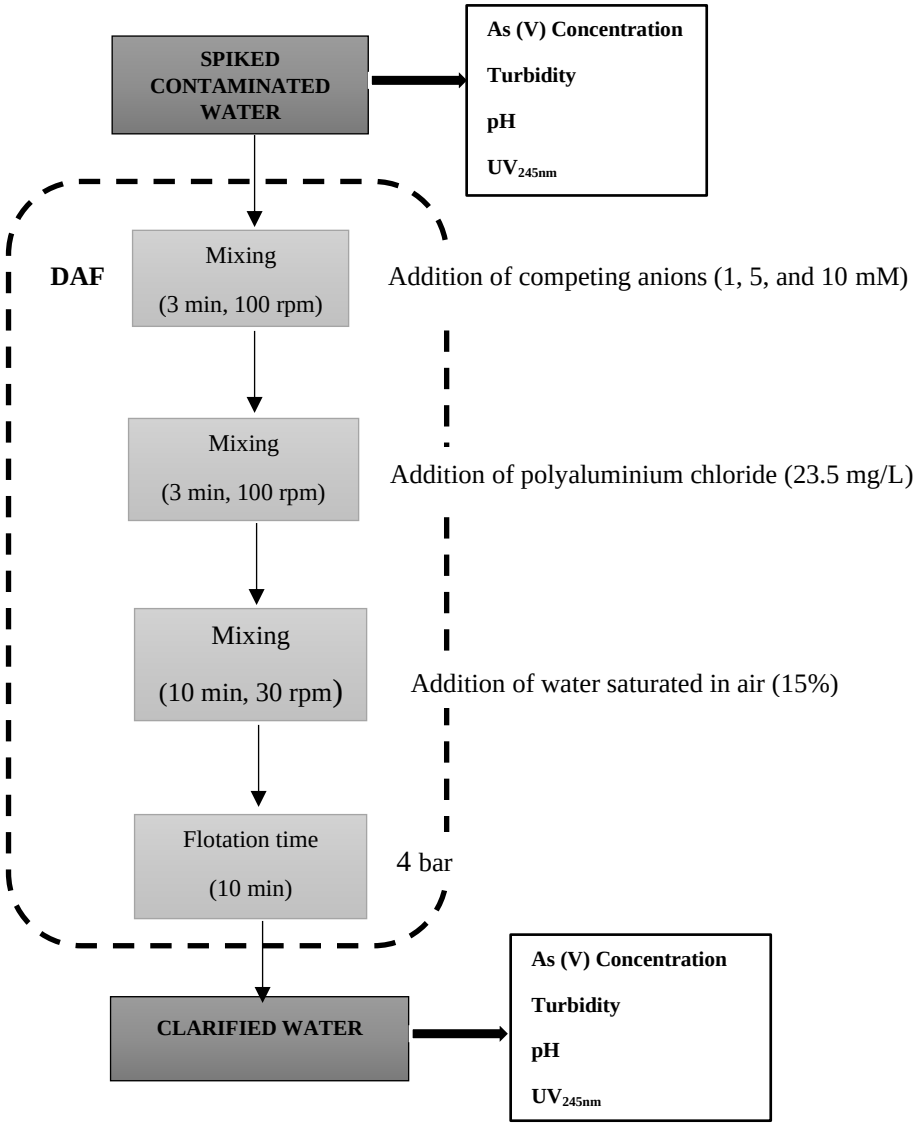

Figure 6-1: Experimental procedure to evaluate As (V) removal from other contaminants by batch dissolved air flotation.

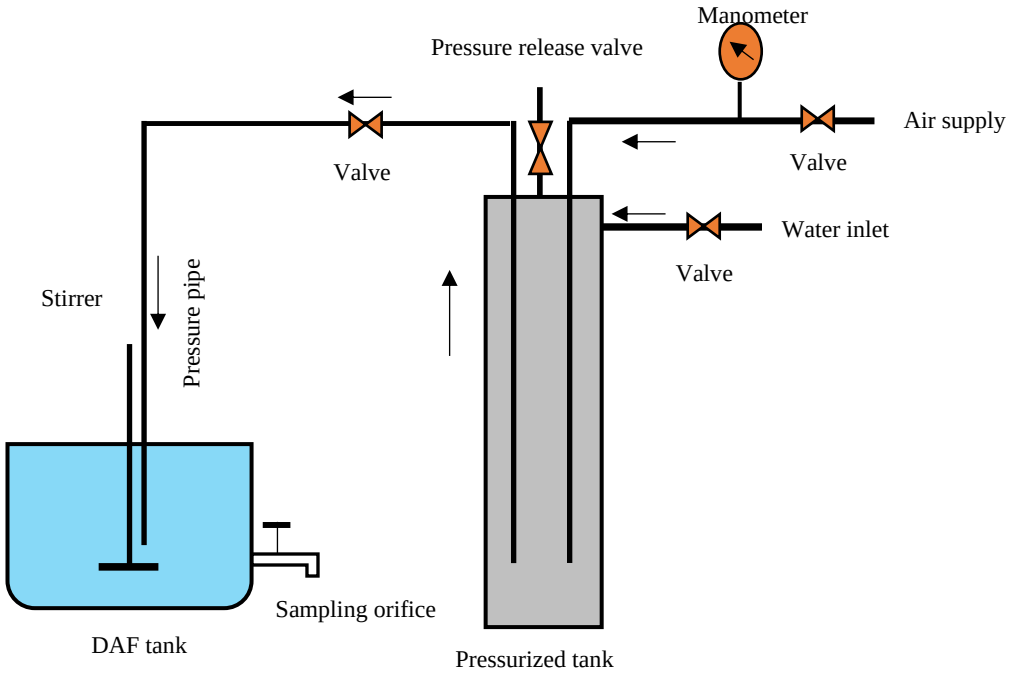

Figure 6-2: Schematic diagram of a batch dissolved air flotation apparatus.

6.3 Results and discussion

6.3.1 Effect of initial pH

In order to evaluate As (V) removal using coagulation/flocculation/DAF process, different pH values ranging from 5 – 9 were investigated using PAC as the coagulant and a DAF saturation pressure of 4 bar. As (V) is known to exist in solution as $H_3AsO_4^0$ (pH $0-2$), $H_2AsO_4^-$ (pH 3-6), $HAsO_4^{2-}$ (7-11) and AsO_4^{3-} (12-14). The pH of the solution has a strong influence on As (V) adsorption (Asmel et al., 2017; Chammui et al., 2014) and is a major parameter steering As (V) deprotonation state and the formation of aggregate polynuclear Al species in PAC (Mertens et al., 2012). Fig. 4-3 shows that As (V) removal was not dependent on pH with the maximum As (V) removal of 96.31 % occurring at pH 6. A similar result was reported by Hu. et al. on arsenic removal during coagulation (Hu et al., 2012). High As (V) removal efficiency resulted from the precipitation of As (V) and aluminium complexes thereby forming a covalent binding due to ligand-exchange reactions (Mertens et al., 2012). The percentage removal efficiency of turbidity follows the same pattern as UV_{254nm}. The lowest turbidity and UV_{254nm} removal percentage was found to be 7.45 % and 32.27 % respectively at pH 6. After

pH 6, there was an increase in turbidity and UV_{254nm} removal with the maximum turbidity and UV_{254nm} removal efficiencies at 90.43 and 86.26 % respectively at pH 9. The final pH value after the addition of coagulant shows a reduction in pH value except for pH 6 which shows no difference in final pH value. The final pH might have been influenced by the addition of 20 % saturated tap water (pH 7.2) which was used in the batched DAF process.

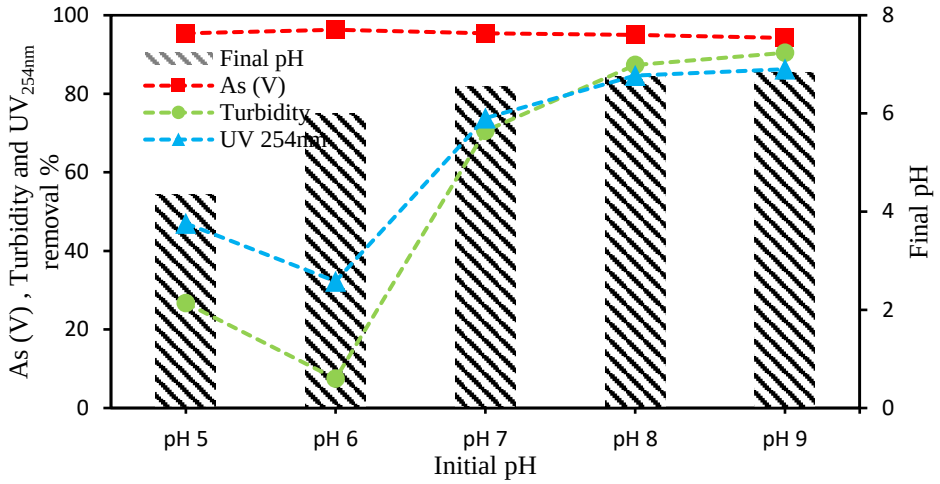

Figure 6-3: The final pH and percentage removal of As (V), turbidity and UV_{254nm} using PAC as coagulant at different pH (5-9) in a C/F/DAF process.

6.3.2 Effect of sulfate ions

The results in Fig. 6-4 (a-c) shows the effect of SO_4^{2-} on As (V), turbidity and UV_{254nm} removal in a contaminated water in a batch C/F/DAF process. Sulfate is one of the major competing anions known to affect the adsorption of arsenic in many surface waters. This study was carried out over a wide pH range of 5 – 9 (Appendix 6A). The results show that SO_4^{2-} addition affected As (V) removal across the pH levels and concentration levels considered in this study although a slight interference was observed at pH 6. The maximum effect was observed at pH 9 when addition of 1 mM of SO_4^{2-} anion showed a 12.25 % reduction in As (V) removal. It was also observed that there was no major difference in As (V) removal at the different SO_4^{2-} concentration levels (1, 5 and 10 mM) over the pH range considered in this study. The low effect on As (V) removal could be a result of weaker SO_4^{2-} binding affinity for PAC than As (V). Guan et al. (2009) showed that the presence of sulfate had a negligible effect in As (III) removal in the $KMnO_4$-Fe (II) process at pH 4 - 5 and was further decreased by 6.50 – 36.0 % over pH 6 – 9 by the presence of 50 -100 mg/L SO_4^{2-} (Guan et al., 2009). Other studies have shown that SO_4^{2-} has

a negligible effect on As (V) removal over a wide pH range (Meng et al., 2000; Tuutijärvi et al., 2012; Youngran et al., 2007a).

As shown in Fig 6-4c, addition of SO_4^{2-} anions showed an increase in turbidity removal from pH 5 – pH 6 where the maximum turbidity removal was 87.85 % at SO_4^{2-} concentration of 1 mM. The turbidity removal percentage flattens out from pH 6 – pH 9 and a reduction in turbidity removal was observed from 90.43 % (without anions) to 86.02 %, 85.96 % and 85.90 % at 1 mM, 5 mM and 10 mM respectively. The percentage of UV_{254nm} removal shows the same removal pattern as turbidity. Addition of SO_4^{2-} also resulted in reduction in UV_{254nm} removal from 86.26 % (without anion) to 80.19 % at pH 9. The final pH after SO_4^{2-} addition at concentration levels 5 and 10 mM shows no major changes from pH 5 – pH 9. However, the final pH at ionic strength 1, 5 and 10 mM shows an increase from 4.34 (after coagulant addition) to 5.60, 5.70 and 5.72 at SO_4^{2-} concentration levels 1, 5 and 10 mM respectively. From Fig. 6-4d, final pH at SO_4^{2-} concentration level 1 mM showed a drop from pH 5 – pH 6 and thereafter an increase from 4.50 (initial pH 6) to 7.07 (initial pH 9).

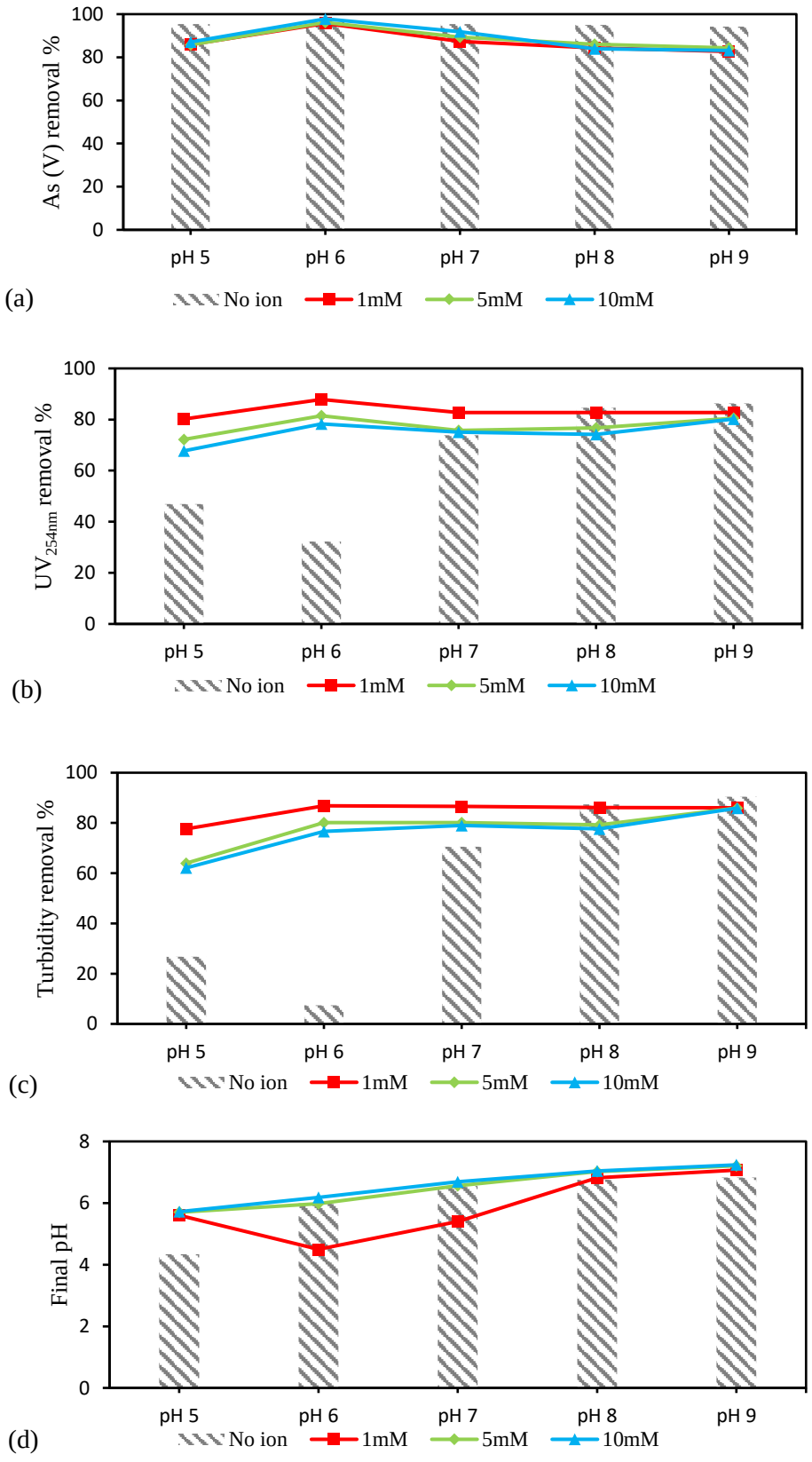

Figure 6-4: The effect of Sulfate (as SO_4^{2-}) on (a) As (V) removal (b) turbidity removal (c) UV_{254nm} removal (d) final pH.

No ion = No anion added.

6.3.3 Effect of nitrate ions

The results shown in Fig. 6-5a illustrate the effect of NO_3^- on As (V) removal by the batch C/F/DAF process. Nitrate showed an insignificant influence on As (V) removal similar to the effect of SO_4^{2-} on As (V) removal. Tuutijarvi et al. (2012) indicated that nitrate (0 – 226 mg/L as NO_3^-N) had an insignificant influence on arsenate adsorption onto Maghemite nanoparticles. This was attributed to the fact that NO_3^- absorbs due to outer-sphere complexation and As (V) adsorbs due to inner sphere complexation, thus nitrate would not compete directly with As (V) for the adsorption sites. Other results showed that there is no or little effect of NO_3^- on adsorption of As (V) using iron and aluminium oxide (Youngran et al., 2007a), functionalized magnetic adsorbent material (Bringas et al., 2015) and Fe^{3+} coordinated to amino-functionalized MCM-41 (Yokoi et al., 2004). The maximum As (V) removal after NO_3^- addition was 83.13 % at 5 mM concentration whereas 94.22 % removal was achieved without addition of the NO_3^- anion. Removal of UV_{254nm} and turbidity as shown in Fig. 6-5 (b & c) shows a similar pattern. There was an improvement in both turbidity and UV_{254nm} removal from pH 5 to pH 9 with a nitrate concentration of 5 and 10 mM. Turbidity removal at pH 8 and pH 9 with addition of 1mM, 5 mM and 10 mM concentrations of NO_3^- anion makes no difference with no NO_3^- addition. The maximum turbidity removal was recorded at pH 9 (90.93 %) by adding 1 mM NO_3^-. Addition of 10 mM of NO_3^- however have a slight effect on UV_{254nm} removal with a removal percentage of 77.64 % as against 86.26 % without nitrate addition. Nitrate addition has a negligible effect on the final pH (Fig. 6-5d).

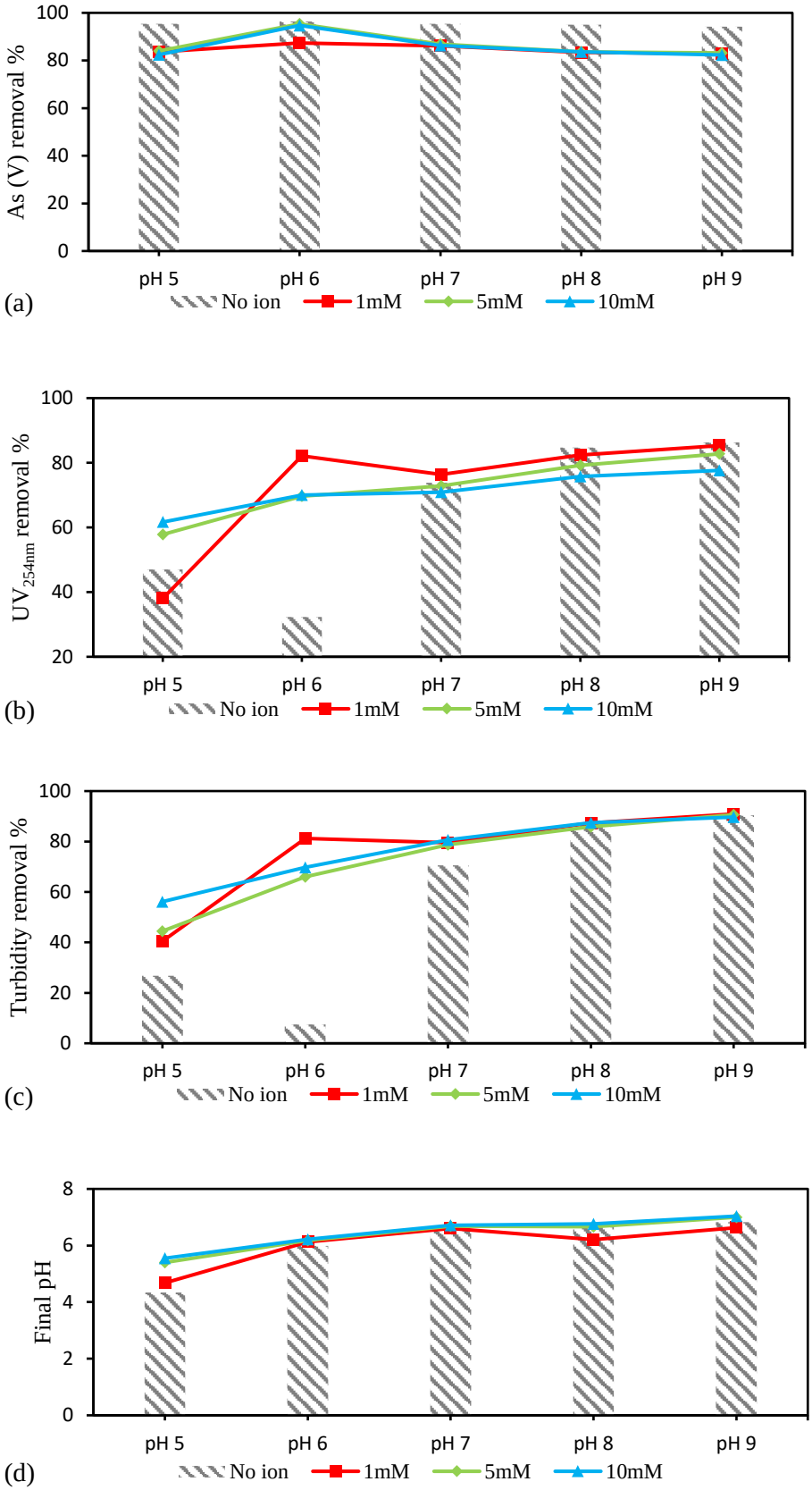

Figure 6-5: The effect of Nitrate (as NO_3^-) on (a) As (V) removal (b) turbidity removal (c) UV_{254nm} removal (d) final pH.

6.3.4 Effect of carbonate ions

It was observed in Fig 6-6a that the removal As (V) via a batch C/F/DAF process was affected by the addition of CO_3^{2-} under all pH and ionic strengths considered in this study with CO_3^{2-} concentrations 1 and 5 mM exerting the most influence. 1 mM CO_3^{2-} addition at pH 5 reduced As (V) removal by 38.00 % compared to when CO_3^{2-} was not added at 95.44 %. As seen from Fig. 6-6a carbonate addition can be seen to significantly affect As (V) removal across all the pH and CO_3^{2-} concentrations with 10 mM CO_3^{2-} exerting the most effect on As (V) removal (29.78 %) at pH 7. Bringas et al. (2015) observed that arsenic adsorption at low values of molar ratio (CO_3^{2-}/As (V) < 12) was not affected by the presence of CO_3^{2-} but when the molar ratio was increased above 20,000, 78 % removal reduction was observed. Kanematsu et al. (2013) also observed that As (V) adsorption onto goethite was not affected by the presence of carbonate (As (V) ~ 1.3 µM, CO_3^{2-} ~ 10 mM). However, Meng et al. (2000) showed that CO_3^{2-} had a slight effect on As (V) removal by coprecipitation of ferric chloride in the pH range 4 – 9.5.

From Fig. 6-6 (b & c), turbidity and UV_{254nm} removal follow the same pattern with a higher removal observed at pH 5 and 6 with the addition of CO_3^{2-} (1, 5 and 10 mM). The addition of CO_3^{2-} however reduces turbidity and UV_{254nm} removal at pH 8 and pH 9. An increase in final pH was observed with the addition of CO_3^{2-} at different concentration levels. Little difference was observed in final pH at CO_3^{2-} concentrations 5 and 10 mM which might be responsible for the similar As (V) removal at all pH levels considered in this study. Frau et al. (2010) suggest that an increase in pH as a result of increase in CO_3^{2-} concentration might be responsible for an increase in surface charge of adsorbent, thus reduced As (V) removal.

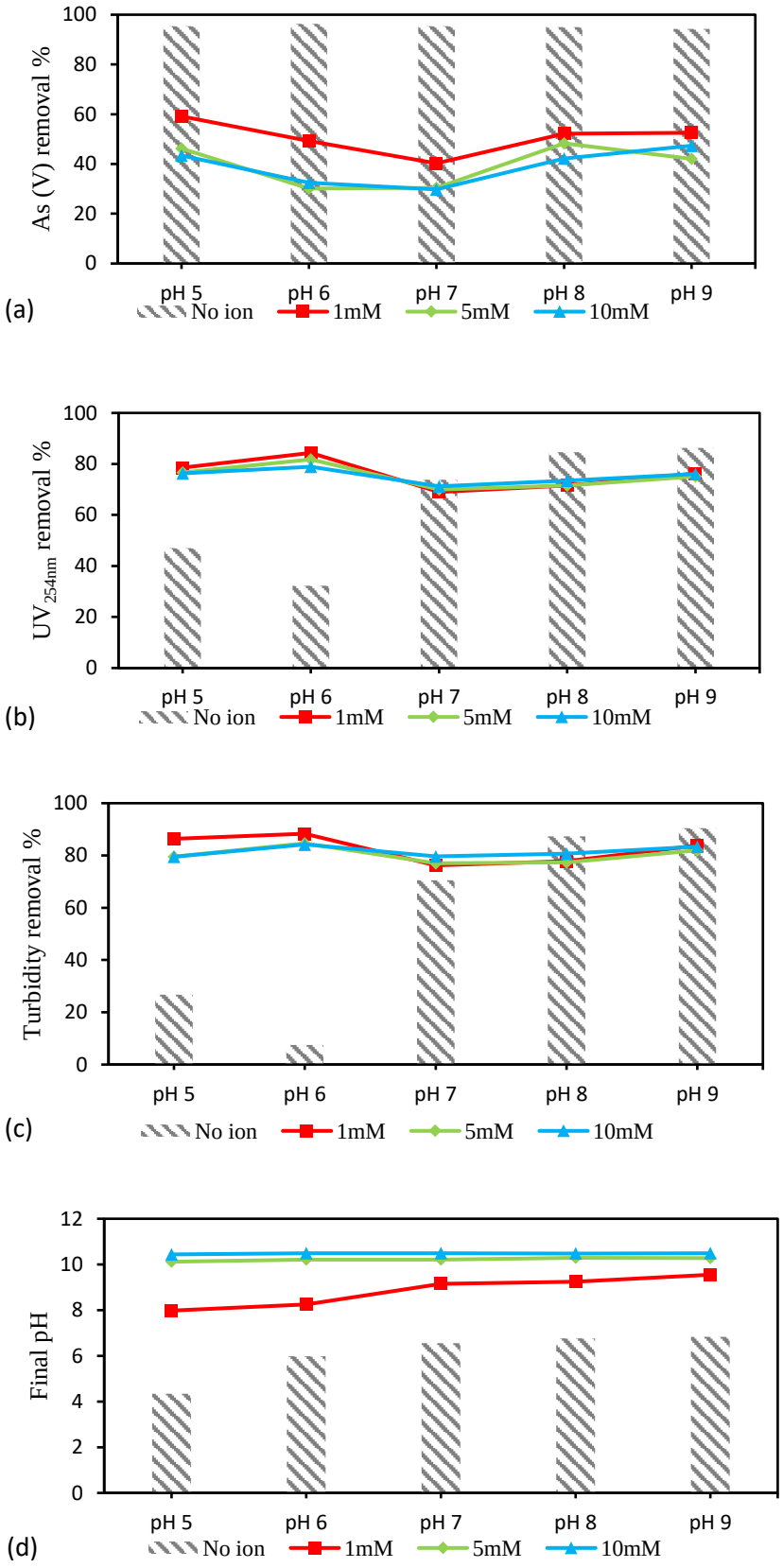

Figure 6-6: The effect of carbonate (as CO_3^{2-}) on (a) As (V) removal (b) turbidity removal (c) UV_{254nm} removal (d) final pH.

6.3.5 Effect of phosphate ions

Phosphate can exist in an aqueous solution depending on pH. This includes dihydrogen phosphate ($H_2PO_4^-$), hydrogen phosphate ion (HPO_4^{2-}), phosphate ion (PO_4^{3-}) and aqueous phosphoric acid (H_3PO_4). From Fig. 6-7a it can be seen that $H_2PO_4^-$ is more prevalent in a weak acid condition, H_3PO_4 ions in a strong acid condition whereas $HPO_4^{2-}$and PO_4^{3-} ions are predominant in the weak and strong basic conditions (Youngran et al., 2007a).

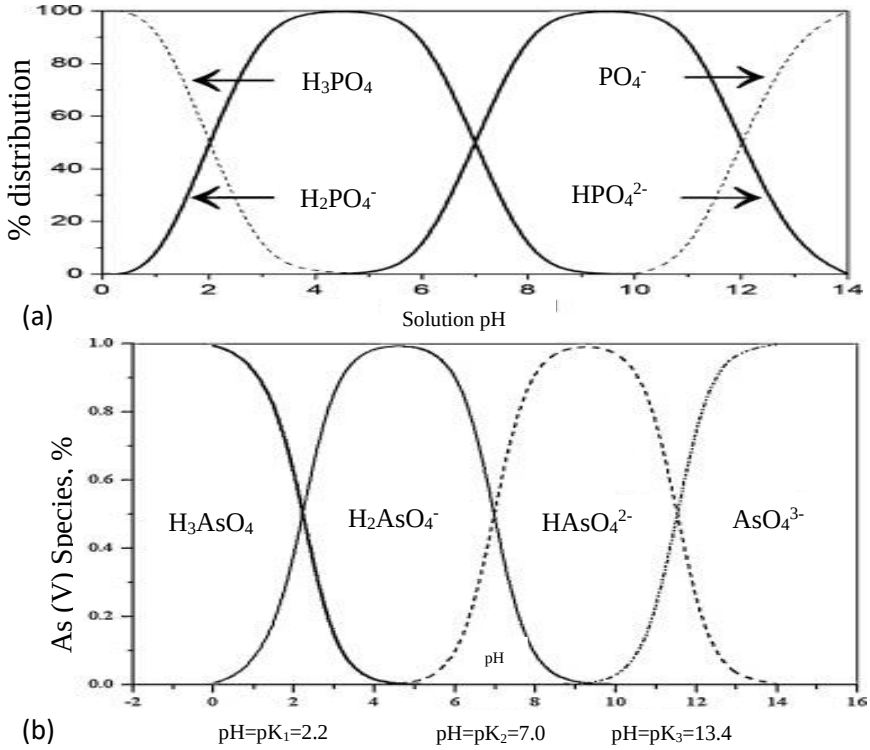

Figure 6-7: The distribution of (a) phosphate and (b) As (V) species as a function of pH (Delaney et al., 2011; Issa et al., 2010).

Phosphate exhibits a chemical structure and protonation constant similar to As (V) ions in solution thus competing with As (V) to form inner-sphere complexes with Al and Fe mineral surfaces (Caporale et al., 2013, 2011; Guan et al., 2009; Nagar et al., 2010). The distribution graphs of As (V) and phosphate (Fig. 6-7) showed that both oxyanions in aqueous solution are pH dependent. From Fig. 6-8a, it was observed that addition of $H_2PO_4^-$ showed a significant effect on As (V) removal. At pH 6, a $H_2PO_4^-$ concentration of 1, 5 and 10 mM resulted in As (V) removal percentages of 15.18 %, 8.62 % and 5.42 % respectively. The removal of As (V) in

the presence of $H_2PO_4^-$ was dependent on pH with the greatest removal to be 38% (pH 9, 10 mM $H_2PO_4^-$) as compared to > 94 % As (V) removal without phosphate addition. This reduction could be attributed to competition for potential binding sites but not as a result of decrease in amount of precipitate formed (Jain and Loeppert, 2000). Likewise, from the species distribution diagram of phosphate, $H_2PO_4^-$ which occurs mainly in weaker acid conditions, could be seen to inhibit As (V) removal at pH 6. Other studies have shown that the addition of $H_2PO_4^-$ ions reduced the amount of As (V) removal even though the removal varied between studies (Guan et al., 2009; Jain and Loeppert, 2000; Tuutijärvi et al., 2012; Youngran et al., 2007b).

Fig. 6-8 (b&c) shows that with an increase in pH, there is a reduction in UV_{254nm} and turbidity removal percentage. However, the addition of phosphate gave a higher turbidity removal at pH 5 – 7 and a higher UV_{254nm} removal at pH 5 and 6. The maximum turbidity and UV_{254nm} removal was 80.19 % and 81.47 % respectively at pH 5 and $H_2PO_4^-$ conc. of 1 mM. Fig. 6-8d indicates that there was an insignificant increase in final pH at $H_2PO_4^-$ concentration of 1 mM except for initial pH 5 where the final pH was 5.60. At $H_2PO_4^-$ concentration of 5 and 10 mM, a slight reduction in pH was observed at pH 6 – 9.

Fig. 6-9 (a & b) compares the effect of competing anions ($H_2PO_4^-$, CO_3^{2-}, NO_3^- and SO_4^{2-}) at different concentration levels (1 mM, 5 mM and 10 mM) in removing As (V), turbidity and UV_{254nm}. At pH 6, the presence of phosphate affects As (V) removal at all concentration levels. However, the presence of phosphate seems to improve both turbidity and UV_{254nm} removal. This result shows that the majority of As (V) remains in solution while the majority of contaminants are removed. Fig. 6-10 (a-d) showed pictures of the As (V) spiked contaminated water before the addition of coagulant and the formation of floc after pH adjustment, coagulant and 1 mM $H_2PO_4^-$ addition. A clear view of the treated contaminated water can be seen from both the side and top view after saturated water at 4 bar was introduced and left to float for 10 minutes. This result showed that the phosphate anion can be used to separate arsenic from other contaminants in a water treatment plant. This means the concentrated sludge at the top may find application in agriculture rather than being sent to landfill since it contains low concentration of arsenic.

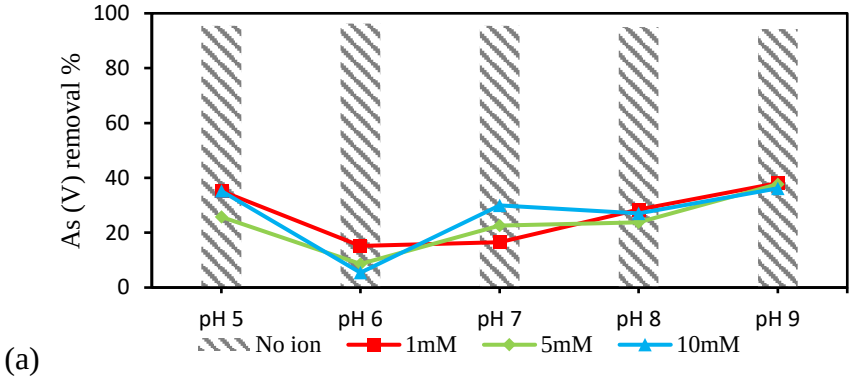

(a)

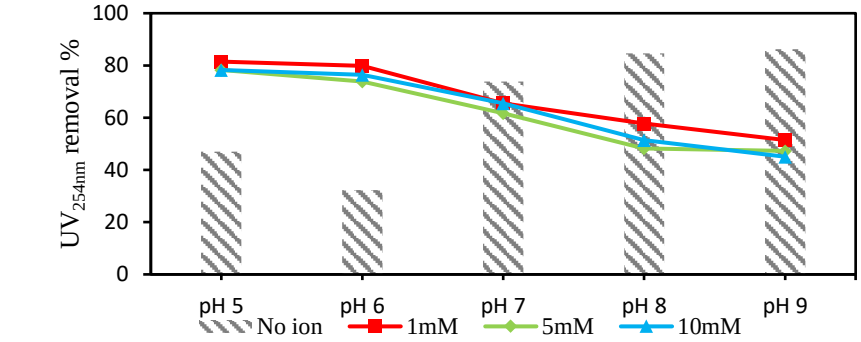

(b)

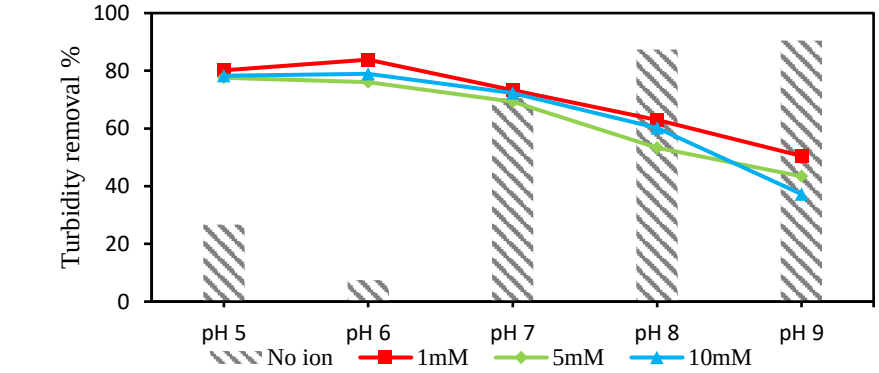

(c)

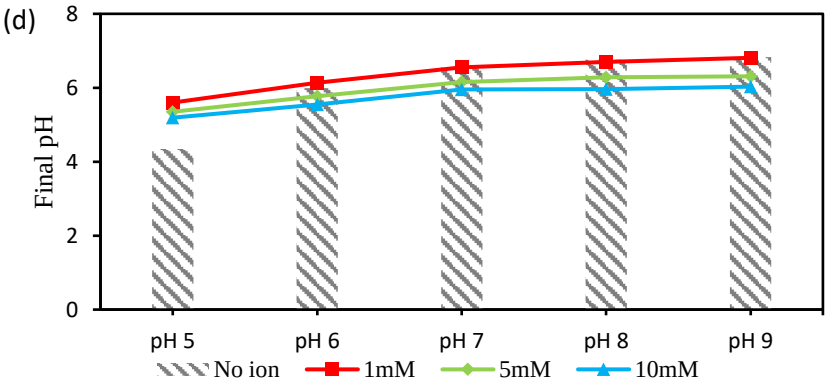

(d)

Figure 6-8: The effect of phosphate (as $H_2PO_4^-$) on (a) As (V) removal (b) turbidity removal (c) UV_{254nm} removal (d) final pH.

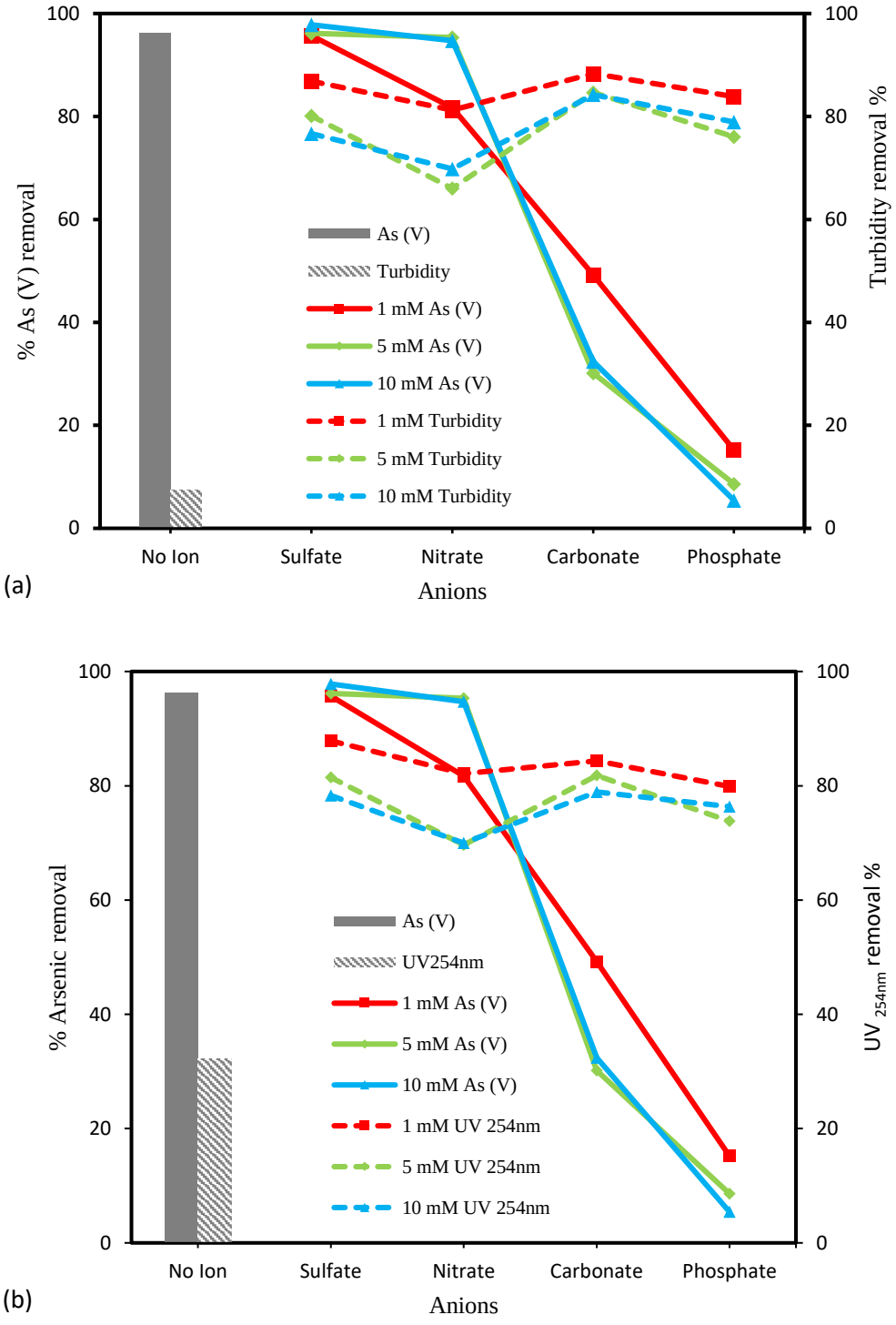

Figure 6-9: Effect of competing anions on (a) As (V) and turbidity (b) As (V) and UV_{254nm} removal at different concentration levels (1, 5 and 10 mM) and pH 6.

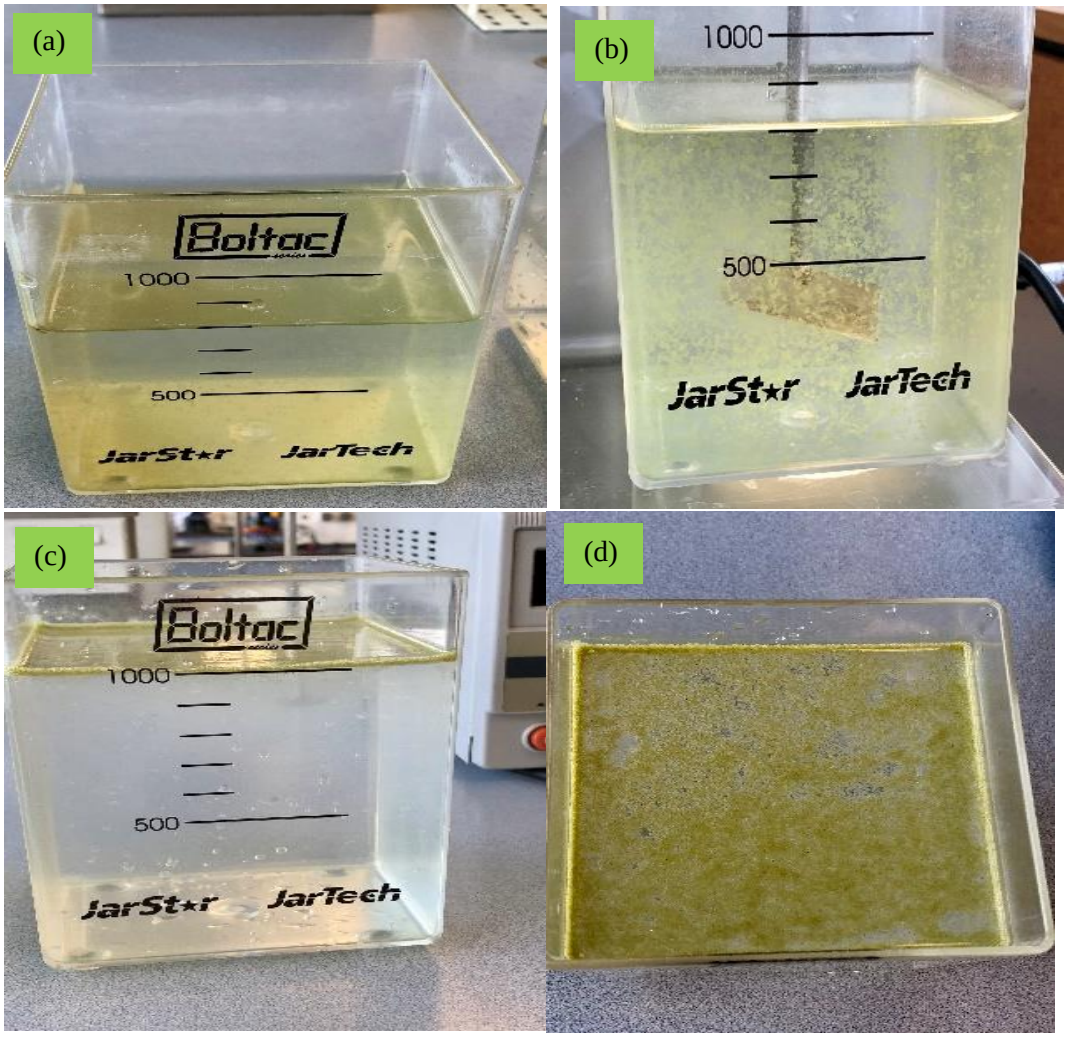

Figure 6-10: Snapshots from C/F/DAF process (coagulant = PAC, 10 mM $H_2PO_4^-$, pH 6, (a) sample water (b) floc formation during the slow stirring coagulation process (c) after DAF treatment (side view) (d) after DAF treatment (top view).

6.4 Conclusions

Polyaluminium chloride as a coagulant is very effective in arsenic removal. This study investigated the effects of sulfate, phosphate, carbonate and nitrate on As (V) removal in a batch C/F/DAF process as a function of pH and concentrations of competing anions. The results in this paper show that PAC was very effective in removing As (V) at all pH level (5 – 9) with a removal rate of > 94 % although a low turbidity and UV_{254nm} removal was observed at pH 6. The following competing anions ($H_2PO_4^-$, CO_3^{2-}, NO_3^- and SO_4^{2-}) at concentration levels (1, 5 and 10 mM) were investigated at pH levels (5 – 9) in a C/F/DAF process. Overall, all the competing anions considered in this study inhibit the removal of As (V) with phosphate and carbonate having a greater effect than sulphate and nitrate. Turbidity

and UV_{254nm} absorbance follow the same removal pattern and the addition of competing anions improved the removal at pH 5 and pH 6. The most significant interference with the removal of As (V) by PAC occurs in the presence of phosphate at pH 6 with a removal rate of 5.52 % at 10 mM phosphate concentration. Overall, the major impact of the competing anions on As (V) removal followed the order of $H_2PO_4^- > CO_3^{2-} > NO_3^- > SO_4^{2-}$. The results from this study showed that the presence of competing anions especially phosphate can be effectively used to separate As (V) from other contaminants. This separation can occur in a two-stage separation process whereby the arsenic in the solution can be removed in the first stage DAF process while other contaminants can be removed in the second stage DAF process. This process will also reduce the composition of As (V) in the sludge which would find application in agriculture instead of going to landfill.

Appendix 6. Supplementary data

- This contains experimental data for effect of competing anions on arsenate removal

References

Aguilar, M.I., Sáez, J., Lloréns, M., Soler, A., Ortuño, J.F., 2002. Nutrient removal and sludge production in the coagulation–flocculation process. Water Res. 36, 2910–2919. https://doi.org/10.1016/S0043-1354(01)00508-5

Ahmad, A.L., Wong, S.S., Teng, T.T., Zuhairi, A., 2008. Improvement of alum and PACl coagulation by polyacrylamides (PAMs) for the treatment of pulp and paper mill wastewater. Chem. Eng. J. 137, 510–517. https://doi.org/10.1016/j.cej.2007.03.088

Al-Zoubi, H., Ibrahim, K.A., Abu-Sbeih, K.A., 2015. Removal of heavy metals from wastewater by economical polymeric collectors using dissolved air flotation process. J. Water Process Eng. 8, 19–27. https://doi.org/10.1016/j.jwpe.2015.08.002

Amaral Filho, J., Azevedo, A., Etchepare, R., Rubio, J., 2016. Removal of sulfate ions by dissolved air flotation (DAF) following precipitation and flocculation. Int. J. Miner. Process. 149, 1–8. https://doi.org/10.1016/j.minpro.2016.01.012

Asmel, N.K., Yusoff, A.R.M., Sivarama Krishna, L., Majid, Z.A., Salmiati, S., 2017. High concentration arsenic removal from aqueous solution using nano-iron ion enrich material (NIIEM) super adsorbent. Chem. Eng. J. 317, 343–355. https://doi.org/10.1016/j.cej.2017.02.039

Biswas, B.K., Inoue, J., Inoue, K., Ghimire, K.N., Harada, H., Ohto, K., Kawakita, H., 2008. Adsorptive removal of As(V) and As(III) from water by a Zr(IV)-loaded orange waste gel. J. Hazard. Mater. 154, 1066–1074. https://doi.org/10.1016/j.jhazmat.2007.11.030

Bringas, E., Saiz, J., Ortiz, I., 2015. Removal of As(V) from groundwater using functionalized magnetic adsorbent materials: Effects of competing ions. Sep. Purif. Technol. 156, 699–707. https://doi.org/10.1016/j.seppur.2015.10.068

Caporale, A.G., Pigna, M., Dynes, J.J., Cozzolino, V., Zhu, J., Violante, A., 2011. Effect of inorganic and organic ligands on the sorption/desorption of arsenate on/from Al–Mg and Fe–Mg layered double hydroxides. J. Hazard. Mater. 198, 291–298. https://doi.org/10.1016/j.jhazmat.2011.10.044

Caporale, A.G., Punamiya, P., Pigna, M., Violante, A., Sarkar, D., 2013. Effect of particle size of drinking-water treatment residuals on the sorption of arsenic in the presence of competing ions. J. Hazard. Mater. 260, 644–651. https://doi.org/10.1016/j.jhazmat.2013.06.023

Chammui, Y., Sooksamiti, P., Naksata, W., Thiansem, S., Arqueropanyo, O., 2014. Removal of arsenic from aqueous solution by adsorption on Leonardite. Chem. Eng. J. 240, 202–210. https://doi.org/10.1016/j.cej.2013.11.083

Chaudhry, S.A., Zaidi, Z., Siddiqui, S.I., 2017. Isotherm, kinetic and thermodynamics of arsenic adsorption onto Iron-Zirconium Binary Oxide-Coated Sand (IZBOCS): Modelling and process optimization. J. Mol. Liq. 229, 230–240. https://doi.org/10.1016/j.molliq.2016.12.048

Choong, T.S.Y., Chuah, T.G., Robiah, Y., Gregory Koay, F.L., Azni, I., 2007. Arsenic toxicity, health hazards and removal techniques from water: an overview. Desalination 217, 139–166. https://doi.org/10.1016/j.desal.2007.01.015

Çiftçi, T.D., Henden, E., 2015. Nickel/nickel boride nanoparticles coated resin: A novel adsorbent for arsenic(III) and arsenic(V) removal. Powder Technol. 269, 470–480. https://doi.org/10.1016/j.powtec.2014.09.041

Delaney, P., McManamon, C., Hanrahan, J.P., Copley, M.P., Holmes, J.D., Morris, M.A., 2011. Development of chemically engineered porous metal oxides for phosphate removal. J. Hazard. Mater. 185, 382–391. https://doi.org/10.1016/j.jhazmat.2010.08.128

Deng, Y., Li, Y., Li, X., Sun, Y., Ma, J., Lei, M., Weng, L., 2018. Influence of calcium and phosphate on pH dependency of arsenite and arsenate adsorption to goethite. Chemosphere 199, 617–624. https://doi.org/10.1016/j.chemosphere.2018.02.018

Domínguez, J.R., González, T., García, H.M., Sánchez-Lavado, F., Beltrán de Heredia, J., 2007. Aluminium sulfate as coagulant for highly polluted cork processing wastewaters: Removal of organic matter. J. Hazard. Mater. 148, 15–21. https://doi.org/10.1016/j.jhazmat.2007.05.003

Duan, J., Gregory, J., 2003. Coagulation by hydrolysing metal salts. Adv. Colloid Interface Sci. 100–102, 475–502. https://doi.org/10.1016/S0001-8686(02)00067-2

DWSNZ, 2008. Drinking-water Standards for New Zealand.

Edzwald, J.K., 2010. Dissolved air flotation and me. Water Res. 44, 2077–2106. https://doi.org/10.1016/j.watres.2009.12.040

Frau, F., Addari, D., Atzei, D., Biddau, R., Cidu, R., Rossi, A., 2010. Influence of Major Anions on As(V) Adsorption by Synthetic 2-line Ferrihydrite. Kinetic Investigation and XPS Study of the Competitive Effect of Bicarbonate. Water. Air. Soil Pollut. 205, 25–41. https://doi.org/10.1007/s11270-009-0054-4

Fu, F., Wang, Q., 2011. Removal of heavy metal ions from wastewaters: A review. J. Environ. Manage. 92, 407–418. https://doi.org/10.1016/j.jenvman.2010.11.011

Ghafari, S., Aziz, H.A., Bashir, M.J.K., 2010. The use of poly-aluminum chloride and alum for the treatment of partially stabilized leachate: A comparative study. Desalination 257, 110–116. https://doi.org/10.1016/j.desal.2010.02.037

Guan, X., Dong, H., Ma, J., Jiang, L., 2009. Removal of arsenic from water: Effects of competing anions on As(III) removal in KMnO4–Fe(II) process. Water Res. 43, 3891–3899. https://doi.org/10.1016/j.watres.2009.06.008

Hernández-Flores, H., Pariona, N., Herrera-Trejo, M., Hdz-García, H.M., Mtz-Enriquez, A.I., 2018. Concrete/maghemite nanocomposites as novel adsorbents for arsenic removal. J. Mol. Struct. 1171, 9–16. https://doi.org/10.1016/j.molstruc.2018.05.078

Hu, C., Liu, H., Chen, G., Qu, J., 2012. Effect of aluminum speciation on arsenic removal during coagulation process. Sep. Purif. Technol. 86, 35–40. https://doi.org/10.1016/j.seppur.2011.10.017

Hua, J., 2018. Adsorption of low-concentration arsenic from water by co-modified bentonite with manganese oxides and poly(dimethyldiallylammonium chloride). J. Environ. Chem. Eng. 6, 156–168. https://doi.org/10.1016/j.jece.2017.11.062

Ihsanullah, Abbas, A., Al-Amer, A.M., Laoui, T., Al-Marri, M.J., Nasser, M.S., Khraisheh, M., Atieh, M.A., 2016. Heavy metal removal from aqueous solution by advanced carbon nanotubes: Critical review of adsorption applications. Sep. Purif. Technol. 157, 141–161. https://doi.org/10.1016/j.seppur.2015.11.039

Issa, N.B., Rajaković-Ognjanović, V.N., Jovanović, B.M., Rajaković, L.V., 2010. Determination of inorganic arsenic species in natural waters—Benefits of separation and preconcentration on ion exchange and hybrid resins. Anal. Chim. Acta 673, 185–193. https://doi.org/10.1016/j.aca.2010.05.027

Jain, A., Loeppert, R.H., 2000. Effect of Competing Anions on the Adsorption of Arsenate and Arsenite by Ferrihydrite. J. Environ. Qual. 29, 1422–1430. https://doi.org/10.2134/jeq2000.00472425002900050008x

Kanematsu, M., Young, T.M., Fukushi, K., Green, P.G., Darby, J.L., 2013. Arsenic(III, V) adsorption on a goethite-based adsorbent in the presence of major co-existing ions: Modeling competitive adsorption consistent with spectroscopic and molecular evidence. Geochim. Cosmochim. Acta 106, 404–428. https://doi.org/10.1016/j.gca.2012.09.055

Karhu, M., Leiviskä, T., Tanskanen, J., 2014. Enhanced DAF in breaking up oil-in-water emulsions. Sep. Purif. Technol. 122, 231–241. https://doi.org/10.1016/j.seppur.2013.11.007

Kofa, G.P., NdiKoungou, S., Kayem, G.J., Kamga, R., 2015. Adsorption of arsenic by natural pozzolan in a fixed bed: Determination of operating conditions and modeling. J. Water Process Eng. 6, 166–173. https://doi.org/10.1016/j.jwpe.2015.04.006

Kurniawan, T.A., Chan, G.Y.S., Lo, W.-H., Babel, S., 2006. Physico–chemical treatment techniques for wastewater laden with heavy metals. Chem. Eng. J. 118, 83–98. https://doi.org/10.1016/j.cej.2006.01.015

Lee, C.-G., Alvarez, P.J.J., Nam, A., Park, S.-J., Do, T., Choi, U.-S., Lee, S.-H., 2017. Arsenic(V) removal using an amine-doped acrylic ion exchange fiber: Kinetic, equilibrium, and regeneration studies. J. Hazard. Mater. 325, 223–229. https://doi.org/10.1016/j.jhazmat.2016.12.003

Litter, M.I., Morgada, M.E., Bundschuh, J., 2010. Possible treatments for arsenic removal in Latin American waters for human consumption. Environ. Pollut. 158, 1105–1118. https://doi.org/10.1016/j.envpol.2010.01.028

Mandal, S., Sahu, M.K., Patel, R.K., 2013. Adsorption studies of arsenic(III) removal from water by zirconium polyacrylamide hybrid material (ZrPACM-43). Water Resour. Ind. 4, 51–67. https://doi.org/10.1016/j.wri.2013.09.003

Manna, B., Ghosh, U.C., 2007. Adsorption of arsenic from aqueous solution on synthetic hydrous stannic oxide. J. Hazard. Mater. 144, 522–531. https://doi.org/10.1016/j.jhazmat.2006.10.066

Meng, X., Bang, S., Korfiatis, G.P., 2000. Effects of silicate, sulfate, and carbonate on arsenic removal by ferric chloride. Water Res. 34, 1255–1261. https://doi.org/10.1016/S0043-1354(99)00272-9

Mertens, J., Casentini, B., Masion, A., Pöthig, R., Wehrli, B., Furrer, G., 2012. Polyaluminum chloride with high Al30 content as removal agent for arsenic-contaminated well water. Water Res. 46, 53–62. https://doi.org/10.1016/j.watres.2011.10.031

Miranda, R., Nicu, R., Latour, I., Lupei, M., Bobu, E., Blanco, A., 2013. Efficiency of chitosans for the treatment of papermaking process water by dissolved air flotation. Chem. Eng. J. 231, 304–313. https://doi.org/10.1016/j.cej.2013.07.033

Mohan, D., Pittman Jr., C.U., 2007. Arsenic removal from water/wastewater using adsorbents—A critical review. J. Hazard. Mater. 142, 1–53. https://doi.org/10.1016/j.jhazmat.2007.01.006

Mondal, P., Majumder, C.B., Mohanty, B., 2006. Laboratory based approaches for arsenic remediation from contaminated water: Recent developments. J. Hazard. Mater. 137, 464–479. https://doi.org/10.1016/j.jhazmat.2006.02.023

Nagar, R., Sarkar, D., Makris, K.C., Datta, R., 2010. Effect of solution chemistry on arsenic sorption by Fe- and Al-based drinking-water treatment residuals. Chemosphere 78, 1028–1035. https://doi.org/10.1016/j.chemosphere.2009.11.034

Pallier, V., Feuillade-Cathalifaud, G., Serpaud, B., Bollinger, J.-C., 2010. Effect of organic matter on arsenic removal during coagulation/flocculation treatment. J. Colloid Interface Sci. 342, 26–32. https://doi.org/10.1016/j.jcis.2009.09.068

Podder, M.S., Majumder, C.B., 2018. Biological detoxification of As(III) and As(V) using immobilized bacterial cells in fixed-bed bio-column reactor: Prediction of kinetic parameters. Groundw. Sustain. Dev. 6, 14–42. https://doi.org/10.1016/j.gsd.2017.10.004

Podder, M.S., Majumder, C.B., 2016. Fixed-bed column study for As(III) and As(V) removal and recovery by bacterial cells immobilized on Sawdust/MnFe2O4 composite. Biochem. Eng. J. 105, 114–135. https://doi.org/10.1016/j.bej.2015.09.008

Roghani, M., Nakhli, S.A.A., Aghajani, M., Rostami, M.H., Borghei, S.M., 2016. Adsorption and oxidation study on arsenite removal from aqueous solutions by polyaniline/polyvinyl alcohol composite. J. Water Process Eng. 14, 101–107. https://doi.org/10.1016/j.jwpe.2016.10.012

Roussy, J., Vooren, M.V., Guibal, E., 2005. Chitosan for the Coagulation and Flocculation of Mineral Colloids. J. Dispers. Sci. Technol. 25, 663–677. https://doi.org/10.1081/DIS-200027325

Saha, J.C., Dikshit, A.K., Bandyopadhyay, M., Saha, K.C., 1999. A Review of Arsenic Poisoning and its Effects on Human Health. Crit. Rev. Environ. Sci. Technol. 29, 281–313. https://doi.org/10.1080/10643389991259227

Sher, F., Malik, A., Liu, H., 2013. Industrial polymer effluent treatment by chemical coagulation and flocculation. J. Environ. Chem. Eng. 1, 684–689. https://doi.org/10.1016/j.jece.2013.07.003

Sigdel, A., Park, J., Kwak, H., Park, P.-K., 2016. Arsenic removal from aqueous solutions by adsorption onto hydrous iron oxide-impregnated alginate beads. J. Ind. Eng. Chem. 35, 277–286. https://doi.org/10.1016/j.jiec.2016.01.005

Smith A H, Hopenhayn-Rich C, Bates M N, Goeden H M, Hertz-Picciotto I, Duggan H M, Wood R, Kosnett M J, Smith M T, 1992. Cancer risks from arsenic in drinking water. Environ. Health Perspect. 97, 259–267. https://doi.org/10.1289/ehp.9297259

Su, C., Puls, R.W., 2001. Arsenate and arsenite removal by zerovalent iron: effects of phosphate, silicate, carbonate, borate, sulfate, chromate, molybdate, and nitrate, relative to chloride. Environ. Sci. Technol. 35, 4562–4568.

Teixeira, M.R., Rosa, M.J., 2007. Comparing dissolved air flotation and conventional sedimentation to remove cyanobacterial cells of Microcystis aeruginosa: Part II. The effect of water background organics. Sep. Purif. Technol. 53, 126–134. https://doi.org/10.1016/j.seppur.2006.07.001

Tuutijärvi, T., Repo, E., Vahala, R., Sillanpää, M., Chen, G., 2012. Effect of Competing Anions on Arsenate Adsorption onto Maghemite Nanoparticles. Chin. J. Chem. Eng. 20, 505–514. https://doi.org/10.1016/S1004-9541(11)60212-7

U.S.EPA, 2016. U.S. Environmental Agency, Drinking Water Contaminants.

Van Benschoten, J.E., Edzwald, J.K., 1990. Chemical aspects of coagulation using aluminum salts—I. Hydrolytic reactions of alum and polyaluminum chloride. Water Res. 24, 1519–1526. https://doi.org/10.1016/0043-1354(90)90086-L

Villaescusa, I., Bollinger, J.-C., 2008. Arsenic in drinking water: sources, occurence and health effects (a review). Rev Env. Sci Biotechnol 7, 307–323.

Wei, H., Gao, B., Ren, J., Li, A., Yang, H., 2018. Coagulation/flocculation in dewatering of sludge: A review. Water Res. 143, 608–631. https://doi.org/10.1016/j.watres.2018.07.029

Wei, N., Zhang, Z., Liu, D., Wu, Y., Wang, J., Wang, Q., 2015. Coagulation behavior of polyaluminum chloride: Effects of pH and coagulant dosage. Chin. J. Chem. Eng. 23, 1041–1046. https://doi.org/10.1016/j.cjche.2015.02.003

WHO, 2011. Guidelines for drinking water quality, fourth edition.

Yang, R., Li, H., Huang, M., Yang, H., Li, A., 2016. A review on chitosan-based flocculants and their applications in water treatment. Water Res. 95, 59–89. https://doi.org/10.1016/j.watres.2016.02.068

Yang, Z., Gao, B., Cao, B., Xu, W., Yue, Q., 2011. Effect of OH−/Al3+ ratio on the coagulation behavior and residual aluminum speciation of polyaluminum chloride (PAC) in surface water treatment. Sep. Purif. Technol. 80, 59–66. https://doi.org/10.1016/j.seppur.2011.04.007

Yokoi, T., Tatsumi, T., Yoshitake, H., 2004. Fe3+ coordinated to amino-functionalized MCM-41: an adsorbent for the toxic oxyanions with high capacity, resistibility to inhibiting anions, and reusability after a simple treatment. J. Colloid Interface Sci. 274, 451–457. https://doi.org/10.1016/j.jcis.2004.02.037

Youngran, J., Fan, M., Van Leeuwen, J., Belczyk, J.F., 2007a. Effect of competing solutes on arsenic(V) adsorption using iron and aluminum oxides. J. Environ. Sci. 19, 910–919. https://doi.org/10.1016/S1001-0742(07)60151-X

Youngran, J., Fan, M., Van Leeuwen, J., Belczyk, J.F., 2007b. Effect of competing solutes on arsenic(V) adsorption using iron and aluminum oxides. J. Environ. Sci. 19, 910–919. https://doi.org/10.1016/S1001-0742(07)60151-X

Yu, J., Wang, D., Yan, M., Ye, C., Yang, M., Ge, X., 2007. Optimized coagulation of high alkalinity, low temperature and particle water: pH adjustment and polyelectrolytes as coagulant aids. Environ. Monit. Assess. 131, 377–386. https://doi.org/10.1007/s10661-006-9483-3

CHAPTER SEVEN

Target separation of arsenic from contaminated drinking water using a batch dissolved air flotation process

Abstract

Dissolved air flotation (DAF) process has been widely used for many applications including water and wastewater treatment. In this study, the effects of pH, saturated pressure, phosphate concentrations, polyaluminium chloride (PAC) concentration, and flotation time on separating arsenic from other contaminants was studied for drinking water treatment using a 2- stage DAF system. Adding low concentrations of phosphate anion, $H_2PO_4^-$ (0.5, 2.5 and 10 mM) have no significant effect on arsenic removal but showed significant effect on turbidity removal with maximum arsenic and turbidity removal efficiencies of 63.71 % and 36.26 % respectively. Increasing the flotation time from 10 to 30 min showed no significant increase in arsenic, turbidity and UV_{254nm} removal efficiencies. It was found that 81.71 % of arsenic was separated from other contaminants in the first stage DAF process at pH 6, while turbidity removal was 3.44 %. In the second stage, the optimum treatment was determined at saturation pressure of 4 bar, pH of 8, PAC concentration of 0.47 mg/L, obtaining removal efficiencies of 64.08 % (turbidity), 27.42 % (arsenic) and 40.33 % (UV_{254nm}). The results demonstrate the effectiveness of a 2-stage batch DAF system in separating arsenic from other contaminants from a contaminated drinking water.

7.1 Introduction

Arsenic is a metalloid and is classified as one of the most toxic and carcinogenic chemicals. It originates from natural and anthropogenic sources and it is found in water, air and soil. It exists in organic and inorganic forms and in different oxidation states namely; -3, 0, +3 and +5 (Hughes, 2002; Wu et al., 2011).

The most common treatment technologies for removing arsenic from drinking water under both laboratory and field conditions are conventional physico-chemical treatment processes; coagulation-flocculation, adsorption, oxidation, ion exchange, membrane processes and electrocoagulation (Ghosh (Nath) et al., 2019; Kordmostafapour et al., 2006). One of the major drawbacks of a coagulation-flocculation process is the large quantities of wastes that are generated, and that can impact processing and disposal cost (Chen et al., 2002). In New Zealand, aluminium-based coagulation with disinfection by chlorination is the most preferred method of water treatment. The current maximum acceptable value (MAV) for arsenic in drinking water of 0.01 mg/l was adopted in 1995 (Gregor, 2001).

Polyaluminium chloride (PAC) and inorganic polymer flocculants have found extensive application worldwide in water and wastewater treatment (Guo et al., 2019; Zouboulis and Tzoupanos, 2009). One of the key factors of PAC that is closely related to its efficiency is its basicity (Guo et al., 2019). PAC has shown to be more efficient in lower dosages and over wider pH, temperature, and colloids concentration ranges than the conventional simpler products. These advantages lead to a more effective and efficient treatment (Sinha et al., 2004; Zouboulis and Tzoupanos, 2009).

Flotation method relies on the difference in the surface properties of different particles in order to separate one particle from another. The particles that are hydrophobic escape from the water to the surface by attaching to air bubbles (Al-Zoubi et al., 2015a). The types of flotation methods are ion flotation, electrolytic flotation, precipitate flotation and dissolve air flotation (DAF) (Al-Zoubi et al., 2015b; Edzwald, 2007).

DAF is used in the purification of water (Zhang et al., 2014). DAF has also found application in pretreating wastewater from a poultry slaughterhouse (de Nardi et al.,

2008), phosphate beneficiation (Al-Thyabat and Al-Zoubi, 2012), removing cyanobacterial cells (Teixeira and Rosa, 2007), treatment of produced water (Younker and Walsh, 2014), feldspar separation (Karagüzel, 2010), emulsified crude oil separation from saline water (Etchepare et al., 2017), sulfate removal (Amaral Filho et al., 2016) and milk industry wastewater treatment (Pereira et al., 2018).

So far, to our knowledge, the selective separation of arsenic from other contaminants by flotation from a contaminated drinking water has not been reported in any literature. In this experiment, coagulation followed by DAF was tested as a means of separating arsenic from other contaminants in drinking water. The main aim of these experiments is to evaluate (a) the effect of coagulant dose (PAC), pH conditions, flotation time, saturation pressure and phosphate concentration by the DAF process (b) the influence of change in pH on the target separation of arsenic from other contaminants focusing primarily on arsenic, turbidity and UV_{254nm} efficiency after optimising the chemical and operating parameters.

7.2 Materials and Methods

7.2.1 Materials

All the chemicals and reagents used were of analytical grade. The solutions were prepared in ultrapure grade water (Milli Q systems: resistivity 18.2 MΩ cm^{-1}; Barnstead, EASYpure). The pH adjustments were performed using 0.1M hydrochloric acid (HCl) and 0.1M sodium hydroxide (NaOH) solutions. Other chemicals used were nitric acid (70 % HNO_3) and ethanol (70 % C_2H_5OH). All chemicals and reagents used were of analytical grade (Merck KGaA, Darmstadt, Germany). Commercial PAC (IXOM Operations Pty Ltd, Melbourne, Australia) with the following properties was used: 23.5 % w/w as Al_2O_3, Basicity of 83 % w/w, specific gravity (SG) = 1.34, pH =3.5 and Freezing point of < 0 ^oC.

7.2.1.1. Natural water sample

A natural surface water sample was collected from the Waikato River (Fig. 7-1 37.806379^o S, 175.306753^o E). The Waikato River contains arsenic, which is higher than the recommended value of 10 µg/L alongside high concentrations of Iron and

Silica. Water samples were collected between the months of May 2019 to July 2019 (winter months in New Zealand). The water samples were collected at the same location, which is just adjacent to Hamilton water treatment plant, and were transported to the environmental research laboratory (The University of Waikato) on the same day. The characterization of the process waters is shown in Table 7-1.

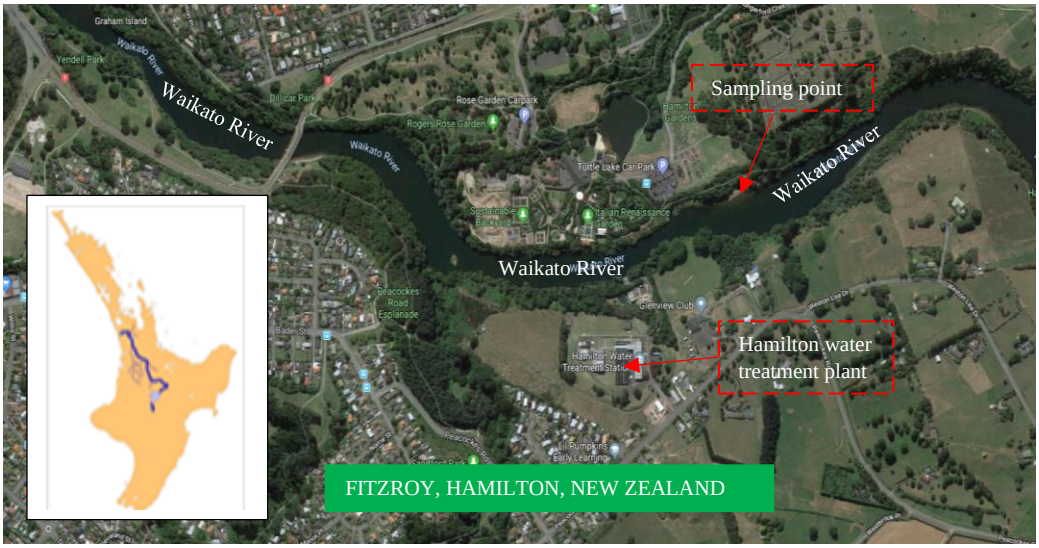

Figure 7-1: Waikato River (Google map) Insert: North Island of New Zealand showing Waikato River (blue).

7.2.1.2. Instrumentation

Sample pH was measured under magnetic stirring using a pH meter (Eutech pH150 pH/temperature). The pH meter was calibrated prior to use using 4.01, 7.01 and 10.04 pH buffers (Merck KGaA, Darmstadt, Germany). Turbidity was determined by the nephelometric method using a HACH 2100N turbidimeter of high resolution (0.001 NTU). UV_{254nm} was measured using a Spectronic Unicam UV300 UV/vis spectrophotometer. A HACH 2100P turbidimeter was used to measure turbidity. The meter was calibrated with 10, 20 and 100 NTU turbidity standards (HACH Turbidity Standard kit model 2100P) before use. Total arsenic concentration was measured by inductively coupled plasma mass – spectrometry (ICP-MS) after sample filtration on 0.45 µm membrane filters. Quality control employed for ICP-MS measurements are shown in APPENDIX 2BA.

7.2.2 Methodology

7.2.2.1 Dissolved air flotation (DAF) tests

In the experiment, a batch DAF system was used as shown in Chapter 6 (Fig. 6-2). The coagulation procedures (by adding PAC) consist of two steps: vigorous stirring after addition of coagulant (100 rpm for 3 min) and mild stirring (30 rpm for 10 min). The coagulation process is then followed by a flotation process (floating time = 10 min). The flotation process was carried out in the same manner in all the tests, where atmospheric air was injected through the upper inlet and dissolved in tap water under pressure in the saturation chamber until the desired pressure, adjusted by the pressure-regulating valve was reached. DAF treated samples were collected after flotation via sampling ports for analysis. All the experiments were performed at room temperature (20 ± 2 ^{o}C). The experimental protocol followed is shown in Fig. 7-2. The efficiency of the different chemical treatments applied was evaluated by measuring arsenic, turbidity, UV_{254nm} and change in pH. The removal percentage (R %) of arsenic, turbidity and UV_{254nm} was determined using the equation below:

$$\text{Removal percentage (R \%)} = \left[1 - \left(\frac{C_f}{C_i}\right)\right] \text{ x } 100$$

Where C_i and C_f are the initial and final concentrations. Experiments were carried out in duplicate.

Table 7-1: Characteristics of Waikato River water sample

Properties	**Values**
pH	7.48 ± 0.5
Turbidity (NTU)	3.12 ± 1.11
Alkalinity (mg $CaCO_3$/L)	20 ± 2
As (mg/L)	0.016 ± 0.003
DO (mg/L)	2.33 ± 1.01
UV_{254nm} (cm^{-1})	0.059 ± 0.016
Temperature (^{o}C)	22.2 ± 2.2
Nitrate (mg/L N)	1.34 ± 0.2
Phosphate (mg/L PO_4)	0.38 ± 0.03
Conductivity (µS/cm)	153 ± 5

7.3 Results and discussion

7.3.1 Effect of coagulant dosage

In this study, the flotation experiments were carried out using PAC as coagulant to investigate the effect the dosage on separating arsenic from other contaminants. The pH, mixing speed, flotation time and saturation pressure were kept constant as shown in Fig. 7-2.

Fig. 7-3a showed the changes of arsenic removal efficiencies as a function of various PAC dosages in a batch coagulation-DAF process (Appendix 7A). With an increase in PAC dosage from 2.35 mg/L to 9.40 mg/L, the removal efficiency of arsenic increased from 54.91 % to 74.70 %. Increasing the PAC dosage further did not result in any significant increase in arsenic removal efficiency. The maximum arsenic removal is 90.50 % at PAC dose of 8 mg/L.

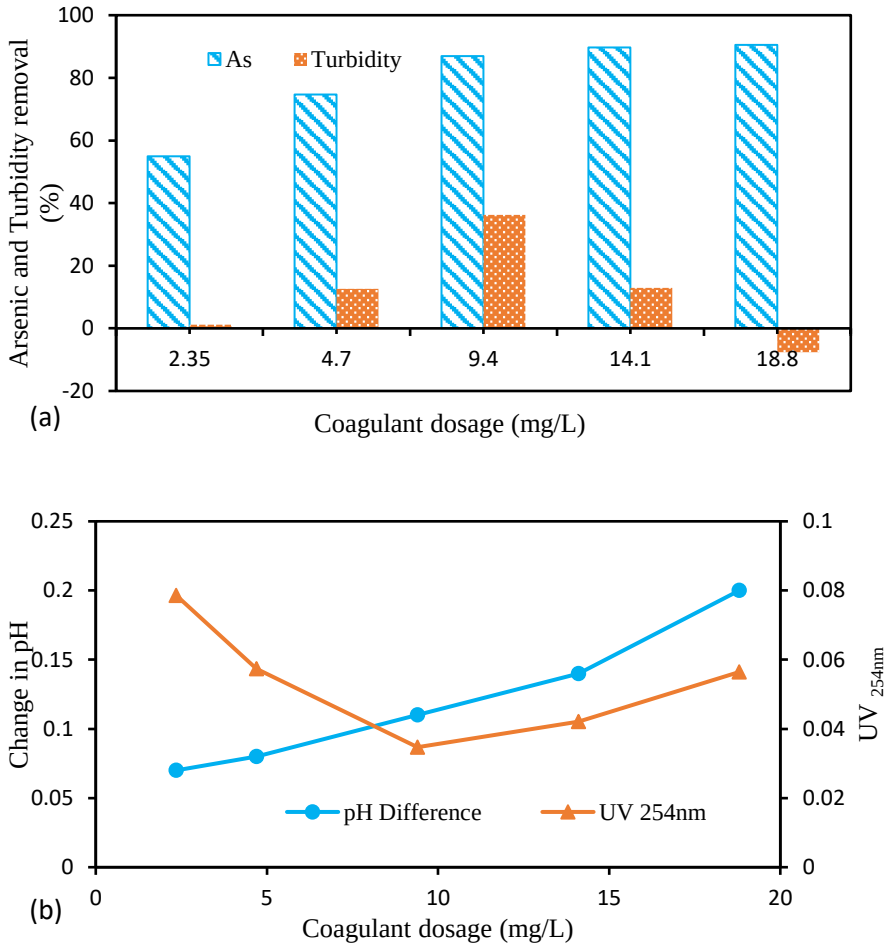

Figure 7-2: Effect of PAC dosage on (a) arsenic and turbidity removal (b) change in pH and UV_{254nm} values.

Figure 7-3: Experimental protocol to evaluate the efficiency of different parameters to separate arsenic from other contaminants using DAF

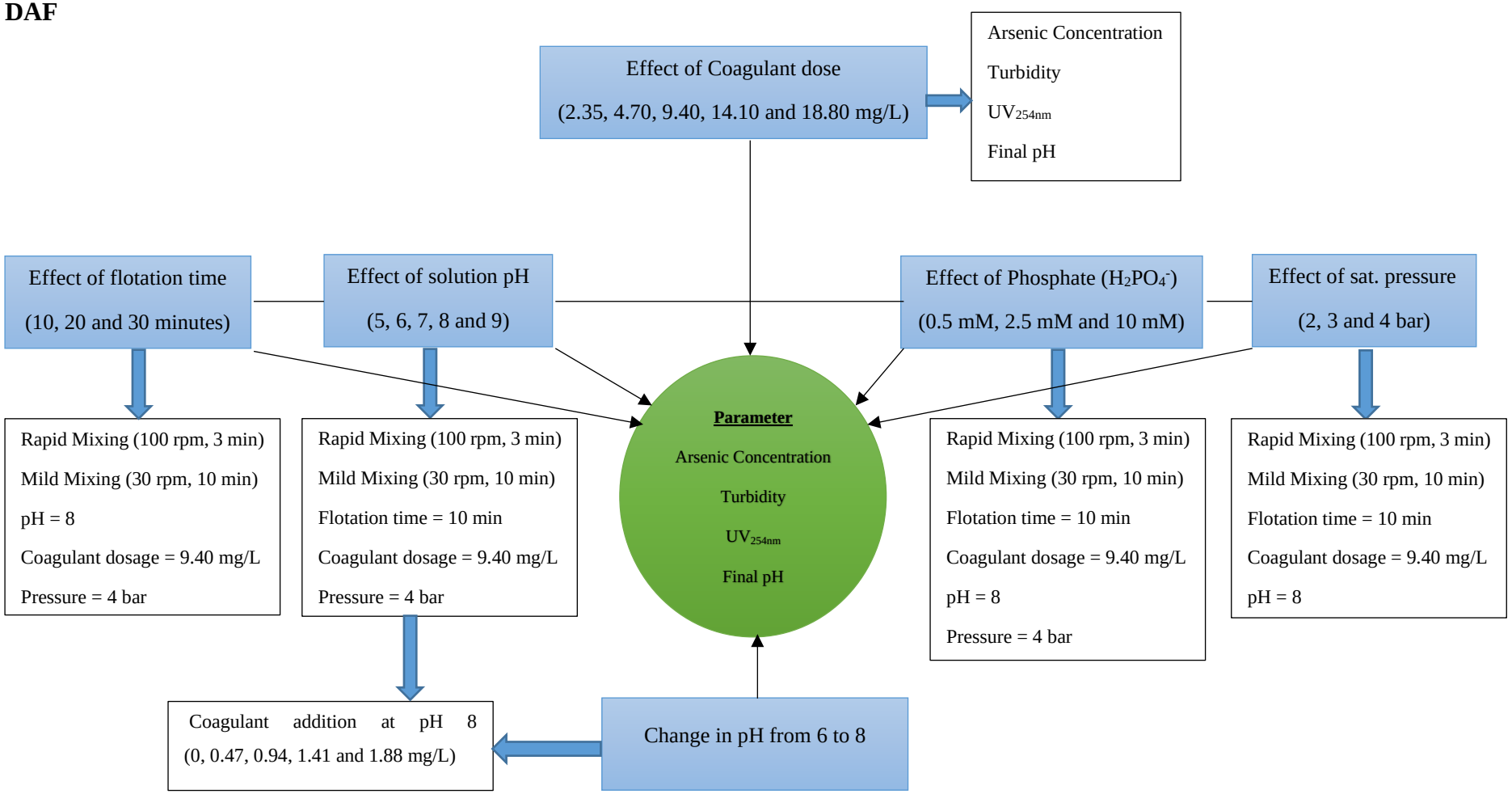

A similar result was also obtained by Wu et al. (2011) who investigated arsenic removal from wastewater using Fe-Mn binary oxide combined with PAC. When the dose of PAC increased from 0 mg/L to 100 mg/L, arsenic removal efficiency increased from 70.20 % to 97.1 %. Hu et al. (2012) studied the effect of aluminium speciation on arsenic removal using different coagulants ($AlCl_3$, PAC1 and PAC2) where they found an increase in arsenic removal from 80 % to 98 % when $AlCl_3$ was increased from 2.0 mg/l to 7.5 mg/L. but no significant increase in removal after that.

There was an increase in turbidity removal from 1.15 % to 12.60 % with a PAC dosage of 2.35 mg/L to 9.40 mg/L. However, beyond 9.40 mg/l, the turbidity removal started to decrease. The function of PAC is to destabilize the negative charge of particles in the solution. Increasing PAC dosage will increase the positive charge; hence, an increase in charge neutralization occurs. Coagulant dose below or greater than 9.40 mg/L did not result in any noticeable floc formation, but cloudiness in solution was observed after 9.40 mg/L indicating that the amount of PAC needed for floc formation had been exceeded. Fig. 7-3b showed that UV_{254nm} removal follows the same pattern as turbidity removal with the highest removal percentage recorded at a PAC dose of 9.40 mg/L. There was no significant change in pH with PAC dose with the highest change in pH of 0.2 observed at coagulant dose of 8 mg/L.

7.3.2 Effect of pH

The effect of pH (5, 6, 7, 8 and 9) on arsenic and turbidity removal was carried out at different pH values at 9.40 mg/l PAC dosage at room temperature (20 ^{o}C) in a batch DAF process (Appendix 7B). Fig. 7-4a showed that there is a slight decrease in arsenic removal from 90.40 % to 81.71 % at pH 5 and pH 6 respectively. The maximum arsenic removal was 90.40 % at pH 5 and gradually decreased to 52.36 % at pH 9. Hu et al. (2011) showed that adding Fe-Mn binary oxide (FMBO) with PAC improves arsenic removal. Almost 100 % of arsenic was removed between pH 4 and pH 9 when 30 mg/L FMBO + 80 mg/L PAC (unfiltered) and 60 mg/L FMBO + 80 mg/L PAC (unfiltered). The removal percentage declined at pH 10 for the two cases because of higher repulsive forces between anionic arsenic species and

FMBO at an elevated pH. Hu et al. (2012) examined the effect of pH on As removal in the pH range of pH 4 to pH 9 at two dosages of 2 mg/L and 20 mg/L. Arsenic removal was higher at 20 mg/L than at 2 mg/L although there is similarity in the curves for the two dosages for arsenic removal using PAC2 as coagulant. This curve is similar to the results obtained in Fig. 7-4a. There is an increase in turbidity at pH 5; this can be attributed to PAC not producing any floc. Turbidity removal was 3.4 % at pH 6 with the maximum removal rate recorded at pH 8 at 33.21 %.

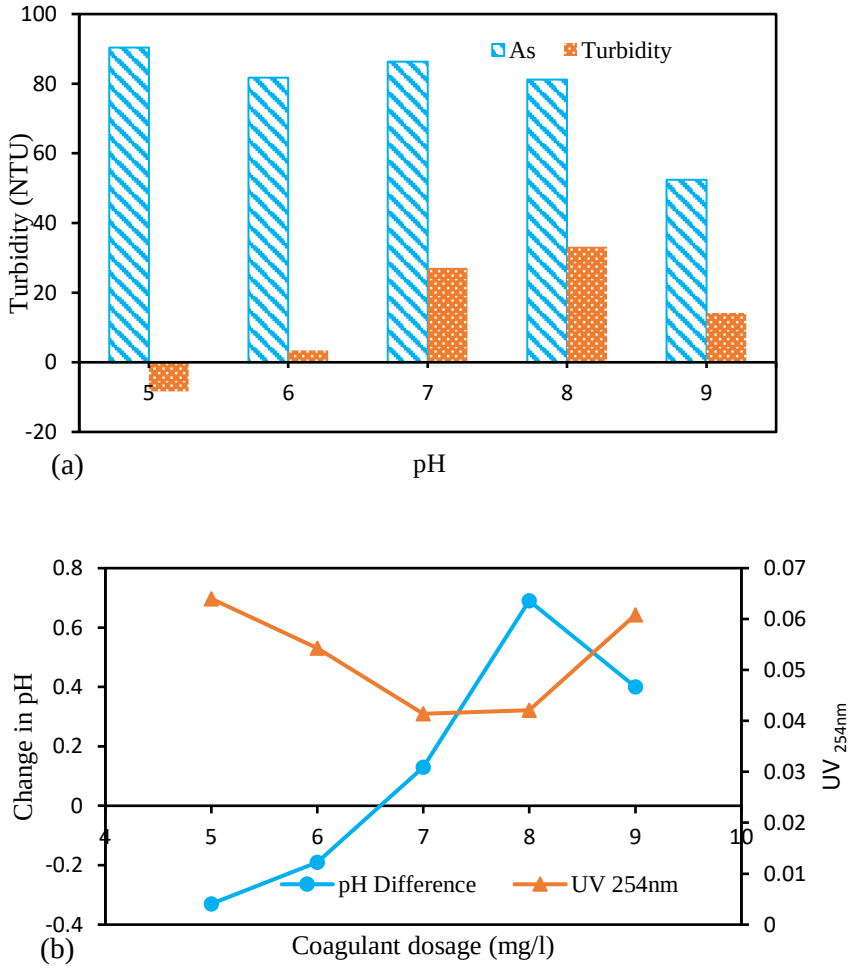

Figure 7-4: Effect of pH on (a) arsenic and turbidity removal (b) change in pH and UV_{254nm} values

Fig. 7-4b showed that there is no significant difference in UV_{254nm} removed across the pH range (4 – 9). The maximum removal percentage was 31.88 % at pH 7. Addition of PAC increases the pH of the treated contaminated water by 0.33 and 0.19 for pH 5 and pH 6 respectively. A decrease in pH was observed in the final solution after PAC addition from pH 7 to pH 9.

7.3.3 Effect of phosphate ($H_2PO_4^-$)

Competing anions are known to affect arsenic removal in solution. The effect of these competing anions was covered extensively in Chapter 6 where phosphate ($H_2PO_4^-$) was shown to exert a much greater inhibitory effect on arsenic removal compared to sulfate (SO_4^{2-}), nitrate (NO_3^-) and carbonate (CO_3^{2-}). Three phosphate concentrations were considered in this study (0.5 mM, 2.5 mM and 10 mM) to determine their effect on arsenic and turbidity removal (Appendix 7C). There was no significant difference in arsenic removal among the three concentrations considered in this study with the a removal of 63.71 %, 60.55 % and 60.55 % at 0.5 mM, 2.5 mM and 10 mM respectively.

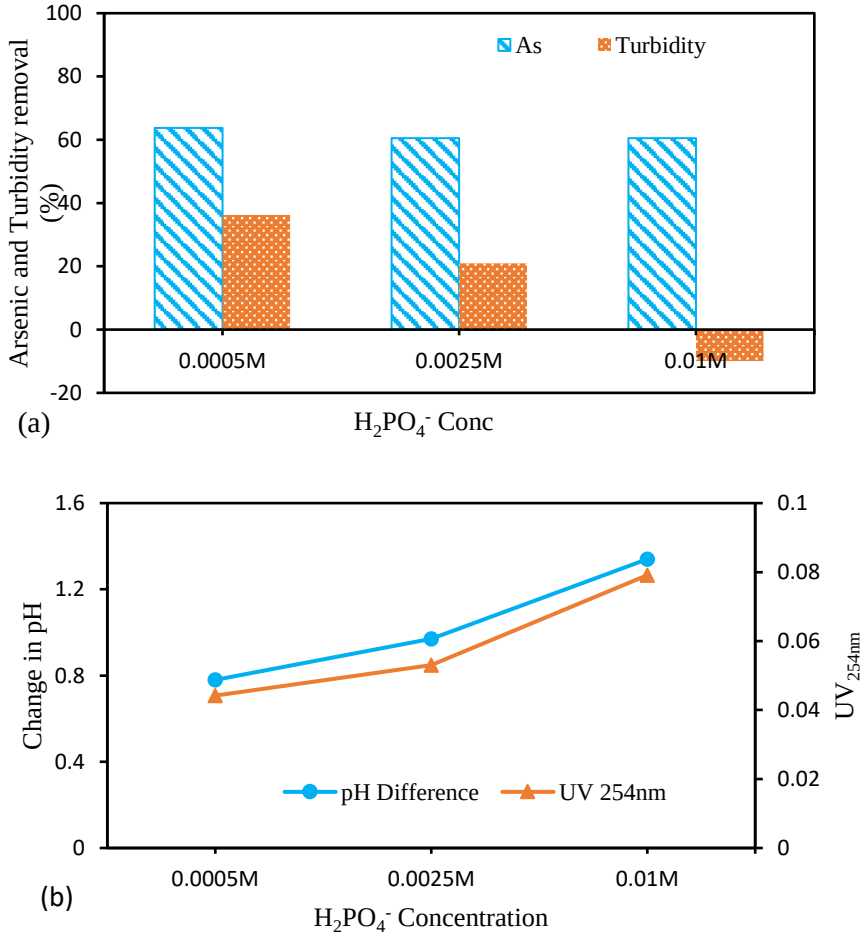

Figure 7-5: Effect of $H_2PO_4^-$ on (a) arsenic and turbidity removal (b) change in pH and UV_{254nm} values

Turbidity removal as shown in Fig 7-5a was significantly influenced by phosphate concentration; the higher the concentration, the higher the turbidity. The maximum turbidity was recorded at 0.5 mM phosphate concentration. There was an increase

in turbidity at 10 mM phosphate concentration due to lack of floc formation. The lack of floc formation can be attributed to the solution containing a high concentration of negatively charged ions (arsenic and phosphate) in the solution which will bond with the positively charged PAC. Increasing phosphate concentration reduced UV_{254nm} removal and result in a higher change in pH (Fig. 7.5b).

7.3.4 Effect of flotation time

Effect of flotation time on arsenic and turbidity removal was determined under the following operating conditions: Rapid mixing (100 rpm, 3 min), mild mixing (30 rpm, 10 min), pH = 8, coagulant dose = 9.4 mg/L and saturated pressure 4 bar (Appendix 7D). There was a slight increase in arsenic removal efficiency with increase in flotation time of 80.42 %, 82.89 % and 82.97 % at a flotation time of 10, 20 and 30 min respectively. The same trend was observed with turbidity removal with a maximum removal efficiency of 39.70 % at 30 min flotation time as compared to 34.35 % at a flotation time of 10 min.

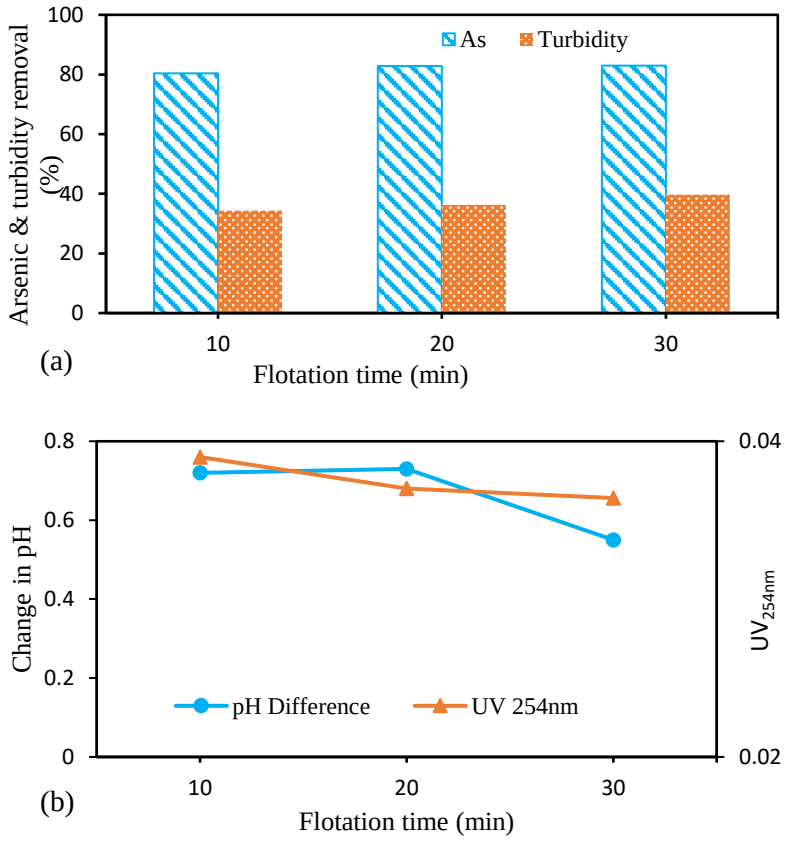

Figure 7-6: Effect of flotation time on (a) arsenic and turbidity removal (b) change in pH and UV_{254nm} values

Fig. 7-6b showed a decrease in pH for all the flotation times from pH 8 to 7.28, 7.27 and 7.45 at flotation times of 10, 20 and 30 min respectively. There was a slight increase in UV_{254nm} removal efficiency (Fig. 7-6b) with an increased flotation time from 36.89 % (10 min flotation time) to 41.10 % (30 min flotation time).

7.3.5 Effect of saturation pressure

Fig. 7-7a shows the effects of saturated pressure on arsenic and turbidity removal efficiency at the following operating conditions: Rapid mixing (100 rpm, 3 min), mild mixing (30 rpm, 10 min), pH = 8, coagulant dose = 9.4 mg/L and flotation time = 10 min (Appendix 7E). Arsenic removal efficiency increased slightly with increase in saturated pressure from 82.82 % (2 bar) to 84.29 % (4 bar). Increase in saturation pressure resulted in a slight decrease in turbidity removal from 37.79 % (2 bar) to 35.88 % (4 bar). The increase in pressure showed a decrease in pH from the initial pH 8 to 7.18 (2 bar), 7.32 (3 bar) and 7.27 (4 bar). The amount of UV_{245nm} remain relatively unchanged at 43.36 % (2 bar), 43.20 (3 bar) and 42.07 % (4 bar).

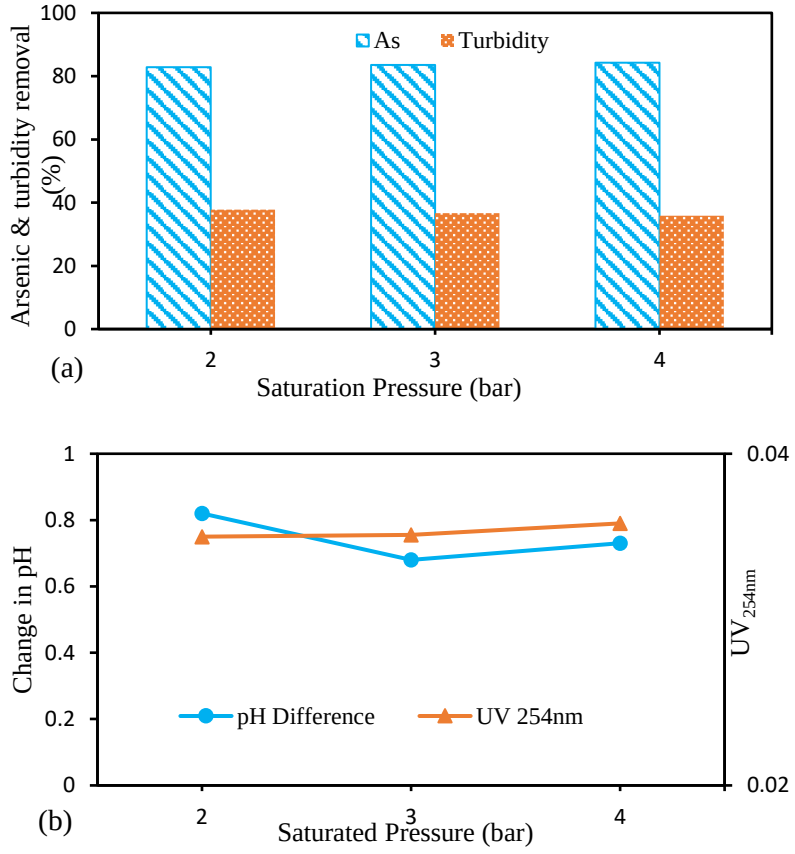

Figure 7-7: Effect of saturation pressure on (a) arsenic and turbidity removal (b) change in pH and UV_{254nm} values

7.3.6 Impact of change in pH in separating arsenic

The performance of change of pH on arsenic separation in a 2-stage batch DAF system (in terms of arsenic, turbidity, UV_{254nm} and final pH) is illustrated in Fig. 7-8 (Appendix 7F).

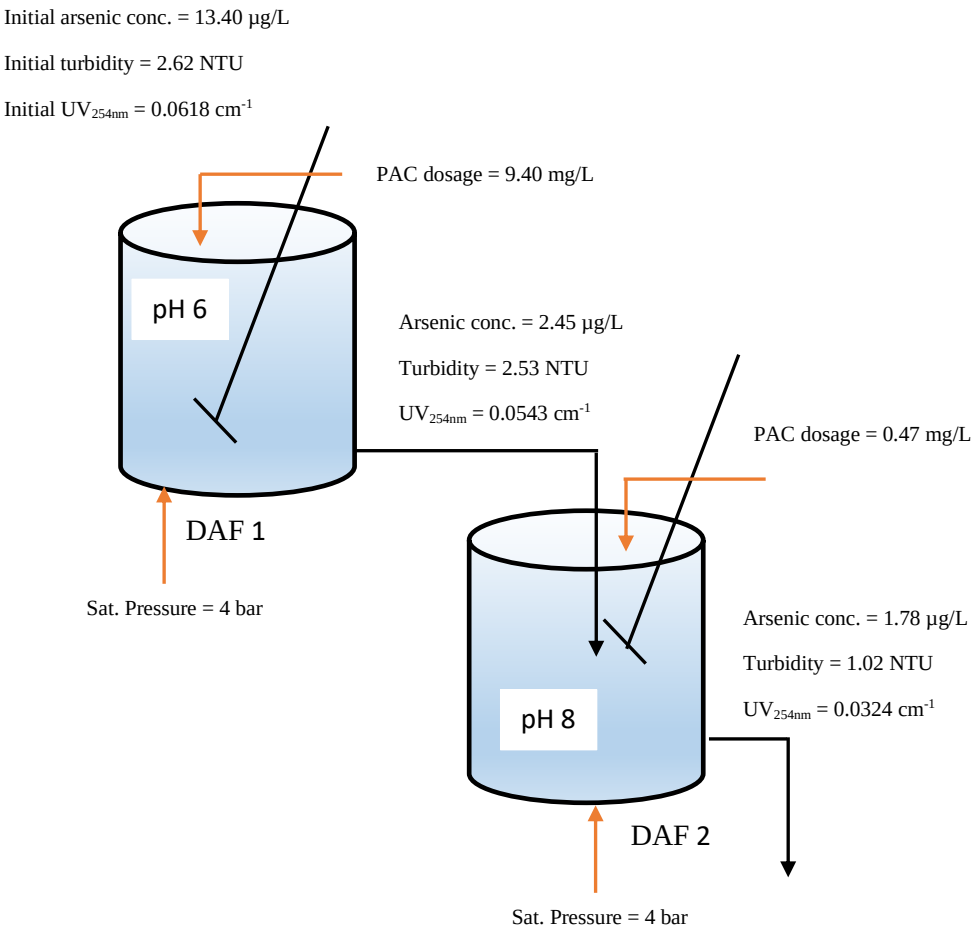

Figure 7-8: Schematic diagram of a 2-stage batch DAF process

Fig. 7-9a illustrates that 81.71 % and 3.44 % of arsenic and turbidity was removed respectively in DAF 1 when the process was operated at pH 6, coagulant dose of 9.40 mg/L and saturation pressure of 4 bar. There was a slight decrease in the value of UV_{254nm} from 0.0618 to 0.0543 cm^{-1}. A slight increase in the final pH of the solution from 6 to 6.19 was recorded. At pH 6, majority of the arsenic was removed at the top (1 cm) while the remaining water solution remained turbid. Increasing the pH of the remaining turbid solution to pH 8 at different coagulant dosage (PAC = 0, 0.47, 0.94, 1.41 and 1.88 mg/L), resulted in bigger floc formation than when the pH of the contaminated water was pH 6. When PAC was added (0.47 mg/L), Table 7-2 showed that arsenic concentration further reduced from 2.45 µg/L to 1.78 µg/L

(percentage removal = 27.42 %) and there is a significant reduction in turbidity from 2.84 NTU to 1.02 NTU (percentage removal = 64.08 %).

Table 7-2: Effect of change of pH in separating arsenic in a 2-stage batch DAF system

Parameters	pH 6	Coagulant dose (mg/L)			pH 8	
		0	0.47	0.94	1.41	1.88
As removal (%)	81.71	11.46	27.41	23.46	34.39	40.76
Turbidity removal (%)	3.44	56.69	64.08	57.04	55.28	52.46
UV_{254nm} (cm^{-1})	0.0543	0.0303	0.0324	0.0340	0.0312	0.0345
Final pH	6.19	7.67	7.59	7.57	7.42	7.12

This indicates that arsenic removal is affected by pH and dosage in a batch DAF process using PAC. The results obtained in this study prove that arsenic can be separated from other contaminants using PAC by changing the pH of the solution and optimising coagulant dosage.

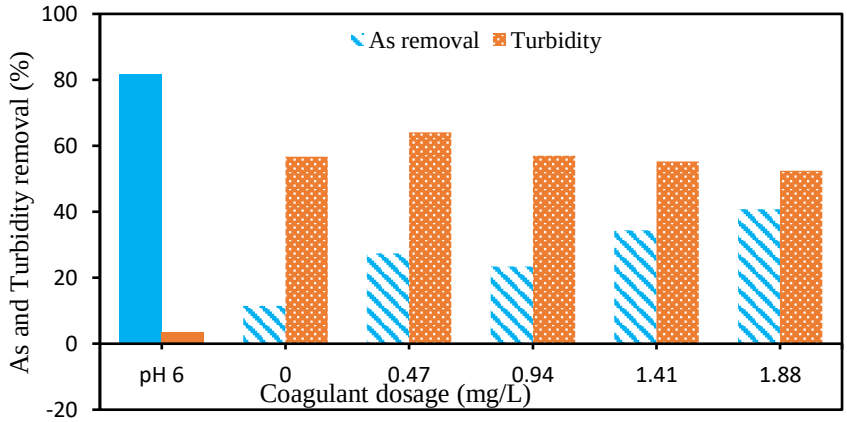

(a)

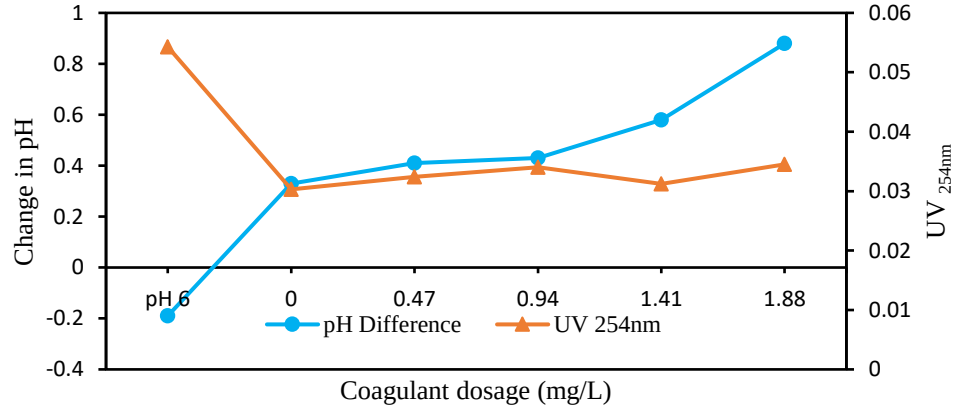

(b)

Figure 7-9: Effect of in pH from 6 to 8 on (a) arsenic and turbidity removal (b) change in pH and UV_{254nm} values.

7.4 Suggested modification to Hamilton Water Treatment Plant

Fig. 7-10 showed the current treatment process of the Hamiton Water Treatment plant. During the winter, approximately 60,000 m^3/day of drinking water is processed at the treatment plant while approximately 90,000 m^3/day is processed during the summer. To assist in settling, alum and polymer are the chemicals used as coagulant and flocculant respectively. In order to separate arsenic from other contaminants, it is suggested that a DAF system be installed before sedimentation as shown in Fig. 7-11. This process (DAF1) would operate at a pH 6, PAC dose of 9.4 mg/L and remove upto 0.96 kg of arsenic per day which would have otherwise been removed at the sedimentation tanks and sent to the wastewater treatment plant (WWTP). The remaining 76,500 m^3/day of treated water which is high in turbidity (2.53 NTU) and low in arsenic concentration (0.22 kg/day) move to the sedimentation tank for further processing. Arsenic removed can be further treated using an adsorbent such as DMI-65 which as been shown to remove arsenic over a wide pH range and can be regenerated. Fig. 7-12 showed two DAFs operating in parallel to separate arsenic from other contaminants. DAF2 operates at pH 8, PAC dose of 0.47 mg/L. This process further removes 0.06 kg/day of arsenic. Only 0.16 kg/day of arsenic is been sent to the WWTP as against the current 0.942 kg/day. That represents 83.01 % reduction in the amount of arsenic that is sent to the WWTP from the WTP per day. This would result in the WWTP biosolids being given a B grade rating. Fig. 7-13 showed a suggested site for DAF installation and a possibility of modifying the exiting sedimentation tank to incorporate two DAFs systems for target separation of arsenic from contaminated drinking water. Table 7-3 showed the different specifications and costs required to install the DAF system(s).

7.5 Conclusions

The conclusions obtained in this research for the experimental conditions studied were as follows:

- Target separation of arsenic from a contaminated drinking water was investigated in this study using a batch DAF process. Polyaluminium chloride (PAC) was used as coagulant throughout this study.
- Lab-scale DAF studies showed that the separation of arsenic from other contaminants in a contaminated drinking water was affected by pH, coagulant dose, saturation pressure, flotation time and phosphate concentration.
- For DAF 1, the optimum separation based on the results was obtained for a saturation pressure of 4 bar, pH of 6 and PAC concentration of 9.40 mg/L. The removal efficiencies of 81.71 % (arsenic), 3.44 % (turbidity) and 12.14 % (UV_{254nm}) was reached.
- For DAF 2, the optimum separation based on the results was obtained for a saturation pressure of 4 bar, pH of 8 and PAC concentration of 0.24 mg/L. The removal efficiencies of 27.42 % (arsenic), 64.08 % (turbidity) and 40.33 % (UV_{254nm}) was reached.
- This study has proven that a 2 stage - DAF process is effective in separating arsenic from other contaminants. This process reduces the amount of arsenic currently going to WWTP from 0.942 kg/day to 0.16 kg/day.

Appendix 7. Supplementary data

- This contains experimental data for effect of coagulant dosage, pH, $H_2PO_4^-$, flotation time and saturation point.
- It contains data for calculating DAF size, saturator size, compressor size and cost of each.

Declaration of Competing Interest

None

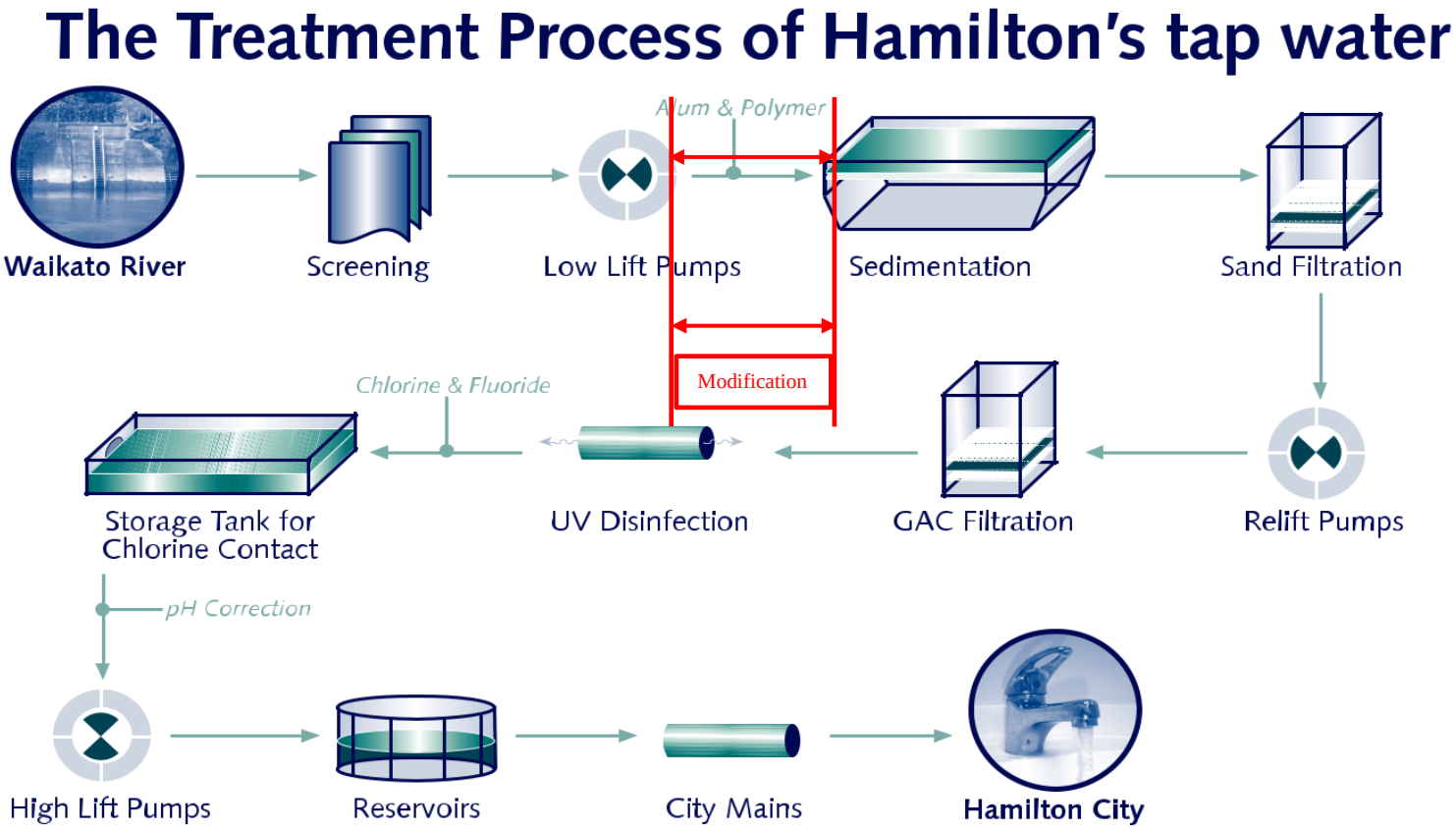

Figure 7-10: The Treatment process of Hamilton`s water treatment plant (Source: Hamilton City Council)

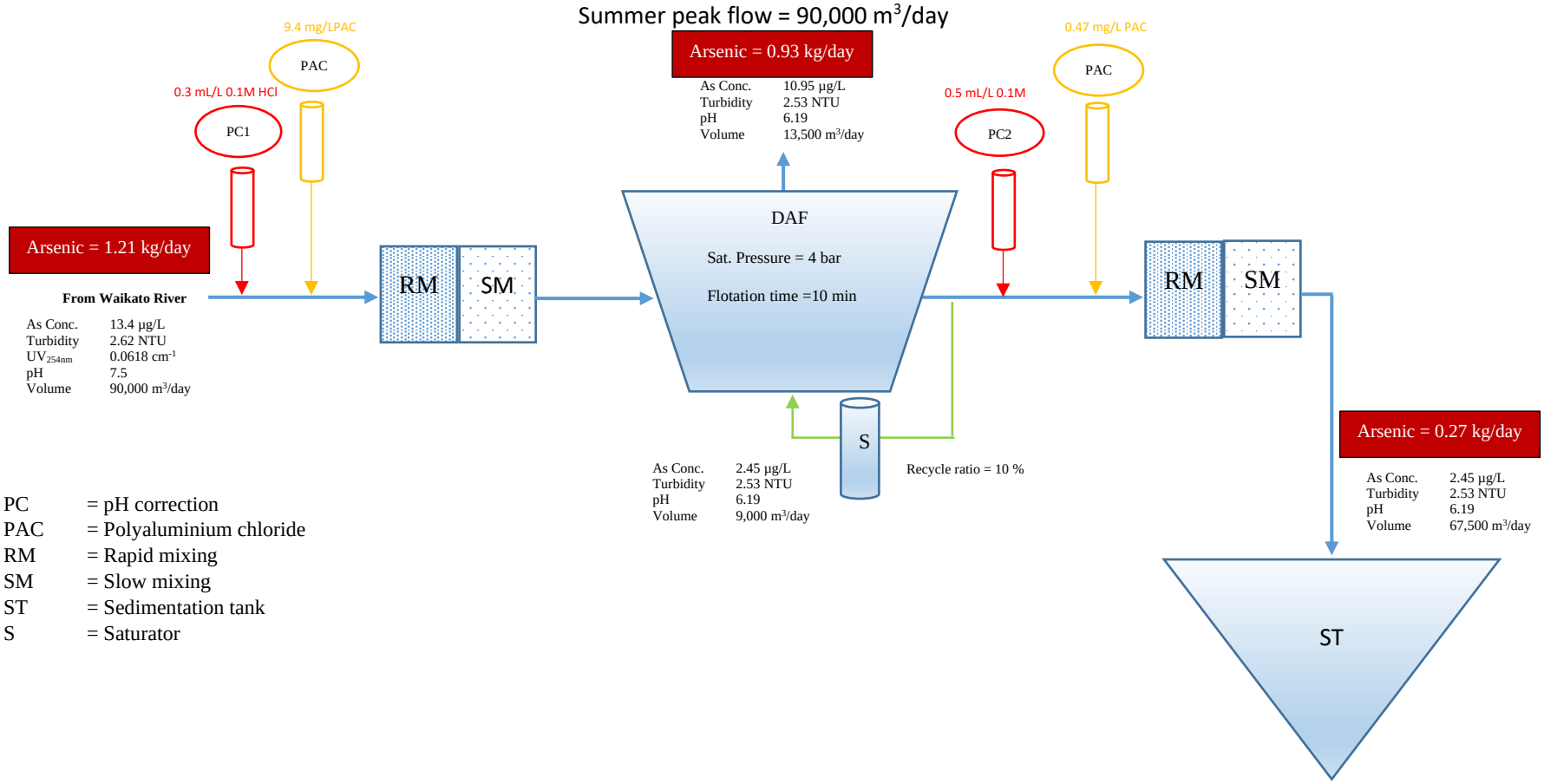

Figure 7-11: Suggested modification to Hamilton`s water treatment plant (DAF before sedimentation)

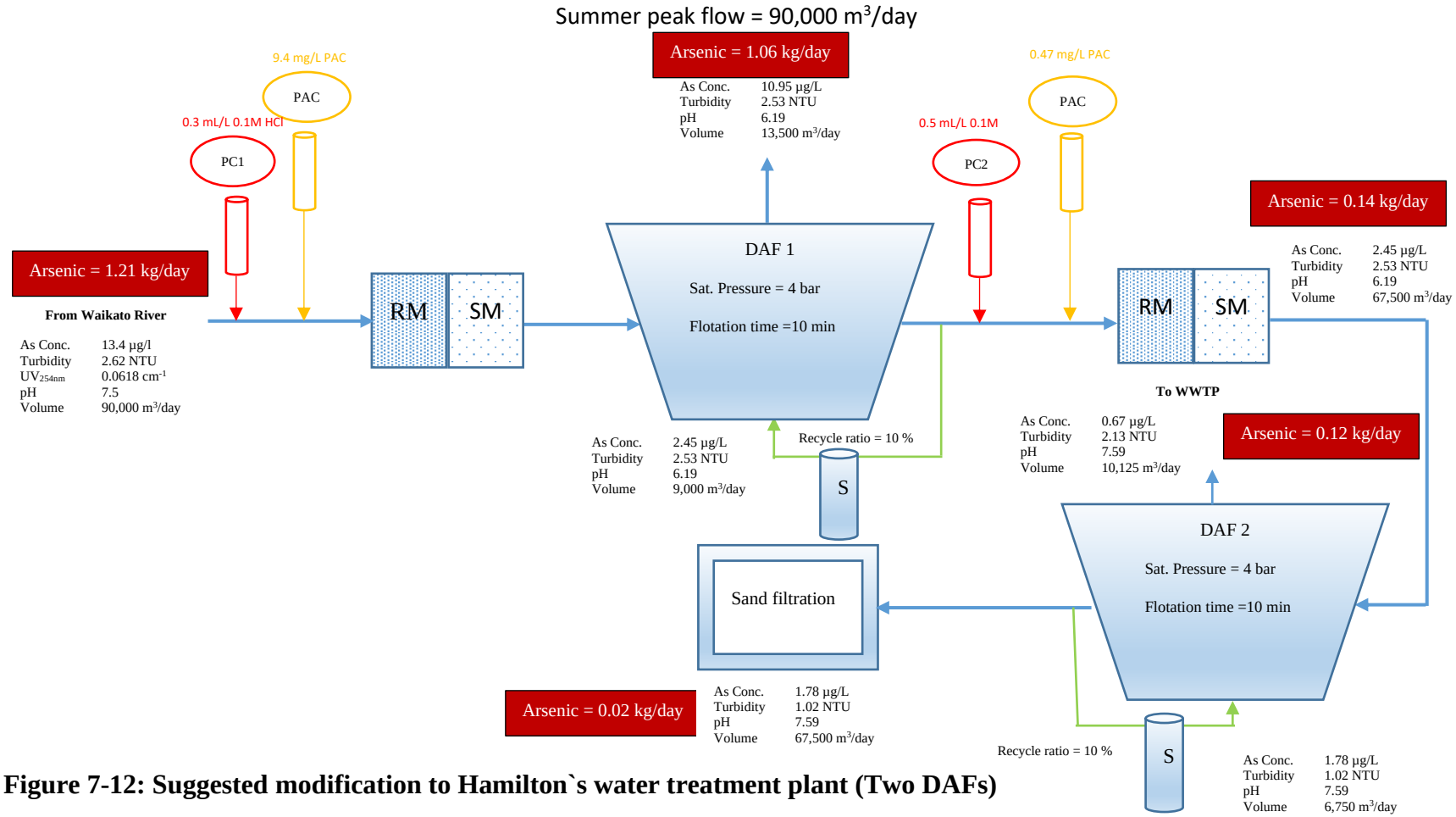

Figure 7-12: Suggested modification to Hamilton`s water treatment plant (Two DAFs)

Figure 7-13: Suggested site for the DAF system and a possible modification to the sedimentation tank (Source: Google map).

Table 7-3: Design specification and cost calculation required for plant modification

Parameters	Specification	Cost ($)
DAF Tank. Included in this price is: - Rectangular flotation tank - Dissolved air system - Feed pumps - Acid dosing and control - Process pipework - Acid storage tank - Foundation - Sludge tank and pumps - Electrical and automation - Installation	(5 X (20 X 2.5 X 3.5) m	7,500,000
Total PAC needed (PAC1 & PAC2) (kg/day)	88.3	30
Mass of NaOH required per day (kg)	180	1,260
Volume of HCl needed per day conc. 37 % (L)	217.91	872
Volume of H_2SO_4 needed per day Conc. 98 % (L)	72	650.88

Air to solid ratio (mg/mg)	0.02255
Volume of air needed DAF1 (m^3/day)	26.95
Volume of air needed DAF2 (m^3/day)	10.19
Air compressor power needed (kW), efficiency 78 % (DAF1 & DAF2)	20
Volume (DAF1 & DAF2) (m^3)	625
Pump size (DAF1), Shaft Power (kW)	5.11
Pump size (DAF2), Shaft Power (kW)	3.83

Calculations are shown in Appendix 7

References

Al-Thyabat, S., Al-Zoubi, H., 2012. Purification of phosphate beneficiation wastewater: Separation of phosphate from Eshydia Mine (Jordan) by column-DAF flotation process. Int. J. Miner. Process. 110–111, 18–24. https://doi.org/10.1016/j.minpro.2012.03.006

Al-Zoubi, H., Ibrahim, K.A., Abu-Sbeih, K.A., 2015a. Removal of heavy metals from wastewater by economical polymeric collectors using dissolved air flotation process. J. Water Process Eng. 8, 19–27. https://doi.org/10.1016/j.jwpe.2015.08.002

Al-Zoubi, H., Ibrahim, K.A., Abu-Sbeih, K.A., 2015b. Removal of heavy metals from wastewater by economical polymeric collectors using dissolved air flotation process. J. Water Process Eng. 8, 19–27. https://doi.org/10.1016/j.jwpe.2015.08.002

Amaral Filho, J., Azevedo, A., Etchepare, R., Rubio, J., 2016. Removal of sulfate ions by dissolved air flotation (DAF) following precipitation and flocculation. Int. J. Miner. Process. 149, 1–8. https://doi.org/10.1016/j.minpro.2016.01.012

Chen, A.S.C., Fields, K.A., Sorg, T.J., Wang, L., 2002. Field Evaluation of As Removal by Conventional Plants. J. - AWWA 94, 64–77. https://doi.org/10.1002/j.1551-8833.2002.tb09540.x

de Nardi, I.R., Fuzi, T.P., Del Nery, V., 2008. Performance evaluation and operating strategies of dissolved-air flotation system treating poultry slaughterhouse wastewater. Resour. Conserv. Recycl. 52, 533–544. https://doi.org/10.1016/j.resconrec.2007.06.005

Edzwald, J.K., 2007. Developments of high rate dissolved air flotation for drinking water treatment. J. Water Supply Res. Technol.-Aqua 56, 399–409. https://doi.org/10.2166/aqua.2007.013

Etchepare, R., Oliveira, H., Azevedo, A., Rubio, J., 2017. Separation of emulsified crude oil in saline water by dissolved air flotation with micro and nanobubbles. Sep. Purif. Technol. 186, 326–332. https://doi.org/10.1016/j.seppur.2017.06.007

Ghosh (Nath), S., Debsarkar, A., Dutta, A., 2019. Technology alternatives for decontamination of arsenic-rich groundwater—A critical review. Environ. Technol. Innov. 13, 277–303. https://doi.org/10.1016/j.eti.2018.12.003

Gregor, J., 2001. Arsenic removal during conventional aluminium-based drinking-water treatment. Water Res. 35, 1659–1664. https://doi.org/10.1016/S0043-1354(00)00424-3

Guo, K., Gao, B., Tian, X., Yue, Q., Zhang, P., Shen, X., Xu, X., 2019. Synthesis of polyaluminium chloride/papermaking sludge-based organic polymer composites for removal of disperse yellow and reactive blue by flocculation. Chemosphere 231, 337–348. https://doi.org/10.1016/j.chemosphere.2019.05.138

Hu, C., Liu, H., Chen, G., Qu, J., 2012. Effect of aluminum speciation on arsenic removal during coagulation process. Sep. Purif. Technol. 86, 35–40. https://doi.org/10.1016/j.seppur.2011.10.017

Hughes, M.F., 2002. Arsenic toxicity and potential mechanisms of action. Toxicol. Lett. 133, 1–16. https://doi.org/10.1016/S0378-4274(02)00084-X

Karagüzel, C., 2010. Selective separation of fine albite from feldspathic slime containing colored minerals (Fe-Min) by batch scale dissolved air flotation (DAF). Miner. Eng. 23, 17–24. https://doi.org/10.1016/j.mineng.2009.09.002

Kordmostafapour, F., Pourmoghadas, H., Shahmansouri, M.R., Parvaresh, A., 2006. Arsenic Removal by Dissolved Air Flotation. J. Appl. Sci. 6, 1153–1158.

Pereira, M. dos S., Borges, A.C., Heleno, F.F., Squillace, L.F.A., Faroni, L.R.D., 2018. Treatment of synthetic milk industry wastewater using batch dissolved air flotation. J. Clean. Prod. 189, 729–737. https://doi.org/10.1016/j.jclepro.2018.04.065

Sinha, S., Yoon, Y., Amy, G., Yoon, J., 2004. Determining the effectiveness of conventional and alternative coagulants through effective characterization schemes. Chemosphere 57, 1115–1122. https://doi.org/10.1016/j.chemosphere.2004.08.012

Teixeira, M.R., Rosa, M.J., 2007. Comparing dissolved air flotation and conventional sedimentation to remove cyanobacterial cells of Microcystis aeruginosa: Part II. The effect of water background organics. Sep. Purif. Technol. 53, 126–134. https://doi.org/10.1016/j.seppur.2006.07.001

Wu, K., Wang, H., Liu, R., Zhao, X., Liu, H., Qu, J., 2011. Arsenic removal from a high-arsenic wastewater using in situ formed Fe–Mn binary oxide combined with coagulation by poly-aluminum chloride. J. Hazard. Mater. 185, 990–995. https://doi.org/10.1016/j.jhazmat.2010.10.003

Younker, J.M., Walsh, M.E., 2014. Bench-scale investigation of an integrated adsorption–coagulation–dissolved air flotation process for produced water treatment. J. Environ. Chem. Eng. 2, 692–697. https://doi.org/10.1016/j.jece.2013.11.009

Zhang, Q., Liu, S., Yang, C., Chen, F., Lu, S., 2014. Bioreactor consisting of pressurized aeration and dissolved air flotation for domestic wastewater treatment. Sep. Purif. Technol. 138, 186–190. https://doi.org/10.1016/j.seppur.2014.10.024

Zouboulis, A.I., Tzoupanos, N.D., 2009. Polyaluminium silicate chloride—A systematic study for the preparation and application of an efficient coagulant for water or wastewater treatment. J. Hazard. Mater. 162, 1379–1389. https://doi.org/10.1016/j.jhazmat.2008.06.019

CHAPTER EIGHT

Summary, Conclusions and Recommendations for Future Work

8.1 Summary

Arsenic is known to be one of the most toxic and carcinogenic elements known to have affected millions of people worldwide. Arsenic in surface and groundwater originates from both natural and anthropogenic sources. Prolonged exposure to arsenic can lead to skin disease, cancer, diabetes and cardiovascular disease. The purpose of this work was to investigate separation of arsenic from contaminated water using the adsorption and coagulation/flocculation/dissolved air flotation (C/F/DAF) processes.

DMI-65 is a silica based catalytic media, traditionally designed to remove iron and manganese from raw water. In this thesis, the focus was to investigate the effectiveness of DMI-65 in removing arsenic in a batch and a fixed-bed adsorption column. Three different kinetic models were applied to determine the kinetic data for arsenic adsorption onto DMI-65. The models are the pseudo first-order, pseudo second-order and Elovich kinetic models. Experimental results showed that both As (III) and As (V) both followed the pseudo second-order kinetic model and equilibrium was reached after 5 hr and 6 hr for As (III) and As (V) removal respectively. Results showed that the maximum adsorption capacity for As (III) and As (V) are 0.318 mg/g and 0.237 mg/g respectively. Thermodynamic analysis showed that the adsorption process was spontaneous and endothermic in nature. The maximum removal efficiency for As (III) was 96.55 % at pH 5 and 90.40 % for As (V) at pH 8.5. Regeneration studies carried out showed that DMI-65 can be regenerated using sodium hydroxide (NaOH) solution and be reused for several cycles. Furthermore, DMI-65 operates over a wide pH range thereby making it suitable for arsenic removal in drinking water.

Designing an adsorption column process requires prediction of the breakthrough curve for the effluent. Thomas, Yoon-Nelson, Adams-Bohart and Clark models were used to identify the best model for predicting the dynamic behaviour of the fixed-bed column. Results showed that both Thomas and Yoon-Nelson models could be used for scaling up and optimising the performance of a continuous fixed-bed adsorption process. DMI-65 used as the adsorbent in this study successfully removed arsenic from the Waikato River water sample to levels below the recommended value of 10 µg/L set by World Health Organisation (WHO), United States Environmental Protection Agency (US EPA) and Drinking Water Standards

of New Zealand (DWSNZ). Fouling of the column is one of the major setbacks in removing arsenic from the Waikato River water sample for all the flowrates studied which resulted in significant pressure drop through the adsorption column.

Polydiallyldimethylammonium chloride (polyDADMAC) and Chitosan from crab shell were used as coagulants in comparing arsenic removal from a coagulation/flocculation/sedimentation (C/F/S) and C/F/DAF process. Both coagulants and processes recorded a low arsenic removal efficiency for all the pH and coagulant doses considered in this study. However, turbidity removal effcicency was higher for both coagulants. This therefore suggested that using polyDADMAC and Chitosan from crab shell alone is not sufficient for removing arsenic from contaminated drinking water.

Adsorbents are vulnerable to chemical interferences that inhibit arsenic removal from contaminated water. Most of the competing ions in natural waters are in the form of organic anions such as nitrate (NO_3^-), silicate (SiO_4^{4-}), sulfate (SO_4^{2-}), bicarbonate (CO_3^{2-}) and phosphate ($H_2PO_4^-$). These anions compete for adsorption sites with arsenic and are also influenced by solution pH, anion concentration and binding affinity. The anions considered in this study ($H_2PO_4^-$, CO_3^{2-} , NO_3^- and SO_4^{2-}) all interfere in arsenate (As (V)) removal by using polyaluminium chloride (PAC) as a coagulant. The phosphate anion recorded the most significant interference in the removal of As (V) at pH 6. Overall, the major impact of the competing anions on As (V) removal followed the following order of $H_2PO_4^- > CO_3^{2-} > NO_3^- > SO_4^{2-}$. Findings from this study showed that correct determination of coagulant dose, pH and anionic strength can be successfully used in separating As (V) from other contaminants. This separation can be in the form of a two-stage separation process whereby the first unit operation removes As (V) and the other unit operation removes other contaminants such as suspended solids. Applying a two-stage separation process will also reduce the concentration of arsenic in biosolids at the wastewater treatment plant which could instead find application in agriculture because the biosolids would be rated as grade B.

In order to separate arsenic from other contaminants in a contaminated water, the effect of coagulant dose, pH, saturation pressure, flotation time and effect of phosphate anion was investigated. Experimental results revealed that at pH 6 using

PAC as coagulant in a C/F/DAF process, arsenic can successfully be separated from other contaminants in a two stage C/F/DAF process. Arsenic removal efficiency is higher in the first stage, while the second stage records high turbidity removal efficiency. Overall, the two stage C/F/DAF process is capable of reducing the amount of arsenic sent to the WWTP from the WTP by 83.01 % from the current 0.942 kg/day to 0.16 kg/day. With this significant reduction in the amount of arsenic leaving the WTP, the biosolids at the WWTP can therefore found application in agriculture instead of going to landfill.

8.2 Conclusions

The primary objective of this work was to address the existing technology gap in the water and wastewater industry by investigating arsenic separation from other contaminants from a contaminated drinking water. With respect to this objective, this research:

1. Demonstrated that DMI-65 was effective in removing arsenic from a contaminated drinking water in a batch and continuous fixed-bed reactor.
2. Showed that using polyDADMAC and chitosan from crab shell alone as coagulants were not sufficient to remove arsenic to a level recommended by WHO, US EPA and DWSNZ in both C/F/S and C/F/DAF processes.
3. Established that phosphate anions interfere with arsenic removal in a C/F/DAF process.
4. Demonstrated that increasing the flotation time and saturation pressure in a C/F/DAF process does not result in significant arsenic removal efficiency.
5. Showed that arsenic can be separated from other contaminants in a two stage C/F/DAF process.

8.3 Limitations of this Study

Below are the limitations of this study

1. Arsenic speciation was not considered in this study.
2. This study was not applied on pilot/large scale application. Other issues that was not considered include
    a. Pressure drop across the column,
    b. Concentrations of arsenic while backwashing,

c. Upward column operating conditions and performance at different bed depths.
d. Concentration of arsenic and volume of sludge from the first DAF process.

3. Polyaluminum chloride was the only coagulant that was evaluated in separating arsenic from other contaminants. Aluminium sulphate which is the coagulant used at the Hamilton WTP was not evaluated.
4. Other parameters such as DOC, SUVA, taste and odour and chlorophyll a, was not considered in this study.

8.4 Recommendation for Future Work

The following are recommendations for further research:

1. **Mechanism of adsorption of As (III) and As (V) on DMI-65**

This thesis addressed the batch/column adsorption of arsenic onto DMI-65. Adsorption kinetics, isotherm, thermodynamics studies and regeneration studies were conducted using both synthetic natural source of water. A further study on the reaction mechanism involved in the removal of As (III) and As (V) before and after adsorption would be beneficial.

2. **Treatment evaluation of filtration – adsorption process**

Fouling of the adsorption column was one of the major challenges observed during arsenic removal from contaminated drinking water using DMI-65 as adsorbent. A study to evaluate filtration as a pre-treatment in a filtration-adsorption process would be necessary to determine if removing other contaminants at the filtration stage would solve the fouling problem in the fixed-bed adsorption column. In order to have a better understanding of the column adsorption process, a study of effect of bed depth and initial concentration on breakthrough curve would be required. Futher work on pilot scale systems would be required to determine the pressure drop during operation through the columns and extent of fouling if it was installed prior to flocculation and clarification. Different modes of operation could be investigated such as upflow expanded bed adsorption to reduce fouling issues, otherwise if flocculation and clarifications were able to be developed by which the solids could be removed without the arsenic, the columns could be installed

between the sand filters and the activated carbon filters. Alternatively, the DMI-65 media could also be used in the filter beds.

3. Investigation of other coagulants and adsorbents

Current work investigated the use of the following coagulants (polyDADMAC, PAC and Chitosan from crab shell) to remove arsenic in a C/F/DAF process. Further studies looking at the possibility of removing arsenic using environmentally friendly coagulants from contaminated water is required. DMI-65 is a silica based catalytic media primarily designed to remove iron and manganese from drinking water. This study has shown that it can successfully remove arsenic to levels below values recommended by WHO, US EPA and DWSNZ. Further studies should be conducted on commercially available adsorbent to determine their arsenic removal efficiencies.

This study has demonstrated that arsenic can be separated from other contaminants in a two-stage C/F/DAF process. It would be necessary to determine the possibility of using other technologies to separate arsenic from other contaminants. This would go a long way in reducing the amount of arsenic in the biosolids at the wastewater treatment plant.

4. Scaling up of coagulation/flocculation/dissolved air flotation

All the experiments in this study were conducted in the laboratory rather than on pilot scale. As such, scaling up the process of separating arsenic from other contaminants in a continuous process rather than in a batch process would be beneficial. Having a better understanding of the performance of the saturator in terms of knowing the bubble sizes on DAF performance would assist in improving the overall performance of the process. Further study should be conducted to determine the overall effect of recycle ratio on the performance of the C/F/DAF in separating arsenic from other contaminants in a continuous process. Impact of such modification(s) to the existing structure need to be assessed in detail.

APPENDICES

APPENDIX 2A: (Section 2.4; Table 2.3)

(a) Groundwater sampling locations (b) Concentrations of arsenic in Waikato groundwater samples.

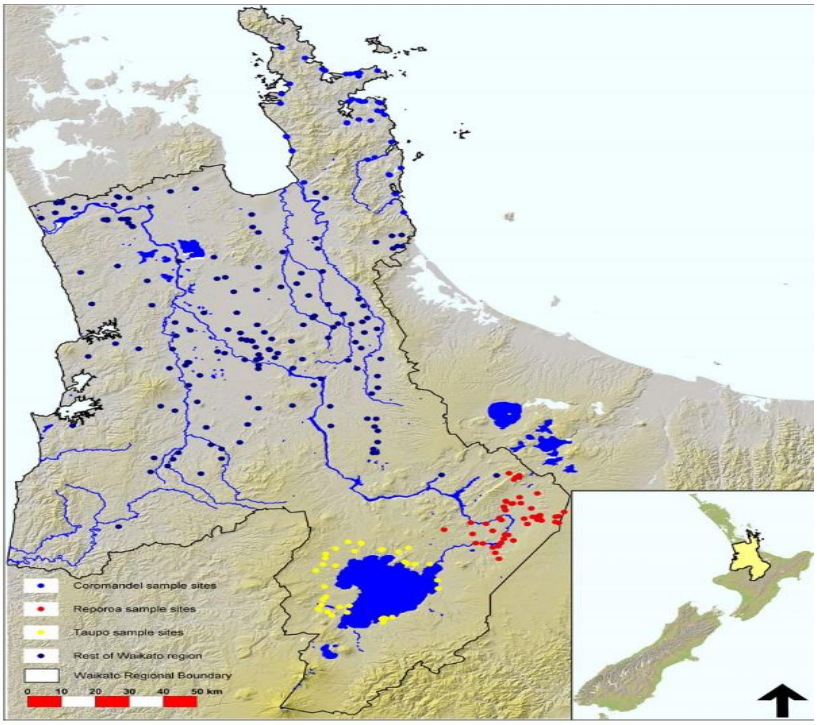

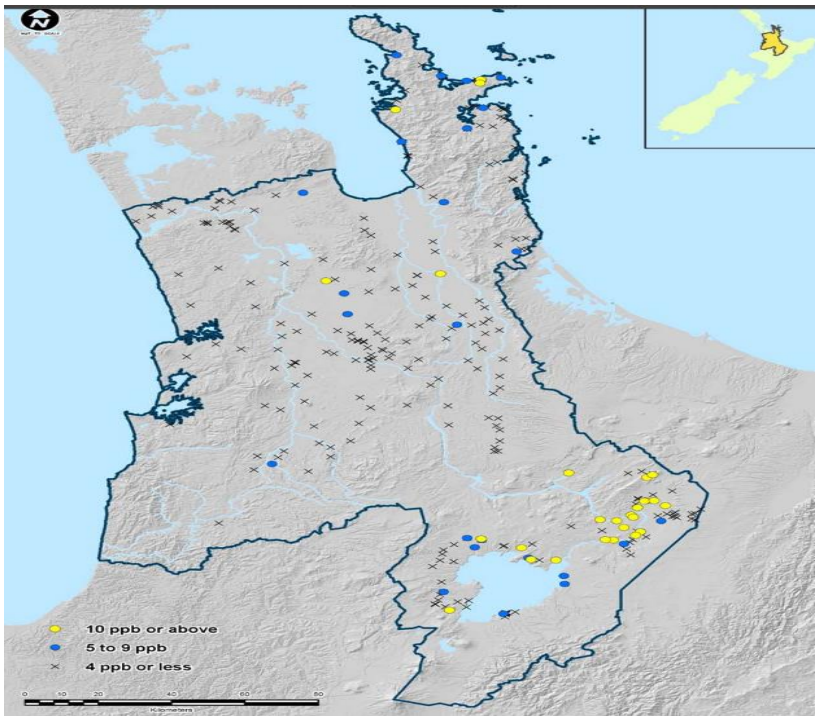

APPENDIX 2B: (Section 2.5)

The ATSDR 2017 Substance Priority List

2017 Rank	Substance Name	Total Points	CAS RN
1	Arsenic	1674	7440-38-2
2	Lead	1531	7439-92-1
3	Mercury	1458	7438-97-6
4	Vinyl Chloride	1358	75-01-4
5	Polychlorinated Biphenyls	1345	1336-36-3
6	Benzene	1329	71-43-2
7	Cadmium	1320	7440-43-2
8	Benzo(A)Pyrene	1306	50-32-8
9	Polycyclic aromatic hydrocarbons	1279	130498-29-2
10	Benzo(B)Fluoranthene	1251	205-99-2
11	Chloroform	1203	67-66-3
12	Aroclor 1260	1191	11096-82-5
13	DDT, P, P`-	1183	50-29-3
14	Aroclor 1254	1172	11097-69-1
15	Dibenzo(A,H)Anthracene	1156	53-70-3
16	Trichloroethylene	1155	79-01-6
17	Chromium, Hexavalent	1148	18540-29-9
18	Dieldrin	1144	60-57-1
19	Phosphate, White	1141	7723-14-0
20	Hexachlorobutadiene	1130	87-68-3

APPENDIX 2BA

Below is the general quality control employed using ICP-MS for analysing arsenic concentration:

A five-point calibration curve, consisting of concentrations between 0.1 and 500 ppb was prepared for all trace elements using stock standard IV71-A (Inorganic Ventures, Christiansburg, VA, USA). A separate calibration curve, consisting of concentrations between 100 and 10,000 ppb was prepared for major elements (Ca, Si, P, S, K, Fe) using single-element standards (Inorganic Ventures, Christiansburg, VA, USA). Check standards were analysed every 20 samples and re-calibration was performed every 100 samples. Blank samples were analysed every 10 samples to ensure minimal carryover between samples. An online internal standard containing ^{45}Sc, ^{72}Ge, ^{103}Rh, ^{193}Ir, and ^{205}Tl was used to monitor and correct for instrumental drift and matrix effects.

Chapter Three

Pore size distribution and pore volume of DMI-65 (Section 3.3.1; Table 3.2)

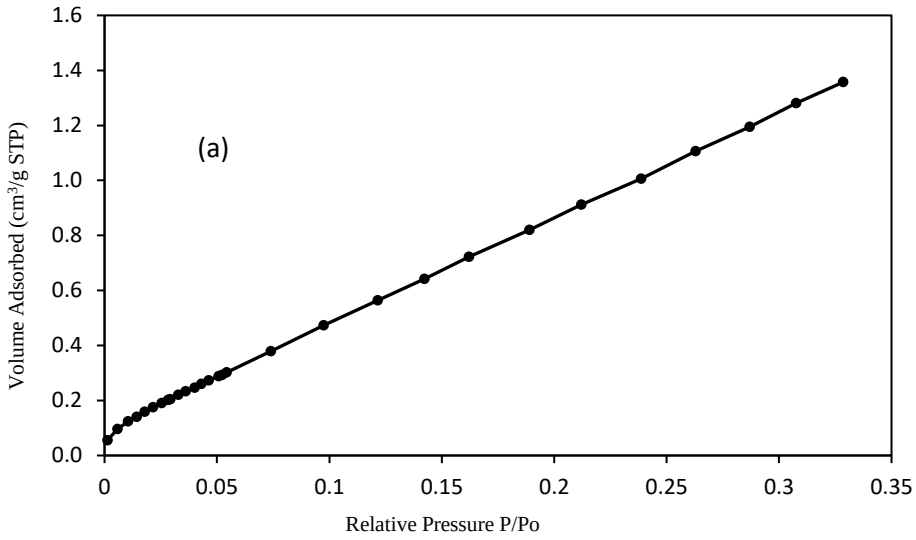

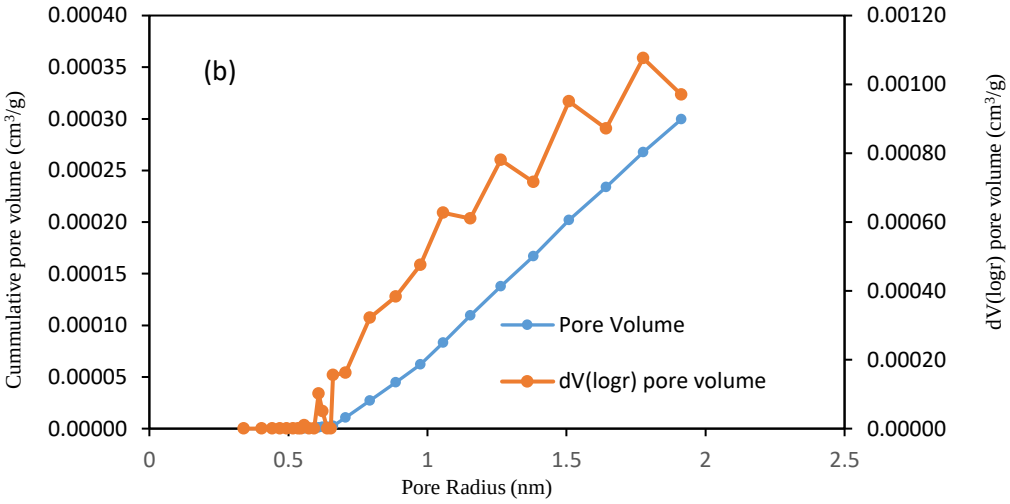

APPENDIX 3A: (a) N_2 adsorption/desorption isotherms (b) pore size distribution and pore volume of raw DMI-65

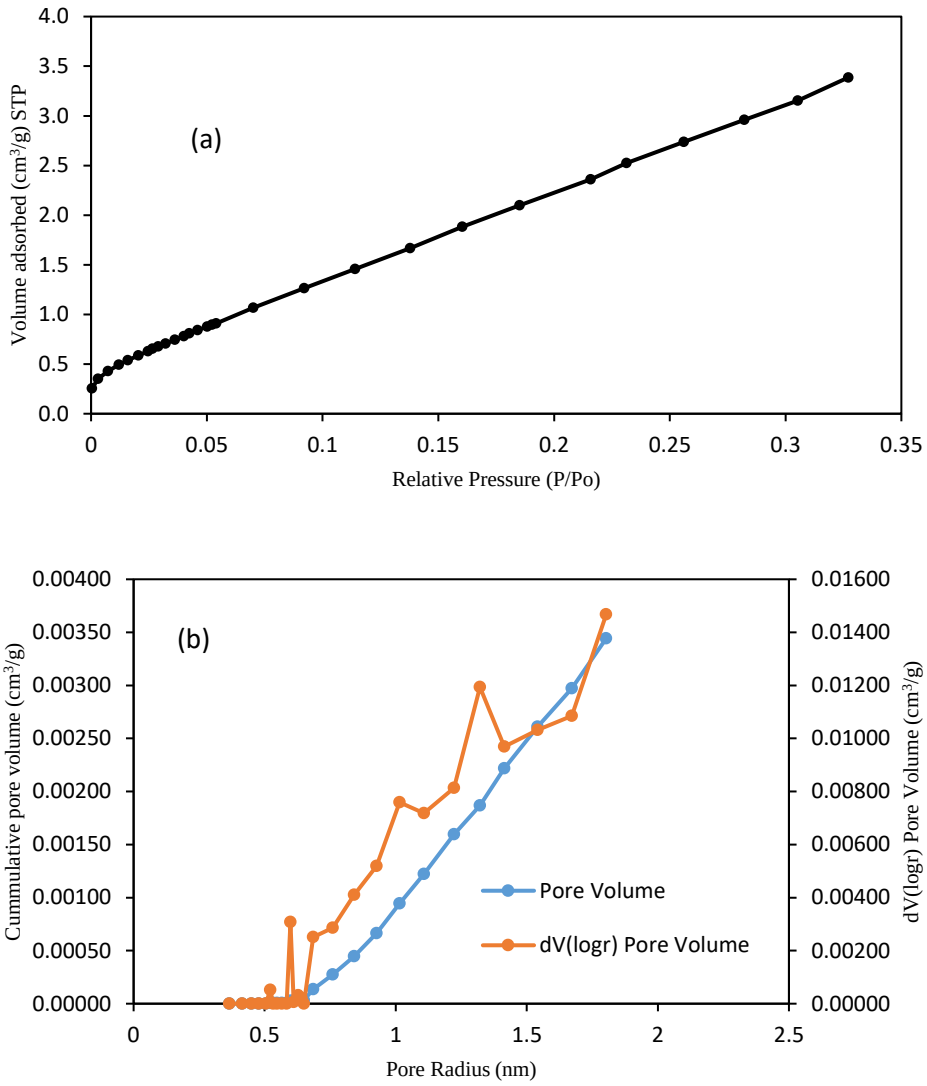

APPENDIX 3B: (a) N_2 adsorption/desorption isotherms (b) pore size distribution and pore volume of activated DMI-65.

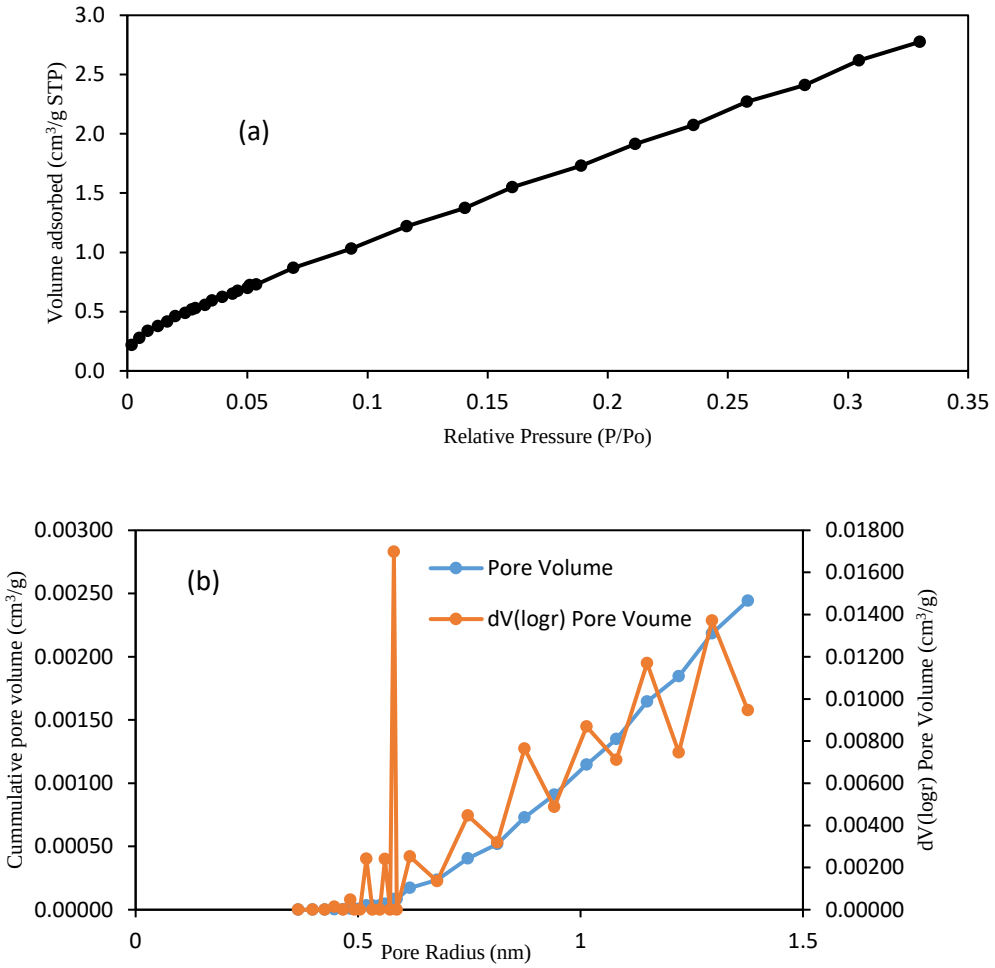

APPENDIX 3C: (a) N_2 adsorption/desorption isotherms (b) pore size distribution and pore volume after contact with As (III).

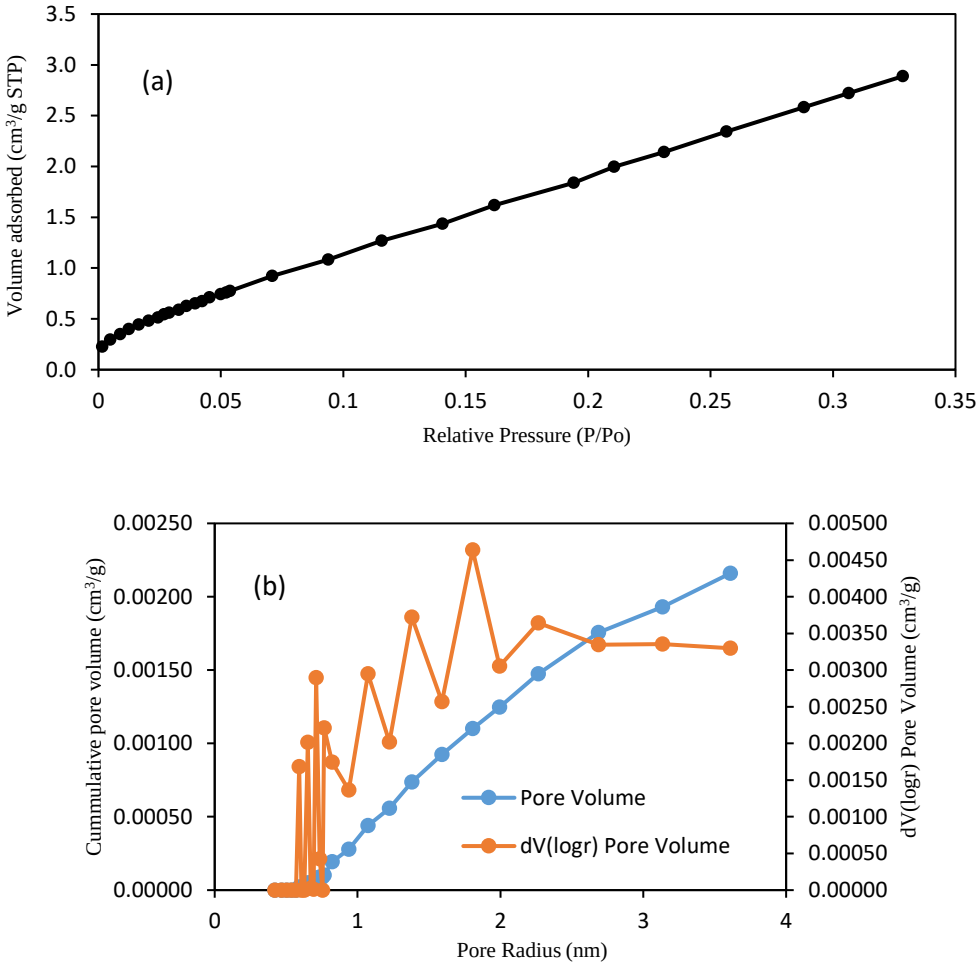

APPENDIX 3D: (a) N_2 adsorption/desorption isotherms (b) pore size distribution and pore volume after contact with As (V).

Surface morphology and EDX (Section 3.3.1; Figure 3.3)

APPENDIX 3F: Raw DMI-65

Element	Element wt. %	Error	Wt. % Atom	Error
C K	16.96	+/- 1.85	29.60	+/- 3.25
O K	29.80	+/- 1.16	39.04	+/- 1.51
Si K	23.62	+/- 0.53	17.63	+/- 0.40
S L	-	-	-	-
S K	2.68	+/- 0.28	1.75	+/- 0.18
Cl L	-	-	-	-
Cl K	5.08	+/- 0.57	3.00	+/- 0.34
K L	-	-	-	-
K K	4.17	+/- 0.59	2.24	+/- 0.32
Mn K	17.68	+/- 1.12	6.75	+/- 0.42
Mn L	-	-	-	-
Total	**100.00**		**100.00**	

APPENDIX 3G: Activated DMI-65

Element	Element wt. %	Error	Wt. % Atom	Error
O K	27.93	+/- 0.95	45.30	+/- 1.54
Al K	0.97	+/- 0.22	0.9	+/- 0.21
Si K	44.72	+/- 0.71	41.31	+/- 0.66
Mn K	26.37	+/- 1.31	12.45	+/- 0.62
Mn L	-	-	-	-
Total	**100.00**		**100.00**	

APPENDIX 3H: DMI-65 + As (III)

Element	Element wt. %	Error	Wt. % Atom	Error
O K	32.34	+/- 1.23	47.40	+/- 1.80
Si K	58.16	+/- 0.85	48.55	+/- 0.71
Mn L	-	-	-	-
Mn K	9.49	+/- 1.23	4.05	+/- 0.52
Total	**100.00**		**100.00**	

APPENDIX 3I: DMI-65 + As (V)

Element	Element wt. %	Error	Wt. % Atom	Error
C K	24.37	+/- 1.98	39.43	+/- 3.23
O K	27.77	+/- 0.91	33.73	+/- 1.10
Al K	0.93	+/- 0.15	0.67	+/- 0.11
Si K	27.68	+/- 0.48	19.15	+/- 0.34
K K	0.66	+/- 0.18	0.33	+/- 0.09
K L	-	-	-	-
Ca K	0.86	+/- 0.22	0.42	+/- 0.10
Ca L	-	-	-	-
Mn K	17.75	+/- 1.45	6.28	+/- 0.52
Mn L	-	-	-	-
Total	**100.00**		**100.00**	

APPENDIX 3J: DMI-65 at different magnification

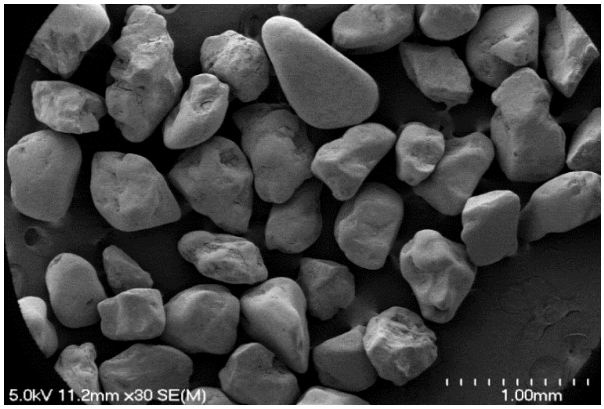

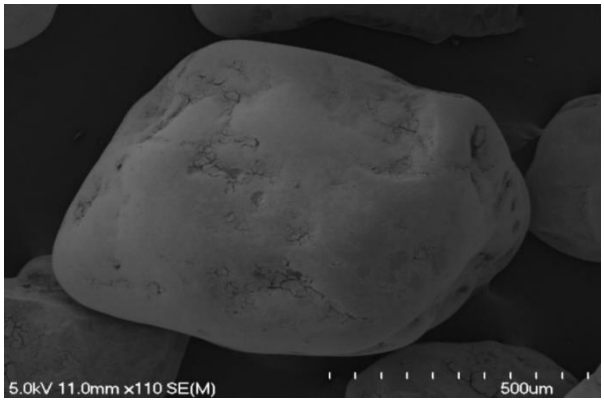

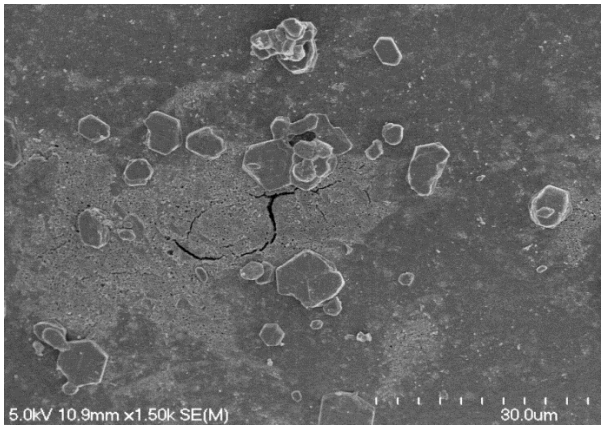

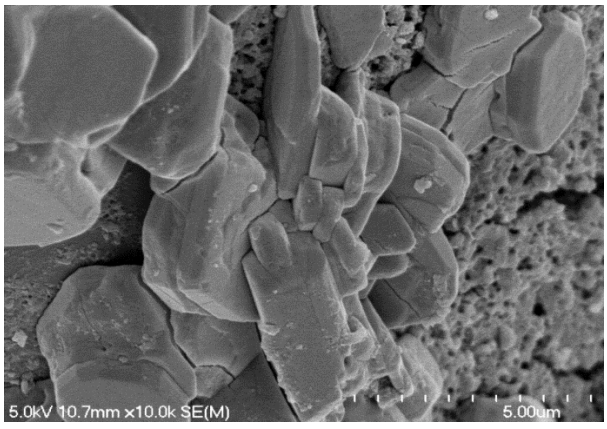

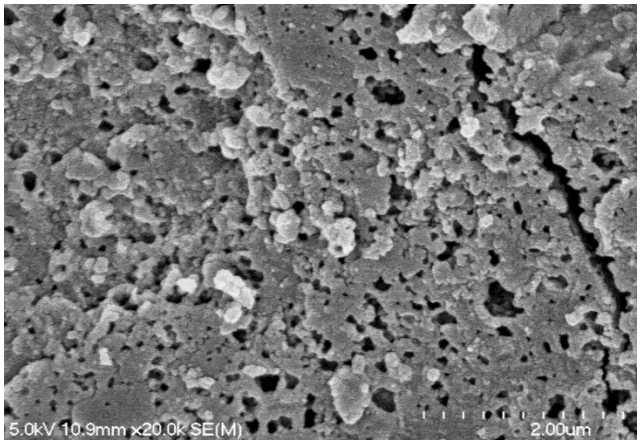
5.0kV 10.9mm x20.0k SE(M)
2.00um

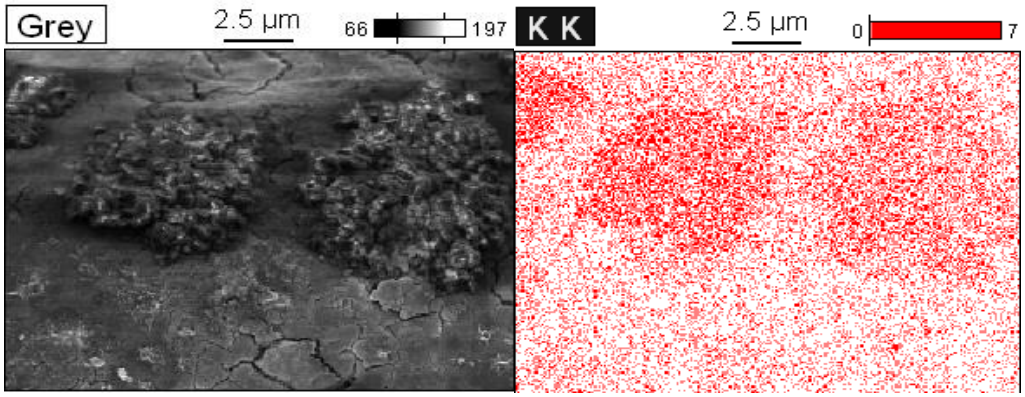
Grey
2.5 µm
66
197
K K
2.5 µm
0
7

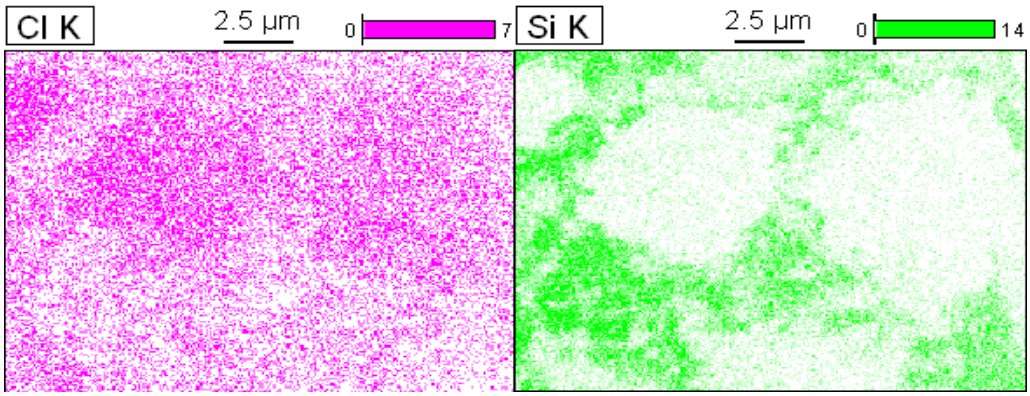
Cl K
2.5 µm
0
7
Si K
2.5 µm
0
14

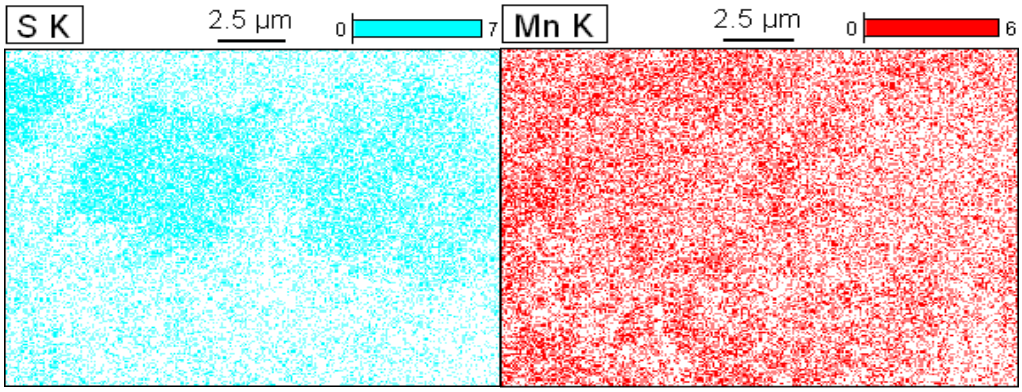
S K
2.5 µm
0
7
Mn K
2.5 µm
0
6

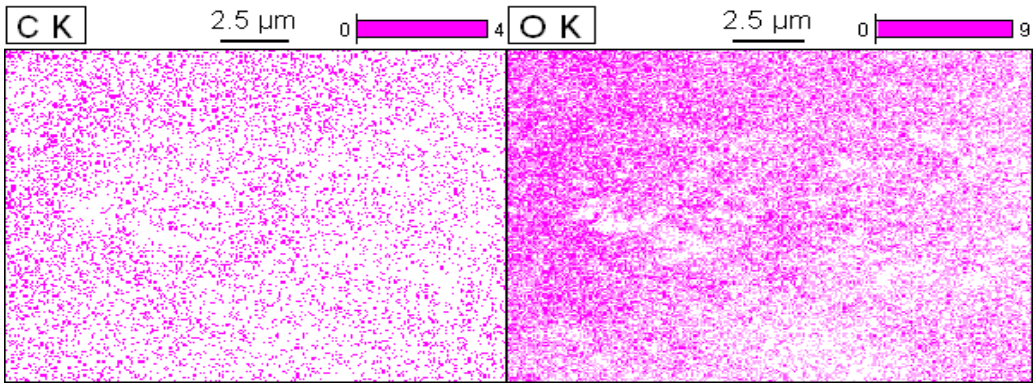
C K
2.5 µm
0
4
O K
2.5 µm
0
9

APPENDIX 3K (Section 3.3.1; Table 3.2)

RAW DMI-65

	1	2	3	4	5	Average	SD	%SD	Min error	Max error	Max error	% error
Surface area (m^2/g)												
MP Bet	0.527	0.474	0.525	0.466	0.501	0.499	0.03	5.69	0.0329	0.0285	0.0329	6.59
LSA	1.06	0.966	1.05	0.911	0.994	0.995	0.06	6.03	0.0840	0.0613	0.0840	8.45
TMESA	0.527	0.474	0.525	0.466	0.501	0.499	0.03	5.69	0.0329	0.0285	0.0329	6.59
DRMMA	0.362	0.320	0.386	0.351	0.380	0.360	0.03	7.34	0.0403	0.0257	0.0403	11.20
Pore volume (cc/g)												
DRMMV	0.000129	0.000114	0.000137	0.000125	0.000135	0.000128	0.00000	7.36	0.0000143	0.00000916	0.0000143	11.22
HKMCPV	0.000118	0.000105	0.000117	0.000107	0.000114	0.000112	0.00000	5.35	0.00000772	0.00000548	0.00000772	6.88
SFMSPV	8.65	1.52	0.000127	0.000116	0.000124	2.03	3.76	184.78	2.03	6.62	6.62	325.46
Pore size (A)												
DRMMHPW	21.3	21.6	22.7	22.4	22.9	22.2	0.70	3.15	0.882	0.518	0.882	3.97
DAMPR	12.7	12.7	13.0	12.9	13.0	12.8	0.15	1.17	0.125	0.075	0.125	0.97
HKMPR	6.96	7.06	8.36	8.46	9.61	8.09	1.10	13.62	1.13	0.370	1.13	13.96
SFMPR	13.8	15.1	16.1	16.3	18.3	15.9	1.67	10.48	2.15	0.430	2.15	13.52

ACTIVATED DMI-65

	1	2	3	4	5	Average	SD	% SD	Min error	Max error	Max error	% error
Surface area (m^2/g)												
MP Bet	4.88	5.49	5.00	5.60		5.24	0.36	6.82	0.365	0.363	0.365	6.95
LSA	8.29	9.31	8.47	9.67		8.94	0.66	7.39	0.643	0.733	0.733	8.20
TMESA	4.88	5.49	5.00	5.60		5.24	0.36	6.82	0.365	0.363	0.365	6.95
DRMMA	3.41	3.94	3.76	4.17		3.82	0.32	8.42	0.412	0.352	0.412	10.77
Pore volume (cc/g)												
DRMMV	0.00121	0.0014	0.00134	0.00148		0.00136	0.00	8.42	0.000146	0.000125	0.000146	10.77
HKMCPV	0.00129	0.00146	0.00133	0.00147		0.00139	0.00	6.65	0.0000972	0.0000818	0.0000972	7.02
SFMSPV	0.00139	0.00157	0.00142	0.00158		0.00149	0.00	6.78	0.000103	0.0000917	0.000103	6.92
Pore size (A)												
DRMMHPW	16.2	17.0	17.8	18.4		17.3	0.93	5.36	1.11	1.03	1.11	6.41
DAMPR	11.3	11.5	11.6	11.8		11.6	0.21	1.80	0.250	0.250	0.250	2.16
HKMPR	1.84	1.84	1.84	1.84		1.84	0.00	0.00	0.00	0.00	0.00	0.00
SFMPR	2.26	2.26	2.26	2.26		2.26	0.00	0.00	0.00	0.00	0.00	0.00

DMI-65 + As (III)

	1	2	3	4	5	Average	SD	% SD	Min error	Max error	Max error	% error
Surface area (m2/g)												
MP Bet	3.91	4.46	3.59	3.61		3.89	0.41	10.49	0.304	0.571	0.571	14.68
LSA	5.71	7.93	6.24	6.38		6.56	0.95	14.53	0.853	1.36	1.36	20.78
TMESA	3.91	4.46	3.59	3.61		3.89	0.41	10.49	0.304	0.571	0.571	14.68
DRMMA	2.61	3.82	3.12	3.18		3.18	0.50	15.59	0.575	0.637	0.637	20.00
Pore volume (cc/g)												
DRMMV	0.000927	0.00136	0.00111	0.00113		0.00113	0.00	15.59	0.000204	0.000226	0.000226	19.99
HKMCPV	0.00121	0.00116	0.000937	0.000923		0.00106	0.00	13.95	0.000133	0.000153	0.000153	14.45
SFMSPV	0.00129	0.00124	0.00101	0.000995		0.00113	0.00	13.53	0.000139	0.000156	0.000156	13.73
Pore size (A)												
DRMMHPW	13.7	21.7	21.4	22.1		19.7	4.01	20.33	6.00	2.39	6.00	30.40
DAMPR	10.6	12.5	12.3	12.5		12.0	0.92	7.7	1.38	52.5	1.38	11.48
HKMPR	1.84	8.39	9.59	9.61		7.36	3.72	50.61	5.5	2.26	5.52	75.01
SFMPR	2.26	13.5	13.4	13.5		10.7	5.61	52.56	8.42	2.84	8.42	78.84

DMI-65 + As (V)

	1	2	3	4	5	Average	SD	% SD	Min error	Max error	Max error	% error
Surface area (m2/g)												
MP Bet	3.79	4.00	3.86	3.88		3.88	0.09	2.31	0.0945	0.121	0.121	3.11
LSA	6.57	7.12	6.84	6.78		6.83	0.23	3.32	0.258	0.292	0.292	4.27
TMESA	3.79	4.00	3.86	3.88		3.88	0.09	2.31	0.0945	0.121	0.121	3.11
DRMMA	3,23	3.47	3.42	3.28		3.35	0.11	3.36	0.120	0.117	0.120	3.58
Pore volume (cc/g)												
DRMMV	0.00115	0.00123	0.00122	0.00117		0.00119	0.00	3.34	0.0000423	0.0000418	0.0000423	3.55
HKMCPV	0.000988	0.00102	0.000994	0.00100		0.00100	0.00	1.30	0.0000121	0.0000178	0.0000178	1.78
SFMSPV	0.00106	0.00109	0.00106	0.00108		0.00107	0.00	1.26	0.0000107	0.0000183	0.0000183	1.70
Pore size (A)												
DRMMHPW	20.9	22.1	22.4	21.1		21.6	0.73	3.37	0.733	0.767	0.767	3.55
DAMPR	12.2	12.5	12.5	12.5		12.4	0.15	1.21	0.175	0.125	0.175	1.41
HKMPR	1.84	8.94	8.94	1.84		5.39	4.10	76.08	3.55	3.55	3.55	65.88
SFMPR	2.26	12.5	17.2	2.26		8.54	7.49	87.81	6.27	8.62	8.62	101.04

APPENDIX 3L: (Section 3.3.1; Table 3.1)

X-ray fluoresecence (XRF) Analysis

Standard operating procedures (Claisse Neo Furnace)

To warm the furnace

Chose Fusion and "Select" program. This will start to heat up furnace to the desired temperature.

Temperature of furnace is on the top right hand corner of screen.

> Use "Disk – general oxide Disk – Extra cooling" for normal samples (basalt, andesite, and rhyolite)

Furnace will now warm up to desired temperature and it takes approx. 30 minutes from cold.

To place mold and crucible in the furnace

- Open safety door
- Use thumb latch to raise crucible guide
- Insert crucible
- Release thumb latch
- Make sure the guide does not touch the crucible
- Make sure the mold is in the rack

Make sure you have the correct fusion program by using the "Select"

Press start

It will ask you to **confirm** that the mold is in the operating point before it starts.

The program will not start until the furnace is upto temperature. Once it reaches the correct temperature, it will start automatically.

You can cancel method or push emergency stop at any time

If an error occurs during the cycle, it may cancel the program

Retrieving the prepared sample

- Open safety door
- Pick up glass disk using provided vacuum cup

- Lift thumb-latch to raise crucible guide
- Pick up crucible
- Check mold to make sure it is clean

To clear “completed” message press OK

You can now start a new sample.

When finished, push the home button and push “turn heat off”

Completion of Tasks/Final Checks:

1. Turn heat off
2. Cleaning crucibles and molds
3. Crucibles should be cleaned after each sample. Molds should be cleaned at least once a day, more frequently if sample is sticking to sides or if you are changing sample type.
4. To clean crucible and mould, place in a beaker with citric acid solution. Mould should be upside down or bottom so that crucible cant scratch surface (20 % weight citric acid and 80 % weight distilled water)
5. Place beaker in ultrasonic bath for about 30 minutes at 60 ^{O}C
6. Rinse crucible/mold 3 times in distilled water and 2 times in ultrapure water
7. Dry with paper towel.

SOP for pressed pellet 40mm size

1. Clean the base, cylinder and plunger with acetone and a paper tissue to make sure they are free from rust and dust.
2. Label sample on back of aluminum cup. Use permanent felt tip pen.
3. Tare a paper cup on the top-loading balance
4. Weigh 8 – 9 grams of sample into paper cup NOTE: the amount of sample varies with the density of the sample, and for low density samples less is required e.g Talc – 5 g
5. Add 25 drops of PVA binder to the sample using a plastic pipette and stir with wooden spatula until it is well mixed.
6. Place aluminum cup in die unit
7. Add sample to aluminum cup

8. Insert piston into die and place into hydraulic press. Pump up press to 100 then release, then pump up to 200 then release and remove. NOTE: For low-density samples, a lower hydraulic pressure should be used otherwise, the sample will immediately swell and distort. It is important that the surface of the pressed pellet remains flat and smooth and does not expand otherwise it will fall apart when inserted upside down in the instrument.
9. Remove cup + sample from unit.
10. Throw away the paper cup and spatula (new ones and used for each sample) and clean the base, cylinder and plunger with acetone using paper tissues.
11. Place the sample in a clean oven for approx. 2 hours to evaporate off the binder.

NOTE

If sample is wet and sticks to piston – you added to much PVA. You can remove sample from the cup and re-press when it has dried out.

If sample is to dry then sample will crumble and fall out of cup (not good)

If sample is above cup sides after pressing then you added too much sample.

SOP Loss on Ignition (LOI)

1. Weigh empty crucible (to 4 decimal places) and record
2. Add 1-2 grams of sample, preferably the larger weight if enough sample. Record weight of sample and crucible.
3. Place in furnace at $1100^{O}C$ for 1 hour (1 ½ if from cold)
4. After 1 hour, turn heat off and open lid to slightly cool samples. Make sure you have safety glasses and lab coat on. Remove crucibles from furnace using long handle tongs. Place crucibles in desiccator in a configuration so that you can remember crucible placement.
5. When cool (wait 20 minutes) weigh crucible. Calculate the difference in sample weight and determine LOI as a weight 5 %.

APPENDIX 3M: (Section 3.3.1; Figure 3.4)

Fourier-transform infrared spectroscopy (FTIR)

Use of the SPECAC Press to form a KBr disc

NB: Prior instruction and a demonstration are mandatory.

1. With sample holder on the block, wind down the top wheel to secure the sample holder in place.
2. Turn the wheel on the side clockwise to the stop position, then pump the handle until the pressure reaches the required level but NEVER exceed 11 tons.
3. Leave for a few minutes for the disc to fuse.
4. Release the pressure by turning the side wheel anticlockwise.
5. Carefully remove the sample holder and turn it upside down. Remove the base and then push the plunger carefully through the assembly to release the disc.

If the disk is stuck, use the press to gently force the plunger through the assembly.

Do not use sharp force, as doing so may damage the assembly and sharp edges may cut and crush objects.

Making a KBr disc for IR analysis of a solid sample

NB: Prior instruction and a demonstration are mandatory.

1. Ensure that the sample and KBr are both dry. The KBr will be kept in an oven for your convenience – please use it sparingly.
2. Using the minimum quality required for the disc, take 1 part sample to 10 parts KBr.
3. Grind the sample and KBr in a mortar to form a fine, homogeneous powder.
4. Assemble the outer parts of the sample holder and insert one of the dies. Make sure that it sits at the bottom of the holder.
5. Carefully add the sample mixture on top of the first die to form a thin, even layer.
6. Gently insert the second die and use the plunger to press that die down to meet the sample layer.

7. Position the sample holder on the press and follow instructions to form a compressed KBr disc.

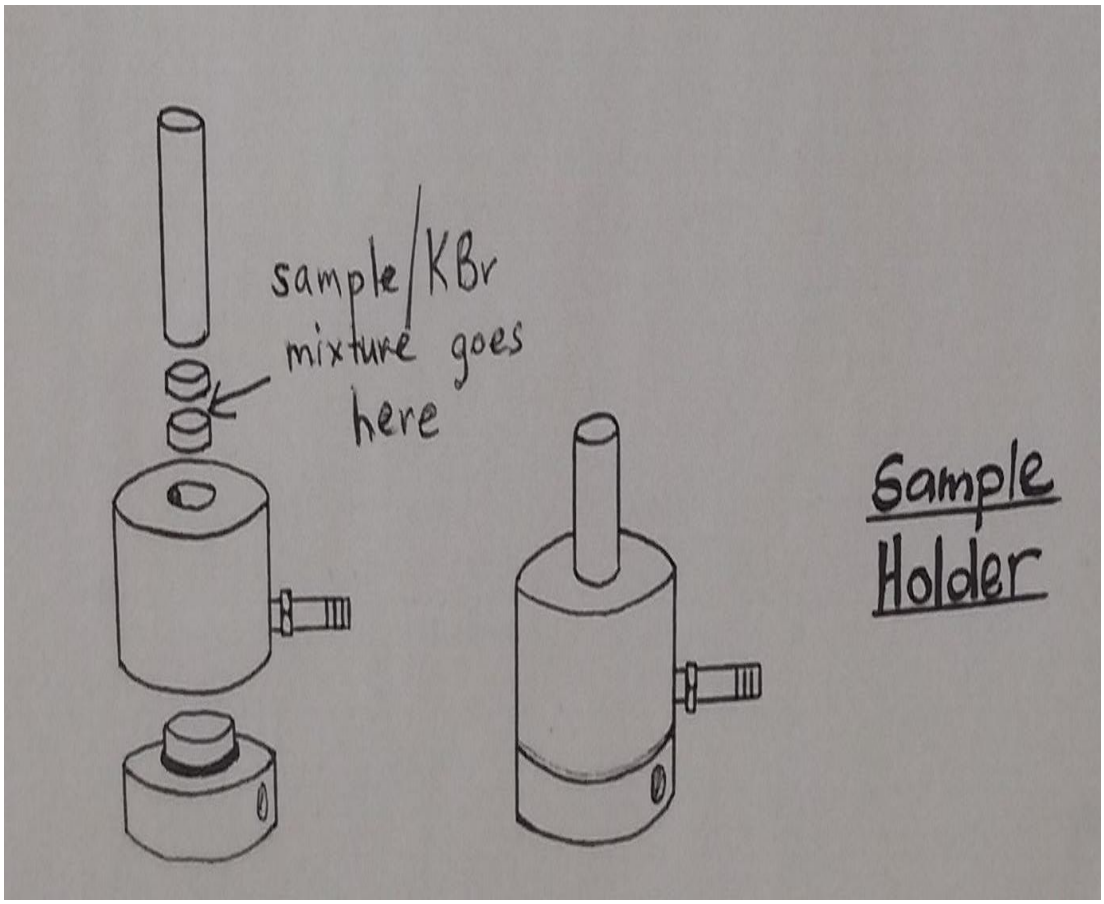

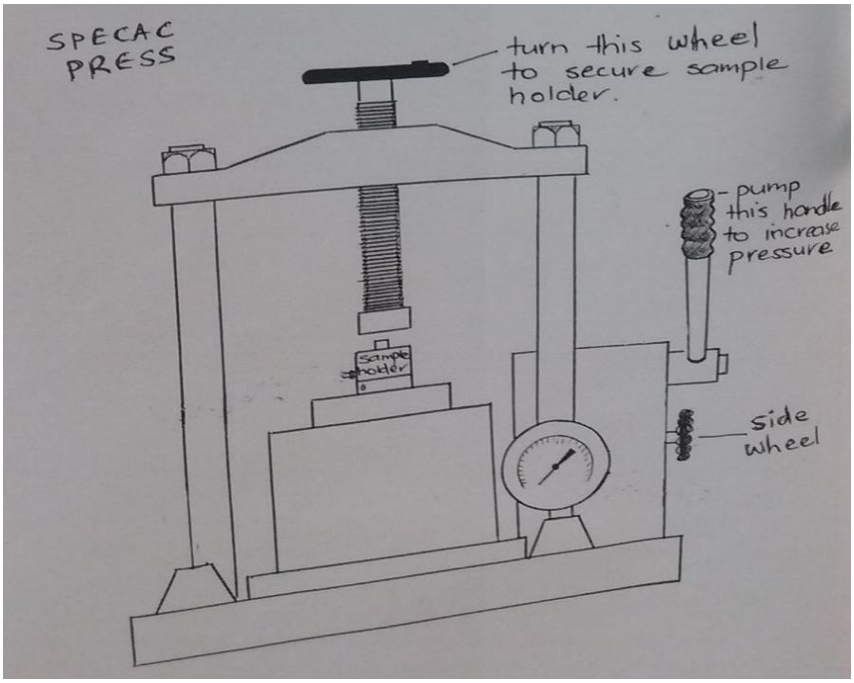

APPENDIX 3

3N: (Section 3.3.2; Figure 3.8)

DMI-65 kinetic data for As (V) batch adsorption

Initial As (V) Concentration (C_o) = 0.05 mg/L

Mass of adsorbent (m) = 1 g

Volume of adsorbate (V) = 0.05 L

Shaking speed (rpm) = 130 rpm

Temperature (T) = 20 ± 2 ^oC

$FeCl_3$ Concentration = 0.25 mg/L

NaOCl Concentration = 0.5 mg/L

pH 5 **pH 6**

Time (min)	As (V) Concentration (mg/L)		Time (min)	As (V) Concentration (mg/L)
10	0.0342		10	0.0287
20	0.0137		20	0.0240
30	0.0130		30	0.0218
45	0.0120		45	0.0209
60	0.0092		60	0.0158
90	0.0091		90	0.0149
300	0.0080		300	0.0087
660	0.0067		660	0.0070
1260	0.0046		1200	0.0041
1440	0.0046		1440	0.0037

pH 7 **pH 8.5**

Time (min)	As (V) Concentration (mg/L)		Time (min)	As (V) Concentration (mg/L)
10	0.0300		10	0.0433
20	0.0262		20	0.0379
30	0.0230		30	0.0369
45	0.0199		60	0.0313
60	0.0172		90	0.0259
90	0.0158		120	0.0220
240	0.0117		240	0.0148
720	0.0075		660	0.0088
1195	0.0063		1200	0.0057
1440	0.0063		1440	0.0048

Pseudo-first-order kinetic model

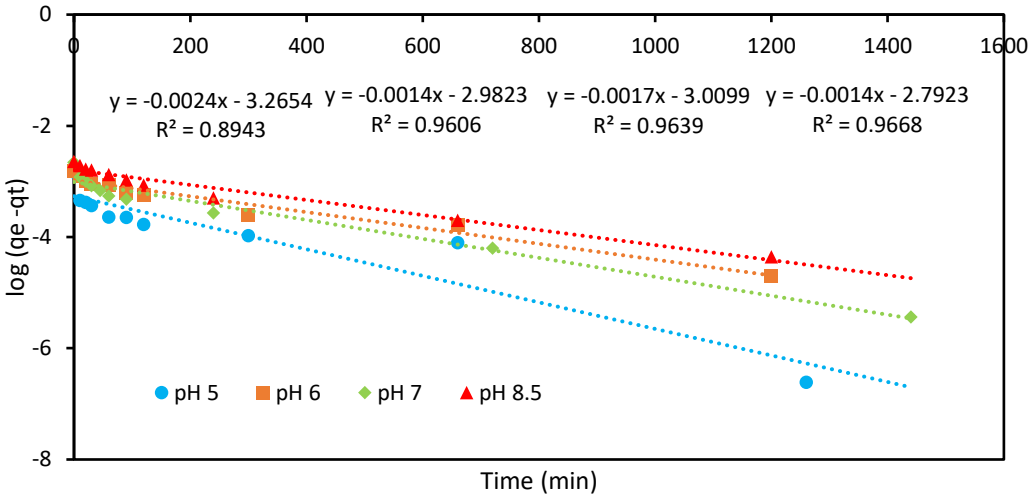

Pseudo-second-order kinetic model

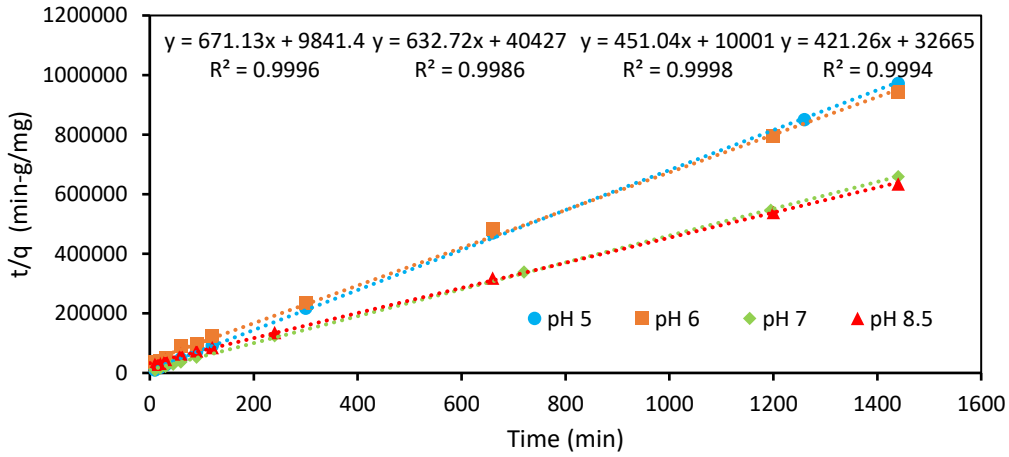

Elovich model

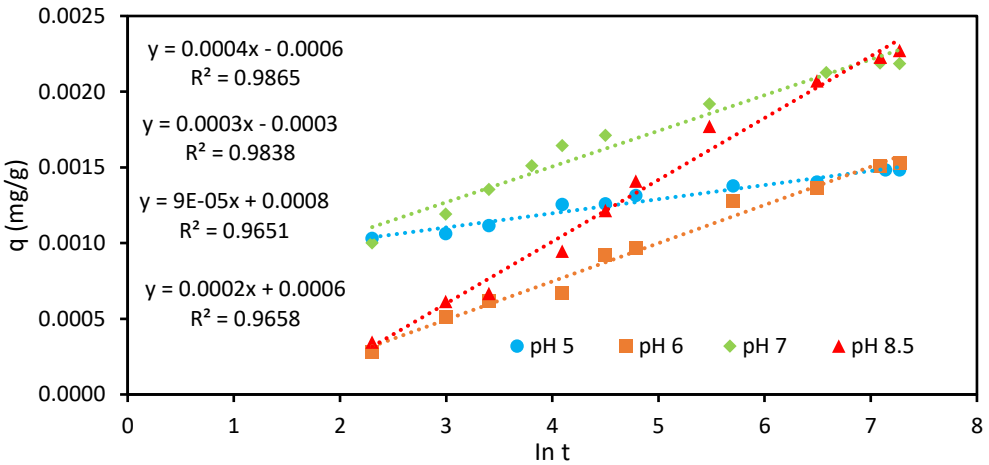

3O: (Section 3.3.2; Figure 3.9)

DMI-65 kinetic data for As (V) batch adsorption

Initial As (III) Concentration = 0.05 mg/L

Mass of adsorbent = 1 g

Volume of adsorbate = 0.05 L

Shaking speed (rpm) = 130 rpm

Temperature = 20 ± 2 ^{o}C

$FeCl_3$ Concentration = 0.25 mg/L

NaOCl Concentration = 0.5 mg/L

pH 5

Time (min)	As (III) Concentration (mg/L)
10	0.0331
20	0.0267
30	0.0195
60	0.0148
90	0.0118
120	0.0111
286	0.0071
610	0.0052
1200	0.0017
1440	0.0016

pH 6

Time (min)	As(III) Concentration (mg/L)
10	0.0376
20	0.0300
30	0.0250
45	0.0187
60	0.0148
90	0.0149
286	0.0080
610	0.0028
1260	0.0022
1440	0.0019

pH 7

Time (min)	As (III) Concentration (mg/L)
10	0.0385
20	0.0341
30	0.0318
60	0.0278
90	0.0233
120	0.0189
247	0.0111
613	0.0060
1290	0.0032
1440	0.0025

pH 8.5

Time (min)	As (III) Concentration (mg/L)
10	0.0396
20	0.0366
30	0.0329
60	0.0265
90	0.0242
120	0.0174
240	0.0122
480	0.0077
900	0.0040
1440	0.0032

Pseudo-first-order kinetic model

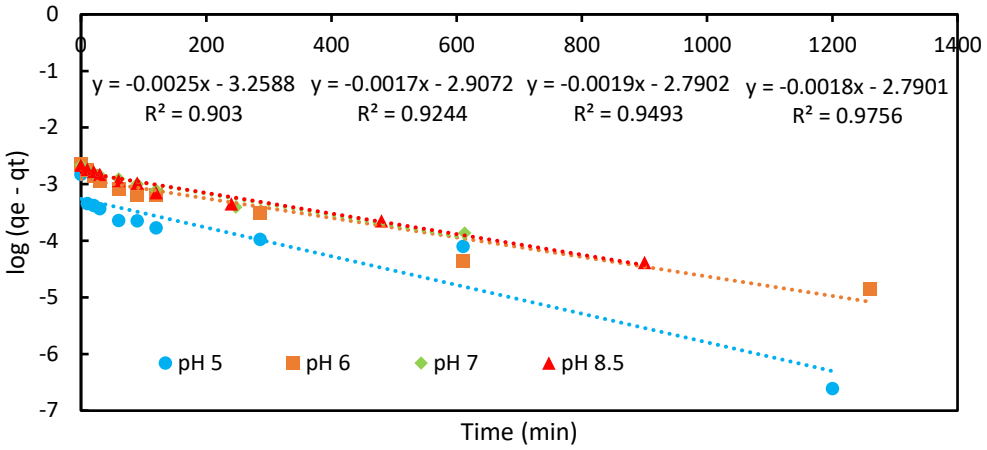

Pseudo-second-order kinetic model

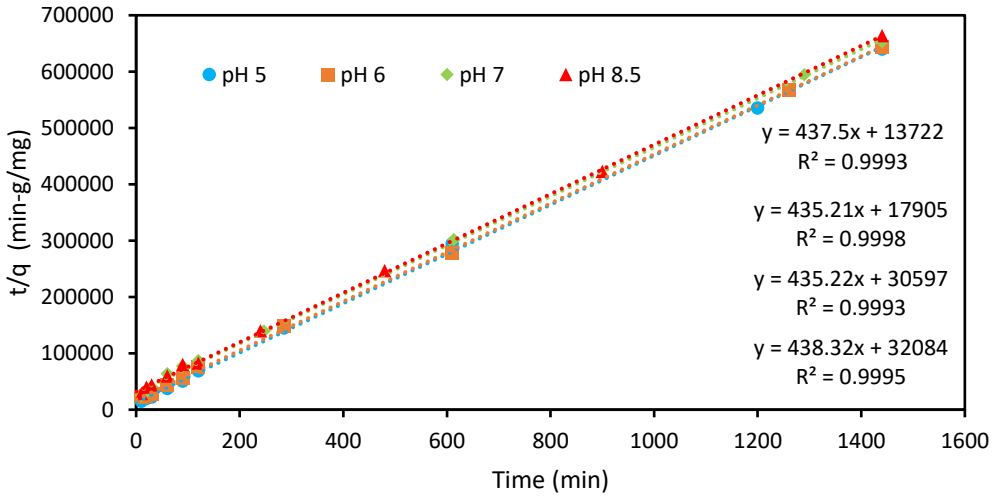

Elovich model

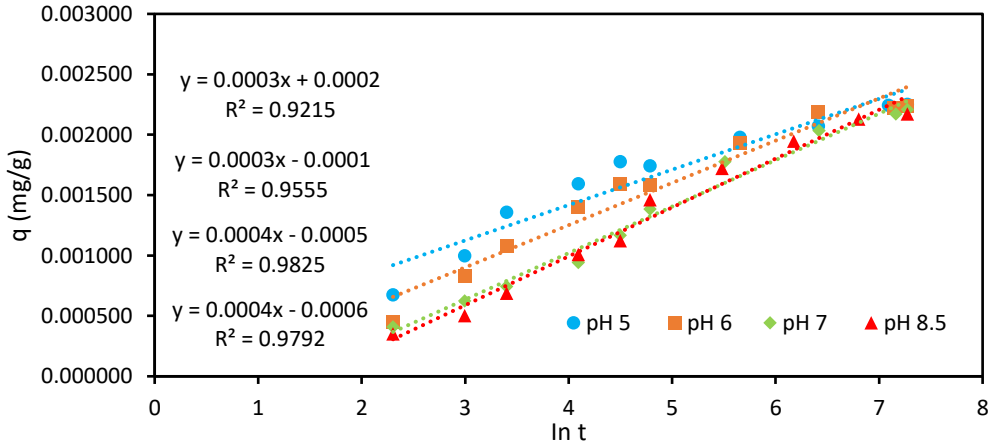

APPENDIX 3P:

Comparison between As (III) and As (V) Kinetics (Pseudo-second-order kinetic model)

(a) pH 5

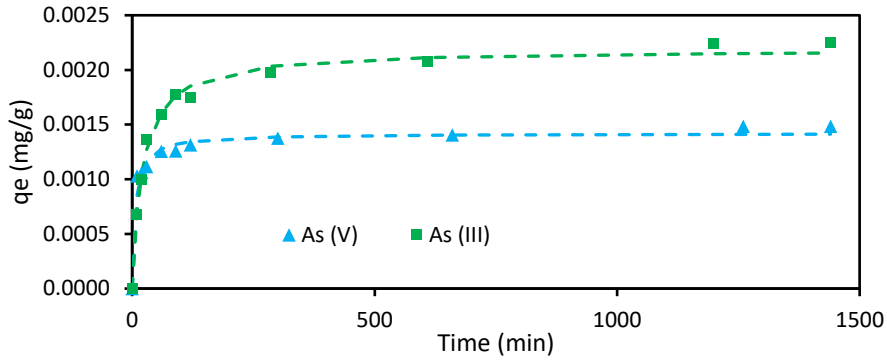

(b) pH 6

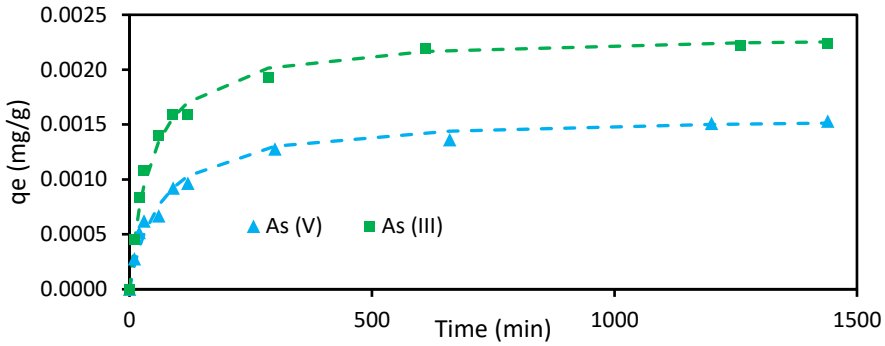

(c) pH 7

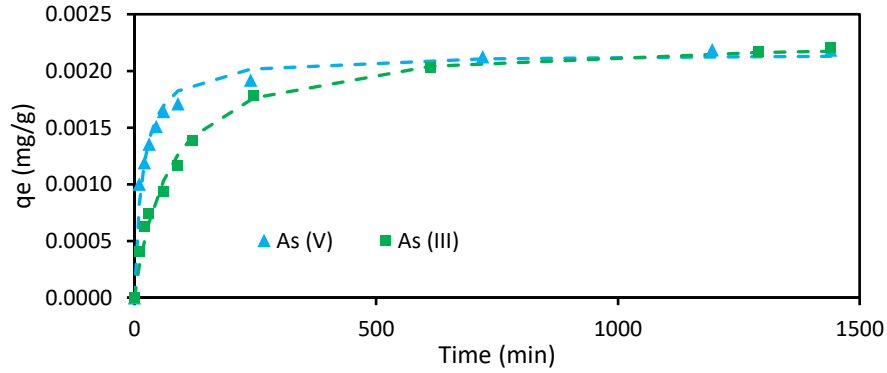

(d) pH 8.5

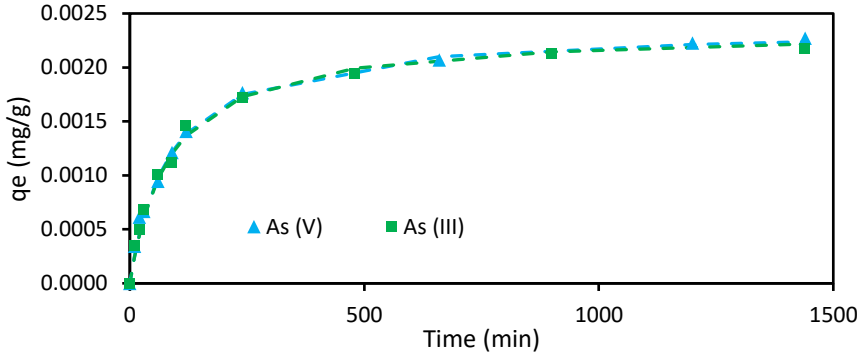

3Q: (Section 3.3.3; Figure 3.11 & 3.12)

Data for adsorption isotherms

Initial As (V) Concentration = 0.015 – 10.00 mg/L

Mass of adsorbent = 1 g

Volume of adsorbate = 0.05 L

Shaking speed (rpm) = 130 rpm

Temperature = 20 ± 2 ^{o}C

$FeCl_3$ Concentration = 0.25 mg/L

NaOCl Concentration = 0.5 mg/L

Total time = 24 hrs

Initial As (V) Conc. (mg/L)	**Final As (V) Conc. after 24 hrs (mg/L)**			
	pH 5	**pH 6**	**pH 7**	**pH 8.5**
0.015	0.010	0.011	0.012	0.008
0.480	0.121	0.046	0.041	0.035
1.432	0.355	0.370	0.348	0.302
2.624	0.868	1.004	0.843	0.777
3.966	1.845	2.016	1.737	1.480
5.052	2.880	2.904	2.552	2.214
6.536	4.154	4.328	3.806	3.206
7.647	5.326	5.373	4.725	4.101
10.223	7.775	7.900	7.084	6.299

Initial As (III) Concentration = 0.011 – 25.00 mg/L

Mass of adsorbent = 1 g

Volume of adsorbate = 0.05 L

Shaking speed (rpm) = 130 rpm

Temperature = 20 ± 2 ^{o}C

$FeCl_3$ Concentration = 0.25 mg/L

NaOCl Concentration = 0.5 mg/L

Total time = 24 hrs

Initial As (III) Conc. (mg/L)	Final As (III) Conc. after 24 hrs (mg/L)			
	pH 5	pH 6	pH 7	pH 8.5
0.011	0.008	0.008	0.009	0.008
0.855	0.060	0.059	0.058	0.090
3.615	0.906	0.804	0.896	0.960
5.989	2.159	2.102	2.306	2.210
9.039	4.251	4.391	4.570	4.476
11.784	6.495	7.001	7.066	6.910
12.151	6.805	7.201	7.323	7.221
15.675	10.002	10.617	10.586	10.450
25.299	19.264	20.037	20.080	19.596

3R

Comparison of As (III) and As (V) Langmuir adsorption isotherm

(a) pH 5

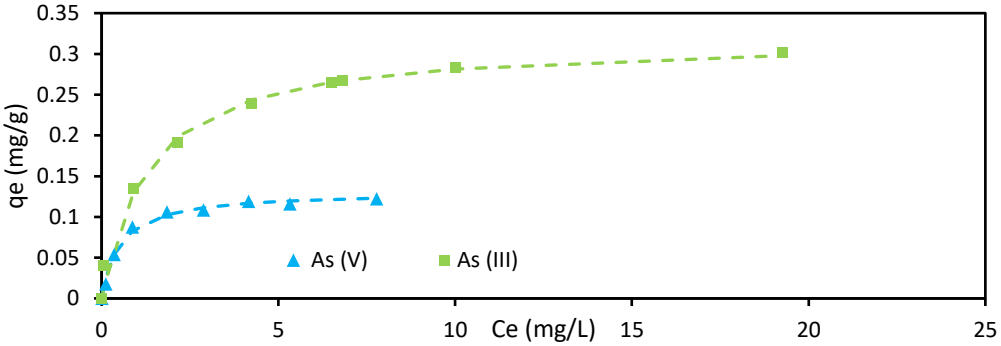

(b) pH 6

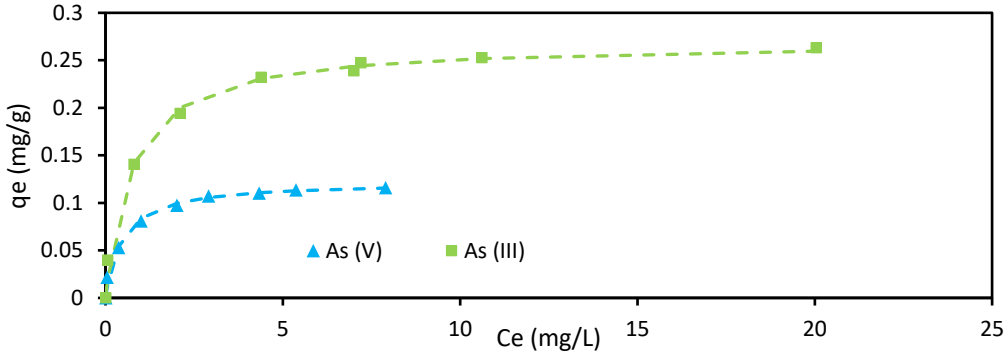

(c) pH 7

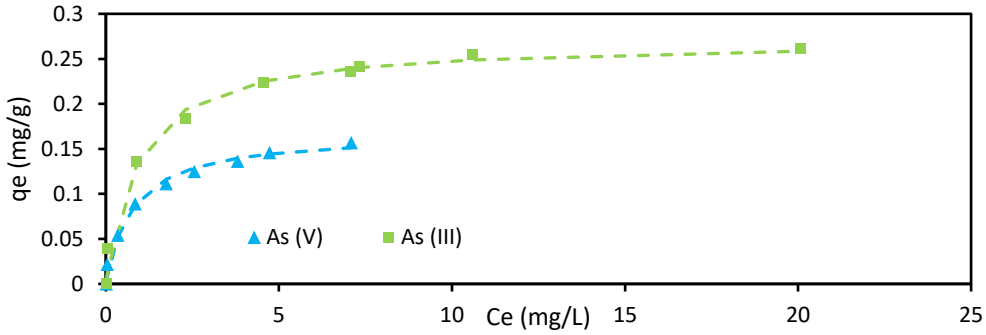

(d) pH 8.5

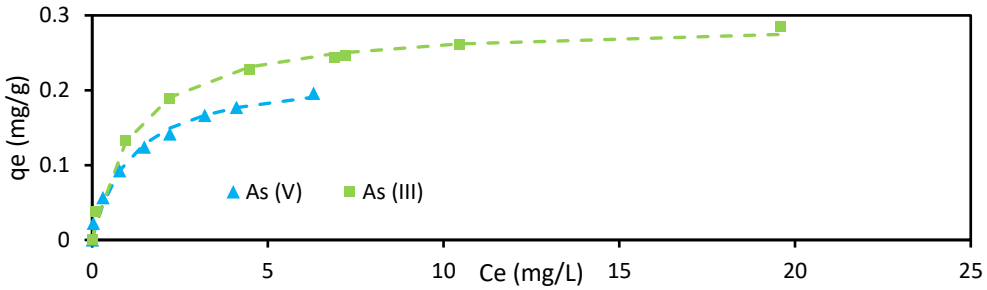

3S: (Section 3.3.4; Figure 3.14)

Data for thermodynamics studies

Initial As (III) Concentration = 0.011 – 25.00 mg/L

Mass of adsorbent = 1 g

Volume of adsorbate = 0.05 L

Shaking speed (rpm) = 130 rpm

$FeCl_3$ Concentration = 0.25 mg/L

NaOCl Concentration = 0.5 mg/L

Total time = 24 hrs

Initial As (III) Conc. (mg/L)	**Final As (III) Conc. after 24 hrs (mg/L)**			
	283 K	**288 K**	**293 K**	**298 K**
0.011	0.008	0.009	0.009	0.009
0.855	0.066	0.060	0.053	0.056
3.615	0.928	0.838	0.819	0.788
5.989	2.300	2.167	1.946	1.807
9.039	4.720	4.650	4.270	4.167
11.784	7.107	7.097	6.776	6.608
12.151	7.594	7.451	7.123	7.082
15.675	10.947	10.602	10.486	10.316
25.299	20.411	20.100	19.890	19.689

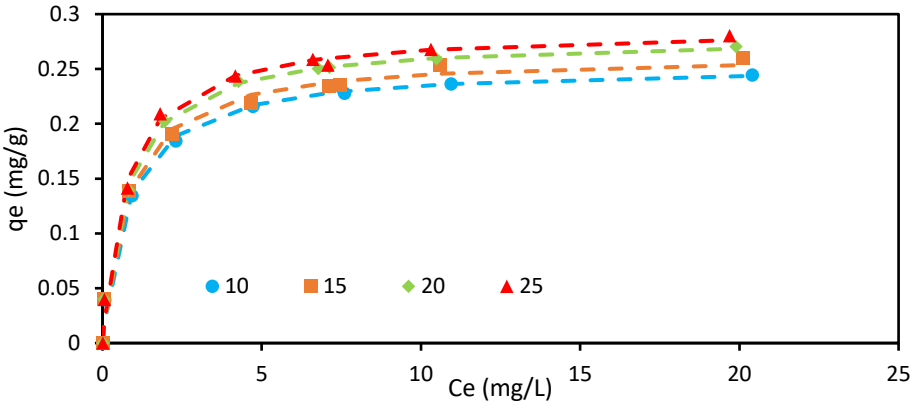

Initial As (V) Concentration = 0.010 – 18.40 mg/L

Mass of adsorbent = 1 g

Volume of adsorbate = 0.05 L

Shaking speed (rpm) = 130 rpm

$FeCl_3$ Concentration = 0.25 mg/L

NaOCl Concentration = 0.5 mg/L

Total time = 24 hrs

Initial As (V) Conc. (mg/L)	**Final As (V) Conc. after 24 hrs (mg/L)**				
	283 K	**288 K**	**293 K**		**298 K**
0.010	0.007	0.008	0.015	0.012	0.008
0.909	0.069	0.061	0.480	0.041	0.073
3.090	1.100	0.901	1.432	0.348	0.591
5.171	2.765	2.326	2.624	0.843	1.934
7.844	5.108	4.775	3.966	1.737	4.276
9.668	6.879	6.539	5.052	2.552	6.088
11.140	8.266	7.992	6.536	3.806	7.448
14.757	11.889	11.527	7.647	4.725	11.018
18.409	15.499	15.179	10.223	7.084	14.715

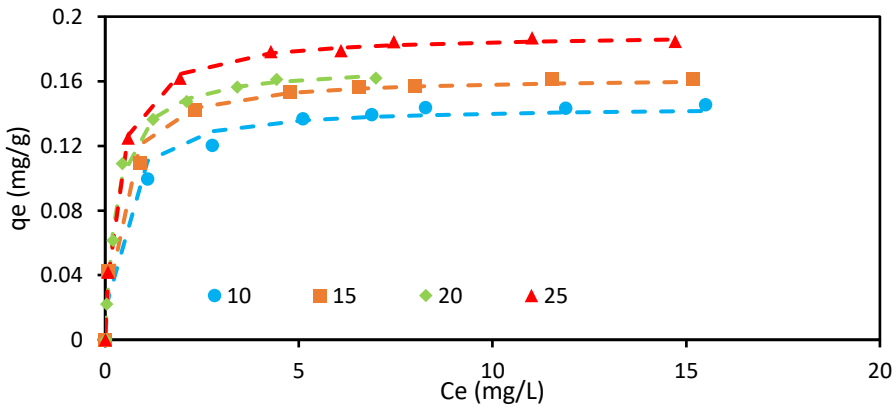

3T: (Section 3.3.5; Figure 3.15)

DMI-65 kinetic data for As (III) and As (V) batch adsorption

Initial As (III) Concentration (C_o) = 0.030 mg/L

Initial As (V) Concentration (C_o) = 0.015 mg/L

Mass of adsorbent (m) = 1 g

Volume of adsorbate (V) = 0.05 L

Shaking speed (rpm) = 130 rpm

Temperature (T) = 20 ± 2 ^oC

$FeCl_3$ Concentration = 0.25 mg/L

NaOCl Concentration = 0.5 mg/L

Number of Cycle	As (III) (µg/L)	As (V) (µg/L)
0	3.02	0.65
1	3.69	0.75
2	3.92	0.77
3	3.93	0.81
4	5.02	1.05
5	5.02	1.05

3AA: Non-Imprinted polymer (NIP)

Kinetic data for NIP

OPERATING CONDITIONS

Mass of NIP = 1.09 g (wet weight) = 1 g dry weight

Volume of Arsenic solution = 0.05 L

Agitation speed = 130 rpm in a shaker

Temperature = 19.8 ^{o}C ± 2 ^{o}C

Initial Arsenic Concentration = 0.06 mg/L (60 µg/L)

Contact time = 24 hours

ARSENIC (V)

	pH 5	pH 6	pH 7	pH 8.5
Time (min)	***Final Conc. (µg/L)***	***Final Conc. (µg/L)***	***Final Conc. (µg/L)***	***Final Conc. (µg/L)***
10	53.66	52.49	51.21	55.25
20	52.48	52.42	48.47	51.60
30	50.52	49.22	44.34	49.21
45	51.64	49.90	43.10	47.53
60	47.24	49.49	42.29	46.41
90	46.89	45.84	41.17	42.46
120	44.47	43.88	40.82	42.98
240	43.11	44.45	38.84	40.38
300	44.85	43.50	38.07	39.19
600	43.57	42.99	37.23	37.52
1200	43.12	44.04	36.52	37.56
1400	43.17	43.70	37.08	38.14

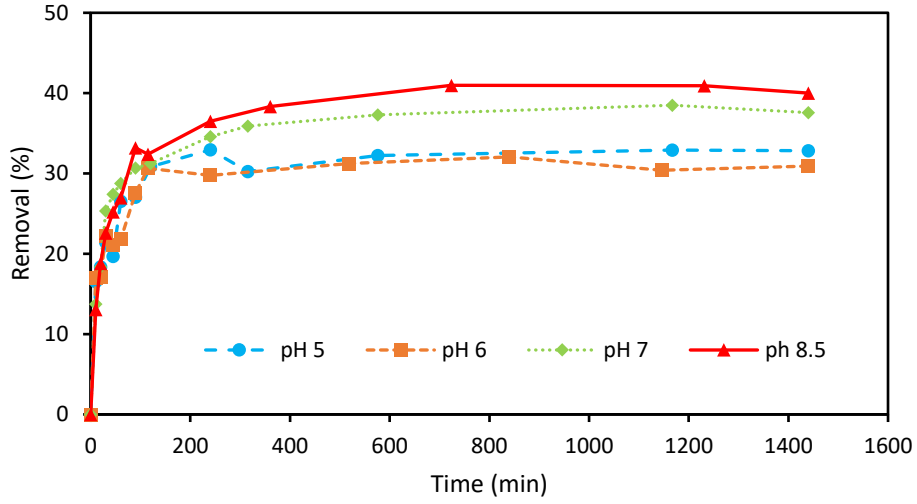

Percentage As (V) removal

(a) pH 5

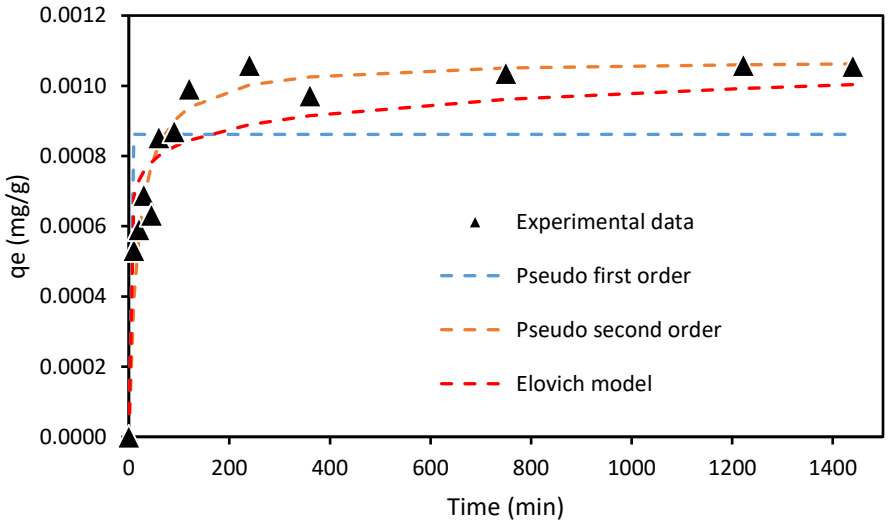

(b) pH 6

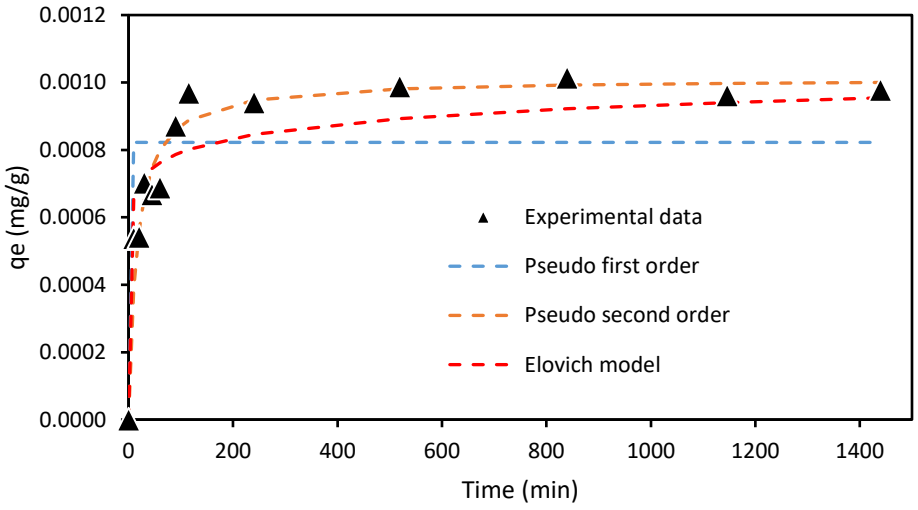

(c) pH 7

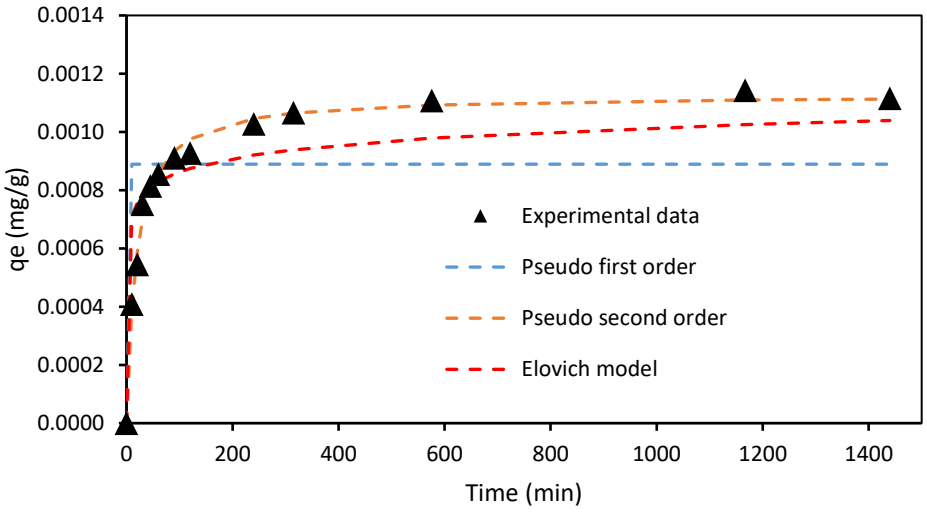

(d) pH 8.5

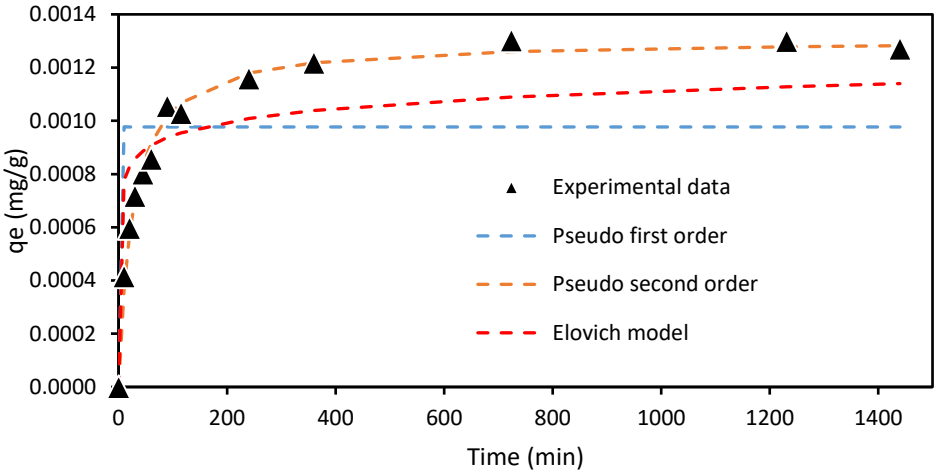

3AB: Pseudo first order kinetic model

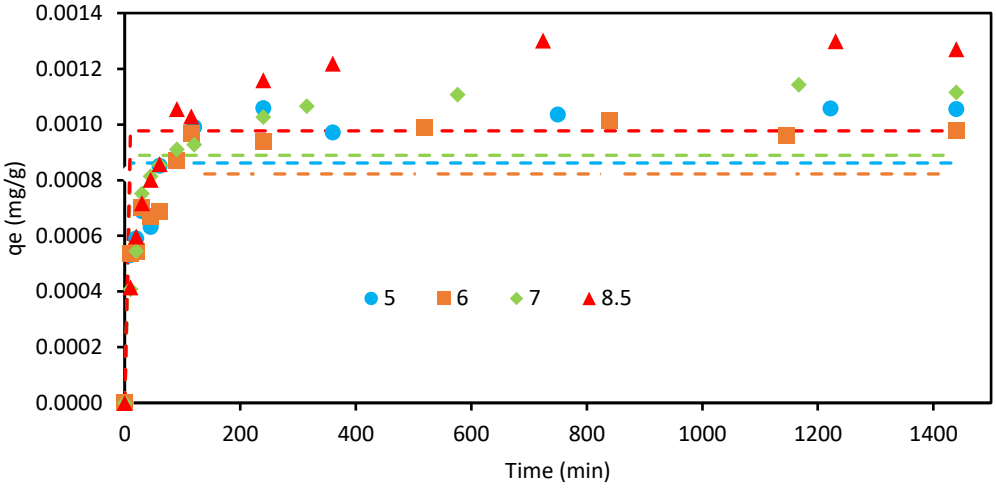

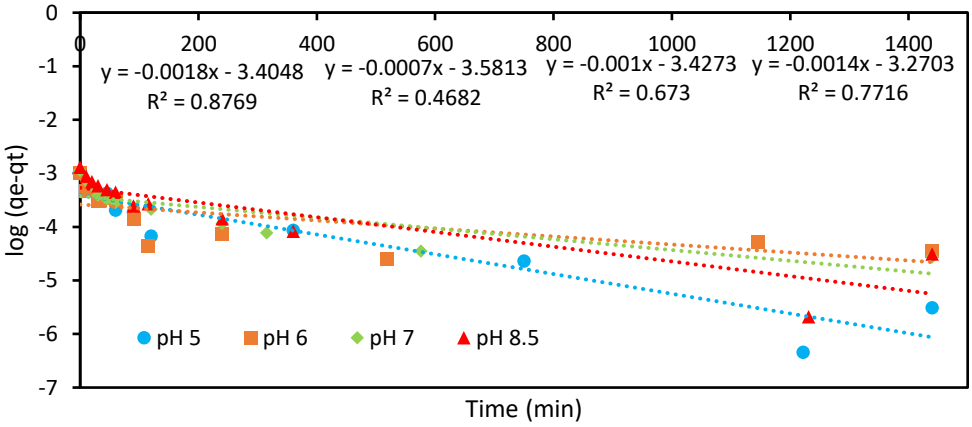

3AC: Pseudo second order kinetic model

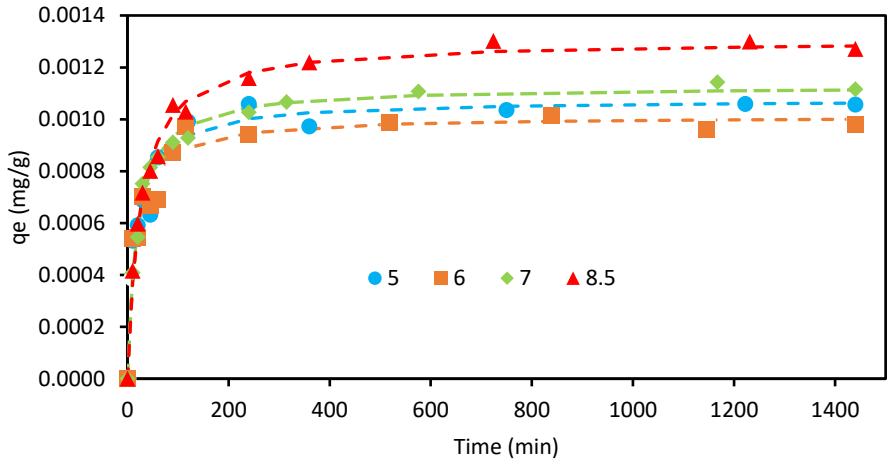

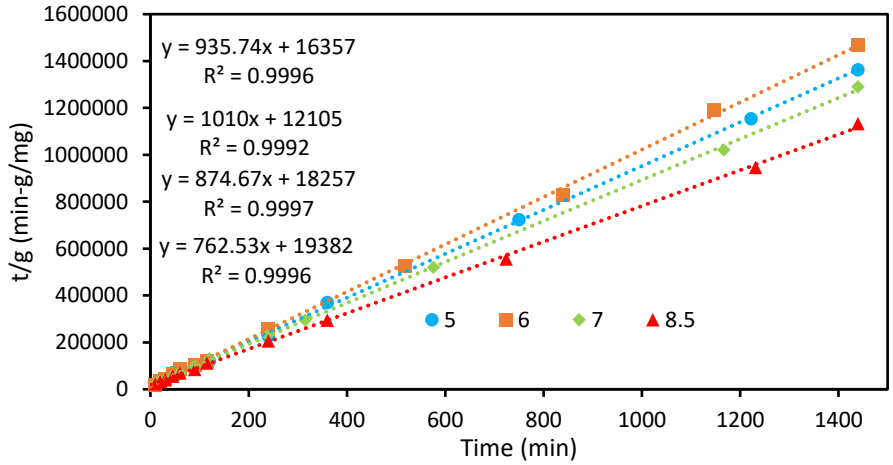

Elovich model

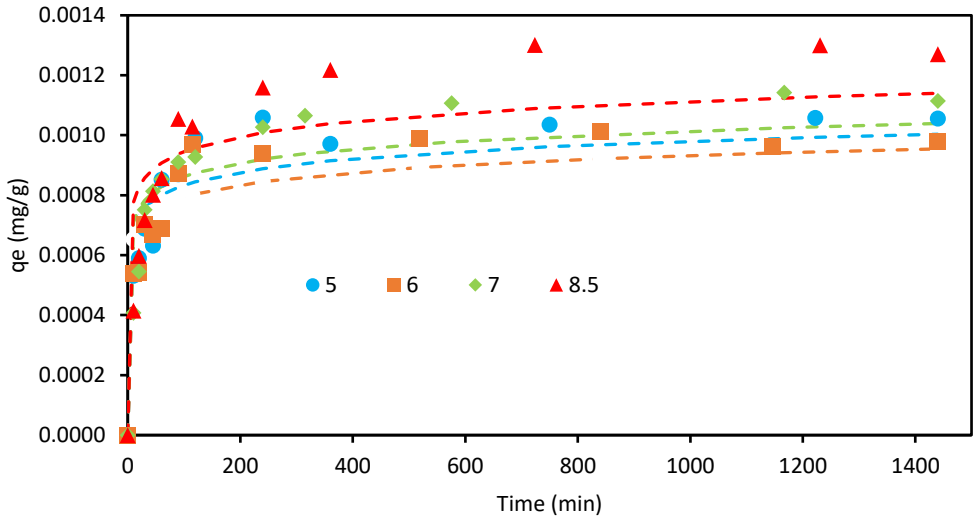

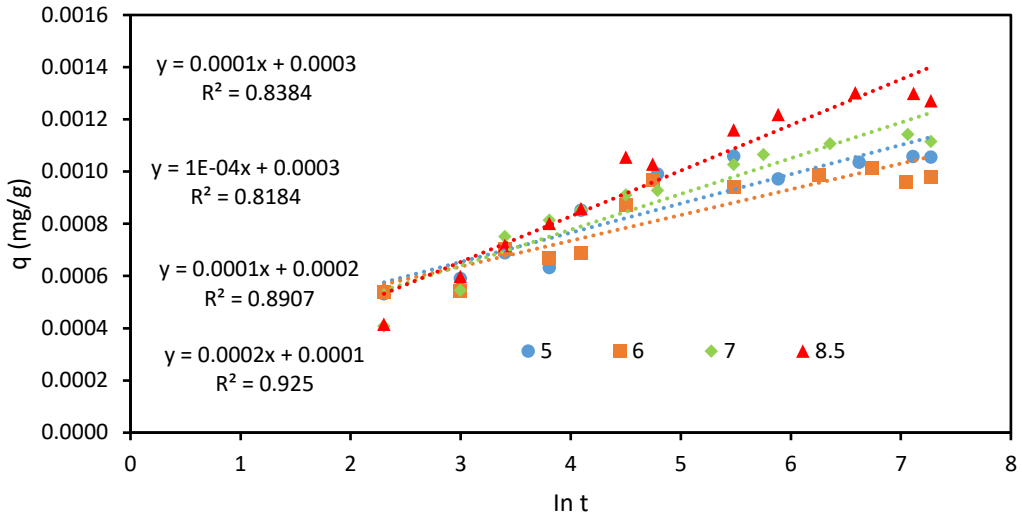

3AD: Adsorption isotherm data

OPERATING CONDITIONS

Mass of NIP = 0.01 g dry weight

Volume of Arsenic solution = 0.1 L

Agitation speed = 130 rpm

Temperature = 19.5 ^{o}C ± 2 ^{o}C

Contact time = 24 hours

ARSENIC (V)

Initial Conc. (µg/L)	*pH 5 Final Conc. (µg/L)*	*pH 6 Final Conc. (µg/L)*	*pH 7 Final Conc. (µg/L)*	*pH 8.5 Final Conc. (µg/L)*
30.77	22.71	28.05	29.52	29.67
823.70	706.98	785.92	772.66	748.39
2621.71	2307.19	2261.48	2245.64	2544.27
4387.45	3844.04	3606.53	3691.33	4308.02
6658.84	5501.52	5529.39	5972.01	6516.73
8976.09	7160.97	7960.07	7985.81	8752.87
11319.65	9233.73	10235.79	10057.32	10757.03
14070.88	11610.80	12473.83	12627.03	13469.80
18398.93	15674.06	16553.92	16890.67	17765.93

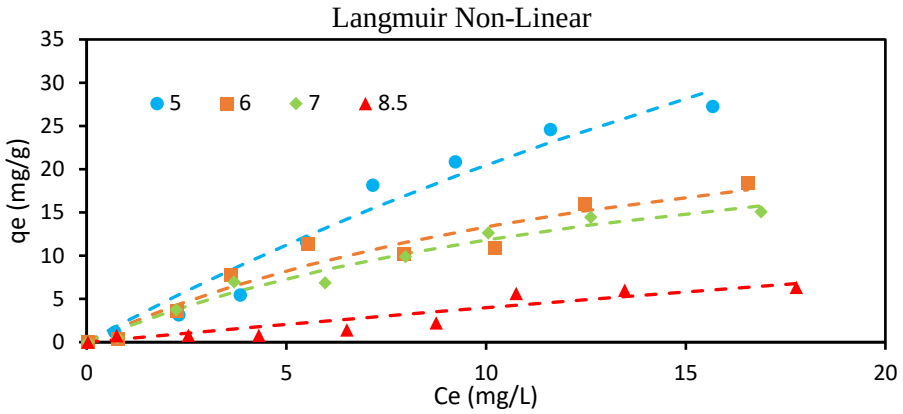
Langmuir Non-Linear
5
6
7
8.5
qe (mg/g)
Ce (mg/L)
0
5
10
15
20
25
30
35

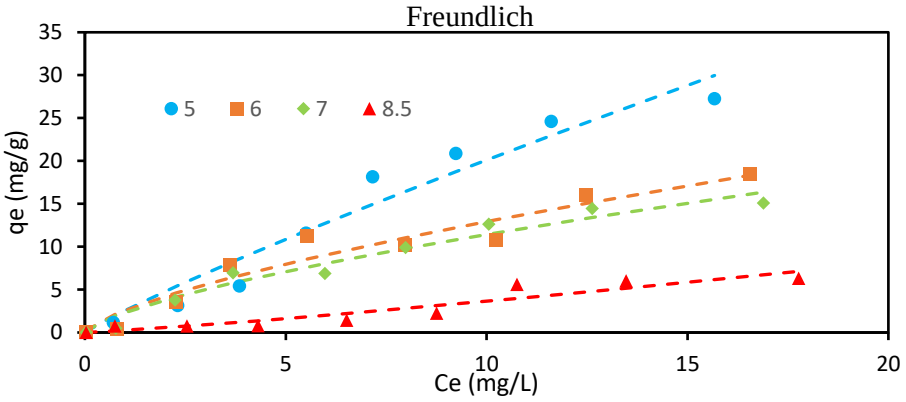
Freundlich
5
6
7
8.5
qe (mg/g)
Ce (mg/L)
0
5
10
15
20
25
30
35

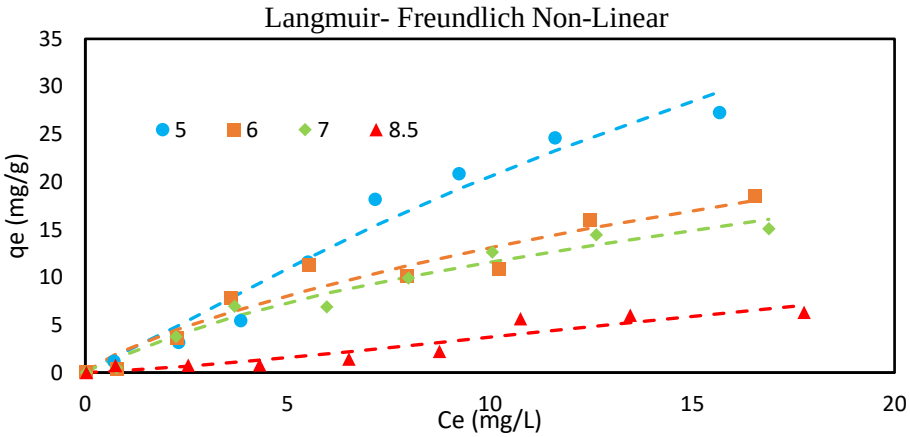
Langmuir- Freundlich Non-Linear
5
6
7
8.5
qe (mg/g)
Ce (mg/L)
0
5
10
15
20
25
30
35

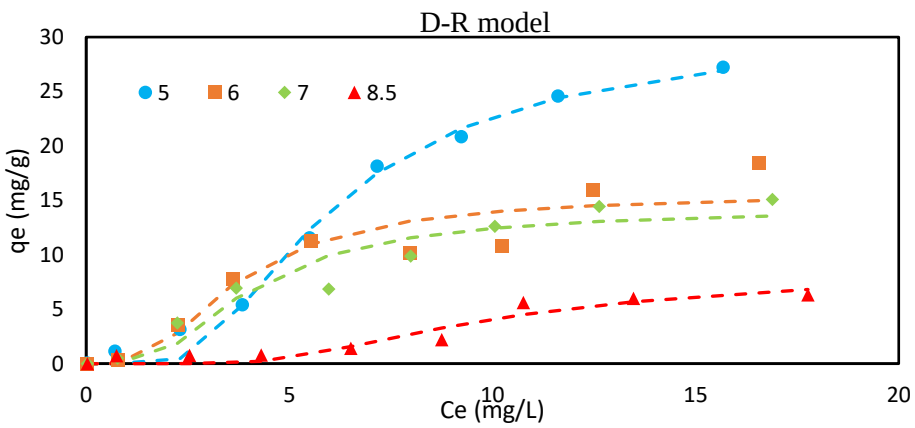
D-R model
5
6
7
8.5
qe (mg/g)
Ce (mg/L)
0
5
10
15
20
25
30

ARSENIC (III)

Initial Conc. (µg/L)	*pH 5 Final Conc. (µg/L)*	*pH 6 Final Conc. (µg/L)*	*pH 7 Final Conc. (µg/L)*	*pH 8.5 Final Conc. (µg/L)*
33.80	4.74	9.58	24.66	28.18
826.16	297.43	41.43	42.32	39.42
2627.94	835.52	741.91	1599.24	837.02
4008.52	2480.51	2316.12	2406.71	2012.10
6333.16	4116.49	3765.20	4696.07	3920.34
9117.86	5903.88	5479.99	7177.53	6232.51
11591.86	7753.51	7313.96	9745.44	8461.06
13962.32	10487.75	9486.84	11833.29	10321.78
18845.94	15159.93	14294.42	16402.91	14990.61

Langmuir Non-Linear

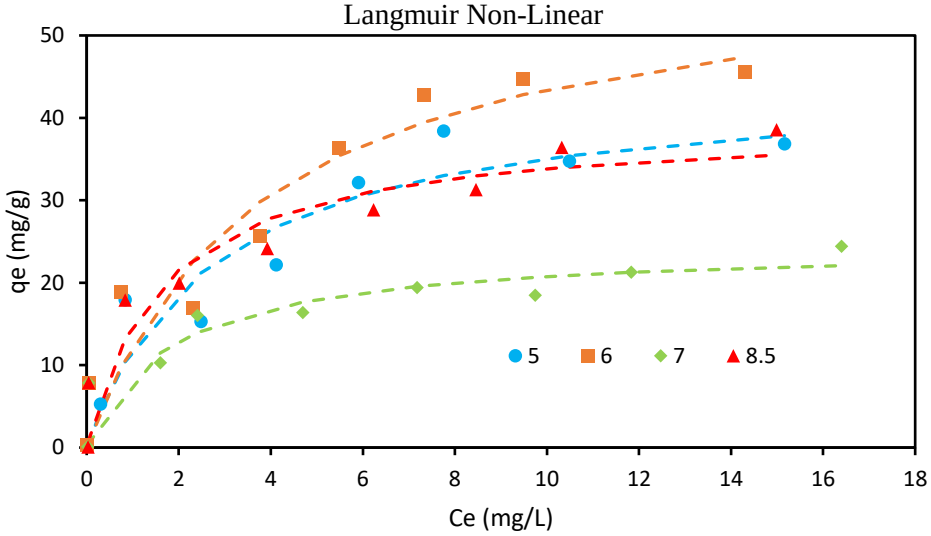

Freundlich

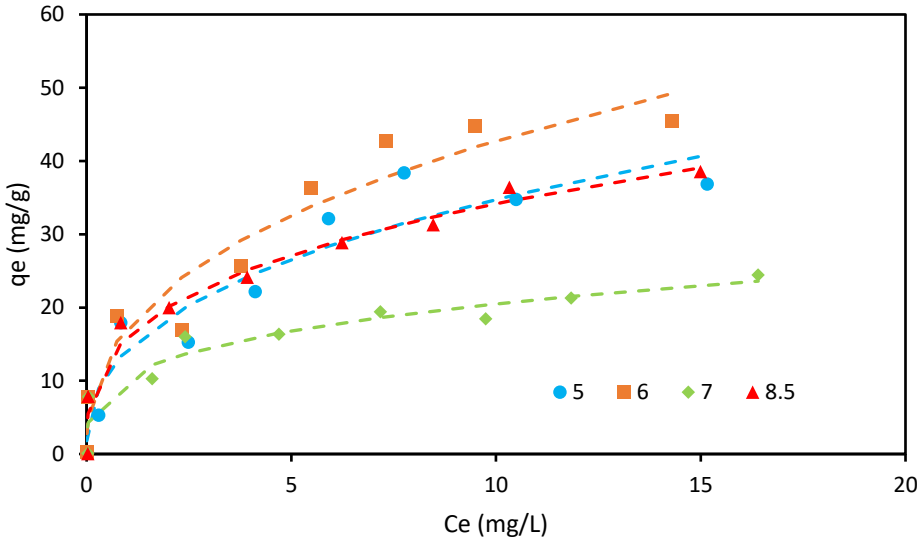

Langmuir- Freundlich Non-Linear

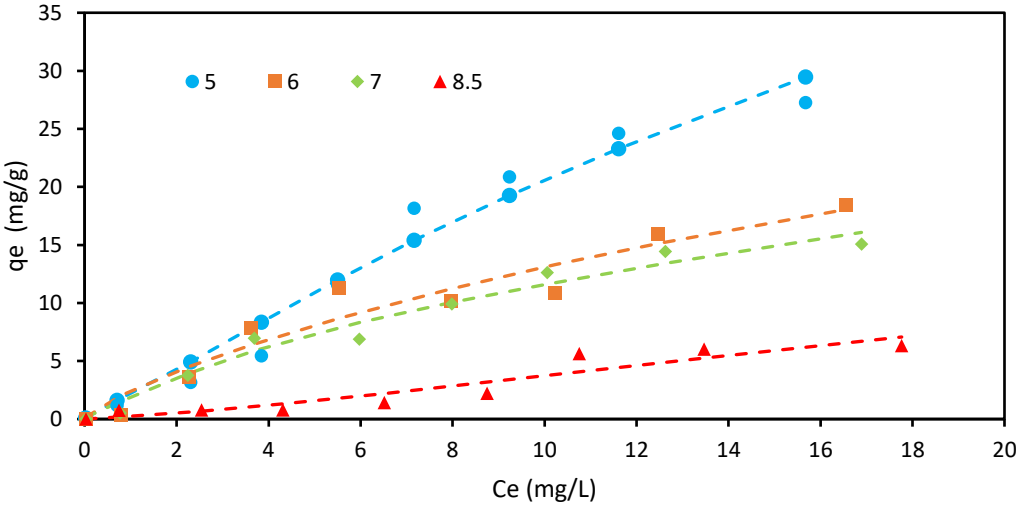

D-R model

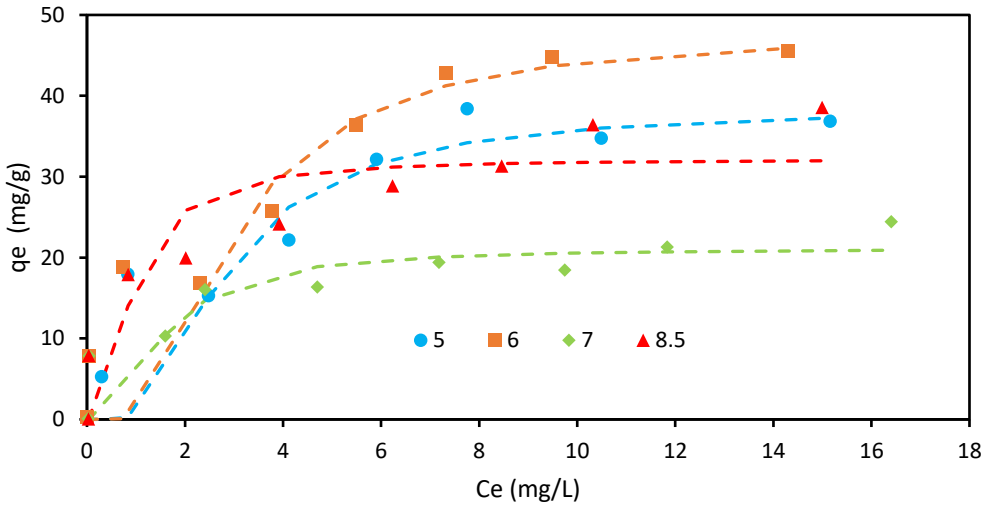

Estimate isotherms parameters for adsorption using NIP

Model	pH 5		pH 6		pH 7		pH 8.5	
	As (III)	As (V)	As (III)	As (V)	As (III)	As (V)	As (III)	As (V)
Langmuir								
q_m (mg/g)	44.72	113.50	60.02	0.122	24.52	0.170	39.41	0.224
K_L (L/mg)	0.363	0.0220	0.262	2.146	0.550	1.297	0.604	0.901
R^2	0.906	0.962	0.915	0.991	0.928	0.990	0.917	0.991
Freundlich								
K_F (mg/g)	0.343	0.072	0.141	0.071	0.135	0.083	0.134	0.095
n	3.409	3.383	3.962	3.214	3.778	2.540	3.481	2.226
R^2	0.960	0.895	0.925	0.934	0.940	0.961	0.953	0.985
Langmuir-Freundlich								
q_m (mg/g)	0.248	0.125	0.254	0.123	0.240	0.165	0.239	0.203
K_L (L/mg)	1.101	1.342	1.125	1.310	1.116	1.001	1.101	0.908
n	2.355	2.116	2.696	2.289	2.577	2.527	2.466	2.428
R^2	0.980	0.961	0.981	0.986	0.989	0.961	0.988	0.979
Dubinin-Radushkevich								
q_s (mg/g)	0.273	0.113	0.248	0.114	0.244	0.146	0.257	0.174
K_{DR} (mol^2/KJ^2)	0.261	0.069	0.162	0.080	0.202	0.117	0.251	0.127
R^2	0.951	0.989	0.969	0.960	0.961	0.951	0.962	0.934

3AC: As (V) Adsorption Kinetics for Molecular imprinted polymer

Operating Conditions

Initial Arsenic Concentration = 63 μg/L

Mass of media = 0.1 g

Temperature = 20.7 ^{o}C

Time = 24 hrs

r.p.m = 130

Volume of solution = 50 mL

Time	pH 5	Time	pH 6	Time	pH 7	Time	pH 8.5
10 min	70.65	10 min	61.09	10 min	61.03	10 min	59.51
20 min	65.30	20 min	64.48	20 min	62.49	20 min	61.00
30 min	60.95	30 min	64.08	30 min	60.75	30 min	61.35
60 min	63.14	60 min	62.34	60 min	60.36	60 min	61.65
90 min	61.94	90 min	63.86	90 min	63.72	90 min	60.17
2 hrs	60.78	2 hrs	60.32	2 hrs	63.33	2 hrs	62.20
4 hrs	60.12	4 hrs	59.02	4 hrs	63.38	4 hrs	59.94
12 hrs	61.74	11 hrs	61.03	10.52 hrs	62.45	12 hrs	60.74
18 hrs	61.77	20 hrs	63.49	18.01 hrs	65.58	18 hrs	62.15
24 hrs	63.10	24 hrs	64.30	24 hrs	60.84	24 hrs	59.23

Values are in μg/l

As (V) Adsorption Isotherm for Molecular imprinted polymer

Operating Conditions

Mass = 0.1g Temperature = 20 ^{o}C

Time = 24 hrs Volume of Solution = 50 mL

r.p.m = 130

Initial Conc.	pH 5	pH 6	pH 7	pH 8.5
63.53	63.82	75.66	65.59	71.52
2051.16	2081.28	2021.51	1697.60	1982.26
6532.71	6628.31	6115.24	5625.83	6032.36
11423.65	11344.23	10276.93	9218.75	10139.15
17328.99	16357.14	15590.67	15008.65	15858.56
23511.27	23075.62	21318.39	18899.41	20034.30
28933.74	27703.76	24844.44	26790.45	23622.41
35808.14	32550.52	30343.90	32731.88	29185.35
48239.58	45870.46	40720.52	46124.59	37786.15

Values are in μg/L

APPENDIX 4

4A

Effect of flowrate:

Initial Turbidity = 2.19 NTU, Initial As Conc. = 13.058 µg/L, Initial UV_{254nm} = 0.0584, pH = 7

10mL/min		**12.5 mL/min**		**20 mL/min**	
Time (min)	As Conc. (µg/L)	Time (min)	As Conc. (µg/L)	Time (min)	As Conc. (µg/L)
20	0.147	20	0.111	10	0.361
40	0.164	40	0.139	20	0.317
103	0.210	103	0.285	30	0.337
260	0.413	260	0.351	50	0.356
573	0.484	573	0.545	85	0.465
1238	0.829	1238	1.177	198	1.126
1410	0.907	1410	1.448	286	1.537
1590	1.029	1590	1.840	369	1.969
1761	1.093	1761	2.150	635	3.898
2000	1.723	2000	2.712	765	4.940
2642	2.190	2642	4.287	815	5.026
3090	2.777	3090	5.410	1370	7.315
3450	3.109	3450	6.718	1440	7.822
3570	3.453	3570	7.967	1555	8.550
4080	3.752	4080	8.066	1710	8.673
4265	4.244	4265	8.282	1782	9.197
4440	4.308	4440	9.305	2046	10.281
4590	4.444	4590	9.586	2151	10.483
4860	4.491			2709	11.695
5345	5.533			2880	11.874
5776	5.675			3090	12.063
6128	6.822			3464	12.500
				4320	12.860

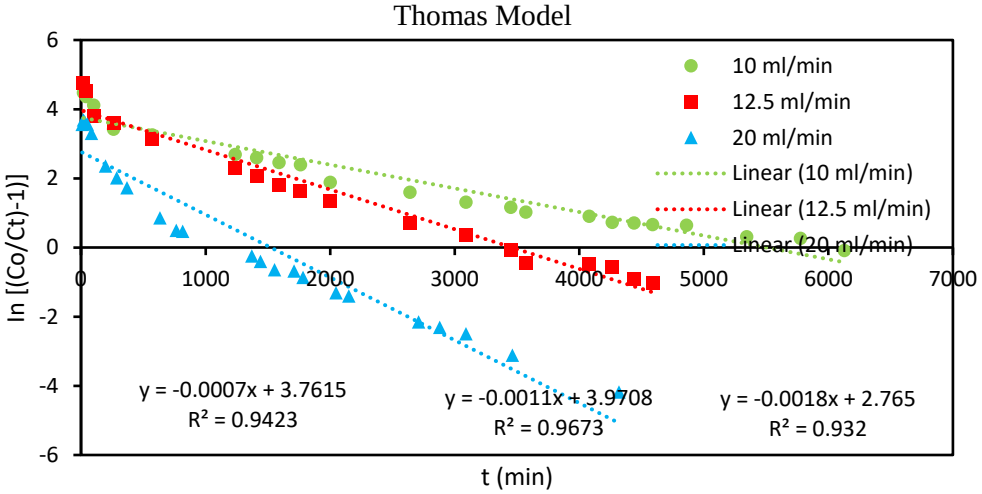

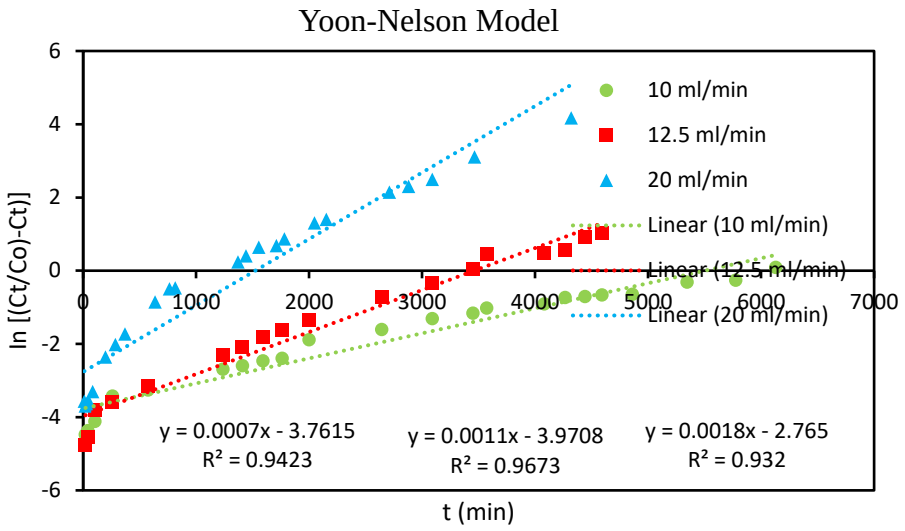
Yoon-Nelson Model
ln [(Ct/Co)-Ct)]
t (min)
10 ml/min
12.5 ml/min
20 ml/min
Linear (10 ml/min)
Linear (12.5 ml/min)
Linear (20 ml/min)
y = 0.0007x - 3.7615
R² = 0.9423
y = 0.0011x - 3.9708
R² = 0.9673
y = 0.0018x - 2.765
R² = 0.932

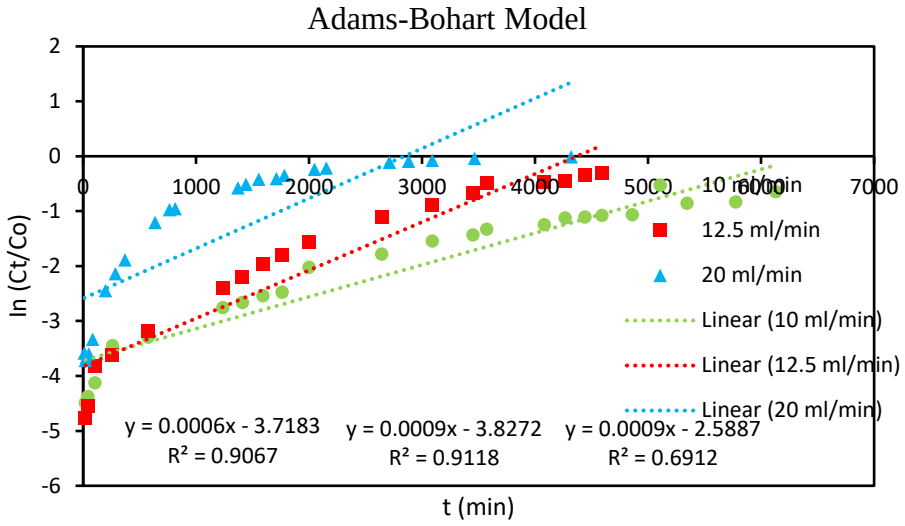
Adams-Bohart Model
ln (Ct/Co)
t (min)
10 ml/min
12.5 ml/min
20 ml/min
Linear (10 ml/min)
Linear (12.5 ml/min)
Linear (20 ml/min)
y = 0.0006x - 3.7183
R² = 0.9067
y = 0.0009x - 3.8272
R² = 0.9118
y = 0.0009x - 2.5887
R² = 0.6912

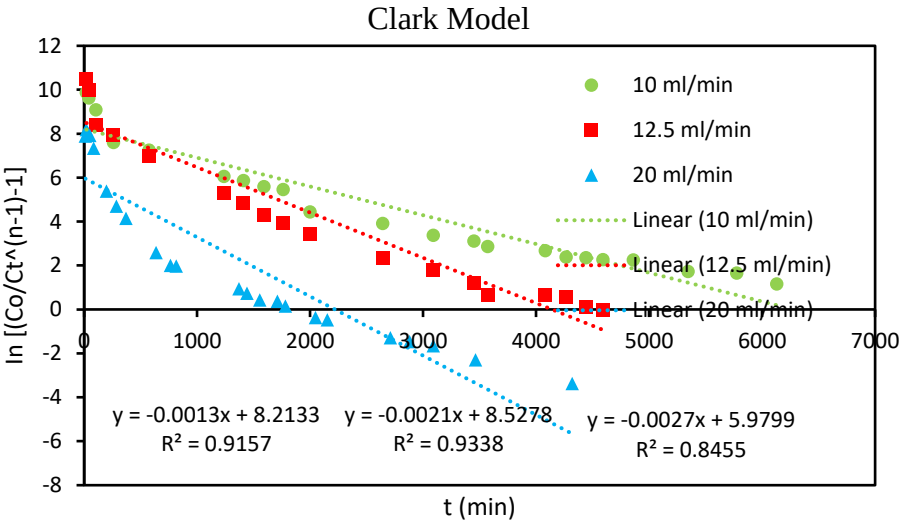
Clark Model
ln [(Co/Ct^(n-1)-1]
t (min)
10 ml/min
12.5 ml/min
20 ml/min
Linear (10 ml/min)
Linear (12.5 ml/min)
Linear (20 ml/min)
y = -0.0013x + 8.2133
R² = 0.9157
y = -0.0021x + 8.5278
R² = 0.9338
y = -0.0027x + 5.9799
R² = 0.8455

4B

Effect of pH:

pH = 5: Initial Turbidity = 4.23 NTU, Initial As Conc. = 18.521 µg/L Initial UV_{254nm} = 0.0746

pH = 7: Initial Turbidity = 2.19 NTU, Initial As Conc. = 19.872 µg/L Initial UV_{254nm} = 0.0492

pH = 9: Initial Turbidity = 2.19 NTU, Initial As Conc. = 13.058 µg/L Initial UV_{254nm} = 0.0584

pH 5		**pH 7**		**pH 9**	
Time (min)	As Conc. (µg/L)	Time (min)	As Conc. (µg/L)	Time (min)	As Conc. (µg/L)
10	0.880	10	0.361	10	2.097
20	0.998	20	0.317	20	2.215
30	1.020	30	0.337	30	2.662
50	1.174	50	0.356	50	4.139
80	1.199	85	0.465	120	9.862
144	1.371	198	1.126	245	10.923
312	1.454	286	1.537	615	13.347
487	1.489	369	1.969	740	15.418
720	1.530	635	3.898	1295	15.862
1393	2.121	765	4.940	1460	15.927
1590	2.489	815	5.026	1685	16.396
1781	2.644	1370	7.315	2008	16.971
2192	3.447	1440	7.822	2170	17.003
2390	4.518	1555	8.550	2690	17.020
2865	6.900	1710	8.673	2842	17.076
3050	7.639	1782	9.197	3000	17.241
3560	11.297	2046	10.281	3320	17.523
3850	12.965	2151	10.483	3460	17.981
4250	15.028	2709	11.695	4095	18.059
4750	16.430	2880	11.874	4287	18.646
5530	16.660	3090	12.063	4450	18.926
6000	17.780	3464	12.500	4850	19.022
7000	18.104	4320	12.860	5100	19.245

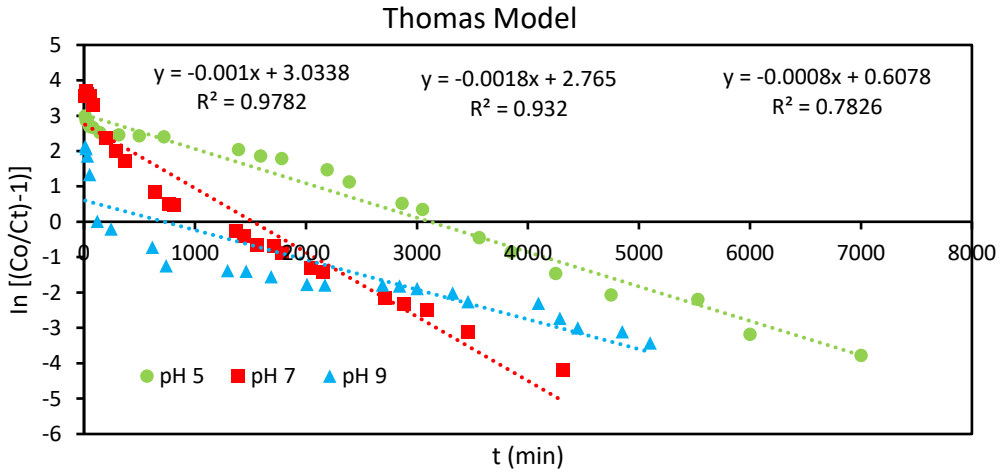

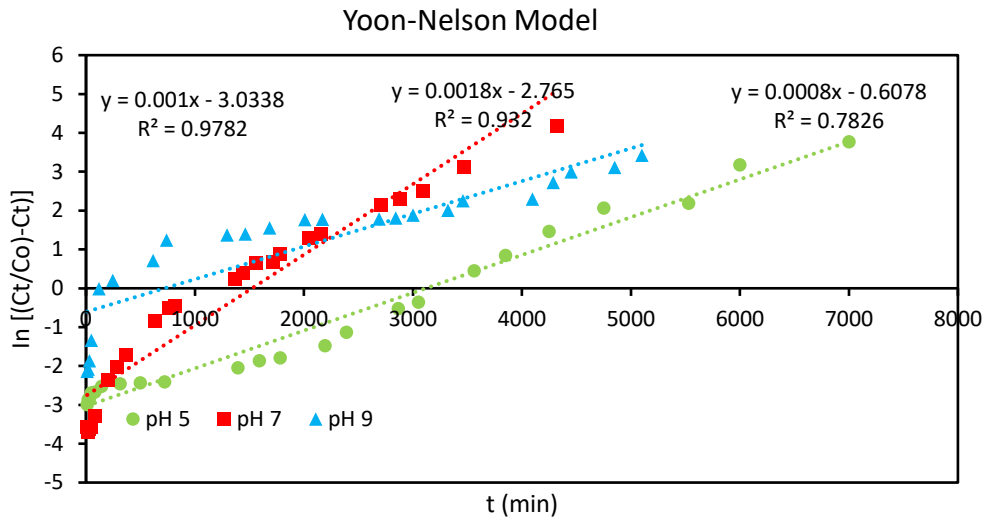
Yoon-Nelson Model
y = 0.001x - 3.0338
R² = 0.9782
y = 0.0018x - 2.765
R² = 0.932
y = 0.0008x - 0.6078
R² = 0.7826
ln [(Ct/Co)-Ct)]
t (min)
pH 5
pH 7
pH 9

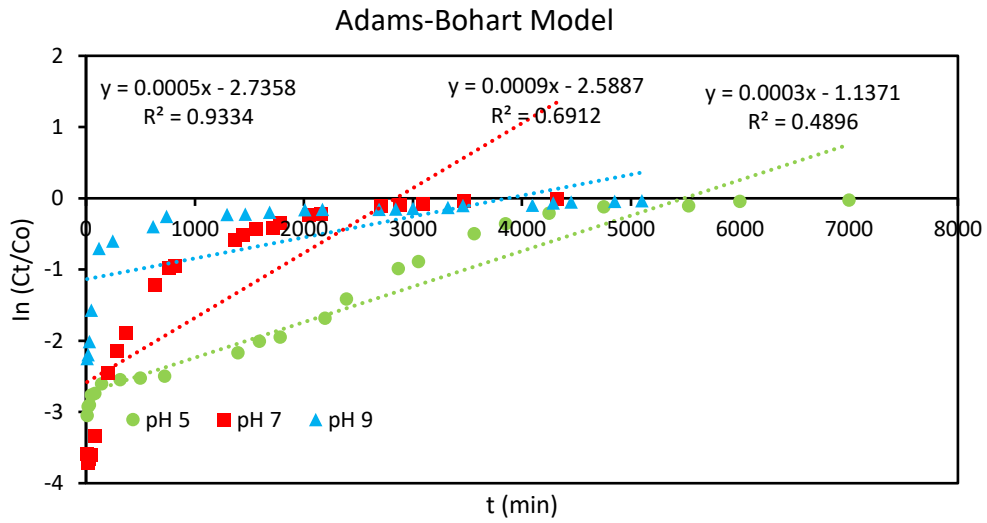
Adams-Bohart Model
y = 0.0005x - 2.7358
R² = 0.9334
y = 0.0009x - 2.5887
R² = 0.6912
y = 0.0003x - 1.1371
R² = 0.4896
ln (Ct/Co)
t (min)
pH 5
pH 7
pH 9

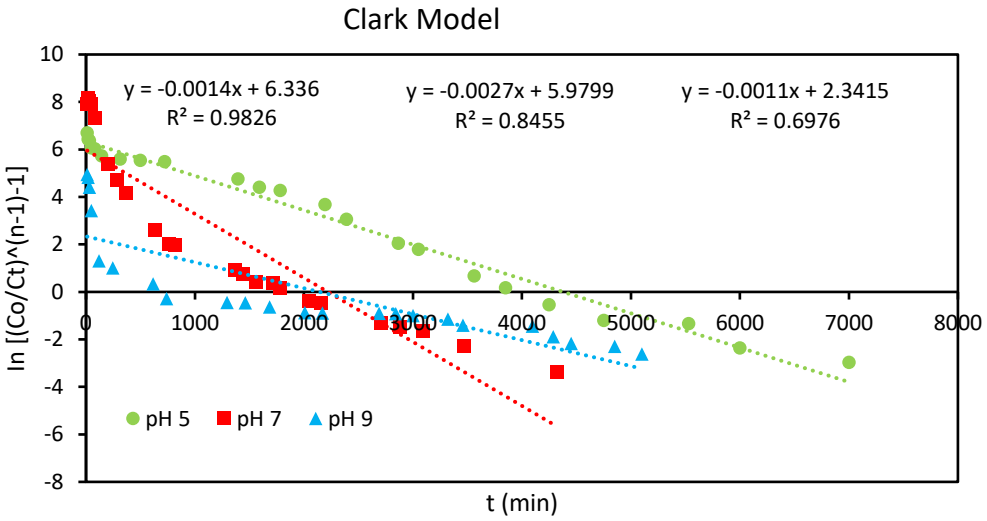
Clark Model
y = -0.0014x + 6.336
R² = 0.9826
y = -0.0027x + 5.9799
R² = 0.8455
y = -0.0011x + 2.3415
R² = 0.6976
ln [(Co/Ct)^(n-1)-1]
t (min)
pH 5
pH 7
pH 9

4C

Adsorption column design

Initial arsenic concentration C_o (mg/L)	0.0185
Arsenic Conc. at breakthrough point C_{tb} (mg/L)	0.00764
Total volume of water to be treated per day (L/day)	90,000,000
Maximum adsorption capacity (mg/g)	0.0066
Total mass of arsenic adsorbed (kg/day)	0.98
Mass of DMI-65 required (tonnes/day)	147.54
Density of DMI-65 (tonnes/m^3)	1.46
Volume of column (m^3)	101.06
Column height (m)	4.5
Column diameter (m)	4
No of column(s) required	= 2 X (2 X 3.142 X 2^2 X 4.5)
Recommended number of adsorption column	= 3
Therefore total mass of DMI-65 required	***= ~225 tonnes***

Cost of DMI-65 ($270 per bag) 1 bag = 21 kg

Cost of DMI-65 (225 tonnes) ***= ~$3,000,000***

Source: https://dmi65.com/dmi-65/technical-datasheet/

Appendix 5A

COAGULANT	PH	SAMPLE	DOSAGE (mL)	FINAL PH	FINAL ZP(mV)	OD_{680nm}	UV_{254nm} (cm^{-1})	TSS (i) (mg/L)	TSS (f) (mg/L)	TSS (20mL)	TURBIDITY (NTU)	As. (µg/L)
POLYDADMAC	4	G1	2	4.01	203	0.063	0.092	0.8848	0.8865	0.0017	2.64	19.00
		G2	2.2	3.98	282	0.063	0.094	0.8829	0.8847	0.0018	2.26	16.82
		G3	2.4	3.98	286	0.061	0.093	0.9003	0.9019	0.0016	2.23	15.48
		G4	2.6	3.95	233	0.061	0.092	0.8876	0.8894	0.0018	2.11	17.01
		G5	3	3.88	257	0.062	0.096	0.8801	0.8824	0.0023	2.22	17.60
		G6	2	5.91	-104	0.064	0.103	0.8808	0.883	0.0022	3.92	21.64
		G7	2.2	6.02	-73	0.065	0.101	0.8926	0.8949	0.0023	3.82	21.13
		G8	2.4	6.08	23	0.064	0.105	0.8955	0.8978	0.0023	3.82	20.89
		G9	2.6	5.94	15	0.064	0.103	0.8872	0.8993	0.0121	3.73	20.90
		G10	3	5.95	165	0.061	0.102	0.886	0.8884	0.0024	3.51	21.05
	5	H1	2	4.76	196	0.054	0.123	0.885	0.8863	0.0013	4.58	18.76
		H2	2.2	4.9	187	0.057	0.102	0.8773	0.8786	0.0013	3.78	18.22
		H3	2.4	5.08	135	0.057	0.095	0.8791	0.8804	0.0013	3.55	17.74
		H4	2.6	5.1	175	0.05	0.095	0.8792	0.8806	0.0014	3.21	16.22
		H5	3	5.09	198	0.07	0.092	0.8778	0.879	0.0012	2.81	17.21
		H6	2	6.96	-103	0.059	0.097	0.887	0.889	0.002	4.63	19.47
		H7	2.2	6.88	-72	0.054	0.095	0.8916	0.8932	0.0016	4.04	21.16
		H8	2.4	6.79	49	0.058	0.089	0.8831	0.8851	0.002	3.83	20.25
		H9	2.6	6.78	102	0.058	0.085	0.8808	0.8825	0.0017	3.65	19.92
		H10	3	6.79	172	0.053	0.085	0.877	0.8788	0.0018	3.62	20.59
	6	I1	2	5.78	24	0.06	0.093	0.888	0.8841	-0.0039	4.25	18.49

	I2	2.2	5.88	54	0.059	0.113	0.8888	0.89	0.0012	5.19	17.36
	I3	2.4	6.3	63	0.061	0.108	0.8901	0.8912	0.0011	5.8	17.66
	I4	2.6	6.38	102	0.052	0.097	0.8874	0.8884	0.001	3.73	19.14
	I5	3	6.47	115	0.056	0.094	0.9026	0.9036	0.001	2.9	18.49
	I6	2	6.77	-88	0.057	0.103	0.8912	0.8926	0.0014	4.84	19.80
	I7	2.2	6.84	-58	0.063	0.11	0.8895	0.8909	0.0014	4.49	21.66
	I8	2.4	6.9	37	0.058	0.103	0.8893	0.8903	0.001	4.13	20.75
	I9	2.6	7.08	43	0.054	0.094	0.8815	0.8832	0.0017	3.83	20.57
	I10	3	6.89	141	0.056	0.09	0.8838	0.885	0.0012	3.18	20.90
7	J1	2	7.06	-74	0.061	0.089	0.8884	0.888	-0.0004	4.5	18.85
	J2	2.2	6.88	-54	0.062	0.107	0.891	0.8907	-0.0003	4.87	16.66
	J3	2.4	7.37	38	0.06	0.115	0.8911	0.8909	-0.0002	5.43	18.26
	J4	2.6	7.35	93	0.059	0.104	0.896	0.8958	-0.0002	4.56	19.90
	J5	3	7.43	148	0.056	0.09	0.8895	0.8893	-0.0002	3.01	18.60
	J6	2	7.6	-72	0.057	0.067	0.8962	0.8963	1E-04	3.2	20.05
	J7	2.2	7.67	-92	0.06	0.085	0.845	0.8946	0.0496	4.1	21.62
	J8	2.4	7.67	23	0.059	0.09	0.8922	0.8924	0.0002	4.08	20.26
	J9	2.6	7.65	79	0.059	0.093	0.8932	0.8935	0.0003	4.08	22.02
	J10	3	7.59	99	0.052	0.087	0.8958	0.896	0.0002	3.75	21.20
8	K1	2	7.24	98	0.058	0.127	0.888	0.889	0.001	5.15	16.28
	K2	2.2	7.51	4	0.062	0.116	0.8966	0.897	0.0004	5.52	17.66
	K3	2.4	7.75	44	0.053	0.111	0.8834	0.8837	0.0003	5.04	17.85
	K4	2.6	7.78	93	0.059	0.107	0.8862	0.8865	0.0003	4.07	16.43
	K5	3	7.88	152	0.062	0.097	0.8882	0.8886	0.0004	3.09	17.06

	K6	2	7.87	83	0.06	0.097	0.8953	0.8953	0	3.97	21.80
	K7	2.2	7.91	44	0.063	0.117	0.8842	0.8845	0.0003	4.09	22.01
	K8	2.4	7.92	2	0.063	0.116	0.8814	0.8815	1E-04	4.29	21.87
	K9	2.6	7.9	34	0.057	0.116	0.8734	0.8735	0.0001	3.9	22.37
	K10	3	7.88	105	0.054	0.107	0.8963	0.8963	0	3.85	23.60
9	L1	2	7.06	-30	0.063	0.118	0.8846	0.8851	0.0005	4.7	18.80
	L2	2.2	7.87	2	0.06	0.12	0.8886	0.889	0.0004	4.18	20.04
	L3	2.4	7.91	23	0.056	0.14	0.8873	0.8875	0.0002	5.27	18.86
	L4	2.6	7.88	64	0.059	0.117	0.8868	0.8868	0	4.91	19.37
	L5	3	7.98	91	0.062	0.113	0.8871	0.8871	0	3.73	18.55
	L6	2	8.01	-37	0.061	0.096	0.8825	0.8824	-1E-04	4.32	23.57
	L7	2.2	8.13	-47	0.058	0.086	0.8991	0.8989	-0.0002	3.64	23.65
	L8	2.4	8.15	-54	0.062	0.102	0.8415	0.8913	0.0498	4.38	22.45
	L9	2.6	8.16	-9	0.057	0.105	0.8464	0.8964	0.05	4.02	22.55
	L10	3	8.04	60	0.056	0.091	0.8898	0.8898	0	3.41	24.12

Appendix 5B

COAGULANT	PH	SAMPLE	DOSAGE (mL)	FINAL PH	FINAL ZP	OD_{680nm}	UV_{254nm} (cm^{-1})	TSS (i) (mg/L)	TSS (f) (mg/L)	TSS (20mL)	TURBIDITY (NTU)	As. (µg/L)
CHITOSAN	4	M1	0.2	4	-66	0.079	0.138	0.8856	0.8859	0.0003	5.89	18.96
		M2	0.4	3.91	-24	0.061	0.099	0.8808	0.8812	0.0004	4.1	18.35
		M3	0.6	3.89	22	0.069	0.113	0.8828	0.8831	0.0003	3.95	18.54
		M4	0.8	3.88	152	0.074	0.123	0.8847	0.8852	0.0005	4.09	17.76
		M5	1	3.86	202	0.072	0.121	0.8747	0.8752	0.0005	4.51	17.67
		M6	0.2	4.94	-207	0.07	0.115	0.8868	0.8874	0.0006	6.27	14.20
		M7	0.4	4.78	-117	0.068	0.08	0.8853	0.8856	0.0003	3.17	13.38
		M8	0.6	4.51	-27	0.068	0.096	0.8816	0.8821	0.0005	3.73	12.98
		M9	0.8	4.38	0	0.07	0.096	0.8932	0.8937	0.0005	3.34	13.15
		M10	1	4.34	119	0.068	0.098	0.8952	0.8957	0.0005	3.59	12.87
	5	N1	0.2	4.35	-72	0.064	0.151	0.8823	0.8823	0	6.67	18.52
		N2	0.4	4.27	-84	0.057	0.111	0.8911	0.8909	-0.0002	4.75	17.52
		N3	0.6	4.19	-12	0.058	0.116	0.8897	0.8895	-0.0002	3.72	17.82
		N4	0.8	4.14	2	0.058	0.123	0.8829	0.8828	-1E-04	4.05	18.06
		N5	1	4.08	173	0.062	0.129	0.8845	0.8845	0	5.02	17.61
		N6	0.2	5.23	-312	0.061	0.118	0.885	0.8854	0.0004	5.05	14.99
		N7	0.4	4.75	-201	0.056	0.079	0.885	0.8851	1E-04	3.76	15.83
		N8	0.6	4.52	-111	0.054	0.103	0.8878	0.8881	0.0003	3.69	15.12
		N9	0.8	4.39	1	0.056	0.112	0.8844	0.8848	0.0004	3.43	15.31
		N10	1	4.37	130	0.052	0.106	0.8915	0.8917	0.0002	3.33	15.69
	6	O1	0.2	4.92	-304	0.068	0.153	0.891	0.8919	0.0009	6.94	17.40

	O2	0.4	4.62	-257	0.052	0.125	0.8807	0.8815	0.0008	4.91	17.68
	O3	0.6	4.5	-224	0.048	0.12	0.8884	0.8893	0.0009	3.48	18.31
	O4	0.8	4.39	43	0.054	0.127	0.8925	0.8935	0.001	3.45	17.14
	O5	1	4.28	143	0.054	0.13	0.9021	0.9029	0.0008	4.2	17.55
	O6	0.2	5.9	-302	0.057	0.134	0.8759	0.8771	0.0012	5.03	14.97
	O7	0.4	5.19	-296	0.06	0.101	0.8955	0.8968	0.0013	3.38	14.70
	O8	0.6	4.78	-282	0.052	0.109	0.8733	0.8744	0.0011	3.37	14.44
	O9	0.8	4.59	-42	0.059	0.109	0.9007	0.9018	0.0011	2.87	14.08
	O10	1	4.5	168	0.051	0.111	0.8819	0.8832	0.0013	3.42	14.29
7	P1	0.2	5.52	-346	0.061	0.146	0.8888	0.8891	0.0003	5.93	17.81
	P2	0.4	4.95	-336	0.056	0.122	0.8825	0.8828	0.0003	5.03	16.71
	P3	0.6	4.66	-302	0.056	0.107	0.8966	0.8968	0.0002	3.7	15.73
	P4	0.8	4.46	67	0.055	0.113	0.8879	0.8883	0.0004	3.27	16.33
	P5	1	4.4	147	0.062	0.123	0.8957	0.8958	1E-04	3.99	16.28
	P6	0.2	6.44	-356	0.065	0.124	0.8842	0.8847	0.0005	5.98	13.40
	P7	0.4	5.74	-312	0.059	0.111	0.8897	0.8899	0.0002	3.86	14.14
	P8	0.6	5.05	-322	0.05	0.094	0.8764	0.8769	0.0005	3.31	13.15
	P9	0.8	4.73	-16	0.059	0.101	0.8877	0.8879	0.0002	2.74	15.69
	P10	1	4.69	87	0.057	0.107	0.8889	0.8893	0.0004	2.93	14.99
8	Q1	0.2	5.72	-390	0.066	0.146	0.8837	0.8839	0.0002	6.39	15.74
	Q2	0.4	5.12	-276	0.059	0.135	0.8878	0.8878	0	4.95	17.65
	Q3	0.6	4.77	-186	0.057	0.112	0.883	0.883	0	3.95	16.42
	Q4	0.8	4.63	134	0.051	0.121	0.8842	0.8842	0	3.32	17.02
	Q5	1	4.54	229	0.062	0.124	0.8893	0.8893	0	3.61	16.86

	Q6	0.2	6.5	-375	0.057	0.123	0.8893	0.8897	0.0004	5.08	14.49
	Q7	0.4	5.72	-365	0.062	0.111	0.8792	0.8894	0.0102	3.92	15.36
	Q8	0.6	5.17	-308	0.058	0.104	0.8823	0.8827	0.0004	3.56	14.14
	Q9	0.8	4.9	3	0.051	0.105	0.8861	0.8865	0.0004	2.87	13.85
	Q10	1	4.75	177	0.053	0.106	0.8973	0.8979	0.0006	3.05	14.17
9	R1	0.2	5.85	-347	0.067	0.151	0.8915	0.8916	1E-04	6	16.88
	R2	0.4	5.1	-332	0.064	0.133	0.8874	0.8875	1E-04	4.84	16.44
	R3	0.6	4.77	-172	0.06	0.125	0.8909	0.891	1E-04	3.81	15.77
	R4	0.8	4.65	22	0.064	0.129	0.8871	0.8872	1E-04	3.73	16.45
	R5	1	4.58	179	0.063	0.133	0.8743	0.8745	0.0002	3.86	15.94
	R6	0.2	6.65	-326	0.07	0.124	0.8852	0.8858	0.0006	6.32	13.02
	R7	0.4	5.92	-372	0.064	0.104	0.8758	0.8761	0.0003	3.77	12.98
	R8	0.6	5.38	-302	0.06	0.094	0.8868	0.8872	0.0004	3.3	12.18
	R9	0.8	5.01	-65	0.056	0.107	0.8847	0.885	0.0003	2.77	13.42
	R10	1	4.83	164	0.054	0.102	0.8816	0.8824	0.0008	2.7	13.49

Appendix 6A

S = Sulfate ion

C = Carbonate

N = Nitrate

P = Phosphate

pH 5	Final pH	ZP (mV)	UV_{254nm} (cm^{-1})	Turbidity (NTU)	As Conc. (µg/L)
Without Ions	4.34	240	0.166	11.8	1.08
S1	5.6	-28	0.062	3.6	3.315084
S2	5.7	-45	0.087	5.8	3.34442
S3	5.62	-66	0.101	6.1	3.05284
C1	7.98	-355	0.067	2.2	9.619925
C2	10.12	-370	0.073	3.29	12.666625
C3	10.44	-319	0.074	3.3	13.33825
N1	4.68	181	0.194	14.4	3.848
N2	5.4	170	0.132	8.94	3.773
N3	5.55	177	0.12	7.06	4.148
P1	5.6	-258	0.058	3.19	15.26698
P2	5.35	-261	0.068	3.61	17.4859
P3	5.19	-249	0.068	3.5	15.2598

Note = 1, 2, 3 represents 1, 5 and 10 mM respectively

pH 6	Final pH	ZP (mV)	UV_{254nm} (cm^{-1})	Turbidity (NTU)	As Conc. (µg/L)
Without Ions	5.99	109	0.212	14.9	0.87
S1	4.50	7	0.038	2.12	1.01
S2	5.98	-51	0.058	3.2	0.91
S3	6.18	-67	0.068	3.76	0.52
C1	8.25	-309	0.049	1.88	11.96
C2	10.21	-347	0.057	2.47	16.45
C3	10.49	-296	0.066	2.54	15.92
N1	6.13	-69	0.056	3.02	4.31
N2	6.18	-162	0.095	5.47	1.10
N3	6.22	47	0.094	4.86	1.24
P1	6.14	-216	0.063	2.6	19.98
P2	5.77	-223	0.082	3.86	21.53
P3	5.55	-242	0.074	3.39	22.28

pH 7	**Final pH**	**ZP (mV)**	**UV_{254nm} (cm^{-1})**	**Turbidity (NTU)**	**As Conc. (µg/L)**
Without Ions	6.55	-227	0.082	4.74	1.08
S1	5.40	-399	0.054	2.16	2.99
S2	6.56	-356	0.076	3.2	2.50
S3	6.69	-235	0.078	3.37	1.91
C1	9.15	-430	0.097	3.83	14.07
C2	10.21	-424	0.094	3.7	16.40
C3	10.49	-366	0.09	3.28	16.54
N1	6.6	-392	0.074	3.3	3.25
N2	6.68	-388	0.085	3.42	3.11
N3	6.71	-328	0.091	3.11	3.24
P1	6.55	-351	0.108	4.3	19.66
P2	6.15	-376	0.12	4.95	18.23
P3	5.95	-322	0.108	4.47	16.51

pH 8	**Final pH**	**ZP (mV)**	**UV_{254nm} (cm^{-1})**	**Turbidity (NTU)**	**As Conc. (µg/L)**
Without Ions	6.76	-270	0.048	2.04	1.17
S1	6.82	-364	0.054	2.23	3.69
S2	7.02	-295	0.073	3.34	3.27
S3	7.04	-224	0.081	3.59	3.77
C1	9.24	-377	0.089	3.58	11.27
C2	10.29	-414	0.089	3.64	12.18
C3	10.48	-341	0.083	3.1	13.60
N1	6.21	-386	0.055	2.04	3.91
N2	6.66	-383	0.065	2.28	3.85
N3	6.76	-326	0.076	2.02	3.86
P1	6.7	-422	0.132	5.97	16.87
P2	6.28	-377	0.162	7.52	17.96
P3	5.96	-303	0.152	6.41	17.20

pH 9	**Final pH**	**ZP (mV)**	**UV_{254nm} (cm^{-1})**	**Turbidity (NTU)**	**As Conc. (µg/L)**
Without Ions	6.83	-276	0.043	1.54	1.36
S1	7.07	-446	0.054	2.25	4.08
S2	7.21	-338	0.061	2.26	3.69
S3	7.24	-267	0.062	2.27	3.97
C1	9.55	-416	0.074	2.6	11.18
C2	10.28	-415	0.078	2.9	13.65
C3	10.49	-354	0.075	2.68	12.40
N1	6.63	-431	0.046	1.46	4.03
N2	7	-419	0.054	1.51	3.97
N3	7.04	-376	0.07	1.66	4.17
P1	6.81	-470	0.152	7.97	14.59
P2	6.31	-407	0.165	9.11	14.68
P3	6.03	-346	0.172	10.1	15.04

Appendix 7A: Effect of PAC dosage

Dosage (mg/L)	Turbidity (NTU)	UV_{254nm} (cm^{-1})	Final pH	As Conc. (ug/L)
2.35	2.59	0.0786	6.93	6.043
4.7	2.29	0.0574	6.92	3.391
9.4	1.67	0.0347	6.89	1.753
14.1	2.28	0.0421	6.86	1.376
18.8	2.82	0.0564	6.8	1.273

Appendix 7B: Effect of pH

pH	Turbidity (NTU)	UV_{254nm} (cm^{-1})	Final pH	As Conc. (ug/L)
5	2.84	0.064	5.33	2.451
6	2.53	0.0543	6.19	1.287
7	1.91	0.0414	6.87	1.832
8	1.75	0.0421	7.31	2.528
9	2.25	0.0608	8.6	6.384

Appendix 7C: Effect of $H_2PO_4^-$

Concentration	Turbidity (NTU)	UV_{254nm} (cm^{-1})	Final pH	As Conc. (ug/L)
0.0005M	1.67	0.0442	7.22	3.924
0.0025M	2.07	0.053	7.03	4.265
0.01M	2.88	0.0791	6.66	4.265

Appendix 7D: Effect of flotation time

Time (min)	Turbidity (NTU)	UV_{254nm} (cm^{-1})	Final pH	As Conc. (ug/L)
10	1.72	0.039	7.28	2.117
20	1.67	0.037	7.27	1.85
30	1.58	0.0364	7.45	1.841

Appendix 7E: Effect of saturation pressure

Pressure (bar)	Turbidity (NTU)	UV_{254nm} (cm^{-1})	Final pH	As Conc. (ug/L)
2	1.63	0.035	7.18	1.858
3	1.66	0.0351	7.32	1.784
4	1.68	0.0358	7.27	1.699

Appendix 7F: Effect of change in pH from 6 to 8

Dosage (mg/L)	Turbidity (NTU)	UV_{254nm} (cm^{-1})	Final pH	As Conc. (ug/L)
0	1.23	0.0303	7.67	2.17
0.2	1.02	0.0324	7.59	1.779
0.4	1.22	0.034	7.57	1.876
0.6	1.27	0.0312	7.42	1.608
0.8	1.35	0.0345	7.12	1.452

Appendix 7G: Solubility of air at atmospheric pressure depending on water temperature

Temperature (°C)	Solubility in pure water of air (mg/L)
0	29.2
5	25.7
10	22.8
15	20.6
20	18.7
25	17.1
30	15.6

Appendix 7H: Calibration curve of total solids vs turbidity (Waikato River)

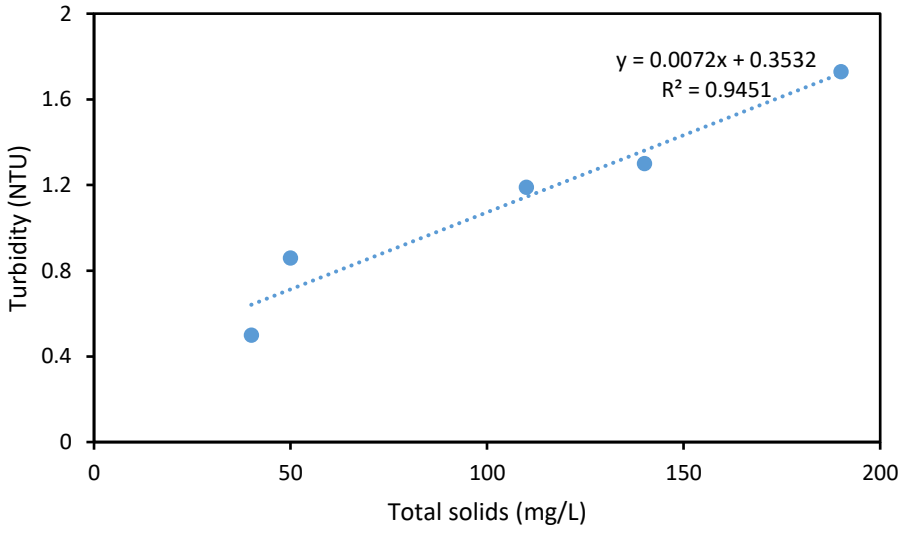

Appendix 7I:

pH Adjustment using HCl

HCl strength (kg HCl/kg solution)	0.38
Molarity	12.39
Solution strength (mol/L)	0.1
Volume solution added per liter of water (mL)	0.3
Liters of solution added	0.0003
Volume of water per day (L)	90,000,000
Moles HCl per day	2,700
Volume 38 % HCl needed per day (L)	**217.92**

pH Adjustment using NaOH

Molecular weight of NaOH (g/mol)	40
Solution strength (mol/L)	0.1
Liters of solution added	0.5
Moles NaOH added per liter	0.0005
Volume of water per day (L)	90,000,000
Moles NaOH per day	4,500

Mass of NaOH per day (g)	180,000
Mass of NaOH per day (kg)	**180**

Mass of PAC per liter of water

DAF

Volume of water per day (L)	90,000,000
Mass of PAC per day (mg)	846,000,000
Mass of PAC per day (kg)	846

SEDIMENTATION TANK/DAF2

Volume of water per day (L)	90,000,000
Mass of PAC per day (mg)	42,300,000
Mass of PAC per day (kg)	42.3
Total PAC needed per day (kg)	**888.3**

Air/solids ratio (Chapter 2: Eq. (47))

Solubility of air *Sa* (mg/L)	18.7
Recycle pressure, *P* (atm)	3.94
Total solids *TS* (mg/L)	190
Recycle ratio (%)	0.1
Recirculation rate *R* (L/min)	6,250
DAF feed rate *Q* (L/min)	62,500
Fraction of saturation, f	0.5
A/S ratio (mg/mg)	**0.02255**

Size of compressor

Water flow (L/day)	90,000,000
Starting solids (mg/L)	190
Mass flow of solids (mg/day)	17,100,000,000
Mass flow of solids (kg/day)	17,100
Removal of solids (fraction)	0.0344
Arsenic concentration (µg/L)	13.4
Arsenic mass flow (µg/day)	1,206,000,000
Arsenic mass flow (kg/day)	1.206
Arsenic removal (fraction)	0.881
Solids removed (kg/day)	588.24
PAC added (kg/day)	846
Total solids removed (Assuming all PAC is floated)	1,434.24
Air to solids ratio (kg air/kg solids)	0.0225
Kg air needed per day	32.34
Density of air (kg/m^3)	1.22
Volume of air needed per day (m^3)	26.95
Compressor power needed (kW), eff. 78 %	**20**

Size of DAF 1

Volumetric flowrate of water (m^3/min)	62.5
Residence time (min)	10

Depth of DAF (m)	3.5
Volume of DAF (m^3)	625
Area (m^2)	350
Hydraulic loading rate (m/min)	0.18

DAF Tank required = 5 X (20 X 2.5 X 3.5) m

Size of DAF 2

Volumetric flowrate of water (m^3/min)	62.5
Residence time (min)	10
Depth of DAF (m)	3.5
Volume of DAF (m^3)	625
Area (m^2)	350
Hydraulic loading rate (m/min)	0.18

DAF Tank required = 5 X (20 X 2.5 X 3.5) m

Size of saturator

Saturation time (min)	10
Water volume (L)	62,500
Ratio packing to water	0.2
Packing volume (L)	12,500
Empty volume (fraction)	0.2
Total saturator volume (L)	93,750
Air saturator volume (m^3)	93.75
Saturator diameter (m)	3
Volumetric spherical ends (m^3)	14.14
Area (m^2)	7.07
Length of cylindrical bit (m)	10

Saturators required = 5 X (10 X 3) m

Pump size DAF 1

Flow of water (m^3/h)	375

Density of fluid (kg/m^3)	1000
Acceleration due to gravity (m/s^2)	9.81
Differential head (m) 4 bar = 41 m head	41 + 4 = 45
Pump efficiency %	60
Shaft power (kW)	5.11

Pump size DAF 2

Flow of water (m^3/h)	281.25
Density of fluid (kg/m^3)	1000
Acceleration due to gravity (m/s^2)	9.81
Differential head (m) 4 bar = 41 m head	41 + 4 = 45
Pump efficiency %	60
Shaft power (kW)	3.83

Appendix 7J: Cost analysis

DAF Tank (DAF 250 X 5 at $1,500,000 each) ***$7,500,000***

Product dimensions (20 m X 3.5 m X 2.5 m)
Included in this price is:

- Rectangular flotation tank
- Dissolved air system
- Feed pumps
- Acid dosing and control
- Process pipework
- Acid storage tank
- Foundation
- Sludge tank and pumps
- Electrical and automation
- Installation

Source: Pal-Singh, S. 2020, Internal communication, Vertex Engineering, Hamilton, New Zealand

https://www.rendertech.co.nz/products/equipment-dissolved-air-flotator/

Polyaluminium chloride (PAC) ($281.40 per ton X 88.3 kg/day) $~30

Source: https://www.kemcore.com/polyaluminum-chloride-pac-03-30.html

(PAC -03 30 %)

Sodium hydroxide (NaOH) (180 kg/day at $175/25 kg) ***$1,260***

Souce: https://www.ecochem.co.nz/order-chemicals/uncategorised/sodium-hydroxide/

Hydrochloric chloride (HCl) conc. 37 % (218/day at $20/5 L) ***$872***

Source: https://www.bunnings.co.nz/bondall-5l-hydrochloric-acid_p0960235

Note $ = New Zealand Dollar

Hydrocloric acid

Strength (%)	37
Molarity (mol/L)	12
Volume per day (L)	217.91
Moles per day	2614.92
Moles per mol HCl	1
Moles of H required	2614.92

Sulphuric acid

Strength (%)	98
Molarity (mol/L)	18.4
Moles H per moles H_2SO_4	2
Moles H_2SO_4 required	1307.46
Liter of H_2SO_4 required	71.06
H_2SO_4 price ($/L)	9.16
Cost of H_2SO_4 ($ per day)	650.89

Source: https://www.ecochem.co.nz/order-chemicals/uncategorised/sulphuric-acid-98/